LEVEL II

USAAVRADCOM-TR-81-D-5

12

ADVANCING BLADE CONCEPT (ABC) TECHNOLOGY DEMONSTRATOR

R. J. Ruddell, et al
SIKORSKY AIRCRAFT DIVISION
UNITED TECHNOLOGIES CORPORATION
Stratford, Conn. 06602

April 1981

Final Report for Period January 1972 - June 1980

Prepared for

APPLIED TECHNOLOGY LABORATORY
U. S. ARMY RESEARCH AND TECHNOLOGY LABORATORIES (AVRADCOM)
Fort Eustis, Va. 23604

APPLIED TECHNOLOGY LABORA' Y POSITION STATEMENT

The Advancing Blade Concept (ABC) rotor system was conceived as a means to alleviate classical retreating blade stall limitations and permit rotary wing flight throughout an expanded flight envelope. Unlike earlier generation compound helicopters, which used wings to unload the rotor at high speeds, an ABC helicopter retains rotor lift under high speed/high altitude conditions and therefore does not need a wing.

This report addresses the research, development, and test efforts involved in demonstrating the feasibility of the ABC rotor system. It covers contractual work spanning 8-1/2 years during which time the ABC rotor evolved through design, small scale wind tunnel tests, miscellaneous laboratory and ground tests, incorporation into the XH-59A demonstrator aircraft, and finally, test of that aircraft. The primary emphasis is on flight test results – as a pure helicopter up to level flight speeds of 156 knots true airspeed (KIAS) and with auxiliary propulsion up to level flight speeds of 238 KTAS.

Test results have been favorable and have verified the feasibility of this type of rotor system. Many of the original concerns relative to handling qualities and rotor stability have been laid to rest. Some insight has been gained into the magnitude of the design compromises needed to accommodate both conventional and high speed flight in one rotary wing aircraft.

A production ABC helicopter would require the application of composite materials technology and rotor redesign to reduce the rotor weight fraction. For missions requiring speeds above approximately 160 knots, an integrated lift/thrust propulsion system would be used to selectively power the rotors for lift or power the fans (or propeller) for thrust. Some type of vibration attenuation device would also be needed.

Results of this program will form a data base from which subsequent ABC designs can evolve. Technical areas requiring further R&D effort to exploit the potential of the ABC rotor have been identified.

Flight testing of the XH-59A under Navy contract DAAK51-80-C-0021 is continuing. The speed envelope has been expanded to 263 KTAS and the aircraft has been flown to a density altitude of approximately 25,000 feet.

Mr. Harvey R. Young and Mr. John A. Macrino from the Aeronautical Systems Division were the project engineers for this program, and Mr. Duane R. Simon was the project test pilot.

Unclassified

SECURITY CLASSIFICATION OF THIS PAGE (When Data Entered)

REPORT DOCUMENTATION PAGE

READ INSTRUCTIONS BEFORE COMPLETING FORM

1. REPORT NUMBER: USAAVRADCOM-TR-81-D-5	2. GOVT ACCESSION NO.: AD-A100181
3. RECIPIENT'S CATALOG NUMBER:	
4. TITLE (and Subtitle): ADVANCING BLADE CONCEPT (ABC) TECHNOLOGY DEMONSTRATOR	5. TYPE OF REPORT & PERIOD COVERED: Final Report. January 1972 — June 1980
	6. PERFORMING ORG. REPORT NUMBER: SER-69065
7. AUTHOR(s): A. J. Ruddell, et al	8. CONTRACT OR GRANT NUMBER(s): DAAJ02-72-C-0920, DAAJ02-75-C-0009
9. PERFORMING ORGANIZATION NAME AND ADDRESS: Sikorsky Aircraft Division of United Technologies Corporation, Stratford, Conn. 06602	10. PROGRAM ELEMENT, PROJECT, TASK AREA & WORK UNIT NUMBERS: 63211A 1F263211D157 17 002 EK
11. CONTROLLING OFFICE NAME AND ADDRESS: Applied Technology Laboratory, U.S. Army Research and Technology Laboratories (AVRADCOM), Fort Eustis, Va. 23604	12. REPORT DATE: April 1981 13. NUMBER OF PAGES: 297
14. MONITORING AGENCY NAME & ADDRESS (if different from Controlling Office)	15. SECURITY CLASS. (of this report): Unclassified 15a. DECLASSIFICATION/DOWNGRADING SCHEDULE

16. DISTRIBUTION STATEMENT (of this Report)

Approved for public release; distribution unlimited.

17. DISTRIBUTION STATEMENT (of the abstract entered in Block 20, if different from Report)

18. SUPPLEMENTARY NOTES

19. KEY WORDS (Continue on reverse side if necessary and identify by block number)

ABC Helicopter
Advancing Blade Concept (ABC)
High-Speed Rotary Wing Aircraft
V/STOL Technology
Hingeless Rotors
Coaxial Rotor
Helicopter Rotors
Helicopter Designs
Helicopter Flight Test

20. ABSTRACT (Continue on reverse side if necessary and identify by block number)

The XH-59A Advancing Blade Concept ABC™ demonstrator aircraft has completed five years of ground and flight tests in both the helicopter and auxiliary propulsion configurations. This testing was supported by wind tunnel tests, analytical developments, and flight simulation studies.

DD FORM 1 JAN 73 1473 EDITION OF 1 NOV 65 IS OBSOLETE

Unclassified

SECURITY CLASSIFICATION OF THIS PAGE (When Data Entered)

Testing as a pure helicopter was accomplished in two phases. To verify control system adequacy, a low speed test program was flown (0 to 80 knots) from July to September 1975. The balance of the flight envelope was explored in progressive steps from November 1975 to March 1977. A power-limited maximum level flight speed of 156 KTAS was reached in this phase, 186 KTAS was achieved in a shallow dive, and an extensive maneuver envelope was developed. Between April 1978 and May 1980 the aircraft was flown with two J-60 engines installed to provide auxiliary propulsion. A maximum airspeed of 238 KTAS in level flight was reached and a sizable maneuver envelope was developed through 220 KTAS. A total of 106 flight hours were accumulated in the pure helicopter and auxiliary propulsion modes.

Test results to date have verified the capability of the Advancing Blade Concept to meet its predicted technical goals. No major surprises or unanticipated problems have been encountered. Specifically:

- Hover performance of the coaxial rotor is excellent with rotor figure of merit as high as 0.79.
- Performance test results of the aircraft have generally verified the performance predictions.
- Rotor control power and damping are very high relative to other rotors; the entire flight envelope has been flown with the Stability Augmentation System (SAS) off.
- The coaxial rotors and absence of a tail rotor minimize control coupling; i.e., nearly pure pitch, roll, yaw, and vertical responses to single control inputs in those directions.
- Rotor system stresses and moments are dominated by one-per-revolution blade loads on the advancing blade, and follow predicted trends.
- Similarly, blade tip clearance in level flight follows predicted trends with approximately 18 inches of clearance remaining at V_{max}.
- Without auxiliary jets running, the aircraft is an unusually quiet helicopter because of its lack of tail rotor and relatively low rotor tip speed.

Aircraft operating limits have been only partially defined. Operation in the pure helicopter mode to an altitude of 14,000 feet raised the rotor nondimensional blade loading, C_T/σ, to 0.14 without rotor stall. At lower altitudes (auxiliary propulsion configuration) in maneuver the rotor thrust reached 22,500 lb, the design limit for the airframe, at speeds up to 220 KTAS. Rotor blade tip clearance is reduced in both high speed pull-ups and rolling maneuvers, but for the conditions flown (zero to 2.0 g's, and left and right roll rates to 60 deg sec), clearance was not limiting.

The aircraft's flying qualities are very good. Five Sikorsky pilots and four government pilots have flown the aircraft to date. Stability augmentation system gains selected to assist the pilot are low. Normal flight throughout the envelope requires no unusual pilot effort. Lift offset or the degree of advancing blade lift employed through the speed range, can be controlled either by differential control inputs to the rotors or by varying the phasing of cyclic control inputs. Establishment of a standard or optimum control schedule was beyond the scope of the flying to date.

The feasibility of the ABC has been demonstrated. It remains for the limits of the system's capability to be defined; for the system to be optimized in terms of handling qualities, vibrations, performance and loads; and for more weight-efficient structural concepts to be developed for the rotor, propulsion and control systems.

PREFACE

This report describes the results of a flight test program conducted with the Advancing Blade Concept (ABC) aircraft, serial number 21942. Tests were conducted in both the pure helicopter and the auxiliary propulsion configuration. Flights were performed by the Sikorsky Aircraft Division of United Technologies Corporation under Contracts DAAJ02-72-C-0020 and DAAJ02-75-C-0009, with the Applied Technology Laboratory, U.S. Army Research and Technology Laboratories, Fort Eustis, Virginia. Testing was conducted at the contractor's flight test facilities in Stratford, Connecticut, and West Palm Beach, Florida, and at Rentschler Field, East Hartford, Connecticut. Program Managers for the contractor were Messrs. G. Stack, D. Jenney, D. Halley, and A. Linden.

Flight testing in the pure helicopter configuration commenced on 21 July 1975 and was completed on 9 March 1977. The aircraft was modified with turbojets for auxiliary propulsion, and flight testing in that configuration began on 6 April 1978 and continued through 31 May 1980. It was conducted under the supervision of Messrs. W. Groth, A. Ruddell and R. McCutcheon. The Sikorsky test pilots were Messrs. B. Graham, D. Wright, J. Wright, C. Evans, and R. Holasek. Government evaluation pilots were Messrs. D. Simon, Applied Technology Laboratory, R. Gerdes, NASA Ames Research Center, and Maj. M. Blair and Lt. Cmdr. T. MacDonald, Naval Air Test Center. Messrs. H. Young, H. Murray, D. Simon, J. Whitman, D. Arents, and J. Macrino were the Army Technical Representatives.

Funding for contract DAAJ02-72-C-0020 was provided by the U.S. Army. Funding for contract DAAJ02-75-C-0009 was provided by the U.S. Army, the U.S. Navy, and the National Aeronautics and Space Administration (NASA). The U.S. Air Force supplied J-60 engines for auxiliary propulsion flight testing.

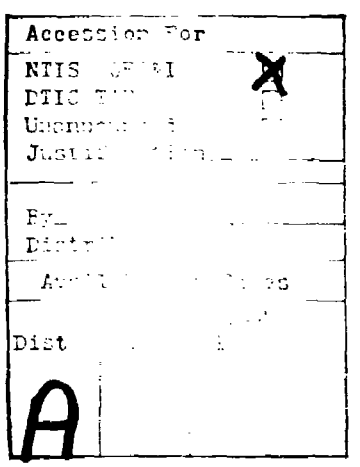

TABLE OF CONTENTS

TABLE OF CONTENTS - (cont'd)

LIST OF ILLUSTRATIONS

LIST OF ILLUSTRATIONS (Cont'd)

LIST OF ILLUSTRATIONS (Cont'd)

LIST OF ILLUSTRATIONS (Cont'd)

LIST OF ILLUSTRATIONS (Cont'd)

LIST OF ILLUSTRATIONS (Cont'd)

LIST OF ILLUSTRATIONS (Cont'd)

LIST OF ILLUSTRATIONS (Cont'd)

LIST OF ILLUSTRATIONS (Cont'd)

LIST OF ILLUSTRATIONS (Cont'd)

LIST OF ILLUSTRATIONS (Cont'd)

LIST OF ILLUSTRATIONS (Cont'd)

LIST OF ILLUSTRATIONS (Cont'd)

LIST OF ILLUSTRATIONS (Cont'd)

LIST OF ILLUSTRATIONS (Cont'd)

LIST OF TABLES

INTRODUCTION

The Advancing Blade Concept (ABC)™ rotor system, with a pair of counterrotating, coaxial, very rigid hingeless rotors, represents a significant departure from all predecessor helicopter rotor systems. It derives its name from the fact that the predominant lift load at high forward speeds is carried by the advancing blades on both sides of the aircraft. Since the retreating blades are not required to carry a significant fraction of the total lift load at forward speed, the speed and load factor limitations of the conventional helicopter due to retreating blade stall are eliminated. Unlike a conventional helicopter, rotor lift capability is retained with increasing speed, and speed capability is maintained at altitude.

In addition to performance benefits, the ABC's unique coaxial rigid rotors represent a significant departure from past practice in handling qualities, acoustics, loads and dynamics. As with other coaxial counterrotating rotors, torque cancellation is provided, thereby eliminating the need for a tail rotor and its associated shafting and gearboxes.

Advancing Blade Concept development began in 1964. Extensive analytical and experimental studies culminated in the test of a 40-foot-diameter rotor in the Ames 40-x-80-foot wind tunnel in 1970 (Reference 1). The wind tunnel tests covered a speed range of 80 to 180 knots and advance ratios of 0.21 to 0.91. Test results confirmed the performance potential of the ABC rotor system. In addition, the full-scale wind tunnel program developed materials technology and fabrication techniques to make construction of a demonstrator aircraft practical.

In December 1971 the U.S. Army awarded Sikorsky Aircraft Contract DAAJ02-72-C-0020 to design, fabricate, and fly the XH-59A to demonstrate the performance, handling qualities, and maneuver capabilities of the ABC rotor system. In August 1973 the first demonstrator aircraft, S/N 21941, was badly damaged in a hard landing during low speed forward flight test. A thorough accident investigation established that the incident was not inherent to any basic flaw in the concept. In November 1974 contract DAAJ02-75-C-0009 was awarded to continue the flight test program with aircraft S/N 21942. This report documents the results of that contract.

---

1. FULL-SCALE WIND TUNNEL INVESTIGATION OF THE ADVANCING BLADE CONCEPT ROTOR SYSTEM, USAAVLABS Technical Report 71-25, Eustis Directorate, U.S. Army Air Mobility R&D Lab, Fort Eustis, Va, August 1971, AD 734338.

Sixty-six hours of helicopter mode flying have been completed with the test envelope expanded to 156 KTAS in level flight and 186 KTAS in a dive. Altitudes of 14,000 feet were investigated.

Auxiliary propulsion flying was done in two phases. The first phase involved testing with the two rotors mounted on the aircraft to cross each other at the 90-degree azimuth position. This testing included 24 hours and expanded the envelope to 204 KTAS. The second phase of flight testing had the rotors installed to cross each other at 0 degree azimuth position. This included 16 hours of flight tests and expanded the envelope to 238 KTAS.

DESIGN DESCRIPTION

The XH-59A Advancing Blade Concept demonstrator aircraft is designed as a research aircraft to investigate the rotor characteristics in both helicopter and auxiliary propulsion modes. Figure 1 shows the aircraft in the helicopter mode, and the auxiliary propulsion configuration is shown in Figure 2. Table 1 summarizes the general aircraft attributes. Detailed design descriptions are presented in the following sections.

TABLE 1. XH-59A AIRCRAFT ATTRIBUTES.

Aircraft Length (rotor turning)	41 ft 6 in.
Fuselage Length	40 ft 10 in.
Main Landing Gear Tread	8 ft
Height	12 ft
Rotor Diameter	36 ft
Number of Rotors	2
Blades per Rotor	3
Rotor Separation	30 in.
Blade Taper Ratio	2:1
Blade Twist (nonlinear)	-10 deg
Total Rotor Solidity $(\frac{bc_{75}}{\pi R})$	.127
Precone Angle	3 deg
Prelag Angle	1.4 deg
Shaft Tilt	0 deg
Design Rotor Speed (helicopter	650 ft/sec
aux propulsion)	450 ft/sec
Drive System Design Power	1500 hp_2
Tail Surface - Horizontal	60 ft^2
- Vertical	30 ft^2
Elevator - % of Horizontal Tail	25
Rudder - % of Vertical Tail	30
Power Plants - Lift	(2) PT6-3
- Thrust	(2) J60-P3A

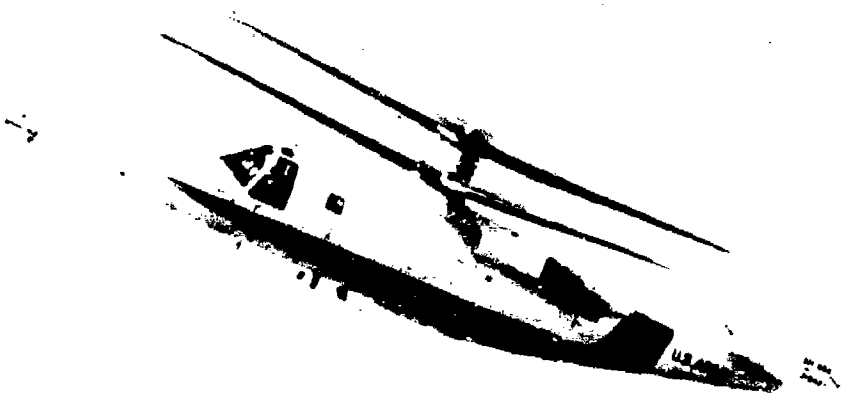

Figure 1. ABC Pure Helicopter.

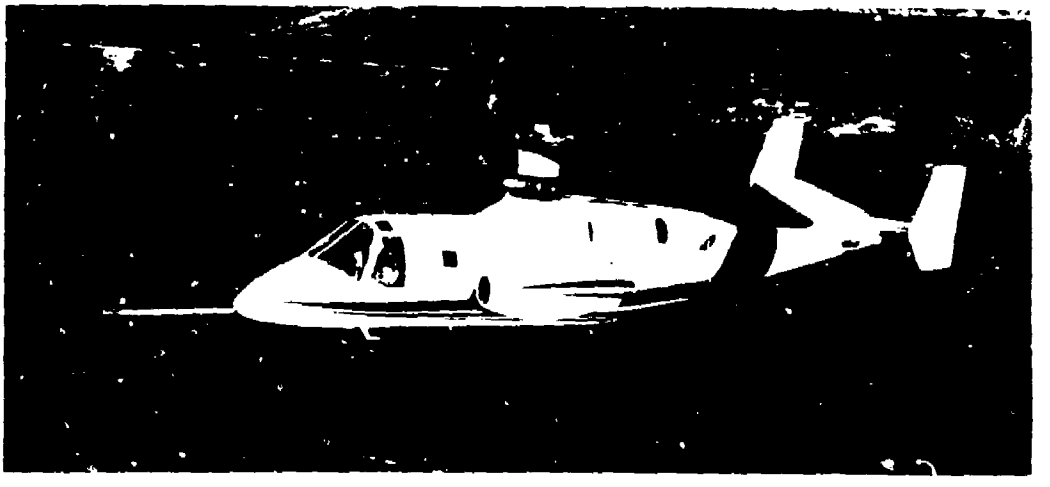

Figure 2. ABC Auxiliary Propulsion Helicopter.

ROTOR SYSTEM

The ABC rotor system consists of two three-bladed counter-rotating rotors classified as rigid or more precisely, stiff inplane hingeless. The latter name refers to that category of rotors which have no mechanical hinges in the two bending degrees of freedom and which have a first chordwise bending natural frequency higher than one times the rotor speed. The flapwise bending stiffness distribution is based on the following design requirements:

(a) The advancing blade concept involves allowing a large part of the rotor lift to be generated in the advancing portion of the rotor disc in high speed flight using conventional one-per-rev cycle pitch. This requires a relatively high flapwise frequency (or effective hinge offset) in the first flapwise bending mode.

(b) The distance between the upper and lower rotors is minimized to reduce drag. This requires sufficient stiffness to prevent the blade tips from contacting in flight.

(c) The stiffness distribution must result in sufficient bending fatigue strength in the selected materials under the high vibratory moments generated by the rigid rotor.

To meet the stiffness requirements at a minimum weight, the rotor blades are tapered in airfoil thickness, the highest taper occurring inboard. In addition, the airfoil chord length is tapered linearly from tip to root to maximize the performance of the rotor. Figure 3 shows spanwise distributions of the airfoil chord length and thickness ratio. The rotor blades have an effective built-in twist of approximately 10 degrees which varies nonlinearly from tip to root as shown in Figure 4.

The rotor radius is 216 inches and normal operating rotor speed is 345 rpm, yielding a tip speed of 650 feet per second.

The primary structural member of the rotor blade is the spar which provides most of the blade's flapwise stiffness requirements. The spar is constructed of 6-4 titanium alloy to maximize the fatigue stress allowable for a given weight in a metal structure. The hollow member, highly tapered in both wall thickness and periphery, is fabricated from a thick-walled extrusion which is machined both internally and externally and then hot formed to the required elliptical shape. The inboard end is round and threaded for attachment to the pitch bearing assembly.

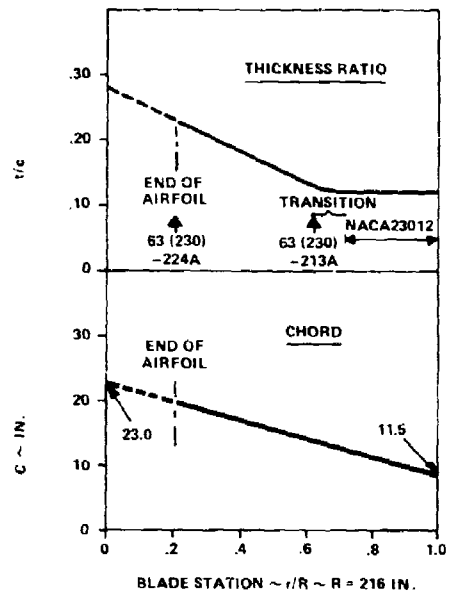

Figure 3. Aerodynamic Geometry.

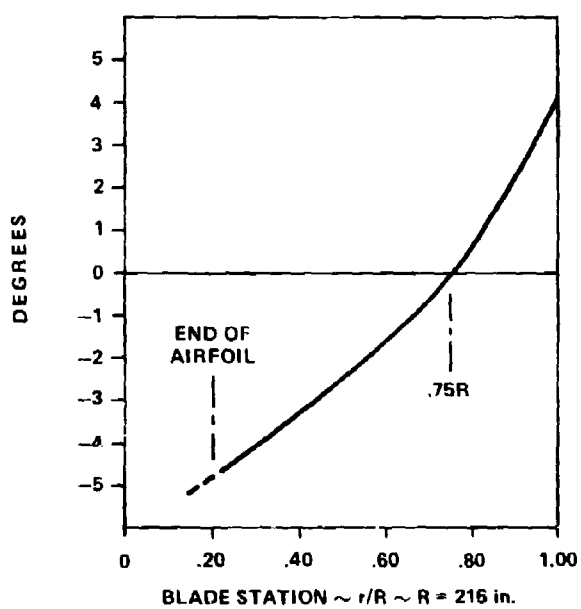

Figure 4. Blade Twist Distribution.

A laminate of boron-composite material is bonded to the upper and lower spar surfaces to increase the stiffness of the structure. A nosecap assembly consisting of shaped balance weights and a polyurethene abrasion strip is bonded to the leading edge of the spar thereby forming the leading edge of the airfoil. The aft fairing of the airfoil is fabricated from a continuous fiberglass (XP114E) skin over a Nomex honeycomb filler; the whole assembly is bonded to the aft end of the boron-stiffened spar. The fiberglass skin contributes significantly to the total chordwise strength and stiffness of the section. A sketch of a typical cross section of the blade is shown in Figure 5. Spanwise distributions of the weight, flap stiffness, chord stiffness, and torsional properties are shown in Table 2. The data are presented as the ordinates and abscissas of straight line segments which approximate the various property curves.

The rotor blade tip incorporates a fitting to which are attached adjustable weights for balancing the blade spanwise and chordwise.

The rotor's pitch bearings are a part of the rotor blade assembly resulting in a very compact root end with a minimum number of joints. A sketch of the rotor blade root end is shown in Figure 6. The blade spar acts as a spindle in the area of the bearings. A pair of roller bearing assemblies transfer bending moments from the spar to the outer sleeve which is rigidly bolted to the hub. Centrifugal loads are transferred from the spar through a spindle nut into the preloaded bearing stack. The ball bearing assembly, located between the two roller bearing assemblies, transfers the centrifugal load to the outer sleeve through a shoulder on the sleeve internal diameter. The bearings are grease lubricated and seals between the spar and sleeve contain the grease within the space occupied by the bearings.

The blades of both rotors are preconed 3.0 degrees upward at the hub to reduce steady flapwise bending stresses. The rotor blade pitch axes are offset forward (in the direction of rotation) of the centerline of rotation by 2.0 inches to relieve the steady chordwise bending stresses due to drag.

The coupled natural frequencies of the rotor blade modes are shown as a function of rotor speed in Figure 7. The rotor is designed to operate near/at 100 percent (345 rpm) in hover and low speed flight and at values as low as 70 percent in high speed cruise flight. All the bending modes below 10 per rev are shown. The first torsion mode is above 10 per rev over the full operating rotor speed range.

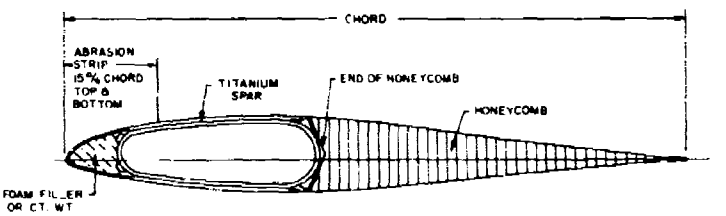

Figure 5. Blade Cross Section.

TABLE 2. ROTOR BLADE SPANWISE DISTRIBUTION OF PHYSICAL PROPERTIES.

Weight		Flapwise Stiffness		Chordwise Stiffness		Torsional Stiffness		Torsional Inertia	
x/R	(lb/in.)	x/R	EI_f ($lb.in^2 \times 10^6$)	x/R	EI_c ($lb.in^2 \times 10^6$)	x/R	GJ ($lb.in^2 \times 10^6$)	x/R	I ($lb.in^2$ in)
1.0	1.24	1.0	8.	1.0	56.	3.0	3.0	1.0	1.63
.973	1.24	.748	16.	.864	80.	.926	3.1	.979	1.63
.973	1.02	.634	28.	.691	144.	.810	5.0	.979	1.81
.939	1.02	.518	52.	.514	212.	.694	9.7	.944	1.81
.939	.32	.403	96.	.403	252.	.579	19.3	.60	4.5
.737	.42	.345	126.	.288	330.	.521	30.0	.40	7.8
.737	.28	.259	196.	.173	460.	.463	47.5	.23	13.5
.576	.42	.202	280.	.115	630.	.405	73.0	.162	14.1
.403	.68	.144	480.	.092	860.	.347	112.0	.162	12.4
.288	.95	.092	860.	0	860.	.289	160.	.139	12.4
.173	1.40	0	860.	"	"	.231	220.	.139	14.7
.115	1.80	"	"	"	"	.174	335.	.116	14.7
.092	2.20	"	"	"	"	.125	575.	.116	17.5
.092	9.70	"	"	"	"	.093	689.	0.	17.5
.030	9.70	"	"	"	"	0.	689.	"	"
0.	0.	"	"	"	"	"	"	"	"

radius = 216 in.

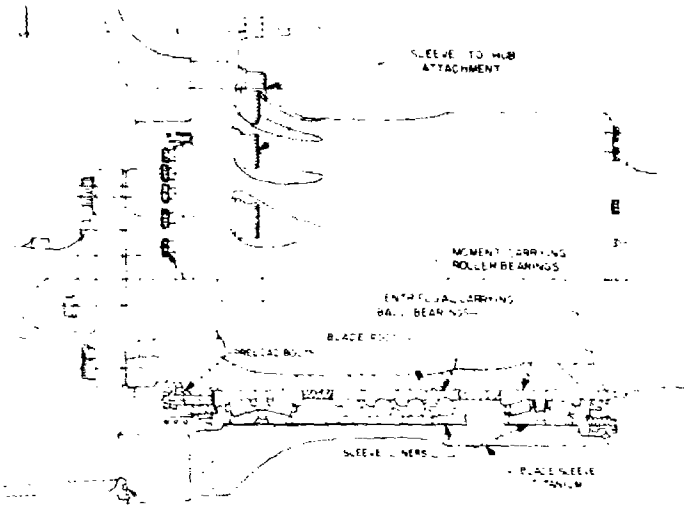

Figure 6. Rotor Blade Root End.

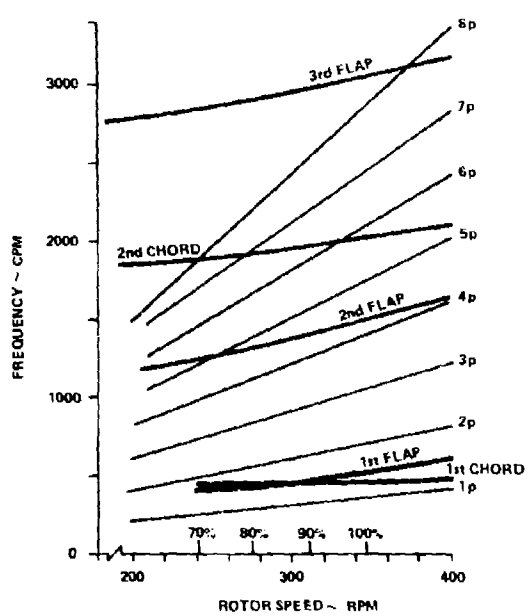

Figure 7. Rotor Blade Dynamic Modes.

The twc lower modes are highly coupled containing both flap and chord simultaneous motion, the coupling being a function of blade pitch, blade twist and rpm. Figure 8 is an exploded frequency plot of these two modes showing the effect of collective pitch. The lower pitch applies to high advance ratio conditions where the rotor is nonpropulsive. The lowest frequency mode is predominantly chordwise at 100 percent but changes to predominantly flapwise at the lowest operating rpm. The chordwise mode remains sufficiently far from two per rev at 70 percent rpm to preclude any stability problems. Note that the first flap mode has a natural frequency of approximately 1.4 per rev at 100 percent rpm which corresponds to an effective hinge offset near 40 percent of the blade radius.

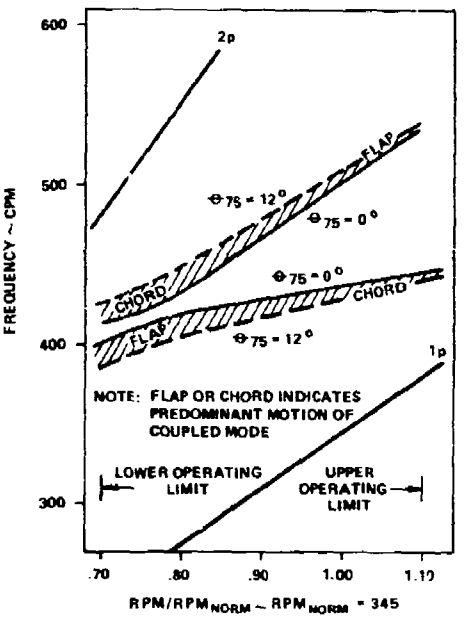

Figure 8. Effect of Collective Pitch Frequency of Lowest Two Modes.

TRANSMISSION SYSTEM

The ABC transmission is designed for 1500 horsepower. In addition to powering the coaxial rotors, an accessory section is provided to power the aircraft subsystems. Provisions are included for a differential rotor speed drive for an alternate yaw control system. However, it was found that the system was not required due to excellent control achieved with differential collective pitch and rudders in forward flight.

Figure 9 shows the general arrangement of the ABC transmission system. A line schematic presenting the gear reduction ratios and speeds of the major components is presented in Figure 10. Gearbox design data are shown in Table 3.

The main gearbox provides a 19.21:1 speed reduction between the PT6T-3 engine and the shafts that power the rotor blades. It supports the main rotor flight control system and is attached to the airframe through four attachment points. These attachment points include provisions for four gearbox isolators whose angles of inclination pass through the effective mass center of the combined gearbox and rotor system. The mounts then would provide isolation in the roll and yaw directions, and a pitch link attached between the gearbox sump and the airframe would provide a rigid support in the pitch direction.

The accessory section, located on the rear of the main gearbox, drives two servo pumps, one yaw pump (if required) and the tachometer. The yaw control drive train is located on the forward side of the main gearbox.

Torque enters the main gearbox through the engine-to-gearbox drive shaft and provides a maximum of 1500 hp at 6600 rpm. Flexible couplings at both ends of the shaft compensate for misalignment and motions of the gearbox relative to the engine output shaft flange. A 3.84 to 1 spiral bevel gear reduction set reduces speed, increases torque, and makes a 90-degree angle change between the engine shaft centerline and the main rotors. The planetary sun gear shaft transfers torque from the bevel gear shaft to the lower pinions of the compound spur planetary reduction set. The 5:1 reduction ratio planetary drives the upper main rotor shaft counter-clockwise, looking down, at 345 rpm via the lower ring gear and drives the lower main rotor shaft clockwise at 345 rpm via the lower planetary cage plate. A torque shaft connects the plate to the bottom end of the lower rotor shaft. A spur gear mounted on the lower ring gear to main shaft connector drives the vane-type lubrication pump located in the sump.

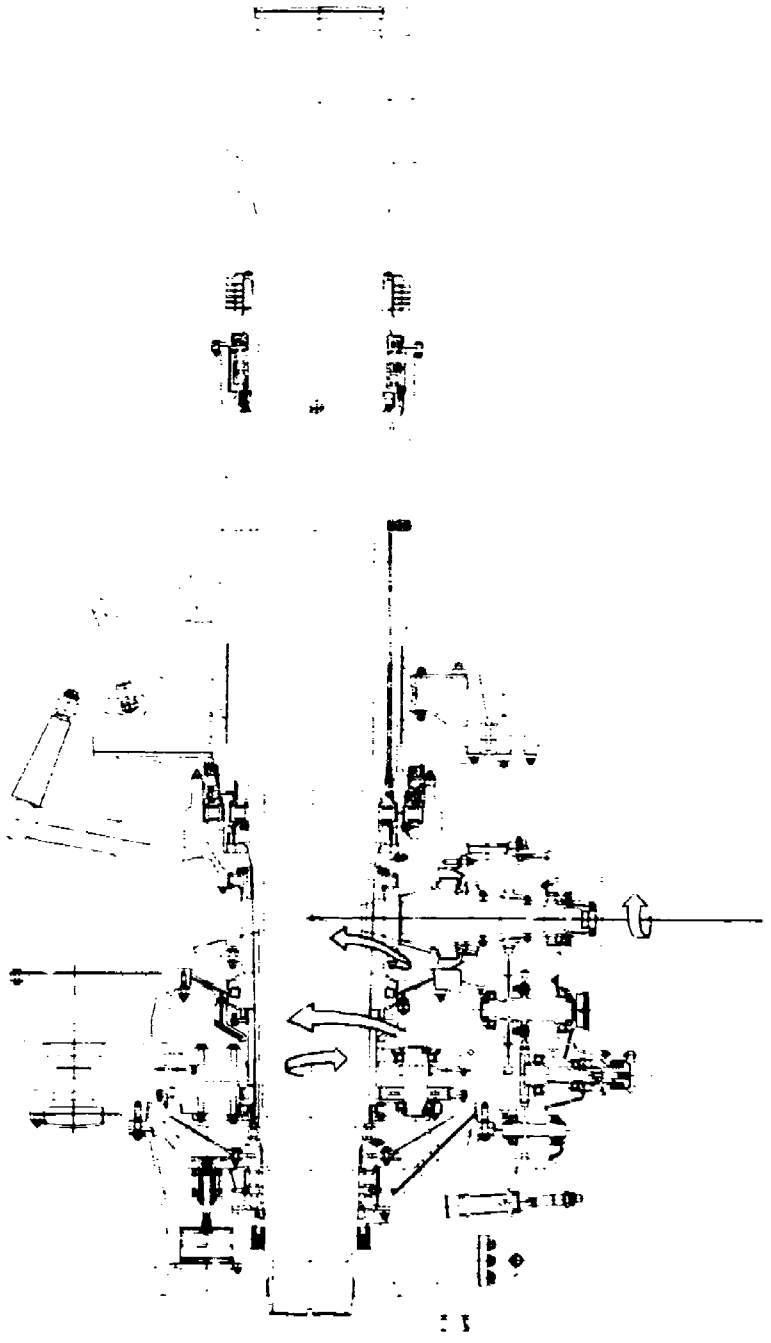

Figure 9. Main Transmission.

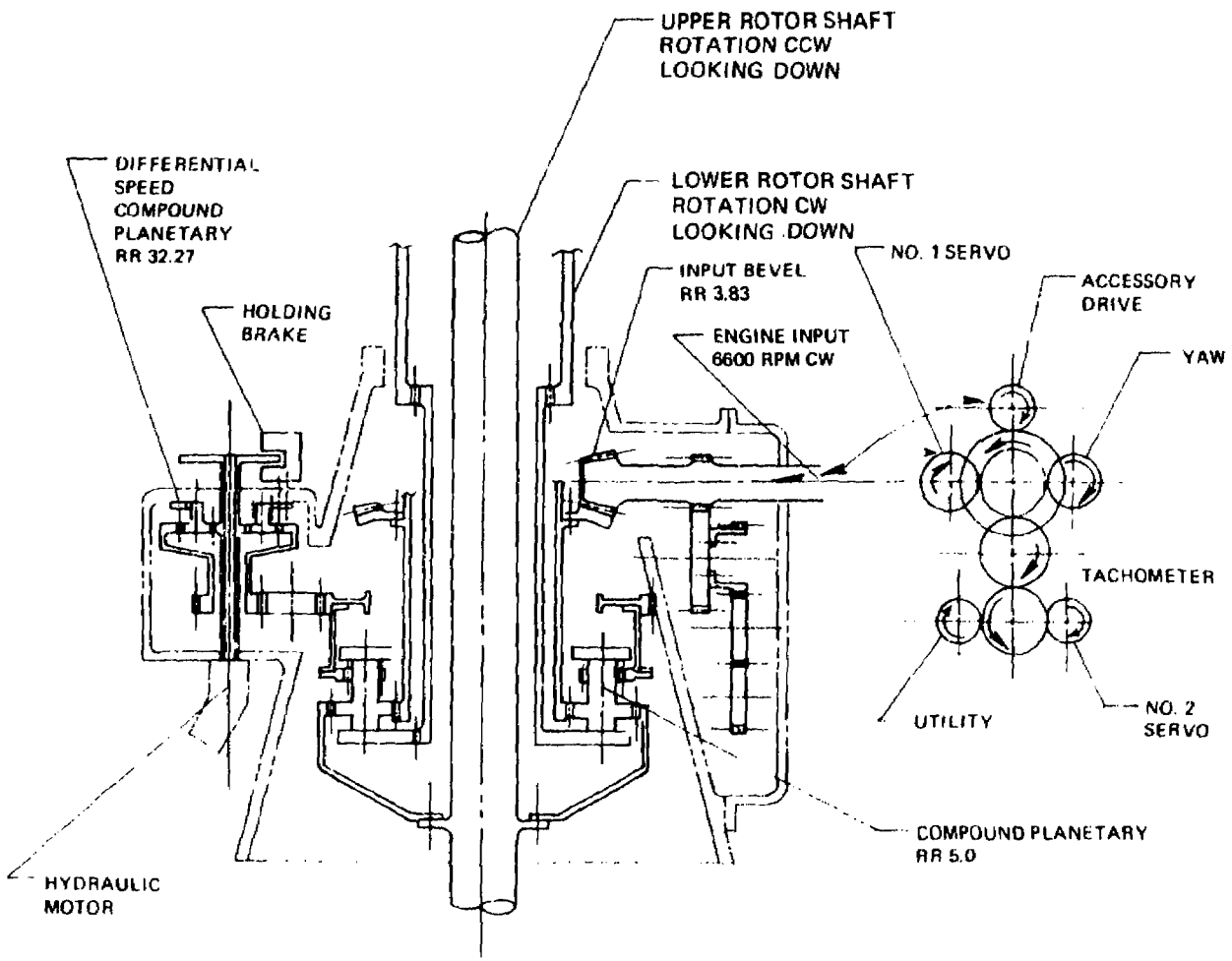

Figure 10. Drive Train Schematic.

TABLE 3. ABC MAIN GEARBOX DESIGN DATA.

Nomenclature	rpm	Gear Design (hp)	Bearing Prorate (hp)
Pinion, input bevel	6600	1500	703
Gear, input bevel	1717.81	1500	703
Sun gear	1717.81	1500	703
Pinion, planetary upper & lower gears	2748.49	1500/750	703
Ring gear, driving	343.56	750	-

From the lubrication pump oil flows through a filter to the oil cooler located with the engine cooling package aft of the main gearbox. A redundant oil filter monitored by a dual indicating system is provided. Cooled oil flows from the oil cooler to the main gearbox. Indicators monitor the pressure and temperature of the oil entering the gearbox, and displays this information on the instrument panel and the advisory caution panel in the cockpit center console. Integrally cored lube lines distribute the oil to the gears and bearings via strategically located oil jets. A screened magnetic chip detector and a temperature bulb monitor oil condition and temperature, respectively, before it reaches the lubrication pump. A low pressure switch located near the last jet and connected to the caution panel warns of a pressure loss between the gearbox oil inlet and the last oil jet in the gearbox.

The differential yaw control power train located at the forward end of the main gearbox transmits power from the yaw control hydraulic motor (when installed) to the upper planetary ring gear in the main gearbox at a reduction ratio of 125:1. This power train consists of a 3.87:1 reduction ratio spur set and a 32.275:1 compound planetary reduction set. Complete provisions permit main gearbox operation either with or without the differential control power train installed in the main gearbox. At no time during the flight test program was the differential yaw control power train installed. All yaw control was derived from either differential rotor collective, which produces differential rotor torque, or from rudders or a combination of these two.

FLIGHT CONTROLS

The XH-59A flight control system is a type III system as defined by MIL-F-18372 and conforms to MIL-F-18372, MIL-F-9490 and MIL-S-8698. It consists of conventional helicopter cockpit controls, stationary and rotating mechanical control linkage systems, dual hydraulic power boost systems, a dual-channel SAS, and an electrically operated differential trim system. With the exception of the rudder controls, the flight control system is irreversible through rotor and elevator hydraulic control servos. In the test configuration, the elevator was locked or powered by the servo of the elevator/collective coupling system. Rudders are controlled through direct mechanical linkage, and control forces are reversible with respect to hinge moments and modifiable by ground adjusted geared trim tab settings. Figure 11 presents a schematic of the XH-59A flight control system.

The pilot's and copilot's manual flight controls are mechanically interconnected, operate in unison, and consist of dual cyclic control sticks, collective pitch levers, and directional control pedals. The upper and lower rotors share cockpit control inputs. Collective pitch lever movement controls rotor system total thrust by simultaneously increasing or decreasing the pitch of each rotor blade. Longitudinal and lateral cyclic controls aircraft pitching and rolling motion by cyclically varying rotor blade pitch and generating control moments. Directional control pedal movement controls aircraft yawing motion by deflecting dual rudders and by controlling interrotor differential collective pitch, producing a resultant torque about the rotor mast. Flight control position indicators are provided on the cockpit instrument panel for longitudinal and lateral cyclic, collective, and directional control pedal.

Control Definitions, Conventions, and Equations

a. Flight control system conventions are as follows:

(1) Subscripts U and L denote upper and lower rotor parameters, respectively.

(2) Rotor plane relative azimuth (ψ) is 0 degree along the reference aligned with the longitudinal axis extending from the rotor hub over the tail and positive in the direction of rotor rotation (clockwise for lower rotor, counterclockwise for upper rotor from planform view).

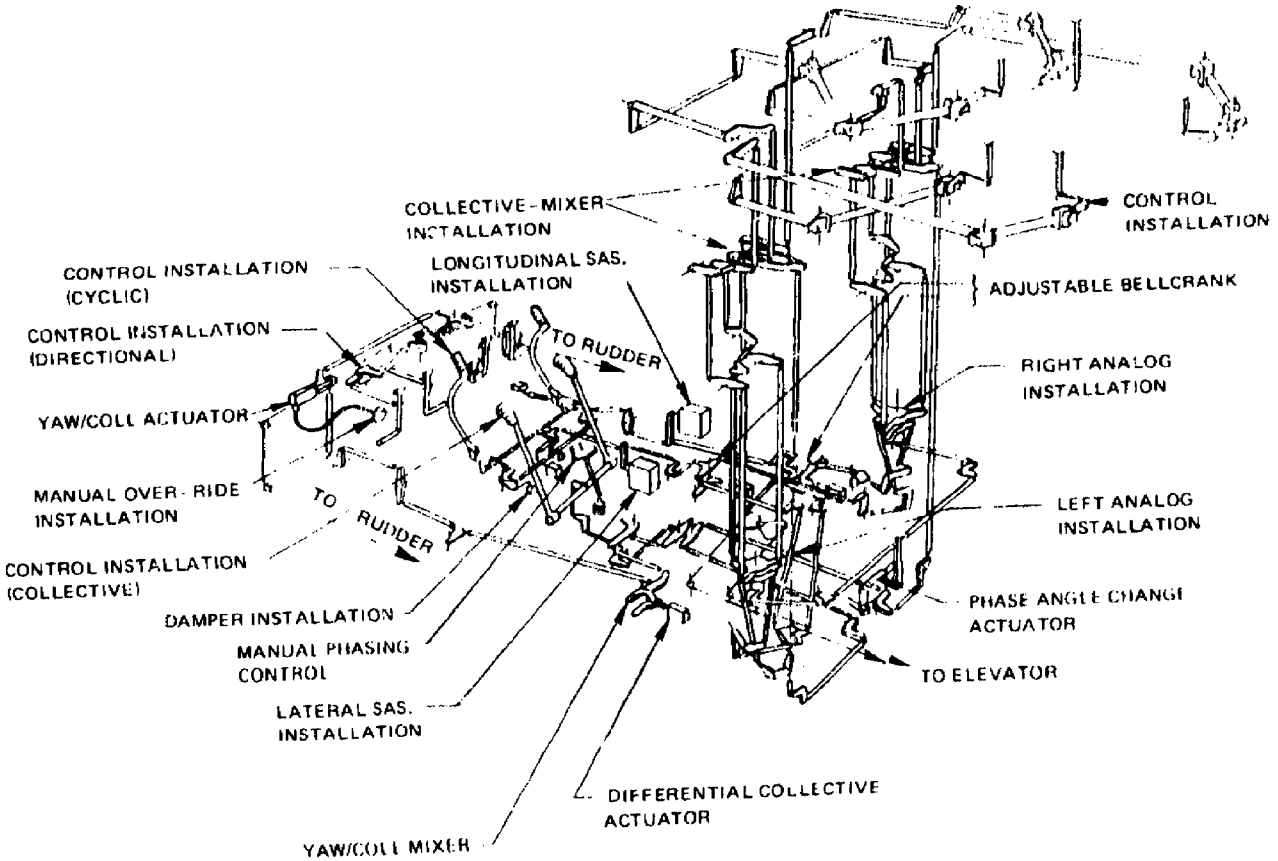

Figure 11. Control System.

(3) A_1 and B_1 are referenced to individual rotor, i.e.:

$+A_1$ = Increased blade pitch in forward blade azimuth quadrants.

$+B_1$ = Increased blade pitch angle, retreating side.

(4) Γ is measured as the number of degrees cyclic control motion is introduced before the blade reaches the respective axis, e.g.:

$-A_1$ with Γ = 40 deg results in blade feathering at ψ = 320 deg

b. Flight control system angle definitions are as follows:

(1) Longitudinal cyclic: $A_1 = \frac{A_{1U} + A_{1L}}{2}$

(2) Lateral cyclic: $B_1 = \frac{B_{1U} - B_{1L}}{2}$

(3) Collective: $\theta_o = \frac{\theta_{oU} + \theta_{oL}}{2}$

(4) Differential longitudinal cyclic: $A_1' = \frac{A_{1U} - A_{1L}}{2}$

(5) Differential lateral cyclic: $B_1' = \frac{B_{1U} + B_{1L}}{2}$

(6) Differential collective: (low speed yaw control) $\Delta\theta_o = \frac{\theta_{oU} - \theta_{oL}}{2}$

(7) Differential collective trim: $\Delta\theta_t = \frac{\theta_{oU} - \theta_{oL}}{2}$

c. Control equations for the rotor system are as follows:

(1) Blade pitch on the upper rotor is

$$\theta_U = [\theta_o + \Delta\theta_o] - [A_1 + A_1'] \cos(\psi_U + \Gamma) - [B_1 + B_1'] \sin(\psi_U + \Gamma)$$

(2) Blade pitch on the lower rotor is

$$\theta_L = [\theta_o - \Delta\theta_o] - [A_1 - A_1'] \cos(\psi_L + \Gamma) - [B_1 + B_1'] \sin(\psi_L + \Gamma)$$

Trim Systems

Longitudinal and lateral cyclic stick force trim is provided for both pilot and copilot via magnetic brake devices in the longitudinal and lateral cyclic control linkages. Differential trim controls are provided to investigate rotor lift sharing and rotor moment distributions. Electric beeping is provided for differential longitudinal (A_1') and lateral (B_1') cyclic and differential collective ($\Delta\theta_t$) trim control. A control box with individual beeper switches and trim indicators for each axis is mounted on the right side of the cockpit center console. In-flight adjustable trim tabs are provided on one rudder and the elevator. Rudder and elevator also incorporate geared trim tabs with ground adjustable ratios of 0.5, 0.75, and 1.0.

Variable Cyclic Control Phase

Because of the high stiffness of the ABC rotor blade, the azimuth at which cyclic pitch must be applied to produce a specific moment output is different from the input azimuth required for the articulated rotor. For the articulated rotor, the cyclic input must be made 80 to 90 degrees in advance of the point where a maximum flapping is desired. For an infinitely stiff rotor, the advance required is essentially zero. For the ABC rotor, the cyclic pitch input must be applied 30 to 40 degrees in advance of the desired moment output (Figure 12). The angle involved in this azimuth shift is defined as the phase angle, Γ, and is considered positive when rotated opposite to the direction of rotor rotation. For example, if a control system phasing angle of $\Gamma = 30°$ is selected, then longitudinal stick will result in maximum cyclic pitch inputs on the blades at rotor azimuths of 150° and 330°. Likewise, lateral stick input will produce maximum cyclic pitch inputs at rotor azimuths of 60° and 240°. Figure 13 illustrates this control system geometry. The optimum value of Γ is actually selected on the basis of several considerations including rotor trim characteristics, rotor performance, and interrotor moment magnitudes in unaccelerated and maneuvering flight.

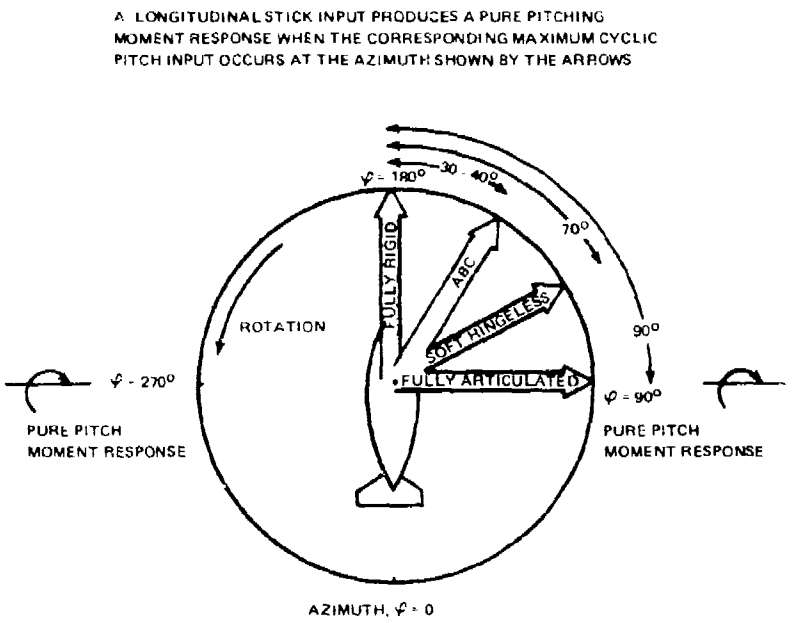

Figure 12. Rotor System Response to Cyclic Control Inputs.

The phase angle is controllable through a range of 0 to 70 degrees through an analog swashplate in the stationary control system (Figure 14). Analog swashplate position is controlled by pilot and copilot beeper switches and a cockpit backup mechanical crank.

Differential Collective Directional Control Washout

Differential collective directional control is washed out between 40 and 80 knots and reintroduced when decelerating from 80 to 40 knots. Pitot sensing of dynamic pressure (q) is converted to an electrical signal that acts to linearly couple/decouple the directional control pedals from the differential collective linkage.

Elevator/Collective Coupling

In order to reduce or avoid rotor shaft damage during high rates of descent the elevator was coupled to the collective stick so that full down collective caused the elevator to deflect 13.9 degrees trailing edge up. This reduced the aircraft pitching moment that had to be balanced by the rotors.

ABC ROTOR SYSTEM ($\Gamma = 30^{o}$ ILLUSTRATED)

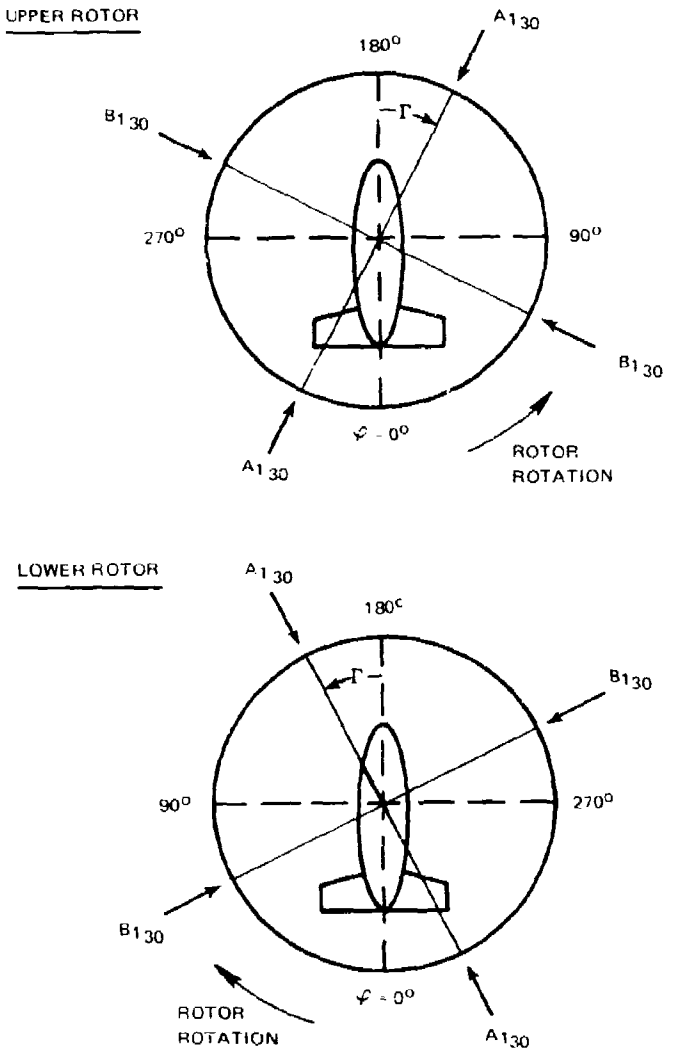

$A_{1\Gamma}$ IS DEFINED AS THE CYCLIC PITCH THAT IS GENERATED BY THE LONGITUDINAL STICK

$B_{1\Gamma}$ IS DEFINED AS THE CYCLIC PITCH THAT IS GENERATED BY THE LATERAL STICK

Figure 13. Rotor Control System Definitions.

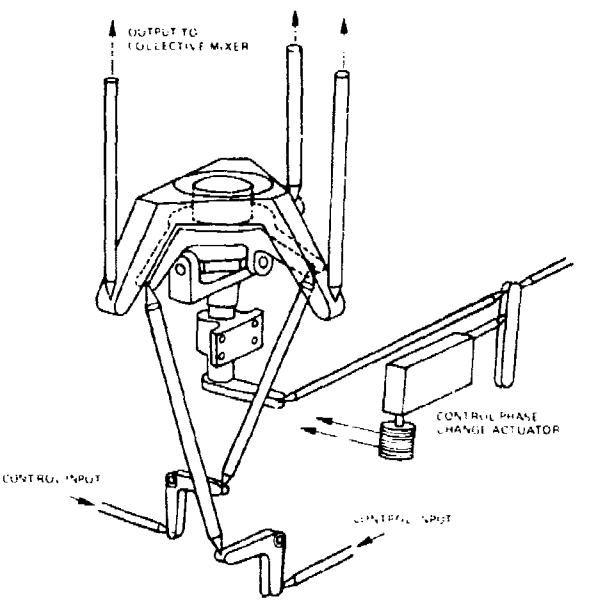

Figure 14. Analog Swashplate.

The coupling was achieved mechanically by the use of a spring strut inserted between the collective system at the directional mixer and the elevator quadrant located in the tub. The spring strut detent was 43 pounds, which required a 15-pound stick force to break-out in the event of a jam condition in the elevator system.

The control cable connected to a single-stage S-61 primary servo adapted for installation in the tail cone of the aircraft. The single-stage servo was connected to the first-stage hydraulic system through a solenoid operated control valve. The operating pressure was reduced to 1500 psi.

During flights with auxiliary propulsion, the elevator/collective coupling was disconnected and the elevator was flown in a locked position.

Servos and Stationary Swashplates

Two sets of linkage components are employed to transfer control motions from the stationary controls to rotating controls for each rotor. Each set consists of three dual hydraulic servos, stationary swashplates, bearings, sleeves, and antidrive (scissors) links. The lower rotor swashplate is mounted above the transmission. The upper rotor swashplate is mounted beneath the transmission in axial alignment with the

rotor mast. The six dual hydraulic servos are attached to the transmission. The output shafts of the three lower rotor servos extend upward to attachment points on the lower rotor stationary swashplate. The output shafts of the three upper rotor servos extend downward to attachment points on the upper rotor stationary swashplate. Two transfer networks comprised of levers, pushrods, torsion tubes, and universal joints (Figure 11) are employed to transfer collective/cyclic composite control motions from the collective mixers to input levers on each dual hydraulic servo. The dual hydraulic servos convert collective and cyclic control motion to stationary swashplate translation and tilt. The servos act in series with the stationary linkage to reduce cockpit control forces and to prevent control force feedback from rotor aerodynamic and vibratory loads.

Primary Servo Actuator

The hydraulic primary servo is unconventional in design and construction, the design philosophy being to mount the housing rigidly on the gearbox, and thus eliminate flexible lines and their associated failure modes.

Figure 15 shows a sectional view of the servo. Stages 1 and 2 are completely separated so that no crack propogation from one unit to the other can occur. Two separate cyclinder housings are bolted together and are provided with attachment flanges for installation on the gearbox. The housings contain one power cylinder and two fluid transfer cylinders. Pressure and return ports are connected to the fluid transfer ports by drilled passages.

The output piston of each stage is mounted on the valve housing. Drilled passages in the piston rod connect the piston head to the valve housing. Drilled passages in the two transfer tubes, one for pressure and one for return, connect the cylinder housing to the valve housing. The configuration is such that the valve housing, power piston rod, and transfer tubes move in unison. The valve housings are completely separated, as are the cylinder housings.

The control valves are of jam-proof design and consist of two spools, the inner spool being spring loaded relative to the outer spool. In normal operation both spools move together and distribute fluid through connected porting. In the event that the normal, outer spool parts are jammed, the inner spool moves against the spring force and distributes fluid through the bypass ports, thus removing system pressure from the power piston. The bypass porting is connected to a sensing unit which activates a cockpit warning light.

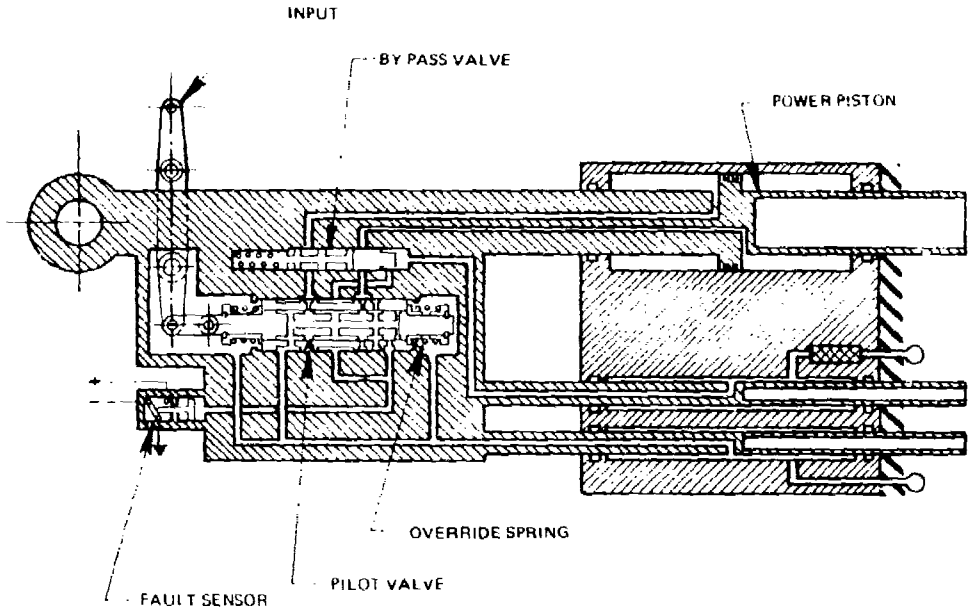

Figure 15. Schematic of Primary Servo.

The separate adjustable valve operating arms are mounted on a common shaft that is connected to the control system.

Servo Input Mechanism

The lever pushrod, torsion tube, and universal joint transfer networks are special design features that permit the use of vibration isolators for soft-mounting the transmission in the airframe lateral axis. (The transmission is hard-mounted to the airframe in the present configuration.) The transfer networks orient linkage connections to the hydraulic servos so that transmission lateral floating motion in future soft-mount configurations will not induce spurious flight control inputs.

Rotating Flight Controls

The rotating flight control linkages for each rotor consist of a rotating swashplate, bearing, and sleeve; a drive link; three pitch change rods; and trailing-edge pitch horns. The rotating swashplates transfer cyclic tilt and collective translation of the stationary swashplates to vertical motion in the pitch change rods. The pitch change rod motion rotates the blade pitch horns and feathers the rotor blades about feather bearings in the blade sleeves. The rotating controls

for the lower rotor are of conventional design and orientation. The swashplate assembly is mounted above the main transmission and displaces externally mounted pitch change rods connected to external pitch horns on the lower rotor blades. The rotating controls for the upper rotor are designed to route pitch change rods through the center of the coaxial rotor mast between the rotating swashplate beneath the main transmission to upper rotor blade pitch horns that are enclosed within the upper mast.

STABILITY AUGMENTATION SYSTEM

Rate damping stability augmentation is provided by the SAS in the longitudinal and lateral control axes. Figures 16 and 17 are functional block diagrams of the pitch and roll SAS channels, respectively. Dual, independent signal paths are provided in each SAS channel. Each path independently senses rate with a rate gyro and routes gyro signals through filter and shaping networks to a servo amplifier. At the input of each amplifier, summers combine trim, gyro rate, hardover test, and derived feedback inputs. The output of each amplifier is applied to an electric actuator which operates one-half of the two-stage hydraulic SAS servo. The output of each servo stage represents a 5% control authority for a total of 10% control authority in each axis. A cockpit hover indicator is used to present SAS servo position for both halves of each channel. Cockpit control panels are provided for SAS gain adjustment and selecting or deselecting SAS channels.

AIRFRAME

The airframe is of conventional semimonocoque construction. The primary structure is 7075 aluminum alloy except for magnesium cockpit skins, tail cone skins, and stabilizer leading edges. The firewall decks are titanium.

The main transmission is mounted on four canted fittings positioned radially about the gearbox. Their load lines intersect at a common point on the gearbox centerline. Each fitting is attached to the transmission via a single 1-inch bolt. Vertical side and drag components are reacted as axial loads in the bolts. Yaw moments are carried by bolt shear forces.

The airframe support structure consists of two fore and aft box beams, symmetrical about B.L. 0, which extend between bulkheads at F.S. 277.0 and F.S. 319.0. The upper web of the beam is at W.L. 152.0 and extends from B.L. 19.7 to the fuselage outer skin. The lower webs are part of the fuel cell deck at W.L. 132.0. The outer webs are formed by the fuselage

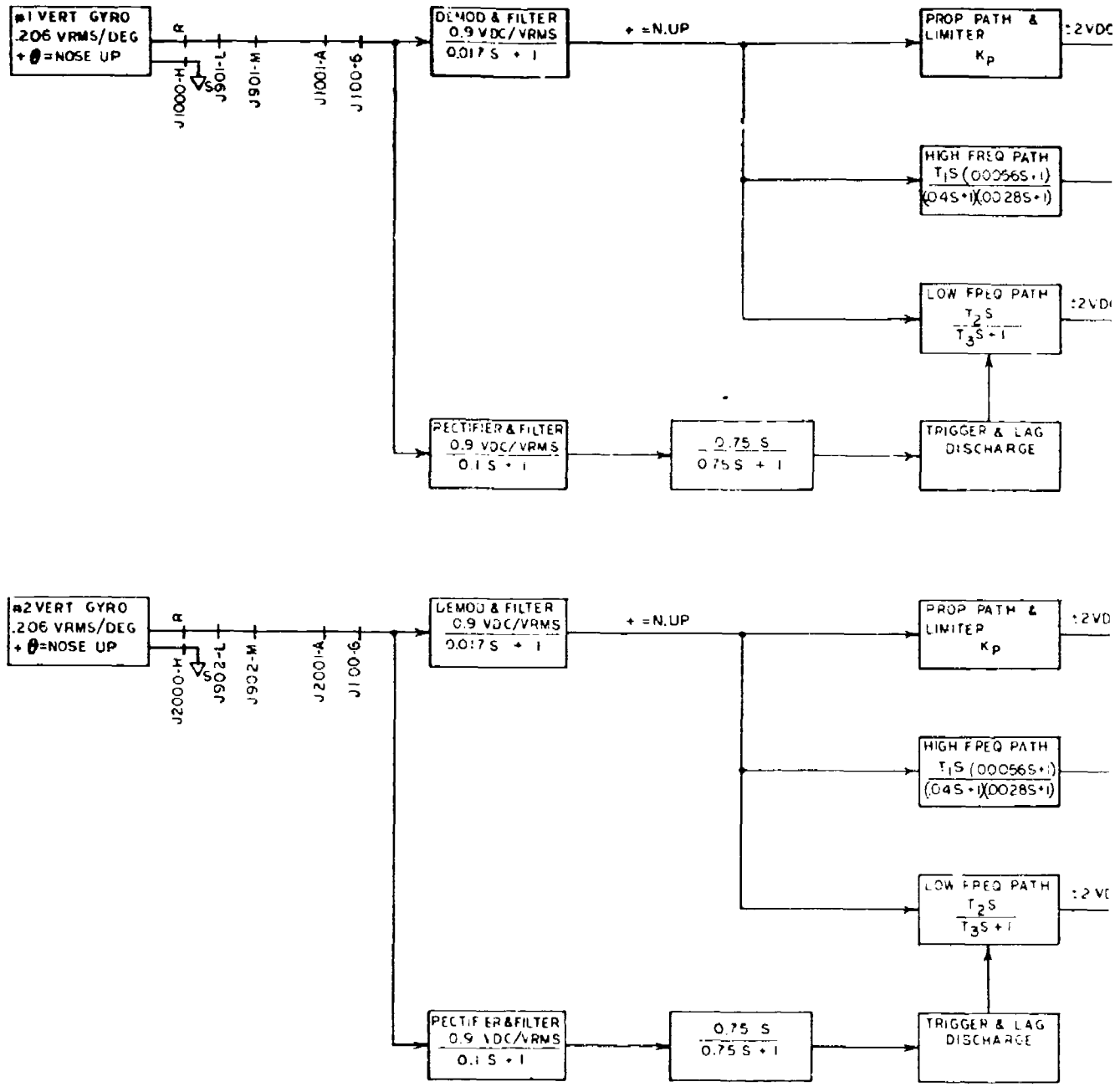

Figure 16. Pitch Dual SAS.

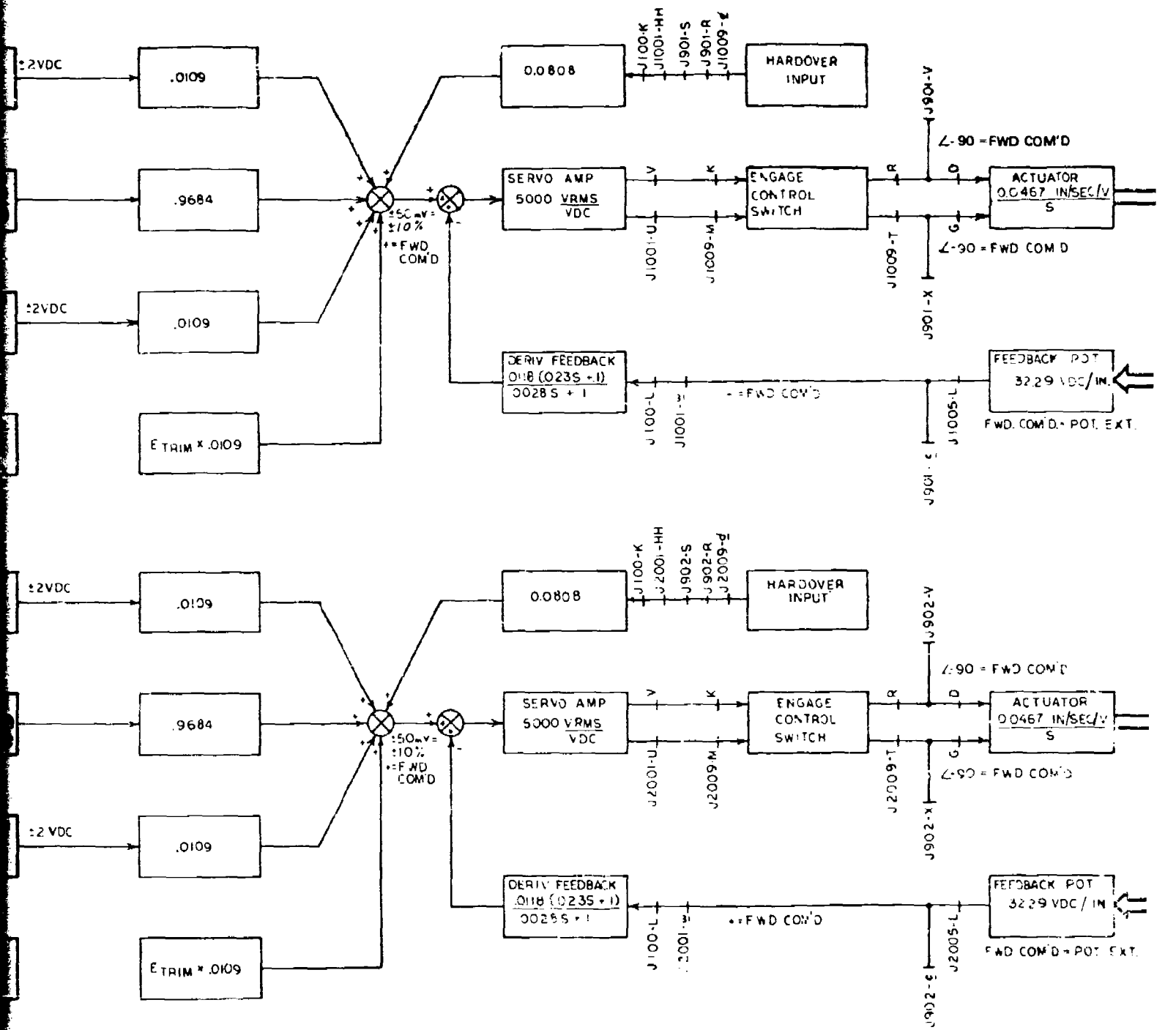
±2VDC
.0109
.9684
±2VDC
.0109
E TRIM x .0109
±50mV = ±10% +=FWD COM'D
0.0808
J100-K
J1001-HH
J901-S
J901-R
J1009-f
HARDOVER INPUT
SERVO AMP 5000 VRMS/VDC
V
K
J1001-U
J1009-M
ENGAGE CONTROL SWITCH
R
D
G
J1009-T
J901-V
∠-90 = FWD COM'D
ACTUATOR 0.0467 IN/SEC/V/S
∠-90 = FWD COM'D
J901-X
DERIV FEEDBACK .0118 (.023S + 1) / .0028S + 1
J100-L
J1001-M
+=FWD COM'D
J1005-L
FEEDBACK POT 32.29 VDC/IN.
FWD. COM'D. = POT. EXT.
±2VDC
.0109
.9684
±2 VDC
.0109
E TRIM x .0109
±50mV = ±10% +=FWD COM'D
0.0808
J100-K
J2001-HH
J902-S
J902-R
J2009-d
HARDOVER INPUT
SERVO AMP 5000 VRMS/VDC
V
K
J2001-U
J2009-M
ENGAGE CONTROL SWITCH
R
D
G
J2009-T
J902-V
∠-90 = FWD COM'D
ACTUATOR 0.0467 IN/SEC/V/S
∠-90 = FWD COM'D
J902-X
DERIV FEEDBACK .0118 (.023S + 1) / .0028S + 1
J100-L
J2001-M
+=FWD COM'D
J2005-L
FEEDBACK POT 32.29 VDC/IN.
FWD COM'D = POT. EXT.

1 7

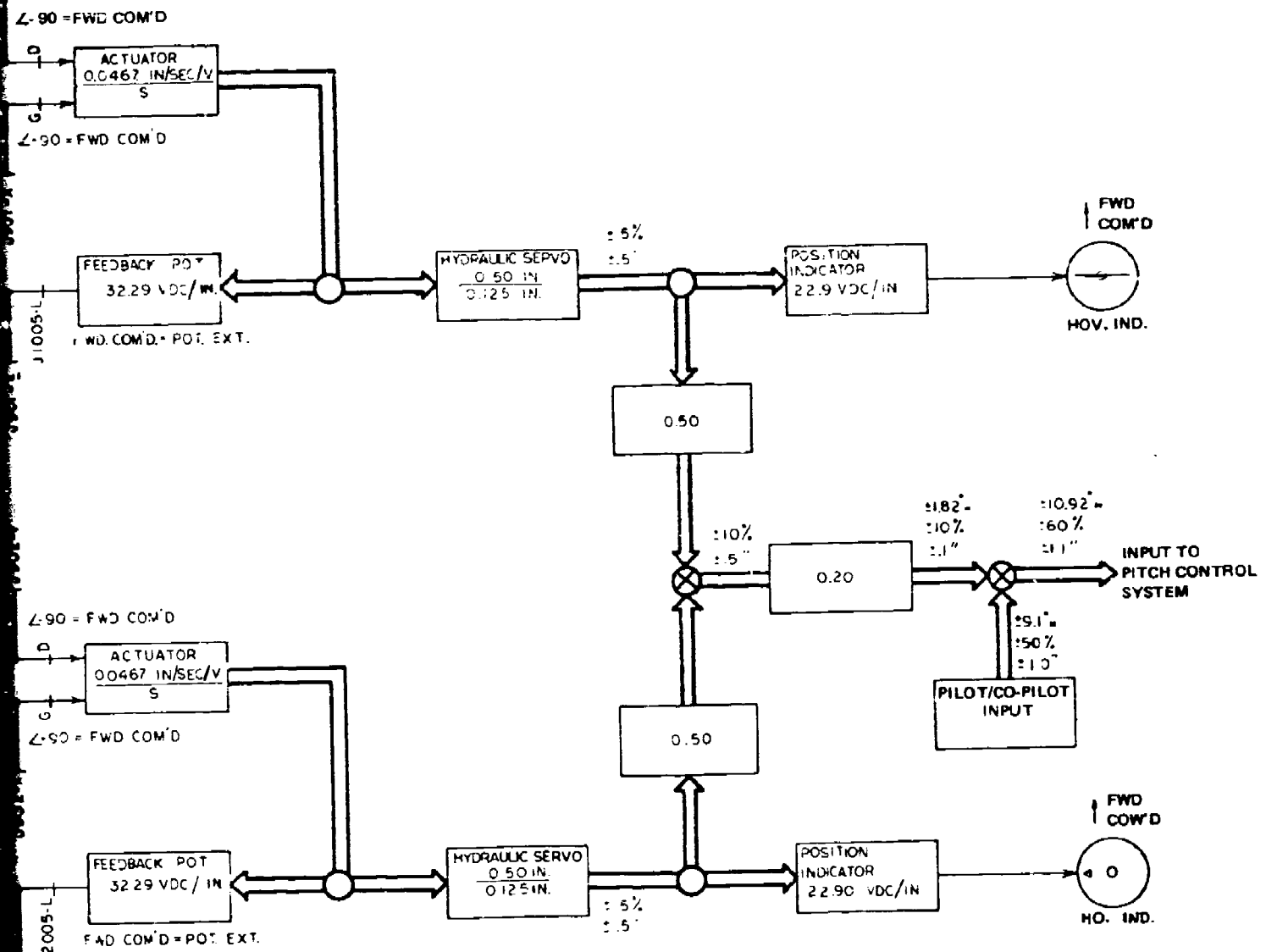
∠-90 =FWD COM'D
D
G
ACTUATOR
0.0467 IN/SEC/V
S
∠-90 = FWD COM'D
FEEDBACK POT
32.29 VDC/IN.
J1005-L
FWD. COM'D. = POT. EXT.
HYDRAULIC SERVO
0.50 IN.
0.125 IN.
±5%
±.5°
POSITION INDICATOR
22.9 VDC/IN
FWD COM'D
HOV. IND.
0.50
±10%
±.5"
0.20
±1.82°
±10%
±.1"
±10.92°
±60%
±.1"
INPUT TO PITCH CONTROL SYSTEM
±9.1°
±50%
±1.0"
PILOT/CO-PILOT INPUT
∠-90 = FWD COM'D
D
G
ACTUATOR
0.0467 IN/SEC/V
S
∠-90 = FWD COM'D
0.50
FEEDBACK POT
32.29 VDC/IN.
J2005-L
FAD COM'D = POT. EXT.
HYDRAULIC SERVO
0.50 IN.
0.125 IN.
±5%
±.5°
POSITION INDICATOR
22.90 VDC/IN
FWD COM'D
HO. IND.

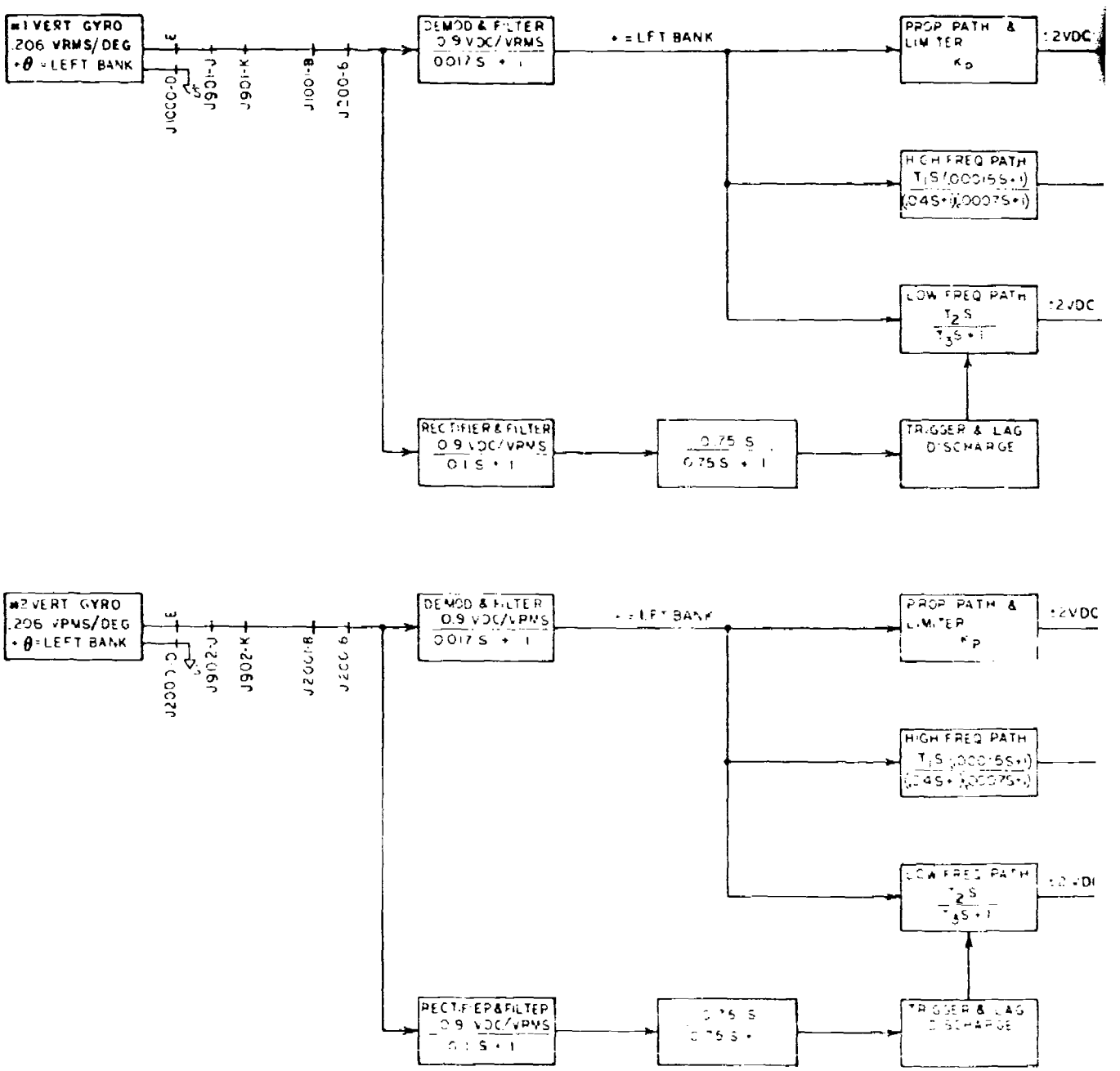

Figure 17. Roll Dual SAS.

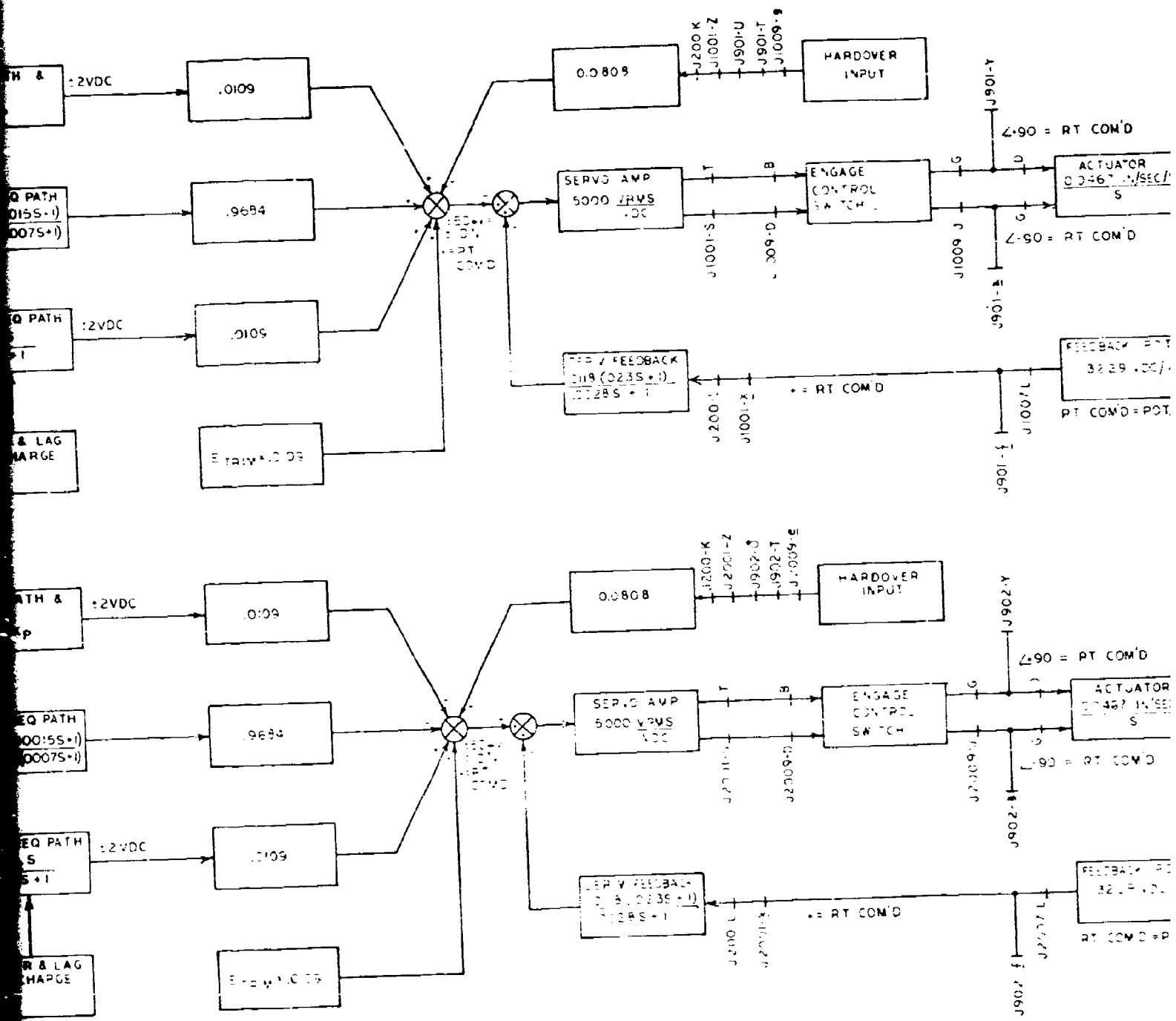
±2VDC
.0109
.9684
±2VDC
.0109
0.0809
HARDOVER INPUT
SERVO AMP
5000 V/RMS
.DC
ENGAGE CONTROL SWITCH
ACTUATOR
S
∠-90 = RT COM'D
∠-90 = RT COM'D
= RT COM'D
RT COM'D = POT.
±2VDC
.0109
.9684
±2VDC
.0109
0.0808
HARDOVER INPUT
SERVO AMP
5000 V/RMS
.DC
ENGAGE CONTROL SWITCH
ACTUATOR
S
∠-90 = RT COM'D
∠-90 = RT COM'D
= RT COM'D

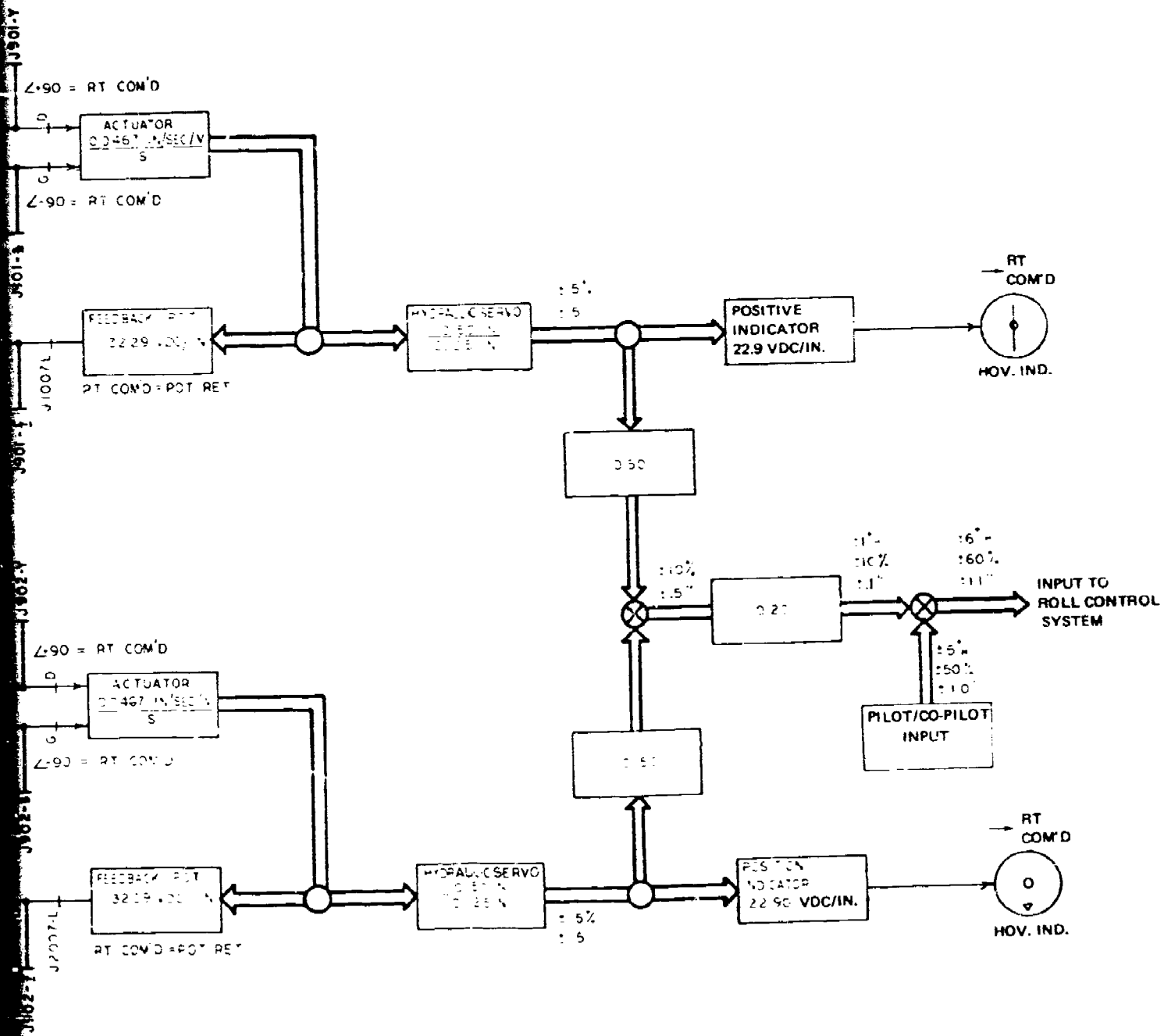
∠+90 = RT COM'D
ACTUATOR
∠-90 = RT COM'D
RT COM'D = POT RET
POSITIVE INDICATOR 22.9 VDC/IN.
RT COM'D
HOV. IND.
INPUT TO ROLL CONTROL SYSTEM
PILOT/CO-PILOT INPUT
∠+90 = RT COM'D
∠-90 = RT COM'D
RT COM'D = POT RET
RT COM'D
HOV. IND.

3

side skins between W.L. 132.0 and W.L. 158.0, and the boxes are closed by webs which are sloped to pick up the transmission attachment fittings. Four canted bulkheads inside the box beams are also attached to the fittings and provide a redundant load path for the gearbox loads.

The support structure is critical for crash conditions (20 G fwd, 20 G down and 10 G side). Limit flight loads are approximately 38% of these and may be transferred through either of the redundant paths.

The aircraft inboard profile is shown in Figure 18. Figure 19 shows the detail structural arrangement.

Conversion to the auxiliary propulsion configuration required two major structural modifications. One was attachment of the J-60 nacelles to the aircraft, and is accomplished through two major fittings at fuselage stations 264 and 277. Stabilizing fittings are located at stations 251.1 and 380. Engine loads are introduced to the aircraft structure through the main fittings. Airframe structural reinforcements were incorporated at fuselage stations 255.5, 277 and 300.23 to accept auxiliary engine flight loads (Figure 20).

Second was installation of a fitting adapter to decrease horizontal tail incidence from +10 deg (trailing edge down) to -5 deg (trailing edge up) and associated modification of the tail fairing. In addition, external straps were installed on the tail cone and tail cone/aft fuselage interface to accommodate the higher auxiliary propulsion tail loads.

ALIGHTING GEAR SYSTEM

The ABC has a tricycle air/oil retractable landing gear. The gear is designed for 60 knots at 8 ft/sec at 9000 lb gross weight and 6 ft/sec at 11,100 lb gross weight with 2/3 rotor lift as per Specification MIL-S-8698.

The main gear oleo has a full stroke of 10-in. and is designed to never exceed 3000 psi during its working range. The metering pin and air volume configurations were determined during drop test at Ozone Corp., Ozone Park, Long Island. Wheel and tire size is 18 x 5.5.

The nose wheel is a dual wheel with a 10-in. stroke and a mechanical trail of 2.40 in. The metering and air volume configurations were also determined during drop test at Ozone. The only design difference between nose and main gear oleo is that the piston head of the nose gear has a built-in centering cam to center the wheels for landing gear well clearance.

The viscous shimmy damper was supplied by Houdaille to Sikorsky's specifications for the XH-59A and is mounted at the bottom of the cylinder and grounded to the wheels by a scissors.

The landing gear's normal retracting and extending system is hydraulic. This supply is provided from the first-stage system. If this system fails, an emergency blow-down system is available. The braking system is a self-contained hydraulic system with master piston mounted on the pilot's pedals.

PROPULSION SYSTEM

Lift Engines

The lift engine consists of a production model Pratt & Whitney PT6T-3 twin power section ("Twinpack") turboshaft power plant with minor modifications for the XH-59A application. A detailed description of the PT6T-3 power plant may be found in Reference 2. The PT6T-3 power plant is hard-mounted to the XH-59A airframe aft of the main transmission between STA 345 and STA 384 at W.L. 159 (Figure 18). The power plant's integral combining gearbox combines the output of each power section and provides an output to the main transmission at 6,600 rpm (100%). The PT6T-3 twin power section ratings are: intermediate 1726 shp and maximum continuous 1452 shp.

The PT6T-3 production fuel controls and mechanical control system have been modified to provide the lower power turbine and ABC rotor system speeds required for high-speed flight in the auxiliary propulsion mode, and to preclude the random electrical control failures encountered during earlier testing in the helicopter phase. The specific modifications incorporated are:

a. The torque balancing unit is disabled.

b. The N_f governors are modified to provide maximum torque in a speed range 105% to 70%.

c. Independent pilot control of each N_f governor is provided to compensate for torque splits that will be encountered with the large power turbine speed changes. The pilot's beep control has also been modified by the incorporation of independent switches on the collective stick that can be actuated simultaneously or independently. Each switch drives one of the electric actuators for speed control. Collective bias is introduced simultaneously to both N_f governors through a torque tube.

d. Switching relays in the beep system electrical circuits were incorporated to preclude random beep switch failures.

2. Specification No. 712B, T400-CP-400 ENGINE SPECIFICATION, Pratt & Whitney of Canada, Ltd.

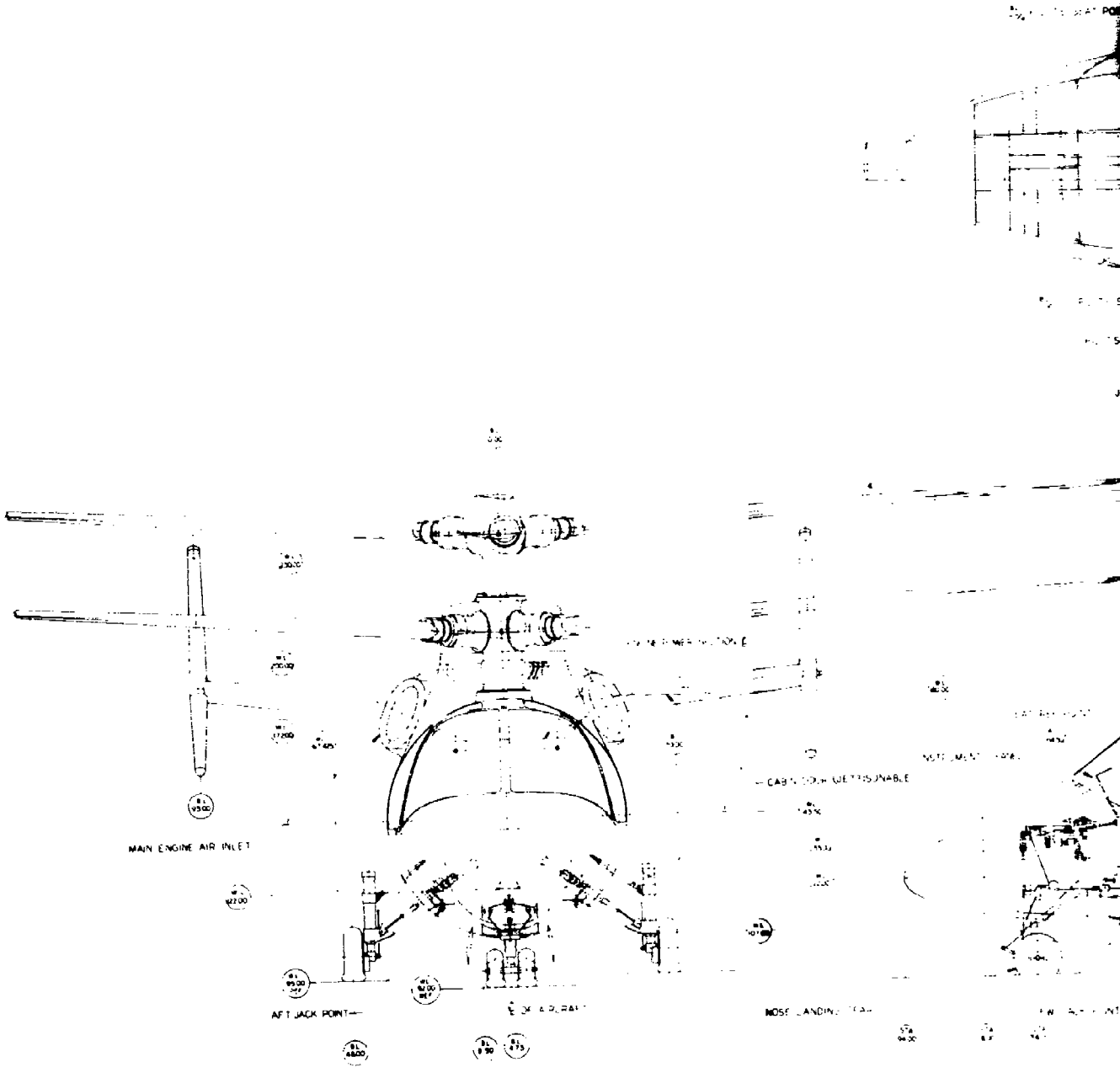

Figure 18. Inboard Profile.

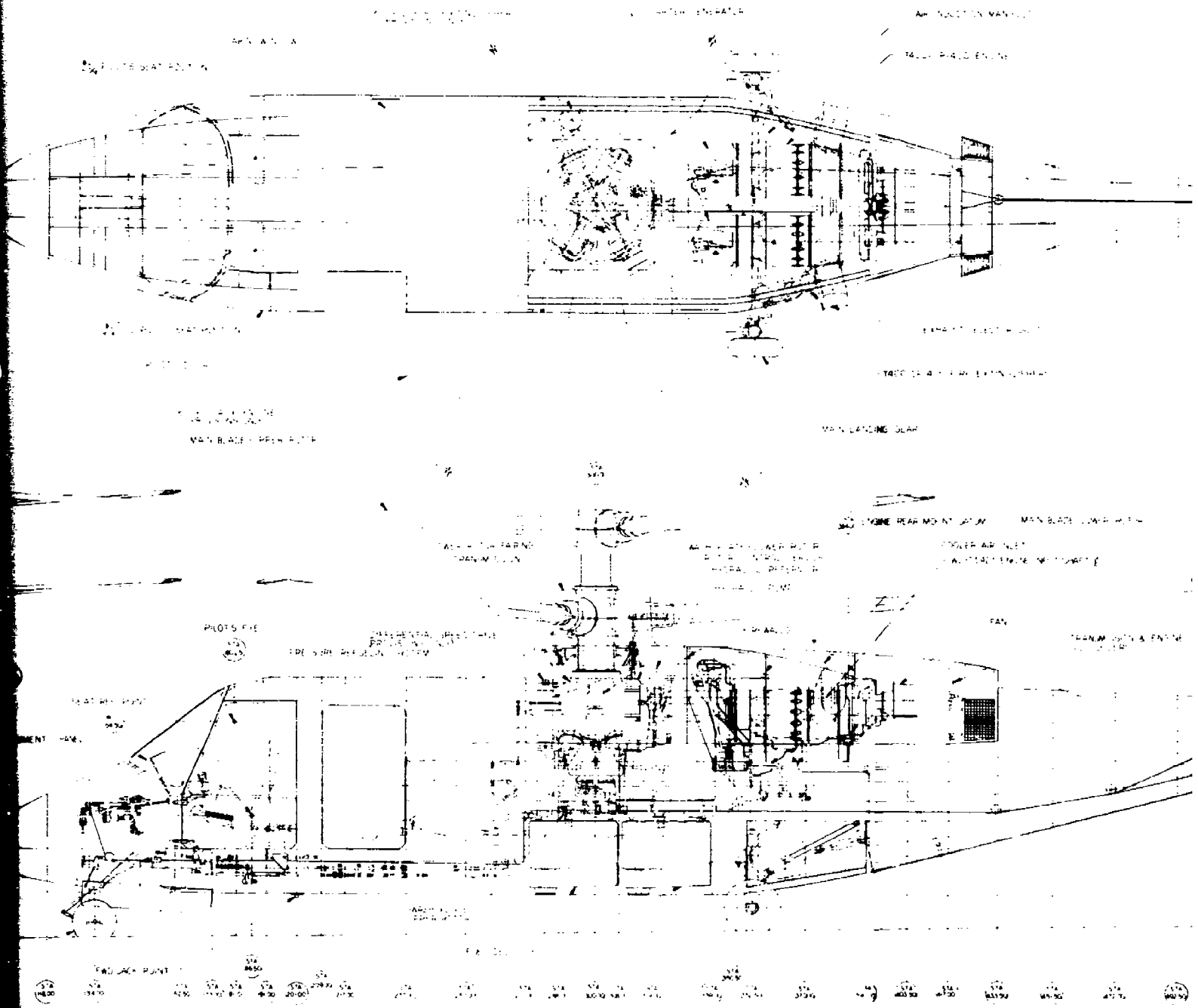
PILOTS FIE
FAN

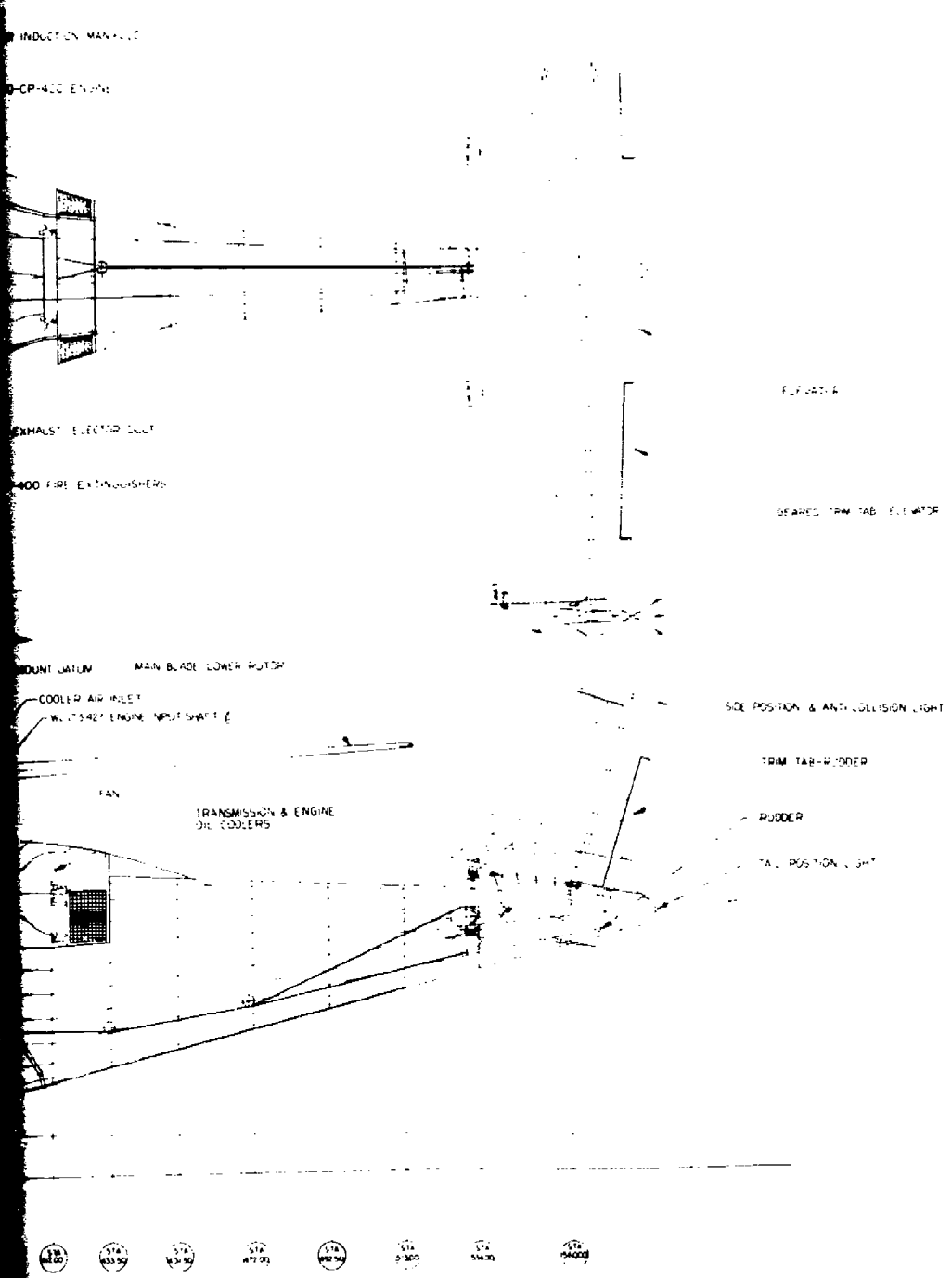
INDUCTION MANIFOLD
CP-420 ENGINE
EXHAUST EJECTOR DUCT
400 FIRE EXTINGUISHERS
ELEVATOR
GEARED TRIM TAB ELEVATOR
MOUNT DATUM
MAIN BLADE LOWER ROTOR
COOLER AIR INLET
W.L. 5427 ENGINE INPUT SHAFT ℄
FAN
TRANSMISSION & ENGINE
OIL COOLERS
SIDE POSITION & ANTI-COLLISION LIGHT
TRIM TAB-RUDDER
RUDDER
TAIL POSITION LIGHT
STA 353.50
STA 434.50
STA 472.00
STA 492.50
STA 514.30
STA 546.00

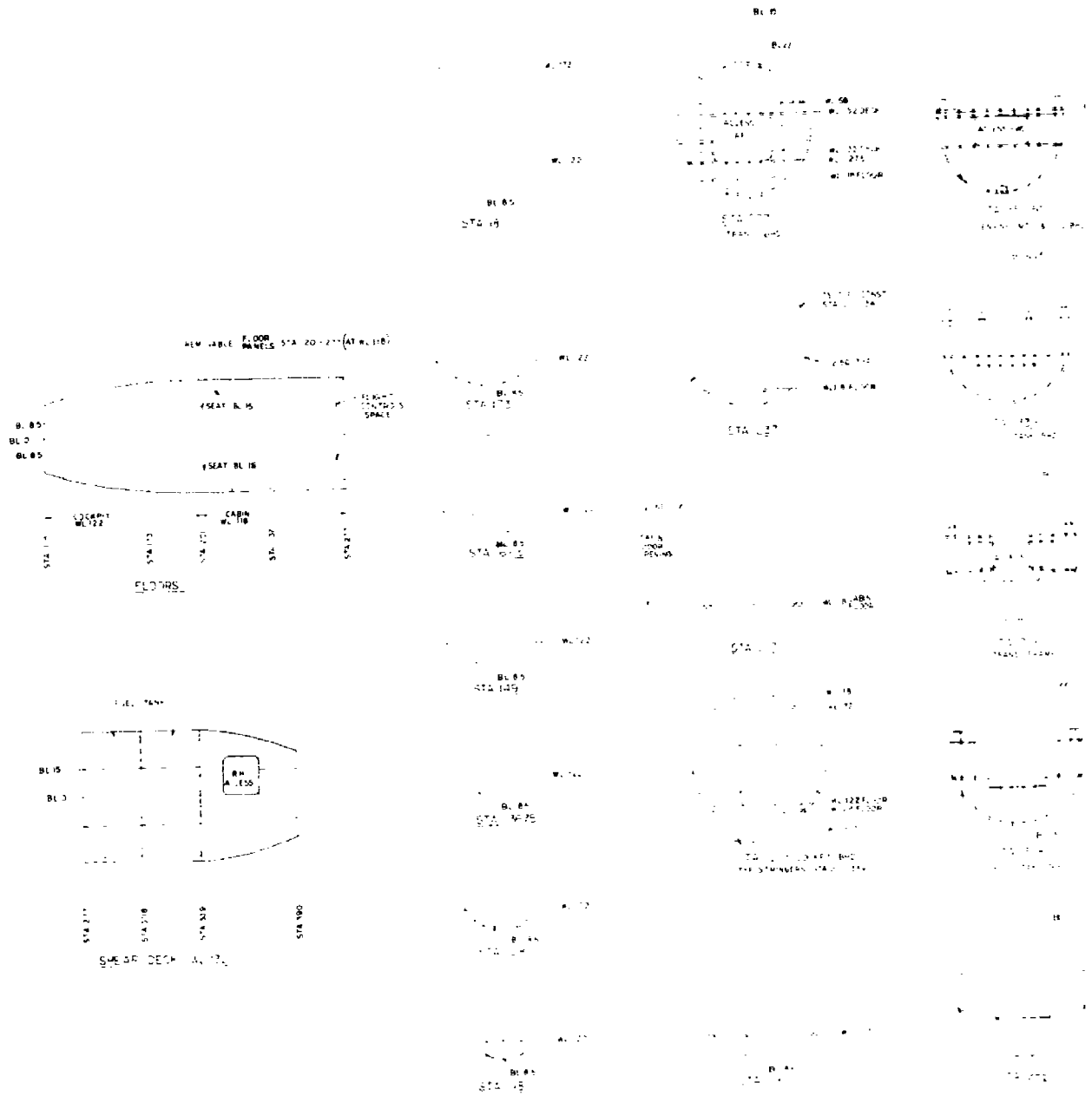

Figure 19. Structural Arrangement.

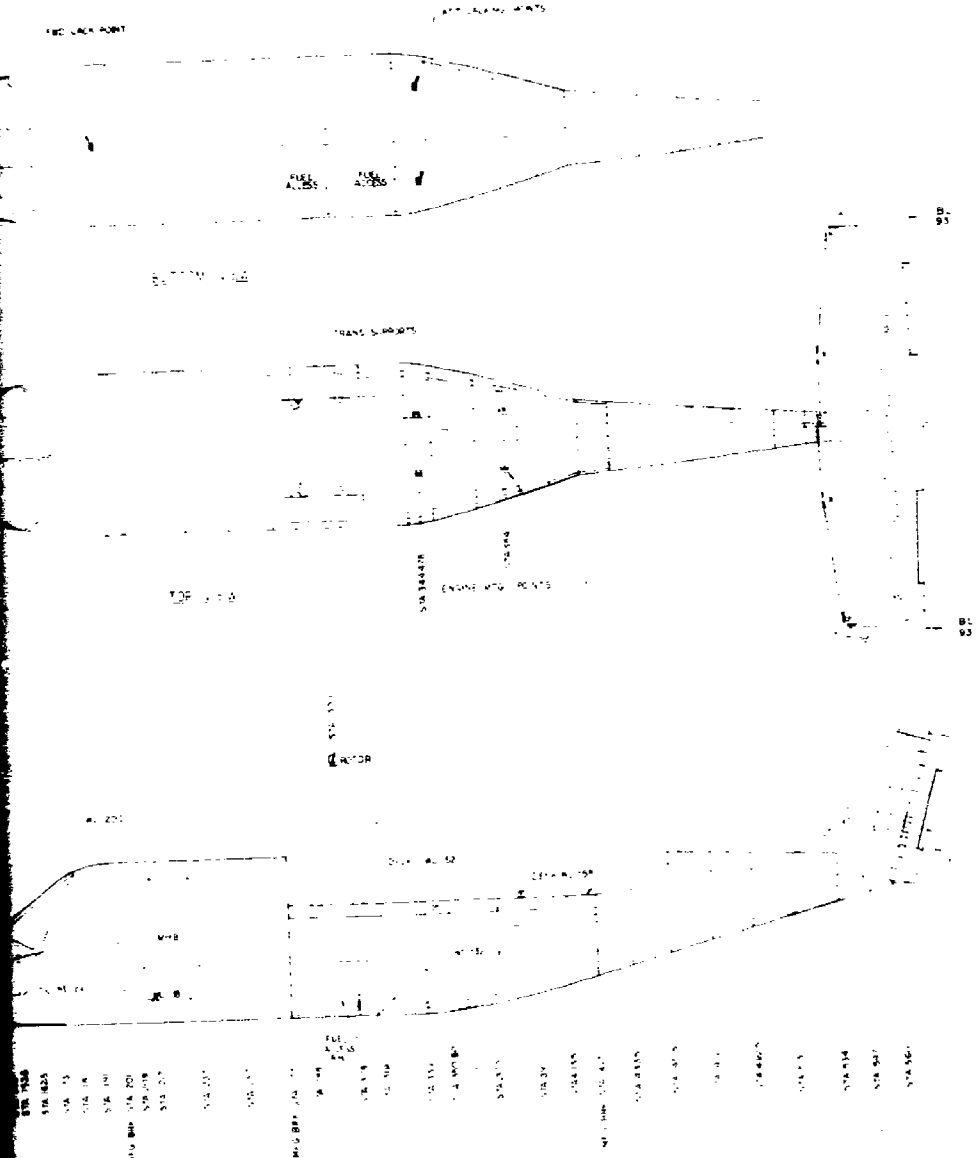

Manual power turbine/rotor speed (N_f/N_r) control is provided by dual speed control levers mounted on the cockpit center console. N_f can be set to govern from 70% to 105% via linkage to the modified fuel controls.

The PT6T-3 start system consists of starter/generators (one mounted on each power section accessory case), individual engine start buttons on the cockpit speed control levers, microswitches in the speed control lever quadrant, and interconnecting relays and wiring to activate fuel valves, ignition circuits, and starters during each power section's start cycle. Starter circuits are powered by 28 vdc from the start bus (Figure 21) with ground electrical power applied, or alternately by the 24v dc battery.

A fire detection system provides warning in the cockpit in the event of fire in either of the PT6T-3 power section compartments. The system consists of four radiation sensing flame detectors - one in each hot section compartment and one in each accessory section. An engine fire extinguishing system is provided for each PT6T-3 power section accessory/hot section compartment. The system consists of two charged containers of liquid dibromodifluoromethane (CF_2BR_2), discharge nozzles, overboard discharge tubes, discharge indicators, pressure gauges, selector valves, and necessary controls. The system provides a two-shot capability which may be directed selectively to either power section or both shots may be directed to a single power section.

10
F

Thrust Engines

The auxiliary propulsion thrust engine installation consists of two Pratt and Whitney J60-P-3A turbojet engines side-mounted in Rockwell International Sabreliner nacelles between STA 264 and STA 277 and aligned with W.L. 145.5. Detailed description of the J60-P-3A engine is contained in Reference 3. The only modification involved for installation on the XH-59A was a reduction in the "stub wing" area between nacelle and fuselage. Each engine provides 3300 lb static thrust at sea level standard day conditions. Engine performance is monitored in the cockpit with tachometers and Engine Pressure Ratio (EPR) gauges which indicate the ratio of total pressure measured at turbine exhaust and compressor inlet face.

3. JT12 INSTALLATION HANDBOOK, Pratt and Whitney Aircraft, 14 April 1966.

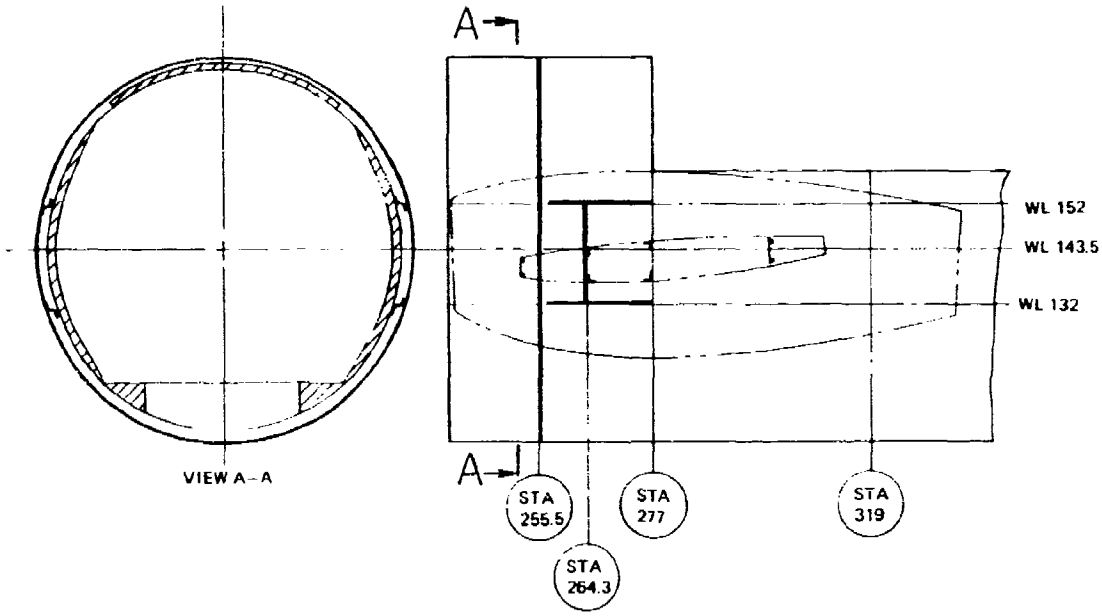

Figure 20. Center Section Detail.

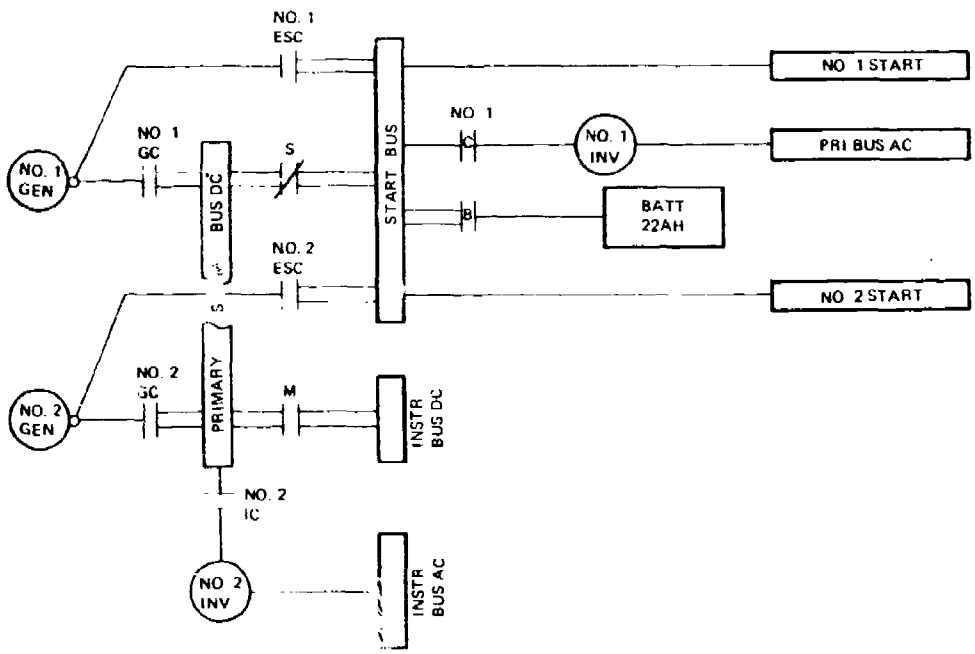

Figure 21. Electrical System.

The J-60 engine control system consists of two tandem twist grips on both the pilot and copilot collective pitch sticks. These grips independently control each engine gas generator. The pilot's twist grips have a positive range selection of stopcock to ground idle and ground idle to maximum power. The copilot's twist grip operating ranges are limited to the control range between ground idle and maximum power. A positive stop is provided between ranges, and detents hold the extreme positions. The twist grip inputs are transmitted coaxially from the top of the collective pitch stick to side-by-side gear tracks at the base of the stick. Flexible push/pull control cables are used to transmit the control inputs individually to the fuel controls in each engine.

The normally furnished starter/generator is replaced by hydraulic starters. Normal start power is furnished by the No. 1 hydraulic system and normal starting sequence is to start J-60 engines subsequent to PT6 start which makes full hydraulic pressure available.

The J-60 fire detection system provides warning in the cockpit in the event of fire in either of the two J-60 engine nacelles. The system consists of continuous wire temperature sensors installed throughout the engine nacelles.

A fire extinguishing system provided for each engine nacelle forward compartment consists of one charged container of liquid dibromodifluoromethane (CF_2BR_2) discharge nozzle, overboard discharge tube, discharge indicator, pressure gauge, selector valve, and necessary controls. The system provides a one-shot capability which may be directed to either engine nacelle as required.

Fuel System

The fuel system is an open-vent type consisting of two tanks, two system strainers, two sump drain valves, two in-line booster pumps, check valves, an electrically operated cross-feed valve, four electrically operated firewall shutoff valves, two float switches, engine filters, fuel flow and fuel quantity indicating systems, and the necessary plumbing lines to convey fuel from the tanks to the engines. The pressure refueling system consists of an adapter, two shutoff valves, two high-level pilot valves, two low-level pilot valves, and interconnecting plumbing. The two fuel tanks consist of neoprene bladder fuel cells tandem-oriented between station 277 and station 339 in the lower fuselage, each having a 122.5-gallon capacity.

HYDRAULIC SYSTEM

Two 3000 psi hydraulic power systems (first-stage servo plus utility and second-stage servo) are installed. A schematic of the hydraulic system is shown in Figure 22. The two system reservoirs are of the "boot strap" pressurized type with air/oil separation and develop a pump inlet pressure to 40 to 45 psi (absolute). The two hydraulic pumps are mounted on the main transmission common with the rotor drive and are independent of engine operation. Test connections on each power system permit ground checking from an external power source.

The two flight control servo hydraulic systems are completely isolated and each supplies one stage of the six dual-stage piston flight control servos. Three servos control the upper rotor and three control the lower rotor. A single system failure can be tolerated without loss of control power. Electrical interlock circuitry prevents shutting off pressure to one stage if the opposite stage is not pressurized and will automatically reactivate the "OFF" stage if pressure becomes low in the opposite stage. Pressure gauges on the instrument panel display each system operating pressure and signals on the Caution and Advisory Panel warn of low pressure in either servo system.

The Stability Augmentation System (SAS) servo systems are also isolated. Each servo system (pitch and roll) consists of two independent servos to which hydraulic power is supplied for each hydraulic system. Power to each servo is supplied through a pilot-controlled ON/OFF switch and a pressure reducer dropping the 3000 psi (absolute) system pressure to the 1000 psi (absolute) SAS servo operating pressure.

The elevator servo is operated from the first-stage hydraulic system upstream from the SAS servos. Power is supplied to the servo through a pilot-controlled 4-way valve and pressure reducer which drops the 3000 psi system pressure to the 1500 psi (absolute) servo operating pressure. A pressure switch, located close to the servo, automatically closes the 4-way valve if a pressure drop is sensed. (This servo was not used during auxiliary propulsion testing.)

The first-stage utility system provides hydraulic power for retraction and extension of the landing gear and J-60 engine start. At reduced rotor speed, flow requirements exceed pump capacity if the J-60 starters are energized. A priority valve installed in the first stage precludes diversion of flow from the primary flight control, SAS, and elevator servos in this case. System design flow rates are listed in Table 4.

Key

1. Pump (First Stage Utility)
2. Pump (Second Stage)
3. Reservoir
4. Filler Coupling
5. Bleeder Valve
6. Relief Valve
7. Check Valve (Reservoir Charge)
8. Check Valve
9. Filter
10. Test Connection (Return)
11. Check Valve
12. Test Connection (Pressure)
13. Manifold
14. Pressure Transmitter
15. Pressure Indicator
16. Restrictor
17. Pressure Switch
18. Servo Actuator
19. Engine Start Motor
20. Engine Start Valve
21. Flow Regulator
22. 4-Way Valve
23. L.G. Emerg. Valve
24. Elec. Actuator
25. Gas Charge Valve
26. Gas Bottle
27. Gas Bottle Release
28. Flow Regulator
29. Flow Regulator
30. Relief Valve
31. Shuttle Valve
32. Uplock Cyl.
33. Cyl. Assy. Main Landing Gear
34. Cyl. Assy. Nose Gear
35. Restrictor
36. Restrictor
37. Priority Valve
38. Master Brake Cyl.
39. Parking Brake Valve
40. Wheel & Brake Assy.
41. Check Valve
42. Positioning Cylinder
43. Restrictor
44. Relief Valve
45. Relief Valve
46. Valve
47. Pressure Reducer
48. Check Valve
49. Pressure Switch

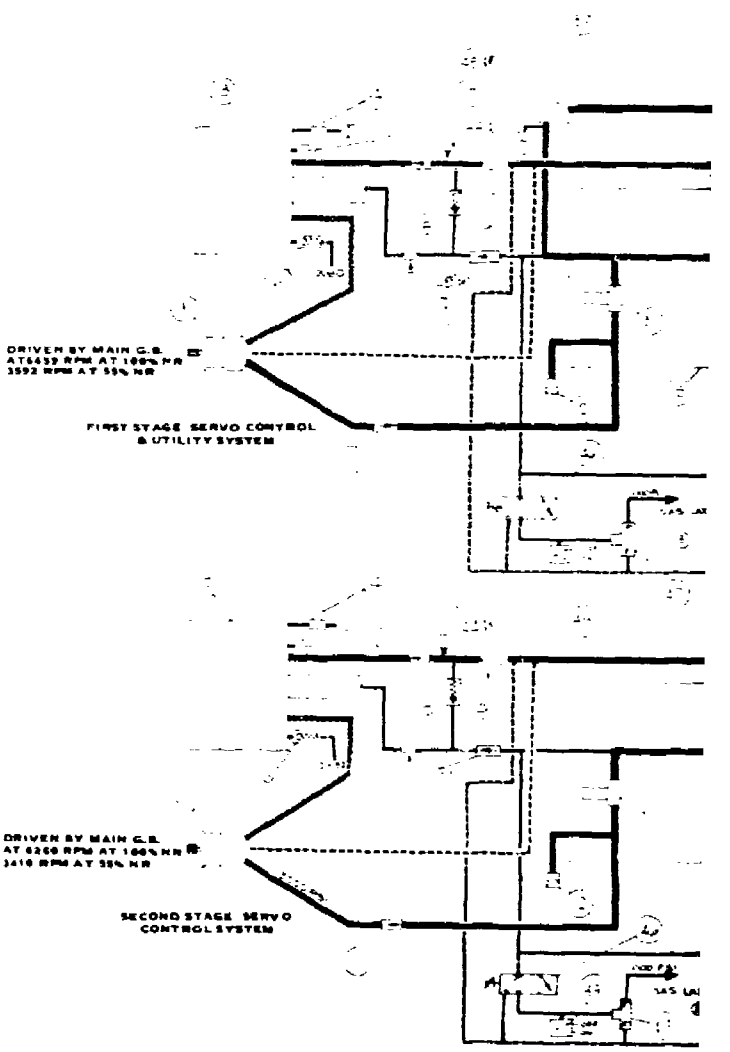

Figure 22. Hydraulic Schematic.

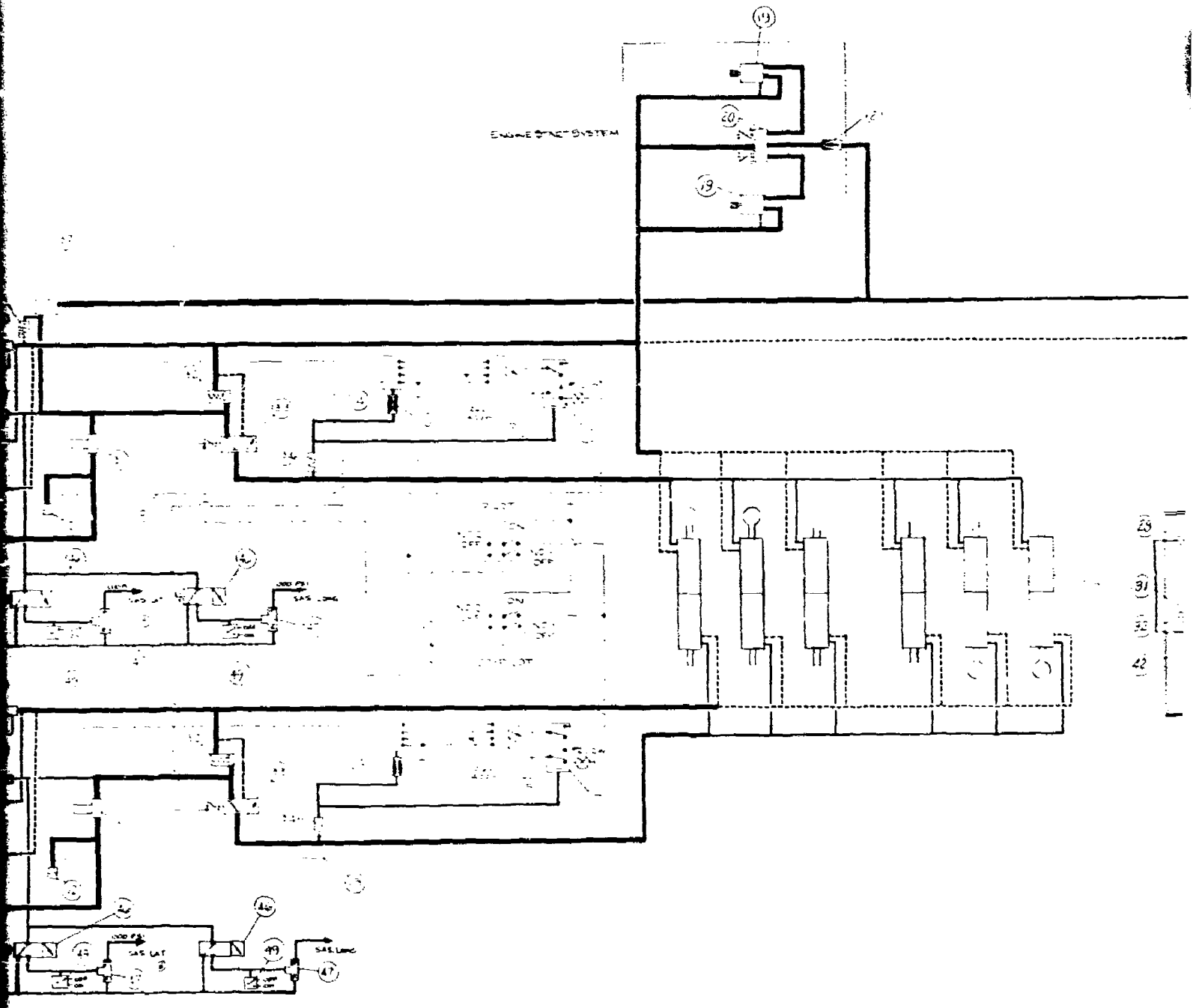
ENGINE START SYSTEM

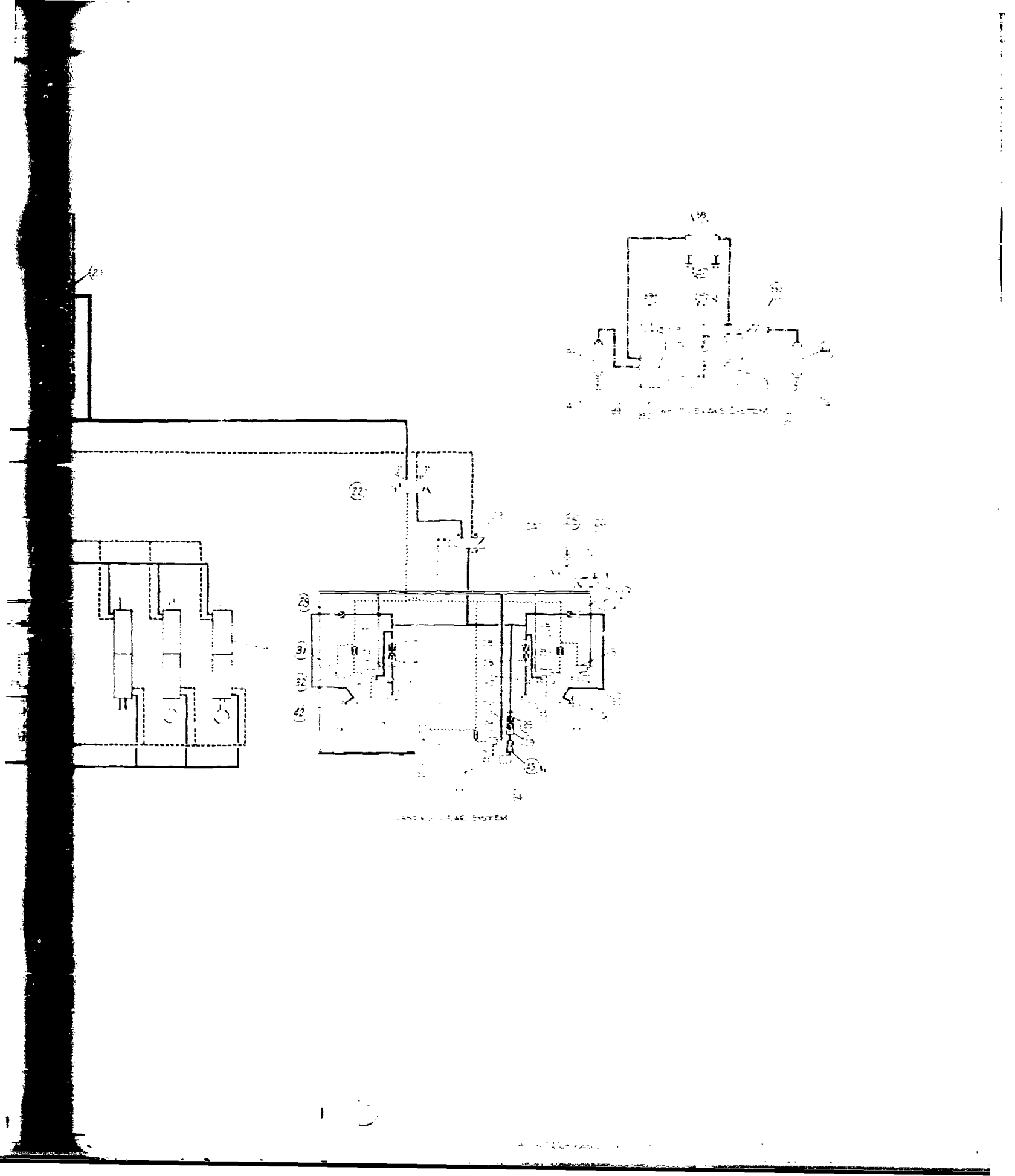

TABLE 4. HYDRAULIC SYSTEM DESIGN FLOW RATES.

Subsystem	Flow Rate (gal per min)
Flight control servos	1.53
SAS servos	.1
Elevator servos	.1
J-60 engine start	7.4
Maximum flow, 1st stage	9.13
2nd stage	1.63
Pump capacity at 100% N_R	12.0
Pump capacity at 70% N_R	8.4

ELECTRICAL SYSTEM

The electrical system is powered by two 200A, 28v dc starter/generators, each driven by a PT6T-3 power section accessory case and a 22 ampere-hour, 24v dc nickel-cadmium (NICAD) battery. A functional diagram of the electrical system is presented in Figure 21. Both generators power the primary and start dc buses. Two 400 Hz, 115v ac, 400v ac static inverters supply ac power. The No. 1 inverter powers the primary ac bus for normal cockpit instruments and ac powered avionics and airframe components. The No. 2 inverter powers the flight test instrumentation ac bus. Should one generator fail, the primary dc bus is deenergized which drops both the No. 2 inverter (and flight test instrumentation ac bus) and the dc flight test instrumentation bus. If both generators fail, the battery supplies dc power for emergency operation selected systems through the start bus.

ANALYTIC DEVELOPMENT

A Sikorsky-sponsored program (Free Flight Normal Modes Analysis) was initiated at the United Technology Research Laboratories in 1965 to establish a dynamic analysis for use in evaluating the ABC coaxial hingeless rotor configurations. A distinguishing feature of an ABC-rotor-equipped aircraft, due to the high blade stiffness and rigid blade-to-hub attachment, is an inherent high degree of elastic and aerodynamic coupling between the rotors, individual blades, and the airframe. Rapid maneuvers made possible by the high available control power substantially couple blade feathering with elastic deformation through both variations in thrust loading and gyroscopic precession. These complex couplings can significantly alter the stability characteristics of the system.

Therefore, the rotor system was simulated dynamically as an integral part of the complete aircraft system, including the individual blades, the individual rotors, interconnecting structural impedences, interacting rotor inflows, interacting rotor/airframe aerodyanmics, and the usual six degrees of freedom of a free-flying airframe. The initial analysis development was completed in 1970 and was used to develop data for the basic report.

This analysis contained means of modelling all of the above effects to some degree, in addition to a sophisticated trim routine which allowed the simulated aircraft to be trimmed in any feasible flight condition. Subsequent development of the analysis has been largely concerned with modifying the formulation of the time-varying aerodynamic interactions as data from model test became available and revising the computer code to decrease the computer time required to calculate a simulated flight condition.

Two major modifications to the analysis were implemented following the acquisition of a substantial data base from wind tunnel tests of a 1/5 (0.1944) scale Froude model. Attempts to correlate the analysis with model test data using model parmeters and low Reynold's Mach number airfoil data demonstrated some significant shortcomings in the analysis. Most noteworthy were the underprediction of longitudinal cyclic required for trim at transition speeds and substantially lower values predicted for the speed ($M\mu$) and angle-of-attack ($M\sim$) stability derivatives than measured in test.

The first modification involved the method by which inter rotor interference was modelled. The original model assumed that for each rotor the inflow contributions from the other rotor were uniformly effective over the rotor disc but reduced

(or augmented) by inflow interference factors. The interference factors were progressively reduced with advanced ratio by a reinforcement factor that was a function of the ratio of the effective momentum disc area to the actual disc area. This reinforcement factor was unity at hover and zero when the two trailing cylindrical wakes cleared each other. The modification consisted of determining an induced flow distribution based on Castles and Deleeuv (Reference 4) and reinforcing the induced velocity of each rotor only on the portion of its disk where the wake of the other rotor actually impinges. In addition, wake contraction factors were added as a ratio of the diameter of the impinging wake at the rotor plane of impingement to the diameter of the rotor generating the wake. The upper on lower factor is generally less than unity, while the lower on upper is generally greater than unity. Contraction factors are consistent with interference factors through the conservation of wake momentum. This modification was found to reduce the longitudinal trim control position error at transition speed by approximately 50 percent.

The first harmonic cosine distribution of self-induced inflow as a function of advance ratio was formulated as suggested by Glauert (Reference 5) and took the form

$$V = Vo + Kv \cdot Vo \cos \psi$$

The coefficient (Kv) was suggested by Payne (Reference 6) to be approximated by

$$Kv = 4\mu / (3.6|\lambda| + 3\mu)$$

---

4. Castles, W., Jr., and Deleeuv, J.H., THE NORMAL COMPONENTS OF THE INDUCED VELOCITY IN THE VICINITY OF A LIFTING ROTOR AND SOME EXAMPLES OF ITS APPLICATION, NACA TN-2912, 1954.

5. Glauert, H., A GENERAL THEORY OF THE AUTOGYRO, RAE R&M 1111, 1926.

6. Payne, P.R., HELICOPTER DYNAMICS AND AERODYNAMICS, Pitman and Sons, London, 1959.

This approximation for Kv approaches 1.333 as advance ratio approaches infinity. Reasoning that the above approximation by Payne was based on experience with lightly loaded articulated rotors, it seems possible that it might be an inadequate representation for the stiff, highly loaded, hingeless ABC rotor. Model test data for single upper rotor, single lower rotor, dual rotors with single rotor control inputs and dual rotors with dual rotor control inputs were used to develop a Glauert inflow function of the same form as that suggested by Payne but with an increased sensitivity to advance ratio approaching 4.65 as advance ratio approaches infinity. The updated term provides total rotor and individual rotor correlation with model test and takes the form

$$Kv = 4.8\,\mu/(3.6|\lambda|+1.03\,\mu)$$

The effect of this modification on the induced velocity ratios at the forward and rear tips of the rotor is shown in Figure 23. The effect of both of the above discussed inflow modifications is shown in Figure 24 as they alter the prediction of longitudinal cyclic control required at low forward speeds.

Additional development activities on the ABC analysis have been extensive but do not directly influence the output data as those discussed above. The extensive complex computations and table look-ups resulted in signficant computer processing time (and therefore excessive computational costs). An effort was undertaken, and continues, to optimize the computational flow and modify data look-up routines with the goal of reducing analytic cost. Improvements to data have reduced the cost of producing analytic data by approximately 50 percent without sacrificing complexity or accuracy of the resulting predictions.

In addition, a rather extensive SAS feedback capability was added to the analysis. Loop closure of attitude, rate, lagged rate and acceleration are available with feedback time constants for simulating lags resulting from a combination f sensors, signal derivations and servo dynamics. This provides the ability to evaluate SAS-ON/ON, SAS-ON/OFF and SAS-OFF/OFF stability as well as transients following single or dual channel simulated hardover failures.

A rather simple model of the effects of auxiliary propulsion on trim has been included, as have various forms of control couplings, detailed modeling of blade prelag, tip path plane separation, and control pushrod steady and vibratory loads.

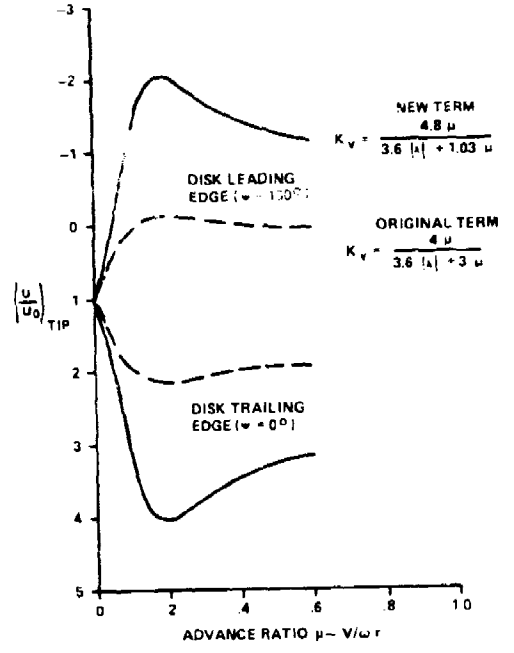

Figure 23. Induced Velocity Ratio Comparison.

13
F

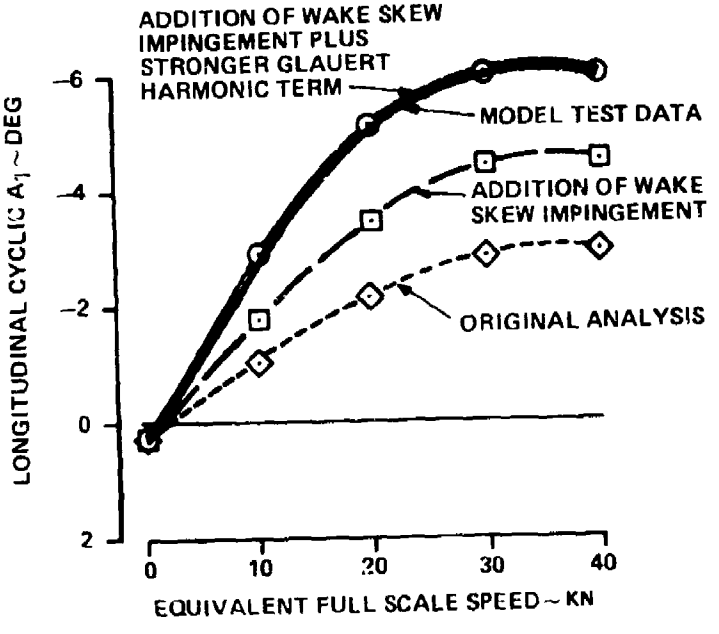

Figure 24. Effect of Inflow Modifications on Longitudinal Cyclic Correlation at 40 Degree Control Phase (Γ).

LABORATORY AND GROUND TESTS

WIND TUNNEL TESTS

Extensive wind tunnel tests were conducted during the development of the ABC helicopter. Two different models were tested in four different facilities. These included a mahogany 1/10 scale fuselage model tested in the United Technology Research Laboratories (UTRL) pilot wind tunnel and a 1/5 Froude scale model with powered rotors tested on the Princeton dynamic model track, in the UTRL main wind tunnel, and in the NASA/ Langley V/STOL wind tunnel.

1/10 Scale Tests

The 1/10 scale model tests were conducted in the UTRL 4 x 6 foot pilot tunnel during the period 31 January to 30 May 1972. The mahogany model was mounted on a pylon attached to a six-component balance located below the test section. Model buildup provisions included seven tail configurations, various J-60 nacelle installations, pressure taps, and tufts. Test objectives were to select the optimum tail configuration for stability and control, locate the J-60 nacelles for minimum drag, determine pressure distributions on the fuselage for structural design, and provide force and moment aerodynamic data for analytical simulation. In addition, the flow field along the fuselage and in the vicinity of the empennage was evaluated by means of tufts and a pressure rake. A coaxial model rotor was mounted on a track support above the tunnel ceiling which was independent of the model and balance. Smoke studies were conducted with the rotor installed for a qualitative evaluation of rotor wake impingement on the tail.

The results of the smoke, pressure rake, and static stability tests clearly indicated that the best tail configuration was the twin-tail "H" arrangement. The effects of the rotor head and fuselage wakes are minimized such that tail effectiveness is maintained over a large range of angle of attack and sideslip. Adding positive dihedral to the horizontal stabilizer and lowering the vertical tail increased angle of attack stability by 25 percent and improved rudder control power at positive angles of attack.

The tufts along the fuselage indicated turbulence around the basic PT-6 inlet and interference between the inlet and the J-60 installation. As a result, the entire PT-6 inlet and cowling area were redesigned. Various J-60 nacelle locations and fairings were also evaluated. Minimum drag was achieved with the nacelles at buttline 52 with a fillet between the fuselage and the nacelles. These results were applied to the final design of the XH-59A flight vehicle.

1/5 Froude Scale Model Tests

A 1/5 (0.1944) Froude scaled dynamically similar model was tested on the Princeton dynamic model track facility, in the UTRL 18-foot-section subsonic main tunnel and in the 21- x 14-foot-section NASA/Langley V/STOL tunnel. Tests were conducted in five phases to investigate the performance, handling qualities, control, and vibration characteristics over the pure helicopter and auxiliary propulsion flight envelopes. Tests in hover and low-speed flight to a simulated 40-knot full-scale speed were conducted in Phase 0 on the Princeton dynamic model tract (Reference 7). Forward flight tests to a simulated 80-knot speed were conducted in Phase I in the UTRL main wind tunnel.

The test speed range was extended to a simulated 100-knots and 40-knot sideward and rearward flight in the UTRL main wind tunnel during Phase II. The test speed range was increased further to a simulated 170 knots in Phase III in the UTRL main tunnel. This test also included single rotor tests, control frequency sweeps, and damping tests which completed the pure helicopter tests. The model was configured with the J-60 nacelles for the auxiliary propulsion configuration tests conducted in Phase IV in the NASA/Langley V/STOL tunnel. Testing included static trim with jets shut down, at ground idle, and at trim thrust as well as trim sensitivity tests with variations in rotor speed, angle of attack, and horizontal tail incidence.

Phase 0 Tests:

A 1/5 (0.1944) scale Froude model of an early ABC helicopter design was constructed at Forrestal Research Center, Princeton University and tested on the Princeton dynamic model track with independent research and development funds. The model was subsequently fitted with the "H" tail configuration selected in the 1/10 scale tests. It was mounted on the facility as shown in Figure 25. Test speed range was 0 to 40 knots simulated full scale. This range was of particular interest because rotor-induced velocity is large relative to forward speed so that mutual interference between the rotors and rotor downwash effects on the airframe are substantial. The long track facility with its large enclosure and good speed control was considered ideal for this speed range.

---

7. Curtiss, H.C., et al, AN EXPERIMENTAL INVESTIGATION OF THE LOW SPEED TRIM AND STABILITY CHARACTERISTICS OF A COAXIAL HELICOPTER WITH HINGELESS ROTOR ON THE PRINCETON DYNAMIC MODEL TRACK, Princeton University, TRN 1196, September 1974.

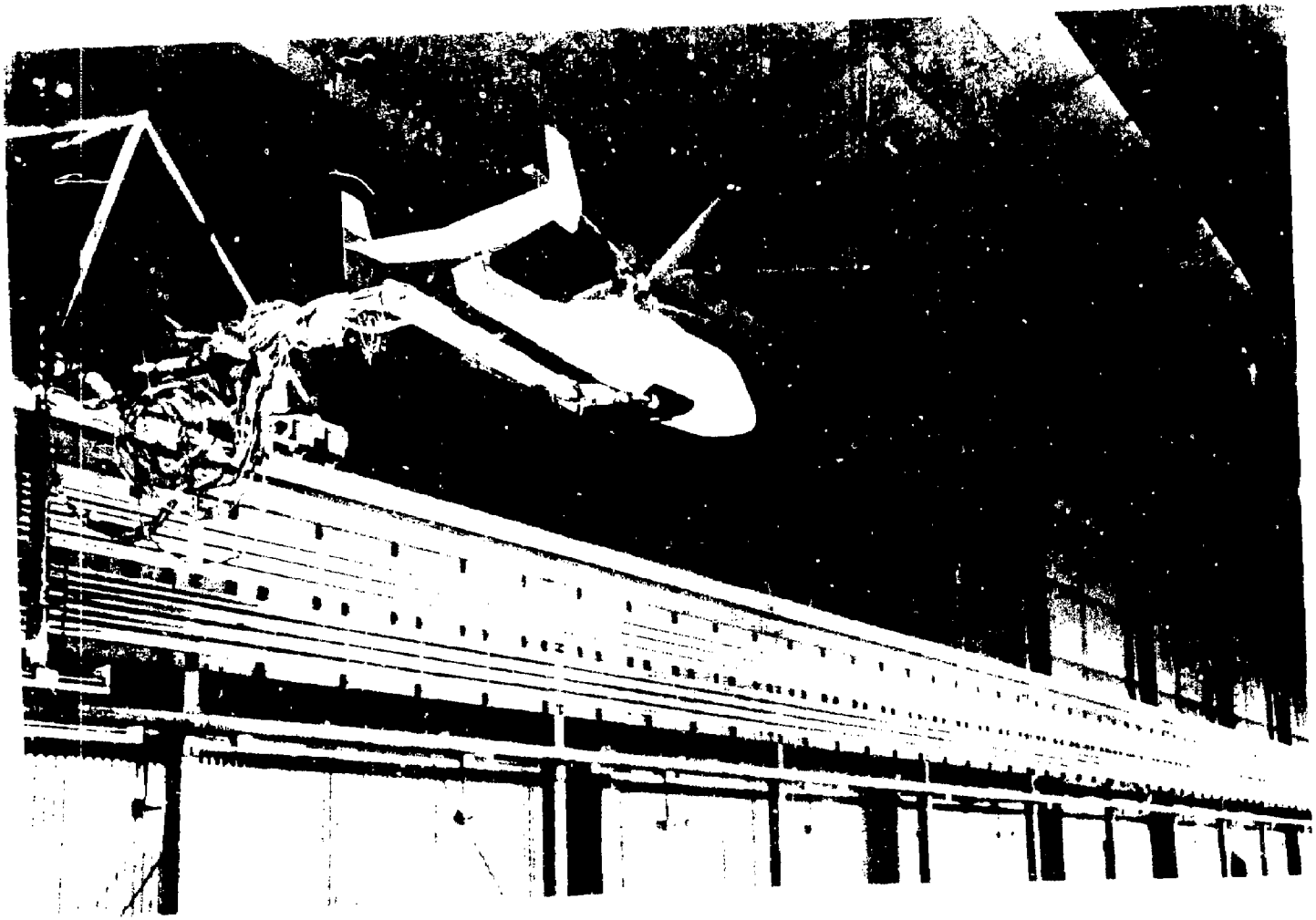

Fig. [illegible] Test of ABS Mounted on Facility at Princeton.

Forces and moments acting on the model were measured as a function of control position and flight condition with primary attention directed toward those parameters pertinent to static trim and stability and control derivatives. The model was also mounted on a gimbal which allowed freedom in the three rotational degrees of freedom. Damping derivatives were determined by freeing selected degrees of freedom and recording the model oscillations in response to an initial offset from trim.

The single most significant static test result was that the model was not trimmable in pitch at a 0.05 advance ratio, 20 knots full scale, with a 70-degree control phase angle (Γ) setting (Figure 26). The model cyclic control limit and the aircraft projected control limit, as established by control system clearance, are shown for reference. Note that neither the model nor the flight vehicle can be trimmed with a 70-degree control phase angle in low-speed flight. This is another implication of the inflow variation over the rotor discussed earlier. The aircraft control phase angle is maintained in the 20- to 40-degree range in low-speed flight.

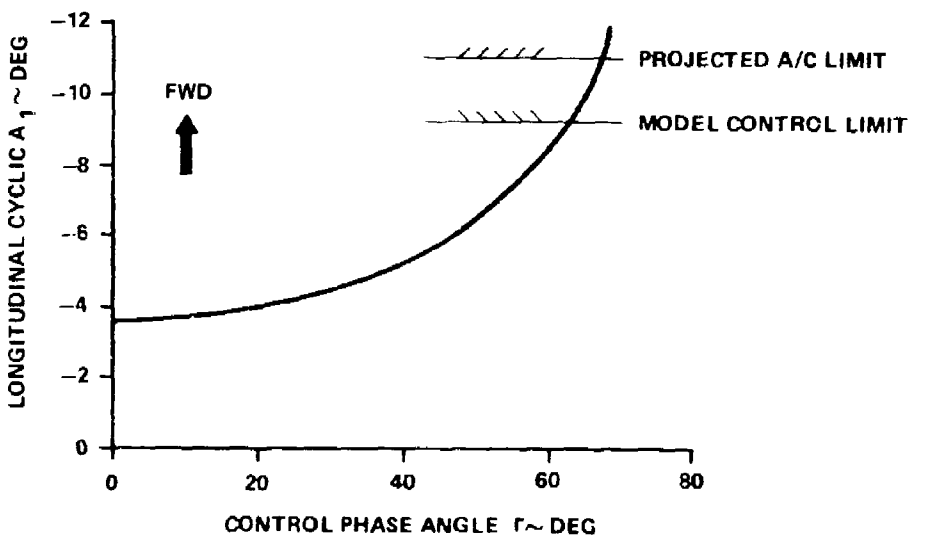

Figure 26. Longitudinal Control Versus Control Phase Angle Characteristic.

Phase I Tests:

At the inception of Phase I testing in the UTRL 18-foot-section main tunnel, pressure surveys across the test section, flow visualization with smoke, and test section wall tufts demonstrated that the flow quality was adequate for acquisition of meaningful data down to 8.5 knots tunnel speed (20 knots simulated full-scale airspeed).

The method of testing was unique in that the model was virtually flown to a desired test condition. This test procedure was possible because of a special model mounting arrangement. Instead of the conventional mounting to the tunnel balance system, the rotor system, control system motor, and fiberglass/epoxy fuselage were mounted through a structural member directly to a TASK six-component strain gage balance system (Figure 27). The TASK balance thus supported the entire model in the tunnel. Task balance data were processed on-line by an integral computer program and displayed to the operator as forces and moments at and about a selected resolving center (normally the center-of-gravity location). Blade feathering of both rotors was operated controllable through an analog computer model of the flight control system. Fuselage attitude was independently controllable by the operator through the tunnel strut system. The operator either nulled all forces and moment values to simulate trimmed flight or selected particular force and moment values to simulate quasi-accelerating flight conditions. Stability and control derivatives were obtained by fixing all trim parameters and changing each appropriate state or control variable in turn.

Level flight controllability tests were conducted in Phase I for forward flight speeds up to 80 knots simulated full-scale airspeed, control phase angles (Γ) from 0 to 40 degrees, and rotor speeds from 88 to 100% N_R. At 88% N_R and with a Γ of 40 degrees, longitudinal cyclic required for trim was excessive. Evaluation of the data showed that blade stall occurred on the retreating side of each rotor. The model blades had 10 percent less solidity than the full-scale aircraft; thus, tests at the equivalent full-scale disc loading resulted in a high blade loading on the model. Reducing model thrust by 10 percent to simulate equal blade loading eliminated blade stall and reduced longitudinal cyclic pitch required for trim to nominal values. No blade stall was apparent on the model at 100 percent rotor speed, even for the 10-percent higher blade loading.

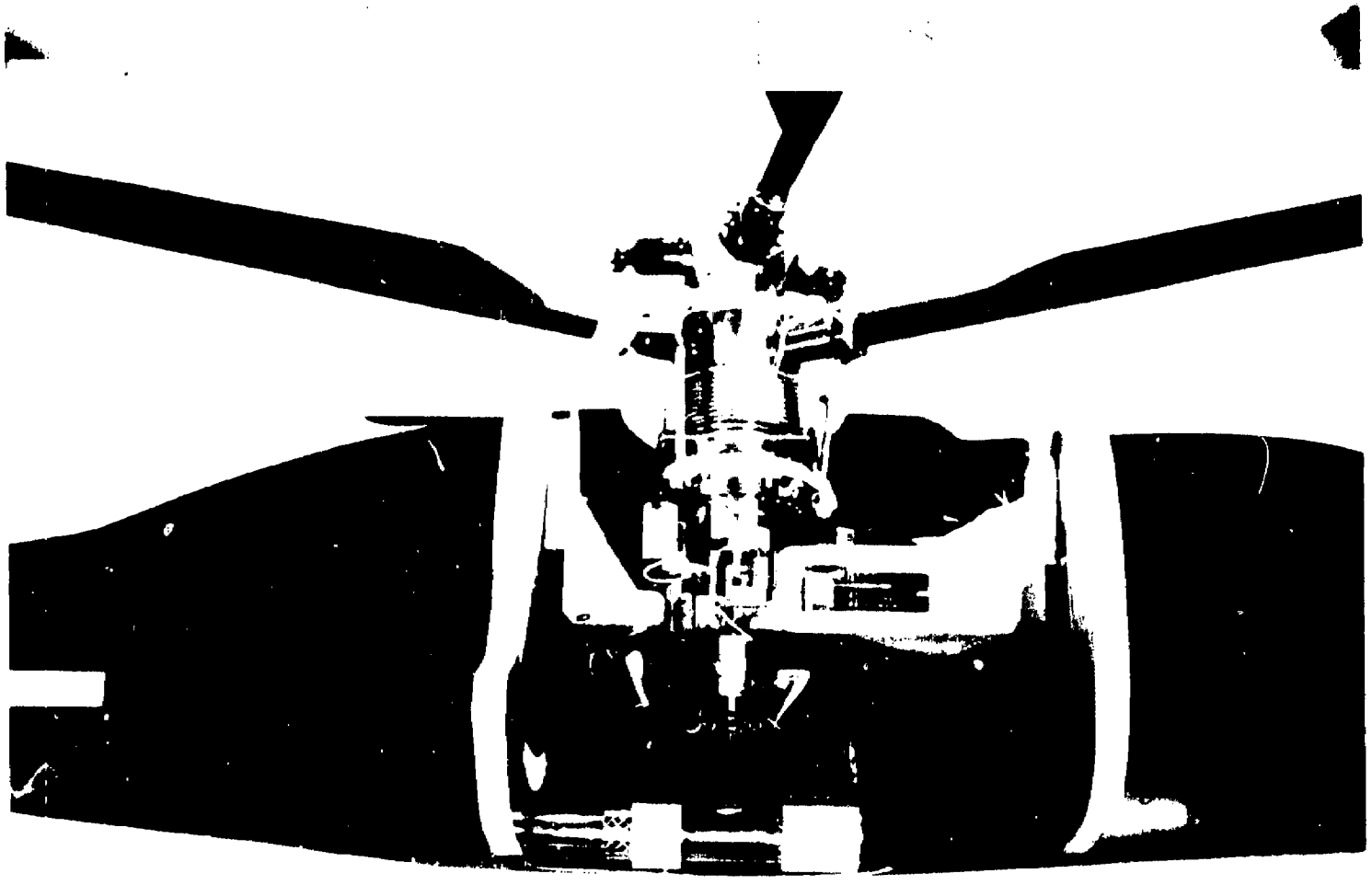

Figure 7.1. Model Six-Component Strain Gage Balance System.

In low-speed flight, the center of lift on each rotor was controllable fore and aft as well as laterally. At a given advance ratio, an increase in control phase angle or a positive differential lateral cyclic pitch input moved the center of lift laterally toward the retreating side of each rotor. Although the fore/aft position of the center of the lift of each rotor is collectively a function of the trim pitching moment, it can be varied differentially between the rotors by introducing differential longitudinal cyclic pitch. In this way sharing of the trim pitching moment requirement is varied between the rotors. The control laws of the ABC rotor system that provide the ability to not only control lift offset laterally and longitudinally but also to control the thrust sharing between the rotors are presented in Figure 28.

Phase II Tests:

This model test phase extended the speed range to a simulated 100 knots full scale, verified conclusions drawn from the Phase I test, evaluated static stability characteristics and maneuver control margins, and provided smoke flow-visualization data.

Test data confirmed that control phase angle (Γ) is an effective parameter for controlling lateral lift offset. Figure 29 demonstrates the degree of lift offset control available with Γ at a fixed airspeed and the migration of offset toward the advancing side with airspeed. Although data for the lower rotor is shown, the upper rotor has the same offset percentages for total system roll balance. This lateral lift offset control is the essence of the ABC concept. It allows optimum use of the higher dynamic pressure on the advancing side of each rotor. Excessive lift offsets result in excessive blade root stresses and vibration and low blade tip clearances. Small lift offsets result in less than optimum lift to drag ratios due to requiring too much lift from the low dynamic pressure high-drag retreating side.

Tests at nose-up and nose-down attitudes verified the maneuver capability of the ABC (Figure 30). Sufficient longitudinal cyclic margin was demonstrated for flare and acceleration maneuvers in excess of 1.5g load factors. Adequate controllability was also demonstrated for trims and flares in rearward and sideward flight.

The ABC model exhibited low-speed stability characteristics typical of a high disc-loading rigid rotor VTOL aircraft. These are a strong instability with angle of attack accompanied by a strong speed stability. At speeds simulating 50 knots full scale, the horizontal tail became effective enough to counter the rotor stability characteristics.

COLLECTIVE CONTROL $\Theta_0 = \frac{\Theta_{0U} + \Theta_{0L}}{2}$

DIFFERENTIAL COLLECTIVE CONTROL $\Delta\Theta_0 = \frac{\Theta_{0U} - \Theta_{0L}}{2}$

LONGITUDINAL CONTROL $A_1 = \frac{A_{1U} + A_{1L}}{2}$

DIFFERENTIAL LONGITUDINAL CONTROL $A_1' = \frac{A_{1U} - A_{1L}}{2}$

LATERAL CONTROL $B_1 = \frac{B_{1U} - B_{1L}}{2}$

DIFFERENTIAL LATERAL CONTROL $B_1' = \frac{B_{1U} + B_{1L}}{2}$

UPPER ROTOR BLADE FEATHERING

$$\Theta_U = [\Theta_0 + \Delta\Theta_0] - [A_1 + A_1'] \cos(\psi_U + \Gamma) - [B_1 + B_1'] \sin(\psi_U + \Gamma)$$

LOWER ROTOR BLADE FEATHERING

$$\Theta_L = [\Theta_0 - \Delta\Theta_0] - [A_1 - A_1'] \cos(\psi_L + \Gamma) + [B_1 - B_1'] \sin(\psi_L + \Gamma)$$

Figure 28. Control Laws.

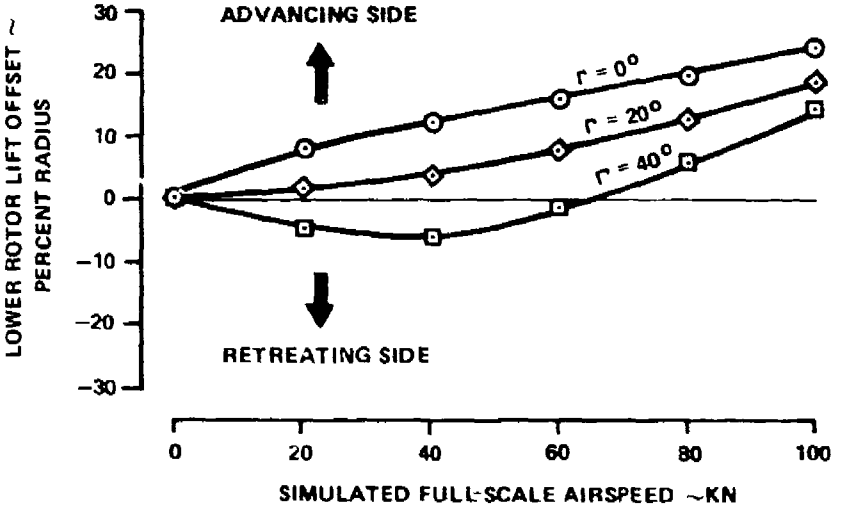

Figure 29. Lift Lateral Offset Movement with Airspeed and Control Phase (Γ).

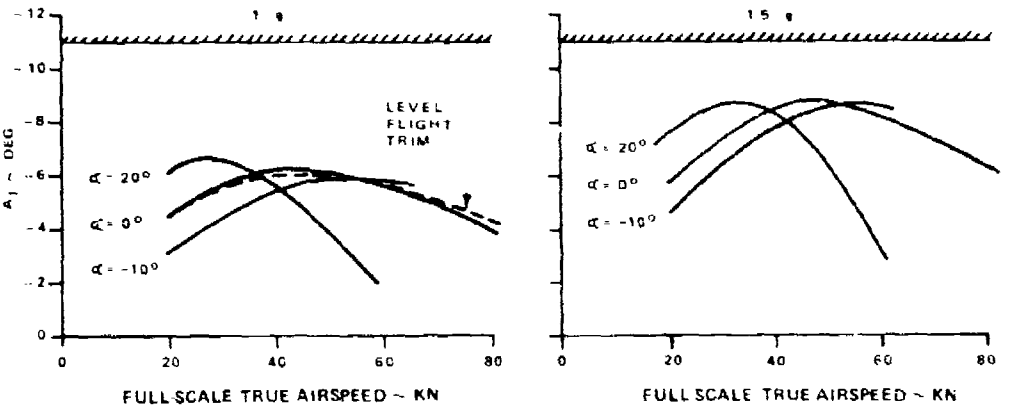

Figure 30. Cyclic Margin for Maneuvering Flight.

Smoke flow-visualization was utilized to obtain qualitative information on the rotor flow field and its effect on the horizontal tail and interrotor interference (Figure 31). Most noticeable is the strong upwash of the wake at the leading edge of the disc, the downwash skew angle at the rear of the disc, and the early wake roll-up as it moves aft. The latter indicates the presence of strong cross-flow and downwash velocity components over the rear of the rotor disc. The strong pitch-up tendency of the aircraft in low-speed flight is attributed to the fore and aft downwash velocity distribution. This is the cause of the peak in forward longitudinal cyclic pitch which occurs in the 25- to 50-knot full-scale airspeed range.

Phase III Tests:

Forward speed range was extended further to 170 knots, Γ changes were evaluated up to a value of 70 degrees, and tail incidence and rotor speed were varied during this test. In addition to forward flight, tests were conducted in sideslip, climb and descent, and single rotor operation. These tests, as well as runs for static stability and damping derivatives, provided data to substantiate the aerodynamic characteristics of the ABC in the helicopter mode. The test results indicated

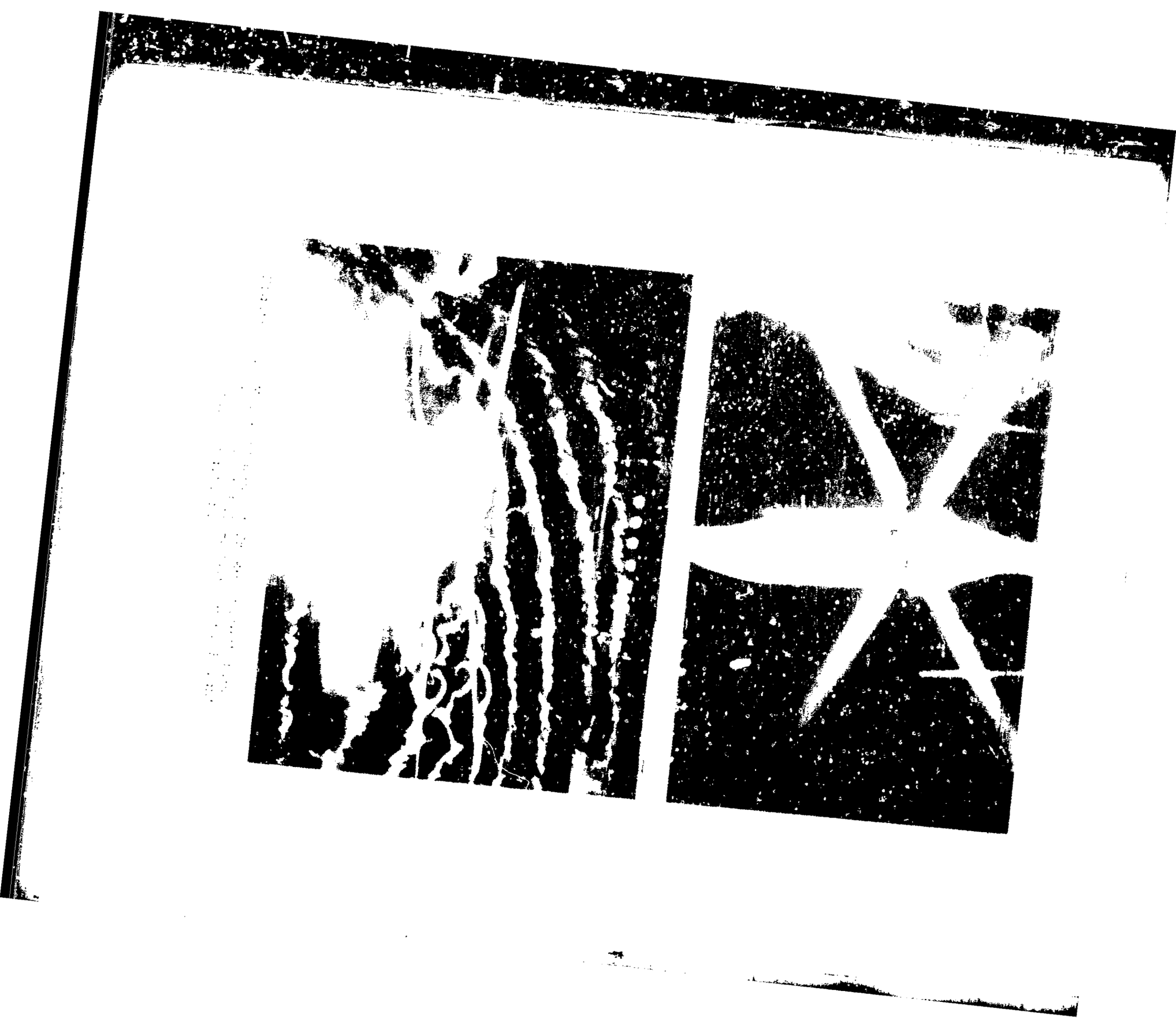

that in a given trim condition, the location of each rotor lift center is influenced primarily by tail incidence and Γ. Γ proportions the azimuthal blade feathering into longitudinal and lateral components. Tail incidence, on the other hand, determines the pitching moment required from the rotors for trim. Thus, in trimmed flight, Γ primarily affects the lateral position of the lift center and tail incidence affects the longitudinal position as shown in Figure 32. In cruise flight, 120 knots full scale, Γ is more effective than tail incidence in controlling the total rotor hub moment (vector sum of pitch and roll moments) and, hence, blade structural loads. The test data in Figure 32, then, suggest that a programmed increase of Γ with forward speed can locate the rotor lift center to control L/D, tip path plane clearance, and blade stresses. Model power and stability were relatively insensitive to Γ so that adjustments of Γ in flight should require little or no increase in pilot workload. It could, however, decrease the low speed adverse stick gradients (Figure 33). Also shown in Figure 33 is the consistency of data between the four test phases even though two totally different types of test facility were used.

The model was tested to angles of attack that simulated rates of descent that were significantly higher than those associated with autorotation, and no structural, stall, blade clearance, control or vibration problems were encountered. Autorotative sink speeds were verified to be 2500 fpm at 80 knots full scale and 3600 fpm at 120 knots full scale. The data also verified that the design collective range for the aircraft was adequate for autorotation entry up to 160 knots full scale airspeed.

The stability derivative test data confirmed the analytical predicted values. Longitudinal control power, pitch coupling with collective, and pitch damping all tended to increase with airspeed. In the lateral directional mode, the test data confirmed that both weathercock and dihedral stability should be good throughout the cruise speed range.

Single rotor operation and dual rotor with individual rotor control inputs were tested to provide data for an evaluation of mutual interference between the upper and lower rotors to support design analyses. The test data verified that mutual interference and airspeed dependent wake distortion effects are significant at low airspeed but diminish with increasing forward speed. Also, the lower rotor, operating in the downwash field of the upper rotor, was less effective in producing moments than the upper rotor.

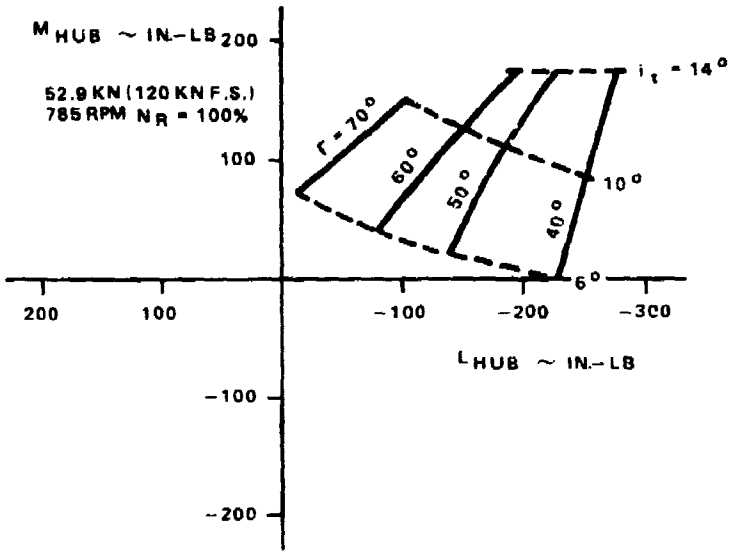

Figure 32. Trim Rotor Hub Moments as a Function of Swashplate Phase Angle and Tail Incidence Angle for 120 Knots Full Scale.

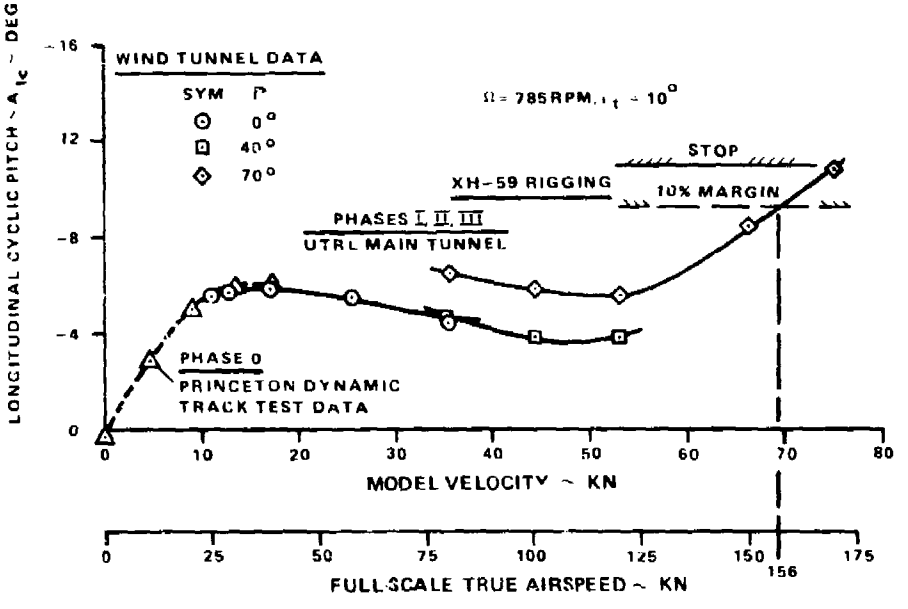

Figure 33. Level Flight Trim Longitudinal Cyclic Pitch Versus Velocity.

Phase IV NASA/Langley Tests:

The 1/5 (0.1944) scale Froude model was tested in the NASA/Langley 21- x 14-foot V/STOL wind tunnel in 1977. Tests of the pure helicopter, nacelles off, validated data continuity with the previous UTRL main tunnel tests. Tests of the pure helicopter, nacelles on, established a flight envelope with J-60 propulsive jets shut down. An envelope to 120 knots was verified (Figure 34). The major tests, however, emphasized the auxiliary propulsion configuration with propulsive force provided by the J-60 jets. These were simulated on the model by NASA-supplied compressed-air ejectors.

The tests were planned to evaluate the complete auxiliary propulsion speed envelope up to the 325-knot dive speed. Data were obtained for trim at 120, 150, and 200 knots simulated full-scale speeds and trim surveys at 150 and 200 knots. Problems were encountered with the model blades during tests at higher airspeeds.

A set of rotor blades was destroyed by blade tip contact while trying to trim at 250 knots with 70 percent rotor speed. It was subsequently determined that inadequate control of the rotor lift center was the basic cause of the blade tip contact. A new set of blades was installed and trim at 250 knots

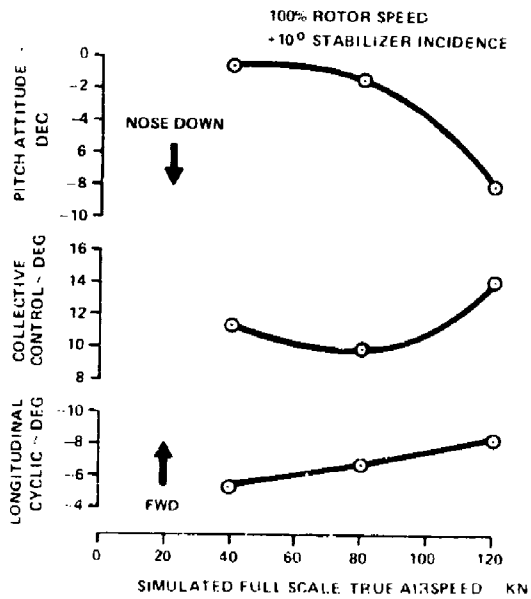

Figure 34. Helicopter Trim (Nacelles On).

was attained. However, before recording the trim data, a cyclic impulse was applied to evaluate blade edgewise damping. A malfunction in the control console resulted in approximately 6 degrees of cyclic impulse being applied, which destroyed the second set of blades. As a result, no trim data were obtained for the 250-knot condition and auxiliary propulsion testing was terminated. A third set of blades that had accumulated many hours of use in prior UTRL test phases was installed on the model and hover tests were conducted expressly for NASA (Reference 8).

A sample of auxiliary propulsion trim data at 100 percent rotor speed and 40 degree control phase angle is presented in Figure 35. Also shown are ABC normal modes analysis predictions which show reasonably good correlation with the test data. The analytic data were obtained by specifying test airspeed and collective control. The computer trim algorithm calculated the corresponding attitude, longitudinal control, auxiliary thrust, etc., required for trim.

Trim surveys involved retrimming the model with successive variations in rotor speed, stabilizer incidence, and angle of attack about level flight trim at 150 and 200 knots. Rotor speed was not varied at the 150-knot condition. Attitude, collective, and longitudinal cyclic requirements resulting from these tests are presented in Figures 36, 37 and 38. The test data indicate that at 200 knots full scale, reductions in rotor speed will be accompanied by an increase in pitch attitude (Figure 36). This positions the rotors in an orientation that approaches autorotation. As a result, collective pitch and, correspondingly, longitudinal cyclic for trim are reduced. At both 150 and 200 knots full scale, an increase in angle of attack also reduces collective and longitudinal cyclic control requirements for the same reason (Figure 37). An increase (less negative) in horizontal tail incidence at constant pitch attitude produces the same downtrend for collective and cyclic pitch, but for a different reason (Figure 38). When horizontal tail incidence is changed to a less-negative setting its down-load and nose-up pitching moment contributions are decreased. Rotor lift and nose-down moment required for trim are correspondingly reduced. This results in a reduction of trim collective and cylic pitch. If collective pitch were held constant, an increase in tail incidence would require a lower pitch attitude to balance the lift and moment change.

---

8. Phelps, A.E., and Mineck, R.E., AERODYNAMIC CHARACTERISTICS OF A COUNTER-ROTATING, COAXIAL, HINGELESS ROTOR HELICOPTER MODEL, NASA TN-78705, May 1978.

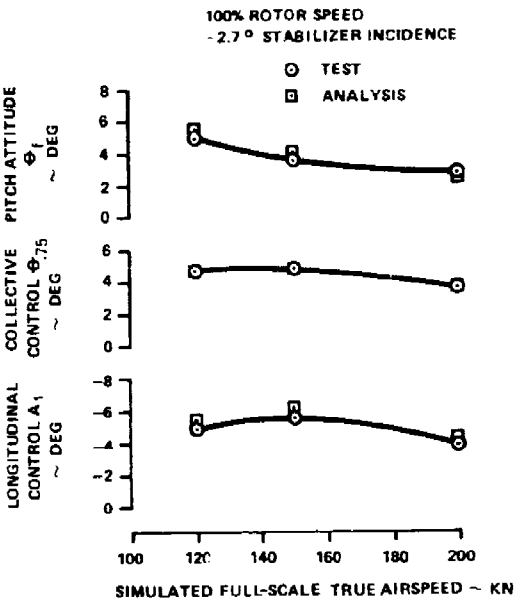

Figure 35. Auxiliary Propulsion Trim Data and Analytic Prediction Correlation.

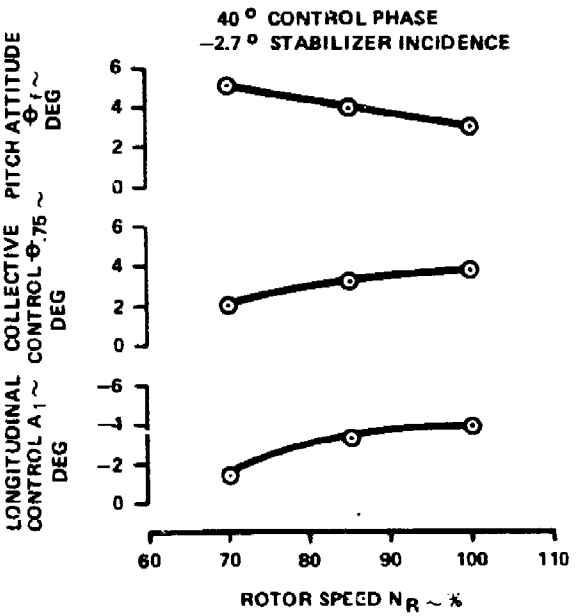

Figure 36. Trim Variation with Rotor Speed at 200 Knots (Full Scale).

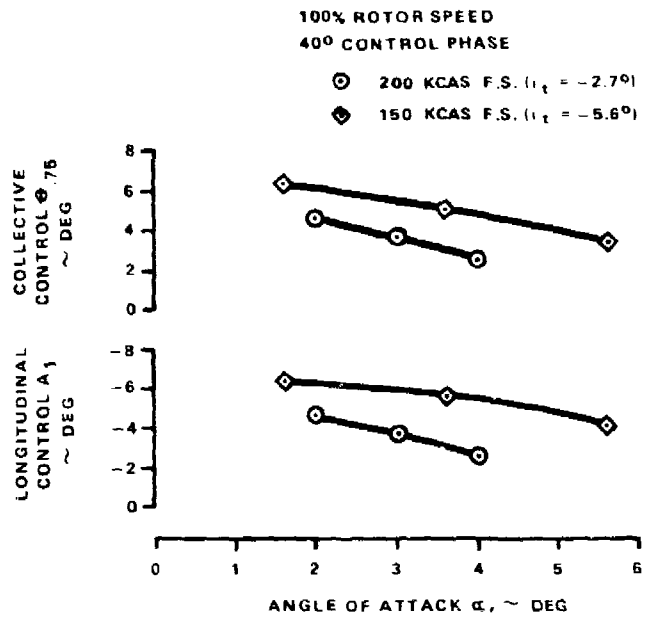

Figure 37. Trim Variation with Angle of Attack.

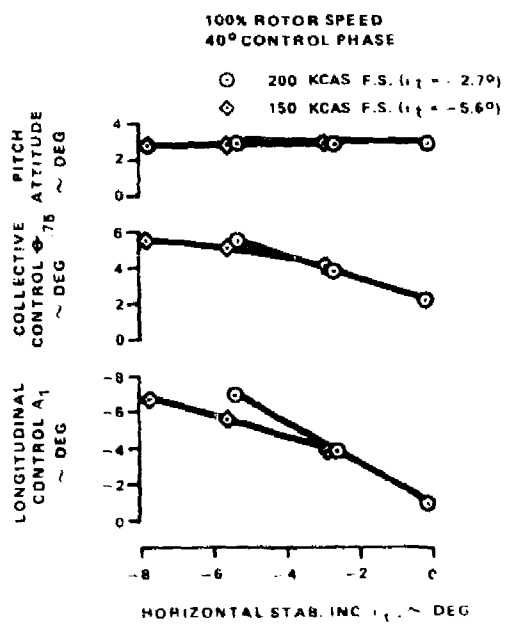

Figure 38. Trim Variation with Horizontal Stabilizer Incidence.

FATIGUE TESTS

Fatigue testing was conducted to demonstrate the structural adequacy for flight testing of the XH-59A technology demonstrator aircraft. Since the aircraft was a one of a kind demonstrator, fatigue testing was limited primarily to components whose design varied substantially from normal production design and fabrication techniques. With one exception, fatigue testing was limited to one specimen. With the exception of the items discussed herein, the endurance and abort limits for components were based on analytical limits backed up by data obtained from testing similar components from other aircraft. In addition to the fatigue tests, the dynamic components were subjected to a minimum of 200 hours of testing on a propulsion system test bed (PSTB).

Upper Rotor Hub Photoelastic Stress Survey

The purpose of these tests was to investigate stress distribution in the XH-59A upper main rotor, providing verification of design analysis and establishing locations of critical strain gage instrumentation for both the subsequent propulsion system test bed and aircraft testing.

This effort consisted of a series of tests conducted on two half-scale plastic models of the XH-59A upper rotor hub and sleeve assembly. Photoelastic and electrical resistance strain measurement techniques were used to investigate stress distribution and to expose potentially critical areas.

An aluminum filled epoxy model was subjected to a range of steady and vibratory load conditions. A portion of the hub was coated with birefringent plastic and examined using a reflection polariscope to reveal areas of high stress. Strain gage measurements were then made which provide a basis for calculating steady and vibratory stress under any combination of flight loads.

A second model, made from a birefringent plastic, was subjected to a selected load condition, and a technique known as 3-D stress freezing was used to lock in the resulting strains in such a way that the model could be sliced and stresses measured in normally inaccessible areas of the hub.

Correlation between the two techniques was very good and provides confidence that data measured by only one of the techniques was valid.

In order to statically simulate the complex loading experienced by the rotor, a simple frame was constructed for testing the aluminum filled epoxy model. Representative blade moment

conditions were simulated in conjunction with a steady centrifugal load by applying suitable combinations of load at each arm. A 1/3 segment of the hub was coated with birefringent plastic using established photoelastic coating procedures and examined under a reflection polariscope. Although limited in scope, this technique gave a clear indication of stress concentrations and areas of high stress. This data was used to select locations and orientation of instrumentation strain gages. The hub loading conditions were repeated with the strain gages installed, and the high readers were then used on the propulsion system test bed to monitor the structural integrity of the upper rotor head during testing. The final flight aircraft strain gage locations were selected from the high readers obtained during the propulsion system test bed program.

The 3-D stress freeze model was installed in a simple loading fixture, simulated loading conditions were applied, and the entire fixture was placed in a large oven and subjected to the required stress freeze temperature cycle. On removal from the oven, the model was disassembled and sliced for analysis. The results of this testing indicated some concern for potential fretting in the area of the blade sleeve attachment bolt. This was subsequently evaluated during the propulsion system test bed phase.

Lower Rotor Hub/Blade Interface Fatigue Test

The lower rotor blade sleeve/hub attachment assembly was subjected to a test program which included static, dynamic and fatigue testing to demonstrate structural adequacy of the assembly for flight testing of the XH-59A technology demonstrator aircraft.

Static bending tests were performed with and without centrifugal load to determine the stiffness of the hub/blade interface attachment. The results of these tests determined sufficient stiffness to avoid rotor dynamic problems.

A static stress survey was performed in conjunction with the stiffness tests to determine stress distributions in the hub/blade interface attachment. The tests were conducted as separate flatwise and edgewise tests with and without centrifugal loading.

A dynamic stress survey was performed with and without centrifugal loading using the data obtained during the static stress survey as a guide. Unlike the static tests, however, this test was conducted with representative combined flatwise and edgewise loadings. The tests were conducted to determine the dynamic stress distribution of the hub/sleeve interface

area and to define critical strain gage locations for subsequent propulsion system test bed and flight aircraft testing.

Upper Rotor Control System Fatigue Test

A fatigue test of the upper rotor control system between the primary servos and the blade control horns was conducted to demonstrate structural adequacy of the assembly for flight testing of the XH-59A technology demonstrator aircraft.

The control system for the upper rotor is a unique design which incorporates servos, stationary and rotating swashplates, walking beams, pitch control rods, and pitch control horns. The control inputs are transferred from the servos to the stationary and rotating swashplate assemblies attached at the base of the main rotor gearbox housing. Walking beam assemblies attach to the rotating swashplate and transfer loads to the pitch control rods, which pass up through the center of the upper rotor shaft and attach to the blade pitch control horns inside at the top of the upper rotor hub/shaft.

Fatigue testing was used to expose the weakest link in the system and to establish critical structural parameters to be monitored during subsequent flight testing.

Testing was conducted in a specially designed test facility which included a rotor transmission housing, an entire upper rotor control system, and a dummy upper rotor hub/shaft and blade sleeve assembly.

Two channels of the control system (control horn, pitch control rod, walking beam, and rotating swashplate arm) were loaded by servo-controlled hydraulic cylinders which attached to the outboard end of the stub blade sections. The third channel was used to maintain positoning and orientation of the control system. Applied loadings were reacted through the control system to the three aircraft servos (from A/C 21941) mounted to the gearbox housing.

Load distributions throughout the system were achieved by positioning the stationary and rotating portions of the system. Phasing of the two loaded channels was also varied so that desired load magnitudes and distributions could be achieved.

Fatigue testing was accomplished at load levels that provided testing in a reasonable amount of time.

In addition to the total system fatigue test, additional bench fatigue tests were conducted on components which were not highly loaded during the total system testing.

Stabilizer Lug Fatigue Test

One additional fatigue test was conducted based on results from the auxiliary propulsion phase of flight testing.

The stabilizer incidence angle was changed from +10 degrees to -5 degrees when the aircraft was reconfigured from the pure helicopter to the auxiliary propulsion configuration. The change was accomplished by installation of an additional fitting between the aft stabilizer mounting lugs and the mating fuselage lugs, making that part of the installation a pin-pin attachment as opposed to the previous fixed attachment point. This modification resulted in a change in the loading characteristics at the forward stabilizer/fuselage lug attachment point. The resultant critical forward lug stress ultimately exceeded the analytical endurance limits.

A fatigue test was conducted on two lug specimens to determine limits based on test rather than on analysis. The data obtained from the lug fatigue testing ultimately raised the limits only slightly. Subsequently, the mean curve, based on test results, was used as a steady state trim flight endurance limit while cycle counting cumulative damage against the test defined 3σ endurance limits. The forward stabilizer lug retirement time was set at 25% of the calculated life.

PROPULSION SYSTEM TEST BED

The propulsion system test bed is a means of verifying (prior to flight test) the airworthiness of the integrated propulsion system. In addition, it represents the first area in which system problems are expected to be uncovered and thus constitutes a tool to effect significant design improvements as required. This approach to testing is carried out by mounting the aircraft propulsion system (and controls) in the same manner as the aircraft and subjecting the whole system and as many of the components as possible to a spectrum of loading similar to but accelerated over that anticipated for the flight aircraft. As in all ground tests, certain inherent limitations are found. The principal limitation is that forward flight is not within the range of test bed operations. In order to develop the loads (and motions) in dynamic components in excess of those that would be encountered in forward flight, a head moment spectrum (and associated power spectrum) is applied.

The XV-15A propulsion system test bed was constructed of structural steel and configured to accept the required aircraft components as well as provide an abundance of permanent work platforms for component accessibility. A hydraulic crane was provided for installation and removal of components. A

275-gallon fuel tank was mounted on supports adjacent to the facility and at the same aircraft waterline with respect to the engines to better simulate the aircraft fuel system. The 275-gallon fuel tank was, in turn, supplied with fuel from a separate 5000-gallon fuel tank which supplied sufficient fuel for long term endurance testing.

The propulsion system test bed configuration is presented in Figure 39.

In additon to the test bed, the facility contained a separate control room. This facility was configured with a control center from which all test bed operations were conducted. The center contained three separate adjacent test consoles. The center console was configured for operation and monitoring of the powerplant and transmission system. The left console was configured for operation of the rotor controls. It contained displays for individual as well as total rotor pitch and roll moments as well as individual and total longitudinal and lateral control positions for the stationary control system. The right console provided on-line data monitoring from information provided by the data instrumentation system. In addition to the three monitoring consoles, a complete separate data recording system was provided. The propulsion system test bed control center is presented in Figure 40.

The propulsion system test bed program consisted of a series of tests chronologically structured to demonstrate satisfactory operation of the test bed and associated aircraft hardware. The final result of this series of tests was the completion of the required 200 hours of endurance testing.

A powerplant to transmission drive shaft natural frequency test was conducted with the rotor blades removed. The test was conducted by powering the transmission to 115 percent normal rotor operating speed with the powerplant to demonstrate the lack of critical shaft speed problems. No critical shaft speeds were found.

The test bed was configured with test clubs installed in place of the rotor blades to establish satisfactory transmission gear patterns and to conduct transmission run in. The test clubs were designed to absorb power as a function of rotor speed and are shown installed on the aircraft in Figure 41. The only problem encountered during this test was a requirement to conduct a minor transmission input pinion gear tooth regrind. This regrind was duplicated on the aircraft transmission.

Aircraft fire detection and extinguisher system tests were conducted to demonstrate proper operation.

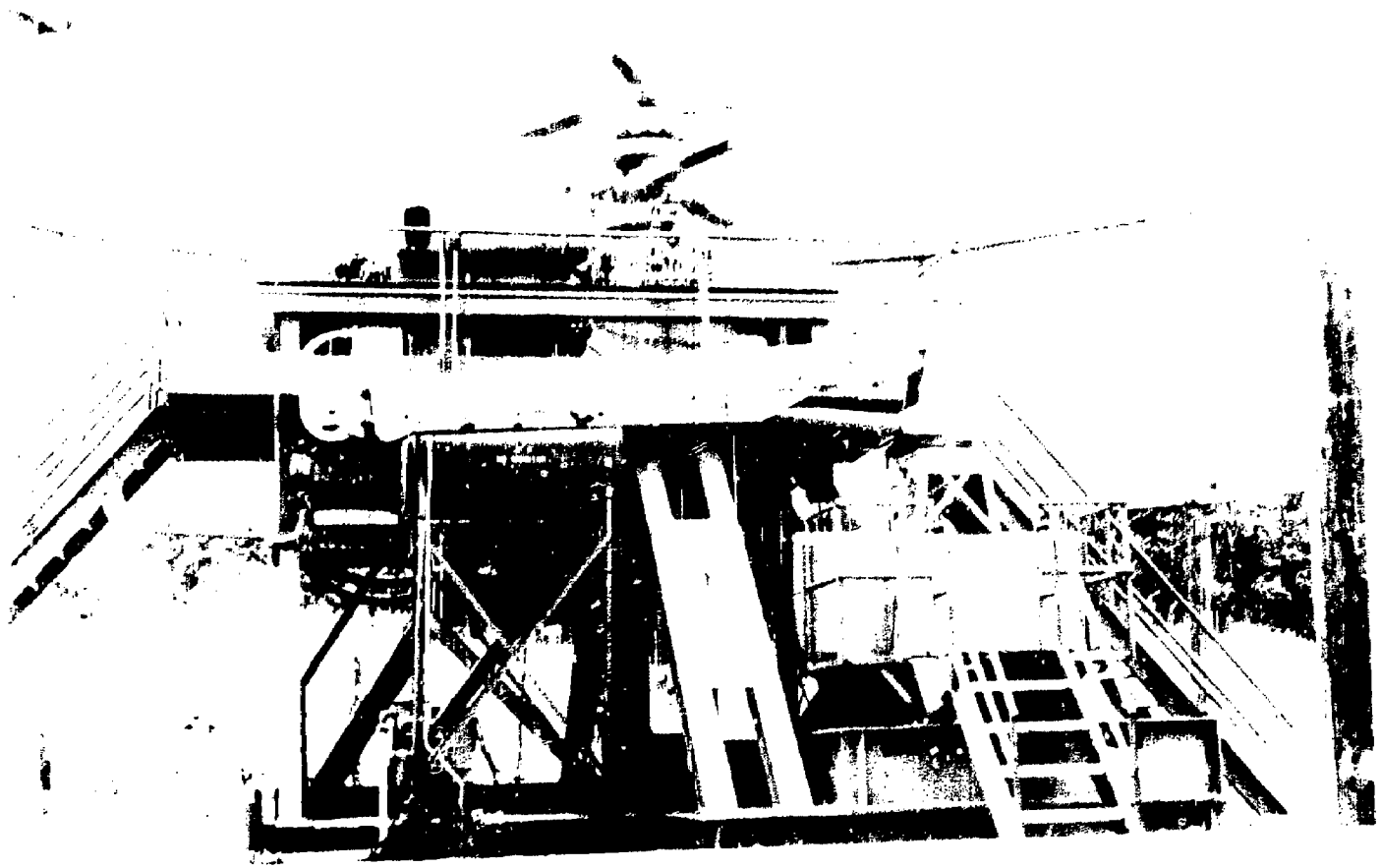

Figure 39. Propulsion System Test Bed Configuration B

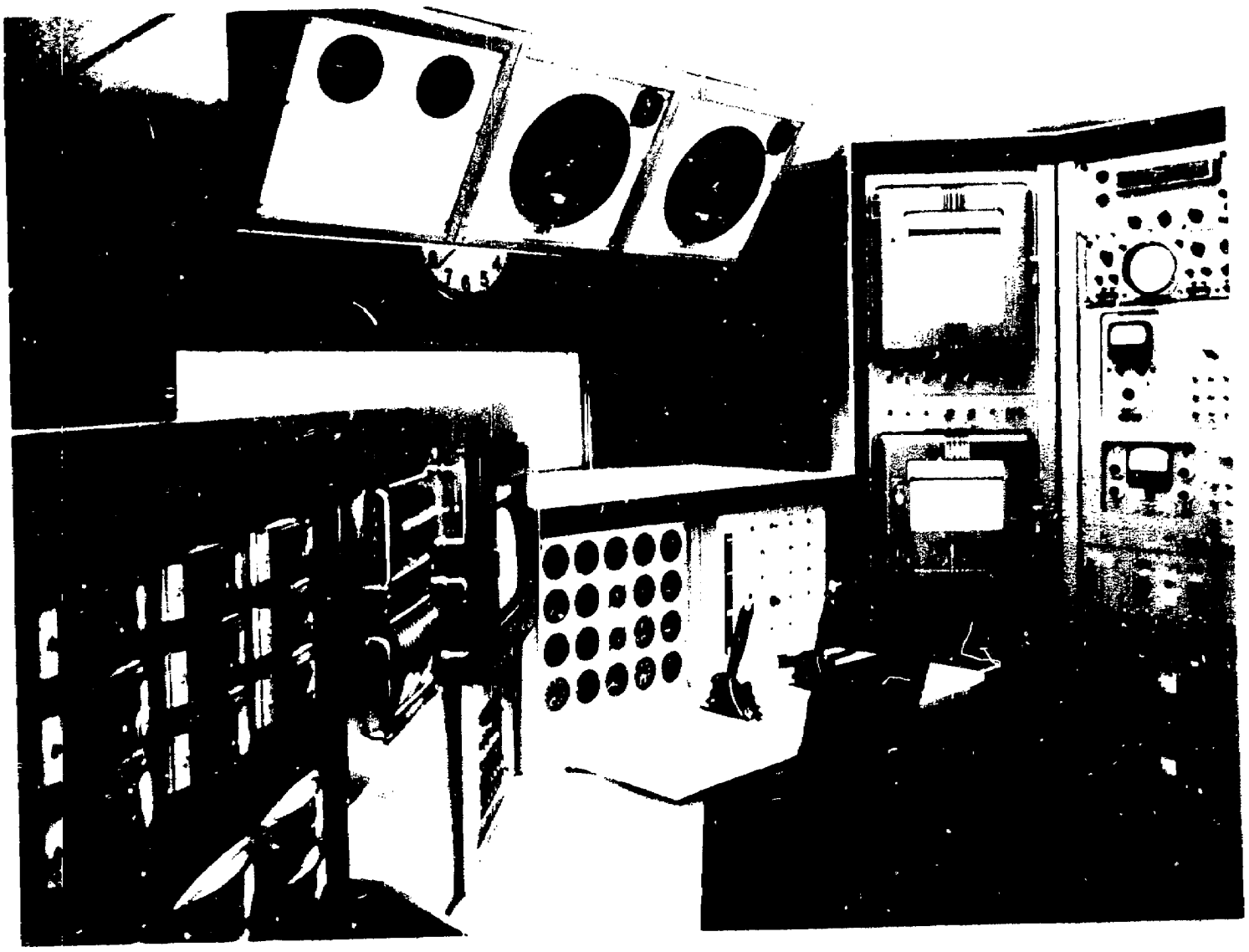

Figure 40. Propulsion System Test Bed Control Room.

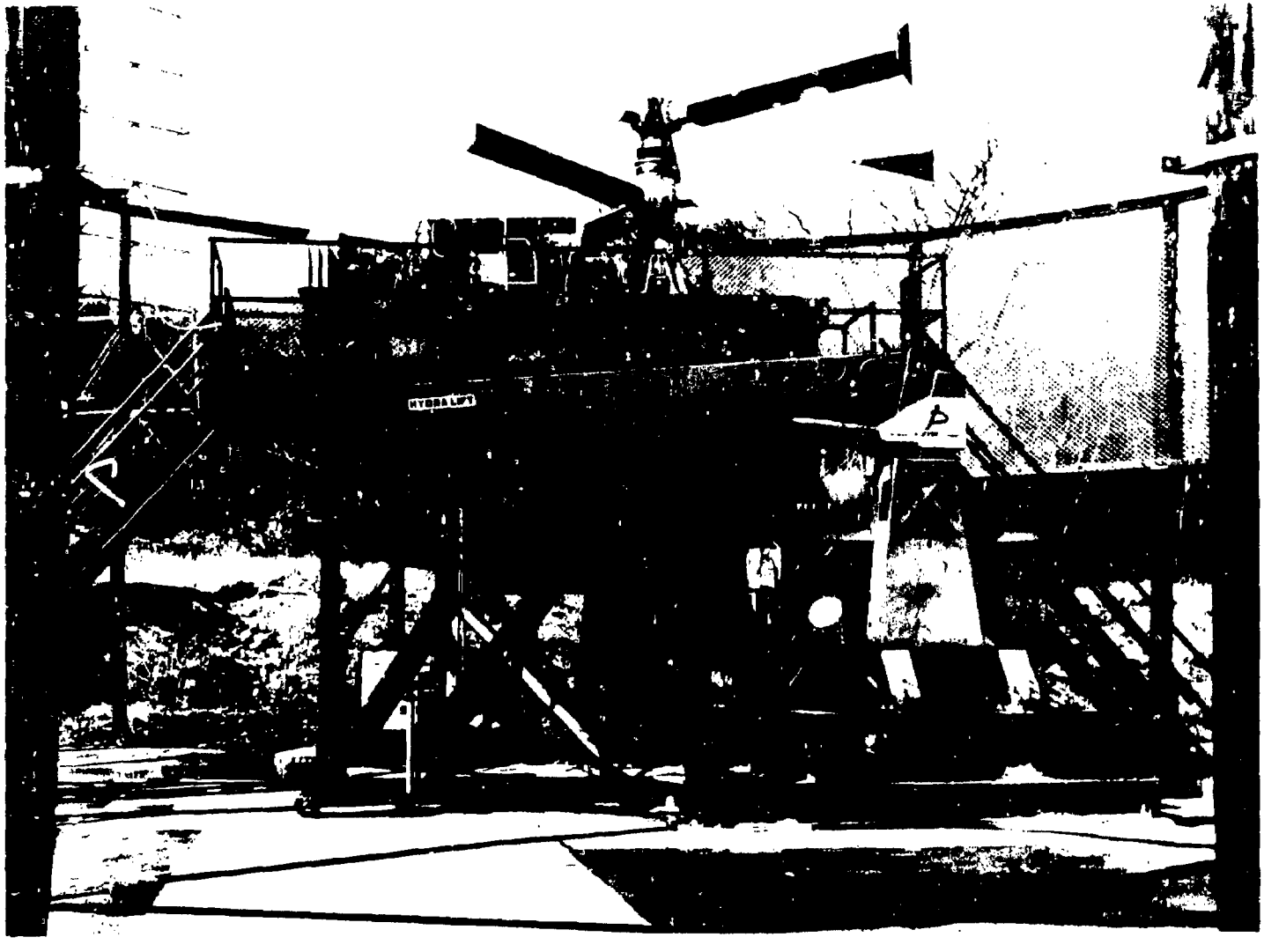

Figure 41. Test Clubs.

The entire facility fuel system, including the associated aircraft fuel system components, was tested for operation suitability.

The entire facility hydraulic system, including the associated aircraft flight control hydraulic system, was proof pressure tested to 4500 psi (1.5 times normal operating pressure).

The aircraft flight control system components between the rotor control servos and the blade horns were subjected to system proof, operation and spring rate tests to demonstrate airworthiness for both the test bed and the flight aircraft.

Powerplant functional and cooling tests were conducted to demonstrate airworthiness for both the test bed and the flight aircraft.

A powerplant transmission vibration survey was conducted to demonstrate airworthiness with the associated aircraft components installed on the test bed.

Rotor stress and motion plus rotor aeromechanical stability testing was conducted to determine loads and stresses in dynamic components for various test conditions as well as to demonstrate the absence of any rotor aeromechanical instability. Additional information obtained from these tests provided master strain gage measurement locations for both the test bed and the flight aircraft and established the test bed structural operating limits.

The final effort on the propulsion system test bed was the conduct of a series of four 50-hour endurance tests to demonstrate operational adequacy, structural integrity and airworthiness of the XH-59A propulsion and rotor systems. Each 50-hour segment was broken into five 10-hour spectrums of horsepower, rotor speed and rotor moments per Table 5. At the conclusion of each 50-hour segment all dynamic components, including the transmission and rotor blades, were disassembled and subjected to a thorough examination. All of the aforementioned tests plus the first 50-hour endurance segment and associated dynamic component teardown and examination were conducted prior to first flight of the aircraft. Subsequent tests were conducted to maintain a minimum of 2 hours of test bed endurance per aircraft flight hour until the final 200 hours of endurance was completed.

TABLE 5. PSTB ENDURANCE TEST SPECTRUM.

Item	Engines	Time (min)	Horsepower	Rotor Speed (%)	Roll Moment Per Rotor (ft-lb)	Pitch Moment Per Rotor (ft-lb)
Normal rated	1&2	30	1500*	100	26700	13500
Takeoff (low)**	1&2	30	900	100	20000	10000
Normal rated	1&2	30	1500*	100	20000	7000
Military (low)**	1&2	30	900	100	20000	7000
100% NRP	1&2	90	1500*	100	20000	8000
80% NRP	1&2	270	1200	100	20000	7000
60% NRP	1&2	90	900	100	20000	8000
Overspeed	1&2	6	1200	Max	31500	15000
Overtorque	1&2	12	1650	100	31500	8000
100% NRP	1	6	750	100	31500	10000
100% NRP	2	6	750	100	31500	8000

* Transmission design limit.
**Condition A-2 of MIL-T-8679.

AIRCRAFT GROUND TESTS

A series of aircraft ground tests were conducted on the aircraft prior to flight to assure that certain systems met their design criteria and that the aircraft and subsystem functioned properly. The majority of the tests were conducted prior to first flight in the pure helicopter configuration. Some of the tests were repeated prior to first flight in the auxiliary propulsion configuration. Ground tests relating to the auxiliary propulsion engines were also performed.

Hydraulic System Proof Pressure Tests

A hydraulic system proof pressure test was conducted for all aircraft hydraulic systems. The tests were conducted utilizing an external hydraulic source which was adjusted to provide one and one-half times the normal system operating pressure. The pressure was maintained for a minimum of 5 minutes while the system components were inspected for leakage and deformation.

A summation of the hydraulic system proof pressure testing is shown in Table 6.

TABLE 6. HYDRAULIC PROOF TEST.

System	Normal Pressure (psi)	Proof Pressure (psi)
Flight Controls - first stage	3000	4500
Flight controls - second stage	3000	4500
Stability Augmentation System	1000	1500
Elevator Control	1500	2250
Landing Gear	3000	4500
Auxiliary Propulsion Start System	3000	4500

Landing Gear Tests

Ground tests were conducted on the landing gear to assure proper operation. The tests were conducted by jacking the aircraft and providing normal hydraulic operating pressure from an external source.

The landing normal extension-retraction time was verified with the aircraft on jacks as follows:

Actuation	Time
Retraction	11.2 seconds
Extension	12.5 seconds

In additon to documenting the normal landing gear operation, testing was conducted to document the emergency landing gear blow-down system operation. This testing was conducted by timing the emergency extension with normal pressure in the nitrogen bottle and then reducing pressure in stages until the emergency extension was unsuccessful. A minimum pressure of 2500 psi was established for emergency blow-down.

Landing Gear Drop Tests

The translational free drop, reduced mass method of impact testing was used with the landing gear installed on a roller-guided basket of a guillotine-type testing machine. The mounting fixture duplicated the aircraft mounting geometry. Tests were conducted by lifting the drop mass to a predetermined height and then allowing it to free fall. The free-fall height was adjusted until the desired sink speed was attained. Testing was conducted with simulated touchdown speeds of zero and 60 knots. The nose gear was tested at a level touchdown attitude only. The main gear was tested at touchdown attitudes of level and 16 degrees nose up. Tests were conducted at an equivalent of 8 feet per second for the pure helicopter configuration and 6 feet per second for the auxiliary propulsion configuration.

During nose gear drop testing, 137 drops were made in determining the configuration of the metering pin. No change was made in the outstroke snubbing orifices. The nose gear performed satisfactorily throughout the test program except that the adiabatic compression of the air charge was producing air pressures that precluded the use of approximately the last 1.5 inches of the strut stroke. This was corrected by adding a spacer under the floating separator, increasing the compressed air volume to 5.03 cubic inches from 3.31 cubic inches. The fully extended inflation pressure was increased to 285 psig from 250 psig to maintain the 2-inch static strut positon. The results of the nose gear drop testing are presented in Table 7.

TABLE 7. XH-59A NOSE GEAR DROP TEST RESULTS.

ITEM	TEST CONDITION 1	2	3
Aircraft Gross Weight - lb	9000	9000	11,100
Sink Speed - ft/sec			
Required	8.0	8.0	6.0
Test Actual	8.18	8.10	6.14
Drop Height - in	11.93	11.93	6.72
Spin Up Speed - kt	0	60	60
Attitude - deg	0	0	0
Design Vertical Load - lb			
Max Allowable	5500	5500	4840
Max Test	5503	5552	4841
Strut Stroke - in.	8.54	8.45	8.33
Strut Inflation Press - psi	285	285	285
Tire Inflation Press - psi	65	65	65

During the main gear drop tests, 124 drops were made in determining the configuration of the metering pin. The main gear performed satisfactorily throughout the test program except that the adiabatic compression of the air charge was producing pressures that precluded use of approximately the last 1.5 inches of the strut stroke. This was corrected by the following:

1. An extension was added to the air side of the floating piston, increasing the fully compressed air volume to 11.88 cubic inches from 5.94 cubic inches.

2. The number of outlet holes which allow the outer oil chamber to fill rapidly was increased from 4 to 8.

3. The static position of the gear was reduced to 1.5 inches from 2.0 inches.

The results of the main gear drop testing are presented in Table 8. Inspections of both the main and nose gear showed no evidence of damage to either test gear.

TABLE 8. XH-59A MAIN GEAR DROP TEST RESULTS.

ITEM	TEST CONDITION 1	2	3	4	5	6
Aircraft Gross Weight - lb	9000	9000	9000	9000	11,100	11,100
Sink Speed - ft/sec						
Required	8.0	8.0	8.0	8.0	6.0	6.0
Test Actual	8.02	8.02	8.02	8.02	5.98	6.08
Drop Height - in	11.93	11.93	11.93	11.93	6.72	6.72
Spin Up Speed - kts	0	60	0	60	60	60
Attitude - deg nu	0	16	0	16	16	16
Design Vert Load - lb						
Max Allowable	6670	6670	7870	7870	5660	6560
Max Test	6560	6670	7870	7775	5660	6562
Strut Stroke - in.	8.61	8.60	8.70	8.68	8.18	8.22
Strut Inflation Press - psi	185	185	185	185	185	185
Tire Inflation Press - psi	135	135	135	135	135	135

Fuel System Calibration

Tests were conducted on the fuel system to verify and determine the following information:

Trapped fuel
Expansion space
Fuel flow rates
Unusable fuel
Pressure refueling
Defueling rate
Fuel system calibration
20 minute warning light

All design conditions were verified and all required information was obtained.

Aircraft Rigging

The rotor and aerodynamic control surfaces were rigged to the required values. Control system linearity and hysteresis tests were conducted to determine control system characteristics. In addition, the cyclic control stick rate damper characteristics were determined. The results of these tests are kept as a part of the permanent aircraft inspection records.

Control System Proof and Operations Tests

A control system proof and operations test was conducted for the rotor and aerodynamic control surfaces. The test was conducted to substantiate the structural integrity of the XH-59A stationary control system and system backup structure. The testing was conducted in the following sequence:

Conformity inspection
No load operation and clearance
Proof load and spring rate test
Post test inspection

Testing was conducted for forty combinations of control settings using the following simulated pilot forces at the cockpit flight controls:

Control	Force
Longitudinal	200 pounds
Lateral	100 pounds
Collective	150 pounds
Directional	300 pounds

All controls passed their respective proof and operations test requirements and the aircraft was cleared for flight.

Ground Runs

Ground runs were conducted on the aircraft in four stages to verify flight readiness. The configuration test sequence was as follows:

Bare head (blades removed)
Test clubs
Blades installed
Auxiliary engines installed

Bare Head Testing:

The aircraft was initially operated without the blades installed to conduct the following system tests and operational checks:

Engines(s) operation
Engine drive shaft critical speed test
System functional checks
System leak checks
Rotor shaft 1/rev. balance check
Data instrumentation checkout

Test Clubs:

The aircraft was configured with test clubs installed in place of the rotor blades as previously shown in Figure 41. The test clubs were designed to absorb power as a function of rotor speed. The initial test runs were designed to allow for a progressive development of transmission gear tooth contact patterns. Once proper gear tooth patterns were developed the test clubs were used to conduct a transmission run-in using an applicable time/power spectrum. The following system tests and operational checks were conducted with the test clubs installed:

Transmission gear pattern development
Transmission run-in
Engine speed control
Engine torque matching
System functional checks
Data instrumentation checkout

Blades Installed:

With completion of all other ground tests, the rotor blades were installed and the following system tests and operational checks were conducted:

Rotor 1 rev balance
Rotor track
Engine operating characteristics
System functional tests
Blade edgewise response
Data instrumentation checkout

With successful completion of all of the ground testing the aircraft was released for first flight in the pure helicopter configuration.

Auxiliary Propulsion:

After completion of the pure helicopter phase of the test program the aircraft was configured for the auxiliary propulsion phase. In addition to rigging, system checks, track and balance, and data instrumentation checkout, the following system tests and operational checks were conducted for the auxiliary propulsion engines:

Operational checkout
Installed performance calibration
Data instrumentation checkout
Fuel system functional check

With successful completion of the required auxiliary propulsion ground testing the aircraft was released for first flight in the auxiliary propulsion configuration.

AIRCRAFT SHAKE TESTS

Shake tests were conducted on the aircraft to provide airframe dynamic frequency response data and the associated airframe mode shapes. Four separate shake tests were conducted during the test program, two of which were conducted with the aircraft suspended and two with the aircraft resting on the landing gear.

The first shake test was conducted prior to the start of the pure helicopter test program phase. The aircraft was suspended using a fixture bolted to the upper rotor head at the blade sleeve attachment flanges. The aircraft was suspended from an overhead chain winch through bungee cords which were tuned to provide a rigid body frequency less than one hertz. The shaker used for this test was of the unbalanced mass type and was mounted to the upper rotor head suspension fixture.

The second shake test was conducted prior to the start of the auxiliary propulsion test phase. The purpose of this test was to determine the dynamic frequency response and associated mode shapes of the auxiliary propulsion thrust engine installation and the tail cone empennage. The tests were performed with the aircraft resting on its landing gear. Excitation was applied, using a constant force electro-dynamic shaker, directly to the auxiliary propulsion engines and to the empennage at several locations.

The third shake test was conducted at the completion of the 90-degree crossover auxiliary propulsion testing. The aircraft was suspended using a much improved suspension test fixture which incorporated hardware to eliminate rotor shaft to transmission case bearing slop which provided a more realistic simulation of actual flight conditons. Excitation was provided by an electro hydraulic inertial constant force shaker mounted to the upper rotor head suspension fixture. The scope of this shake test was substantially expanded over the first suspended shake test. Testing was divided into four separate aircraft configurations. The first configuration was tested simulating 90-degree crossover auxiliary propulsion testing in order to better understand airframe stress and vibration problems associated with the 90-degree crossover test data. The second test configuration was with the 90-degree crossover auxiliary propulsion configuration and two cabin mounted self tuning lateral absorbers. The third test configuration was with the 90-degree crossover auxiliary propulsion configuration with transmission to airframe elastomeric isolation. The fourth test configuration was with the basic auxiliary propulsion configuration, but simulating 0-degree rotor crossover.

The fourth shake test was conducted after initiation of flight testing with the 0-degree rotor crossover configuration. The purpose of this test was to determine the mechanism associated with the rudder control rod dynamic frequency and associated loads corresponding to data obtained from flight testing with the 0-degree rotor crossover configuraion. The testing was performed with aircraft resting on the landing gear. Excitation was applied, using a constant force electro-dynamic shaker directly to the empennage at several locations.

FLIGHT TEST PROCEDURES

TEST PHASES

The XH-59A was designed to be test flown as either a pure helicopter or a helicopter with auxiliary propulsion. The primary difference between the two configurations is the addition of the auxiliary propulsion thrust jets with their associated throttle control, fuel and engine start systems as well as a horizontal stabilizer incidence change. The only major instrumentation changes were for auxiliary propulsion engine monitoring and power measurement systems.

In keeping with the aircraft design philosophy, the total flight test program was structured to first fly in the pure helicopter configuration and then reconfigure the aircraft into the auxiliary propulsion configuration for flight evaluation. Both test phases were structured to provide a logical orderly buildup of the flight envelope. This was accomplished by first providing an incremental airspeed envelope expansion followed by an expansion of both the maneuver envelope and associated simulated system malfunctions at a lesser airspeed consistent with the prior airspeed envelope expansion end point. The maneuver/simulated system malfunction testing consisted of flight evaluations for turns, sideslip, control power, rotor speed, climbs, descents, load factors, roll rates, simulated stability augmentation system malfunctions, and simulated loss of engine power (both lift and propulsive) as applicable. In addition to these tests, the interrotor control trims were evaluated. In general, the magnitude of incremental airspeed envelope expansion was 20 knots.

During the flight test program a conservative approach was used to limit rotor and airframe stresses. A ground rule was established that trimmed flight points would not be attempted at flight conditions where any stress was projected to be above the fatigue endurance limit. A further conservatism was included in that many fatigue limits were determined by analyses, rather than test, and the analytical procedure is itself quite conservative.

Telemetry was used extensively to monitor aircraft data parameters during all phases of flying. This provided not only a reliable method of monitoring the aircraft on a safety basis but also became more important during the auxiliary propulsion testing in assisting the test team in expeditious use of flight time when fuel usage became more critical with four operating engines. The telemetry system was configured to display 20 data parameters. The 10 most critical parameters were displayed full time while the remaining 10 parameters were selectable by the test team, providing on-call monitoring of any recorded data parameter during the flight.

Data analysis was conducted between flights, and data trending versus predictions was correlated. Periodic data reviews were conducted with on-site Government representatives, normally at the completion of major incremental envelope expansion periods.

Pure Helicopter Testing

The pure helicopter test phase was subdivided into three separate test sequences. The first, under Test Plan 69G-3, was conducted to expand the aircraft envelope to 80 knots. The second, under Test Plan 69G-4, was conducted to expand the aircraft envelope to 140 knots. The last, under Test Plan 69G-5, was conducted to expand the envelope to V_D, to obtain classic performance and handling qualities data and to explore areas of interest bypassed during the initial envelope expansion testing. A summary of the pure helicopter testing is presented in Table 9.

Auxiliary Propulsion Testing

The auxiliary propulsion testing was subdivided into two separate sequences under Test Plan 69G-6. The first sequence provided for aircraft check flights after modifications were made to incorporate the auxiliary propulsion engines and to develop normal and emergency takeoff and landing procedures. The second sequence provided for flight testing of the auxiliary propulsion configuration to a maximum airspeed of 204 KTAS with 90-degree rotor crossover and to a maximum airspeed of 238 KTAS with 0-degree rotor crossover. A summary of the auxiliary propulsion testing is presented in Table 10.

TABLE 9. SUMMARY OF PURE HELICOPER TEST PHASE.

Test Plan	No. Flts.	Flt. Hrs.	Accomplishments
69G-3	19	12.4	Established stability augmentation system gains for low-speed flight, completed five-step cyclic control sensitivity evaluation, expanded flight envelope to 80 knots in 20-knot increments, obtained low-speed acoutsics data, obtained low-speed airspeed system calibration, and conducted first pattern flight at 80 knots.
69G-4	16	14.1	Envelope expansion to 140 knots, control power tests to 140 knots, roll reversals to 140 knots, load factor development to 140, elevator setting evaluations
69G-5	58	40.1	Envelope expansion to V_H, autorotation flares, altitude testing, level flight and hover performance, envelope expansion to V_D, airspeed calibration to V_H, yaw control power in descent, Government pilot evaluation, cabin vibration absorber tuning, elevator off flight evaluation, elevator setting evaluations, collective to elevator evaluation in descent, dive evaluation to simulate auxiliary propulsion configuration.

TABLE 10. SUMMARY OF AUXILIARY PROPULSION TEST PHASE.

Test Plan	No. Flts.	Flt Hrs.	Accomplishments
69G-6	9	4.3	Aircraft check flight with J-60 engine supports only, envelope expansion with J-60 engines installed but not operating. verified freedom from nose wheel shimmy, developed normal and emergency takeoff and landing procedures, conducted first pattern flight with auxiliary propulsion engines operating
69G-6	34	19.3	Envelope expansion to 204 knots true with 90° rotor crossover. Government pilot evaluation to 160 knots calibrated.
69G-6	34	15.8	Envelope expansion to 238 knots true with 0° rotor crossover. Government pilot evaluation to 210 knots calibrated

XH-59A DATA SYSTEM

The XH-59A was equipped with a full array of data measurement and recording systems to document the ABC Rotor Concept Demonstration Program. The data system consisted of both data measurement and recording systems typical of systems used throughout the rotary-wing industry, and systems designed or adapted specifically for use on the XH-59A aircraft. Included herein is a summary description of the XH-59A data system.

System Description

Data Acqusition System:

The airborne data acqusition system consisted of 130 data channels multiplexed into 13 tracks of data and recorded on a 1-inch intermediate band analog magnetic tape. The data acquisition system also contained a telemetry subsystem which can transmit two tracks of 10 data channels each via L-Band transmitters to a ground based station for on-line data review and/or processing.

Electrical Power:

The data acquisiton system was powered through a master power distribution box located on the instrumentation rack in the cabin. The power distribution box was connected to the aircraft 28 vdc electrical system through a 100-ampere current limiter and to the 115 vac 400 Hz 3-phase aircraft electrical system through a 15-ampere current limiter in each phase. This unit also contained current limiters for each distribution box output.

In the event of an emergency, power could be disconnected by a master instrumentation power switch located in the cockpit.

Wiring:

Airframe mounted transducers and measurement input sources were wired to centrally located terminal boards which were connected to a programmable patch panel through trunk lines. The patch panel facilitates the interconnection of transducer, signal conditioning, and calibration resistors to FM multiplexing of required measurements for the telemetry and tape recording systems. The cabin instrumentation is shown in Figures 42 and 43.

Rotating system measurements were wired to terminal boards located in the ring-shaped instrumentation cans mounted on each rotor head. Each instrumentation can contained two tracks (20 channels) of signal conditioning and FM encoding equipment. The FM multiplex output of the lower rotor in-

Figure 42. Cabin Instrumentation Rack - Forward Section.

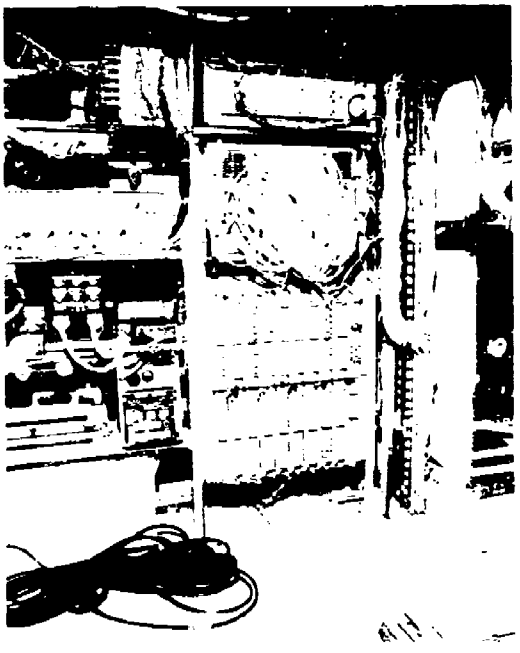

Figure 43. Cabin Instrumentation Rack - Aft Section.

strumentaion was coupled through a slip ring mounted between the lower and upper main rotor heads to join the output of the upper rotor instrumentation. The output of all four tracks (40 channels) or rotating measurements were routed through a second slip ring mounted on the bottom of the main gearbox to the telemetry and tape recording system (Figure 44).

Signal Conditioning

The aircraft contained 130 channels of low level signal processing modules. The basic functions of a module are: (1) condition the transducer signal to a ± 10 millivolt or a 0 to -10 millivolt level for input to the voltage controlled oscillators; and (2) to provide a means of calibrating the measurement on the ground and in the air. The signal conditioning modules were arranged in groups of 10 (10 channels) tape tracks with each group sharing a common mount and power supply. The calibration technique is accomplished by relays in each signal conditioning module which are controlled from the system control box. The type of signal conditioning module depends on the type of transducer installed to obtain the desired measurement. Three types of signal conditioning modules will handle the entire range of transducers installed on the aircraft.

Strain Gage Module:

The strain gage module is used for 1, 2, or 4 active strain gage installations and all potentiometer type transducers requiring external excitation. The module provides bridge power, voltage and balance controls, and series resistance calibration circuits. Potentiometers were wired into wheatstone bridge circuits with wing resistors for utilization with the strain gage module.

Voltage Source Module:

The voltage source module is used for all self-generating voltage transducers which have a voltage output proportional to the measured parameter. The module provides a switch selectable voltage divider that produces an output signal level of ±9 millivolts and a circuit to provide reference voltages for calibration. The full-scale input range for each switch position of the voltage source modules is tabulated as follows:

Switch Position	MS-350B Full Scale	MS-350C Full Scale
1	9 Mv	9 Mv
2	25 Mv	0.5 V
3	50 Mv	1.0 V
4	150 Mv	2.0 V
5	300 Mv	5.0 V

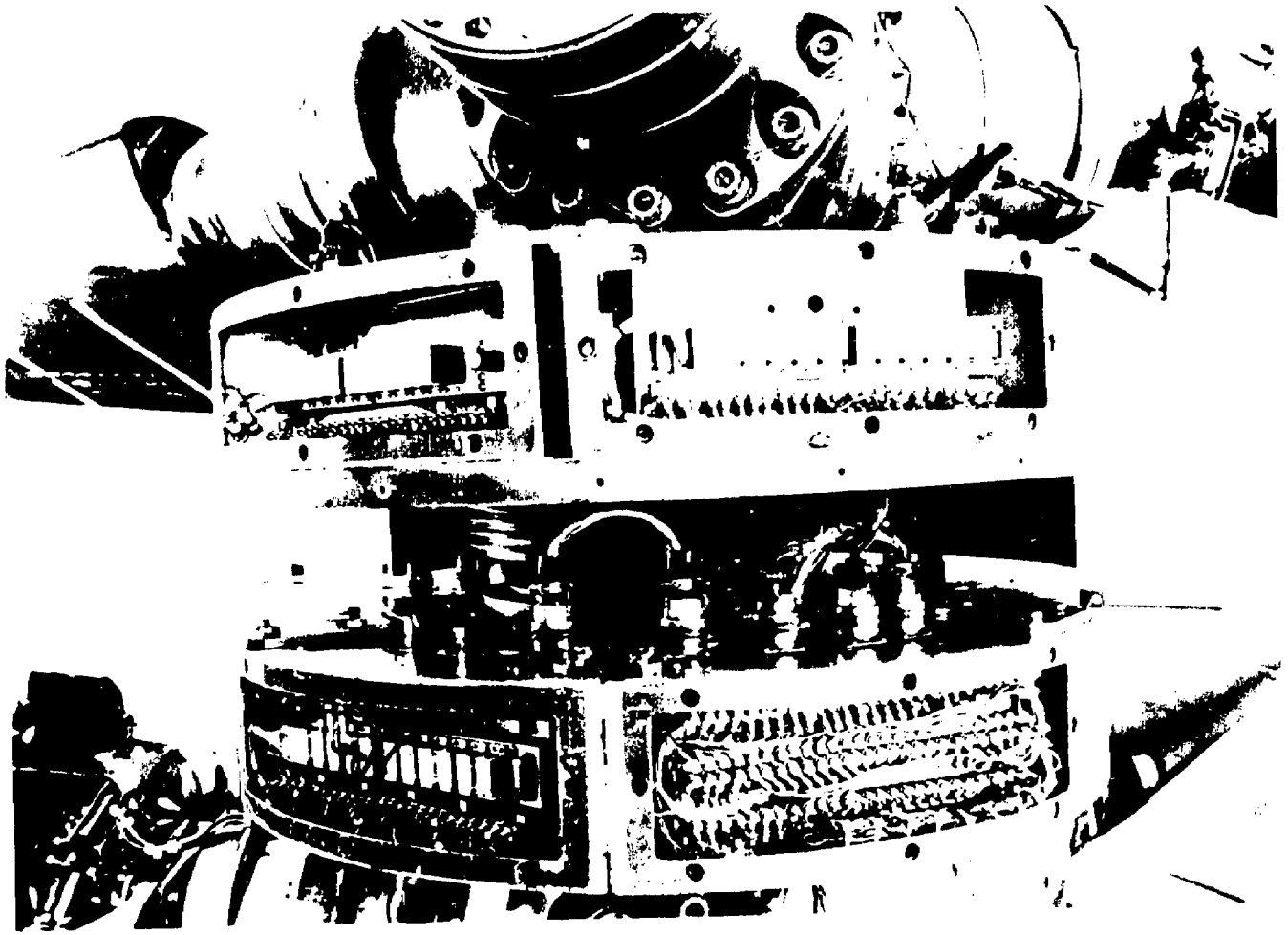

Figure 44. Output of Rotating Measurement Wiring.

Tach Generator Module:

The tach generator module is used to condition the output of the tach generators used to measure the engine and rotor speeds on the aircraft. The module converts the high-voltage, three-phase, low-frequency signal of the generators to a single-phase, low-level signal of three times the input frequency.

Encoding

This system employs Proportional Bandwidth Inter-Range Instrumentation Group (IRIG) low-level micro-minature voltage controlled oscillators (VCOs). IRIG channels 7 through 16 are used to accommodate the measurement frequency range. The VCO, which is basically high level (i.e., ±2.5 volt input), requires a pre-amp to accommodate this low-level (± 10 MV) signal from the signal conditioning module. The pre-amps are installed in the VCO mount adjacent to each high-level VCO. The center frequency and intelligence bandwidth on a per-track basis are as follows:

CHANNEL NO.	CENTER FREQ. (±7.5% DEV.) (Hz)	NOMINAL INTELLIGENCE BANDWIDTH (Hz)
1	2300	35
2	3000	45
3	3900	60
4	5400	80
5	7350	110
6	10500	160
7	14500	220
8	22000	330
9	30000	450
10	40000	600

The voltage controlled oscillator center frequency will deviate ±7½% with a ± 10 MV input signal. The intelligence bandwidth is that frequency, or lower, which can be recorded without signal attenuation at the VCO. (This intelligence bandwidth corresponds to the flat frequency response of galvanometers in light beam oscillographs.)

Each data track has a discrete track identification oscillator with fixed frequencies as follows:

TRACK NO.	OSCILLATOR FREQUENCY(Hz)
1	470
2	520
3	575
4	640
5	710
6	790
7	875
8	975
9	1080
10	1200
11	1335
12	1480

In additon to the 10 VCOs and track identification oscillator, each track incorporates an accurate 50 KHz frequency reference oscillator. The reference oscillator, 10 VCOs, and 1 track identification oscillator frequencies are summed by a summing amplifier with the multiplex available for magnetic tape recording and/or telemetry transmission.

Recording Equipment

The data acquisition system recording media was a Bell and Howell Model MARS-2000 14-track airborne analog magnetic tape recorder. The magnetic tape used was 1.0 inch in width, 1.0 mil thickness on a 10½ inch reel, and 3600 feet in length with a recording speed of 15 IPS providing 45 minutes of record time. The recorder meets the following specifications:

(1) MIL-E-5400K Class I
(2) MIL-I-6181D
(3) MIL-T-5422 (ASG)
(4) MIL-STD-70KA
(5) IRIG Document 106-73.

The recorder data track assignment was as follows:

Track No.	Record Ampl.	Data
1 to 13	Direct record	FM Multiplex Data (10 data channels/tracks)
14	Direct record	Run and Calibration tones

Telemetry

The aircraft was configured with two UHF L-Band telemetry transmitters and associated switching to provide air to ground data transmission of up to 20 FM multiplexed data channels. The primary transmitted signal contains the selected track (track 5) of master parameters. The secondary transmitter, switchable in flight, has the capability of telemetering any of the 12 other multiplexed tracks of data recorded on tape.

System Control and Operation

All data acquisition system control functions were performed by a master control box (P/N SLGNM-1840) installed in the test vehicle cabin with a remote control unit in the cockpit for system record start/stop capability only. The specialized electronic systems can be remotely controlled by the tape control box in addition to being individually controlled. A digital display for data burst number was installed in the cockpit instrument panel.

In addition to the normal static preflight data calibration, the system is capable of "in-flight" simultaneous calibration of all parameters. This is accomplished by relays installed in each signal conditioning module controlled by the tape control box.

The operating mode of the recording system is determined by five different tones (frequencies) which were multiplexed on Track 14. The five tones are identified as follows:

(1) RUN (5.0 kHz) - comes on 2½ seconds after the tape recorder has been started to indicate the tape is up to recording speed and data sampling can commence.

(2) ZERO CAL (6.5 kHz) - indicates the signal conditioning modules have removed bridge power from all transducers.

(3) RESISTANCE CAL (8.0 kHz) - indicates the signal conditioning modules have applied a series calibration resistance which simulates a known percentage of full-scale parameter physical input.

(4) X-DUCER CAL (10.0 kHz) - indicates the signal conditioning modules have returned the transducer to its operating state with bridge power applied.

(5) BEEPER (12.5 kHz) - this tone is used as an alternate to the run code for identification of a particular portion of a data burst (panel). The 12.5 kHz tone is introduced on command and stays on until the off command is initiated.

Transducers

Strain Gages:

Airframe total stress and force measurements were obtained using Micromeasurement 350-ohm temperature compensated strain gages configured in a one, two or four active gage Wheatstone bridge.

Accelerations and Vibrations:

Acceleration and vibration measurements were obtained using a number of different types of transducers. The selection of transducers was dependent on the application and required installation. Tranducers used for general airframe acceleration measurements include:

Statham	AG9TC-5-350
C.E.C.	4-202-0146 4-202-0001
Endevco	2262-25C

A separate measurement was made of cockpit low-frequency acceleration using Kistler 303M123-3 servo accelerometers with an active low pass filter unit TGN95-01016.

Powerplant vibration measurements were made using Vibrametrico Vibramite 14C vibration pickups and Endevco 6233 piezoelectric accelerometers with special cables and the Engine Vibration Measurement System FGN95-01053. The Engine Vibration Measurement System converts the charge output of the accelerometer to a voltage, integrates the voltage to a signal proportional to engine vibration, and band pass filters this output for the desired frequency response.

Engine Performance:

Engine performance measurements were made for electrical and hydraulic tie-ins to the regular aircraft instrument systems. Gas turbine speed (N_1), power turbine speed (Np), and turbine inlet temperature were all measured with electrical tie-ins to the appropriate aircraft instrument systems. Engine torques were measured using pressure transducers (Data Sensor and C.E.C. 4-356-0001) plumbed to the engine torque pressure outputs.

In auxiliary propulsion mode the primary measurement of J-60 engine thrust was the engine pressure ratio (EPR). EPR is measured by electrical tie-in to the standard aircraft instrument transducer. The synchro output of the transducer was converted to a voltage proportional to EPR by Natel synchro to DC converters P/N 416-1C-400-11GLZ.

Air Reference Measurements:

Air reference measurements include airspeed, altitude, sideslip and angle of attack. A sensor head P/N FTD-1 was mounted on the end of an 8-foot-long noseboom to extend it forward out of the influence of the fuselage and rotors. The sensor head combines a self-aligning pitot-static probe (gimballed) with vanes to measure sideslip and angle of attack.

Airspeed was measured with a standard airspeed indicator for cockpit display and a Data Sensors PB409B ±3 psig differential pressure transducer for the instrumentation system.

Altitude was measured with standard cockpit displays and a Rosemount 1241A4BLDEE transducer for the instrumentation system.

The sensor head vanes provided a potentiometer output which was conditioned to a Wheatstone bridge for recording on the instrumentation system. A high level output of the VCO preamplifiers is used to drive cockpit displays of these measurements.

Outside air temperature was measured using a Rosemount P/N 102AUICK resistance total air temperature probe mounted on the aircraft fuselage. The resistance output of the probe is conditioned to a Wheatstone bridge for magnetic tape recording.

Attitudes:

Aircraft pitch and roll attitudes were measured using a Lear Siegler P/N 9000C attitude gyro. Natel synchro to DC converters P/N 416-1C-400-11GLZ were used to obtain analog signals proportional to aircraft attitude.

Angular Rates and Acceleration:

Aircraft pitch, roll and yaw rates and accelerations were measured utilizing Hamilton Standard 3 axis DC/DC rate/acceleration package (P/N 10-08307-009). The package contains three rate gyros and associated electronics which provide three analog signals proportional to rate and three analog signals (derived from the rate signal) proportional to angular acceleration.

Control Positions:

Control positions were measured using a variety of linear and rotary potentiometers conditioned to Wheatstone bridges. Cockpit display of control positions was provided from the high level output VCO preamplifiers. The following control positions were measured on the XH-59A Flight Test Vehicle:

1. Longitudinal Cyclic Stick Pos.
2. Lateral Cyclic Stick Pos.
3. Collective Stick Pos.
4. Rudder Pedals Pos.
5. Differential Longitudinal Actuator Pos. (A_1')
6. Differential Lateral Actuator Pos. (B_1')
7. Differential Collective Trim Pos. ($\Delta\theta_t$)
8. Control Phase Angle (Γ)

Upper and lower main rotor blade pitch was measured using ±30-degree angulators mounted on the main rotor blade cuffs. The angulators are torsional force transducers that provide a Wheatstone bridge output proportional to shaft angular displacement.

Specialized Electronics:

Specialized electronic systems were provided in the data acquisition system to provide signals for cockpit displays and/or magnetic tape data recording.

Load Factor System (Sikorsky Aircraft P/N SLGNM-1472):

This system provided the following capability:

(a) Pilot display for:

(1) continuously monitoring load factor during the maneuvers.

(2) peak reading positive and negative load factor attained during the maneuver (upon pilot's command) at the completion of the maneuver.

(b) Load factor signal for magnetic tape recording utilizing either FM multiples or P.C.M. techniques. The signal was ±1.0 vdc for the measurement range of -1.5 to ±3.5 g's.

The transducer was a Kistler Instruments Model 303M132 or Systron Donner Model 4311AR-3.5-P97 servo accelerometer with power and signal conditioning an integral part of the electronics. The pilot had a remote control unit at his disposal for cockpit display calibration and reading of peak load factors attained.

Expanded NR System:

This system accepts the 3X input frequency output of a tach generator signal conditioning module taken from the high level output of a VCO preamplifier and converts it to a voltage proportional to main rotor speeds. Two precision reference oscillators included in the system can be switched to replace the input for calibration purposes. The voltage output is used for magnetic tape recording and to drive a digital cockpit display of NR with a resolution of 0.1% main rotor speed.

71 + 1/Rev. System:

This system measured rotor azimuth by means of a specially slotted ring mounted on the bottom of the upper main rotor shaft and slotted optical block containing two light sources and two photodetectors. As the ring is rotated the photodetectors are alternately exposed and blocked from the light sources, creating a pulse train with pulses every 5 degrees of rotor azimuth (72 pulses per rotor revolution). To identify 0 degree rotor azimuth the system is configured to generate an inverted pulse polarity such that each rotor revolution creates a pulse strain of 1 negative and 71 positive pulses. This pulse train output was used for magnetic tape recording and to provide rotor azimuth information for the blade tip separation monitor.

Blade Tip Separation Monitoring System:

The Blade Tip Path Monitoring System (TPM) was an electrical system which detected the minimum blade tip separation (air gap capacitance) and crossing point occurrence of the upper and lower rotors, and displayed this information in real time on analog (displacement) and digital (crossing point) meters to the pilot. The system also displayed and held, for at least 30 seconds, this minimum blade tip separation.

The outboard region of all blades contained painted conductive surfaces that functioned as antennas. The lower blades were the transmitters (approximately 16 kHz) and the upper blades were the receivers. The system measured the separation between all pairs of blades during each revolution and displayed the minimum value and corresponding azimuth position for each revolution. This data was linearized (the raw data is approximately inversely proportional to the distance squared), drove the cockpit display, was recorded on the aircraft data tape, and was available for transmittal via telemetry to the ground station.

Cockpit Displays:

In addition to the standard aircraft indicators the XH-59A flight test vehicle contained the following cockpit instruments (Figures 45 and 46):

1. Expanded NR
2. Load Factor
3. Tip Path Clearance and Azimuth
4. Longitudinal Cyclic Stick Position
5. Lateral Cyclic Stick Position
6. Collective Stick Position
7. Rudder Pedal Position
8. Differential Longitudinal Control Position
9. Differential Lateral Control Position
10. Differential Collective Control Position
11. Control Phase Angle Position
12. Sideslip
13. Angle of Attack

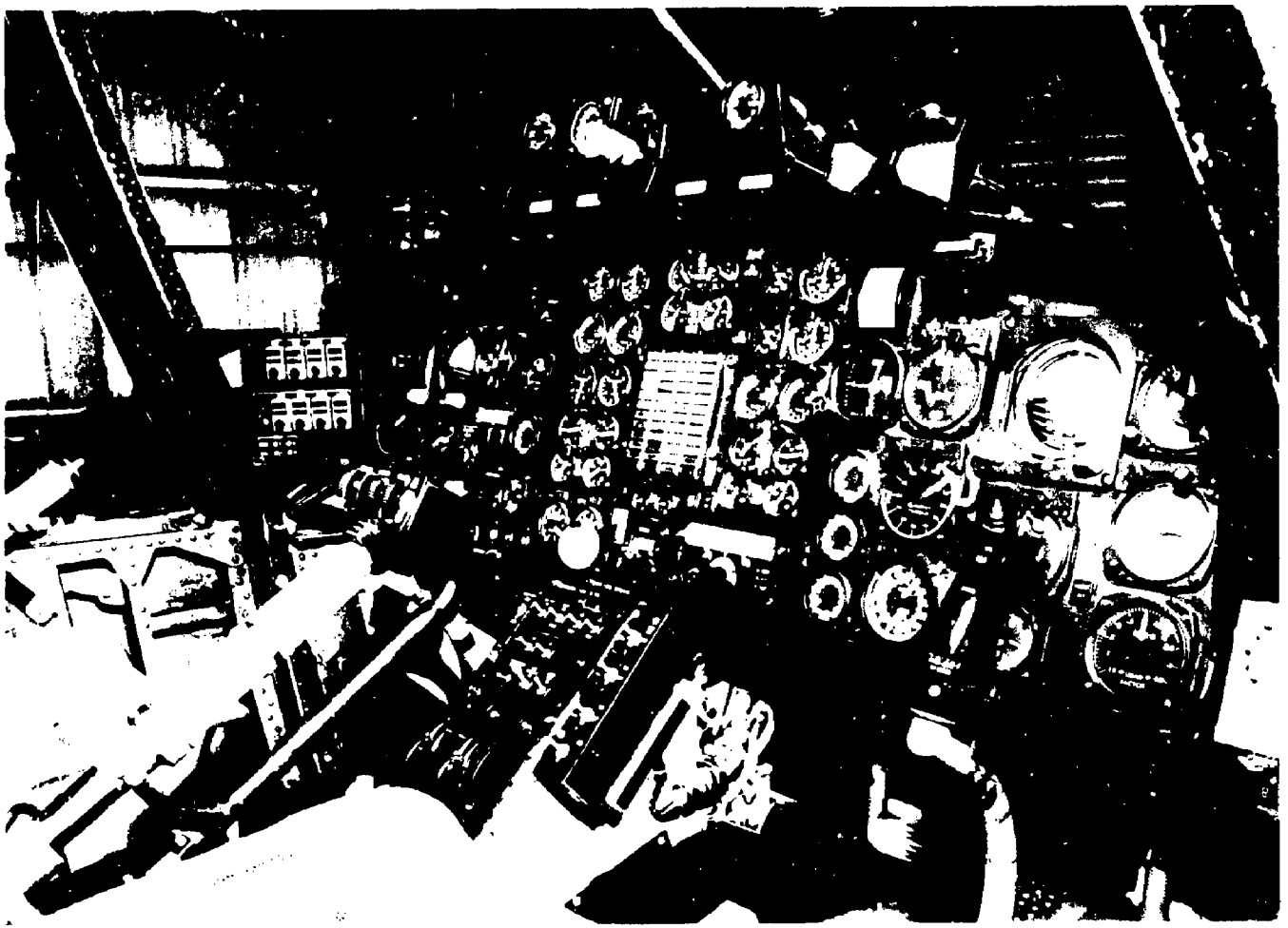

Figure 45. Cockpit Instrument Panel - Pilot's Side.

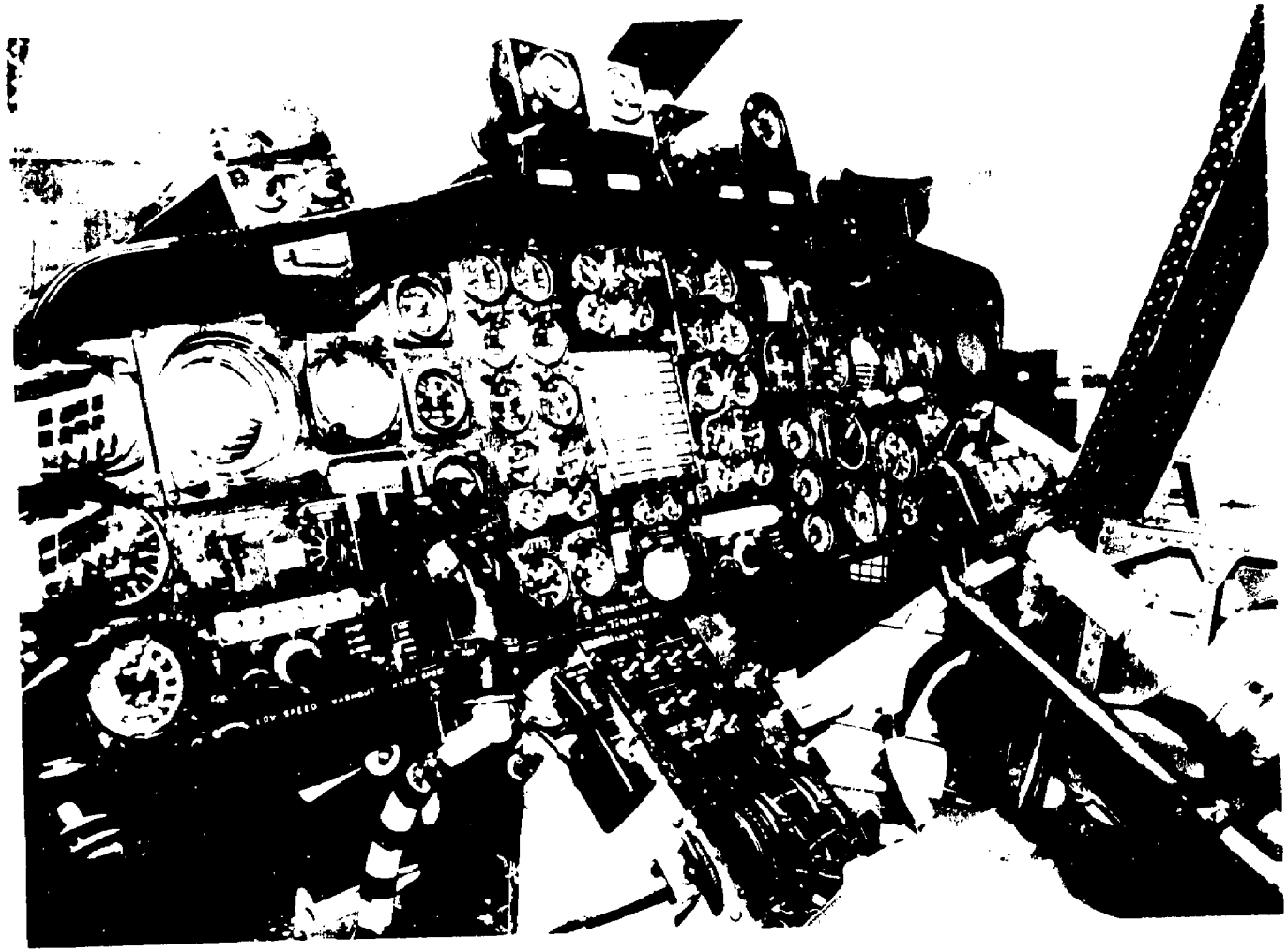

Figure 46. Cockpit Instrument Panel - Copilot's Side.

PURE HELICOPTER TEST RESULTS

FLIGHT ENVELOPE

In general the helicopter flight envelope was opened up in 20-knot increments in forward flight. In addition, sideward and rearward flight envelopes were established using a pace method. Maximum velocities obtained in each flight regime are presented in Table 11.

TABLE 11. PURE HELICOPTER SPEED ENVELOPE.

Regime	True Airspeed (knots)	Limit
Forward Flight - Nominal Sea Level	156	Power Avail
Forward Flight - Nominal 10,000 ft	150	Power Avail
Sideward Flight - Right	40	10% Control Margin
- Left	35	10% Control Margin
Rearward Flight	30	10% Control Margin

The demonstrated XH-59 lift capability is shown in the load factor envelope (Figure 47). This figure presents the actual rotor lift developed to trim and maneuvering flight and relates it to the helicopter design gross weight of 9000 lb in terms of load factor.

The maximum nondimensional blade loading (C_t/σ) developed throughout the flight envelope is presented in Figure 48. The ABC rotor's ability to maintain lift with increasing speed is clearly evident.

The range of density altitude covered in the envelope expansion for both level flight trim and dive conditions is shown in Figure 49.

Sideslip and bank angle envelopes are presented in Figures 50 and 51.

Rotor speed ranges for power-on and power-off flight conditions are shown in Figures 52 and 53.

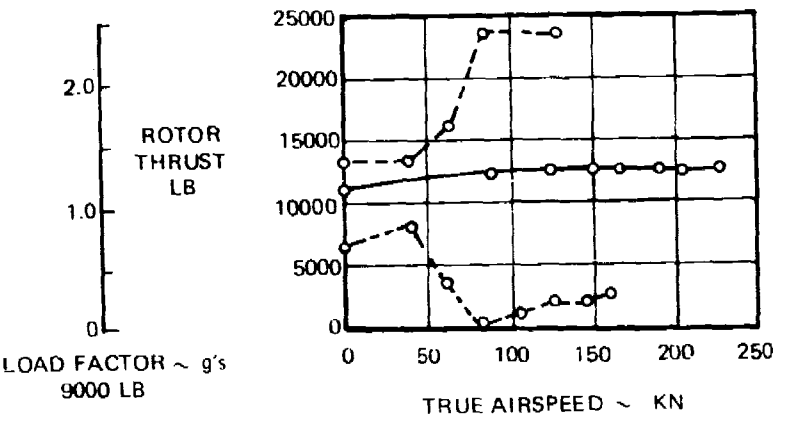

Figure 47. Helicopter Load Factor Envelope - Power On.

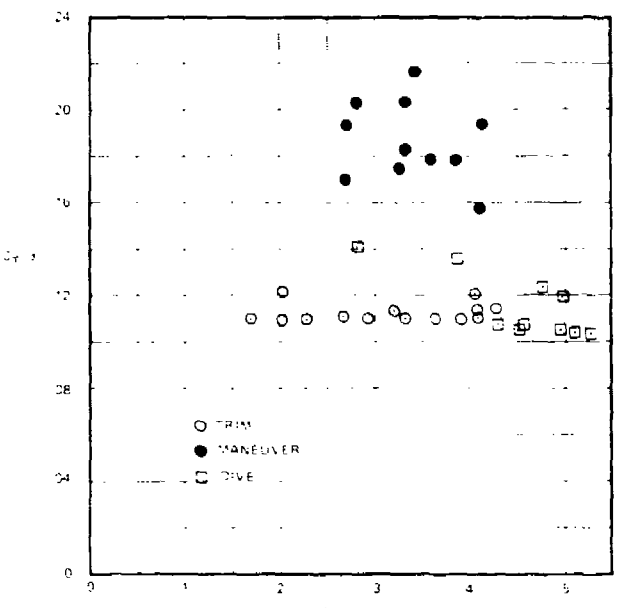

Figure 48. Maximum Blade Loading, Helicopter Configuration.

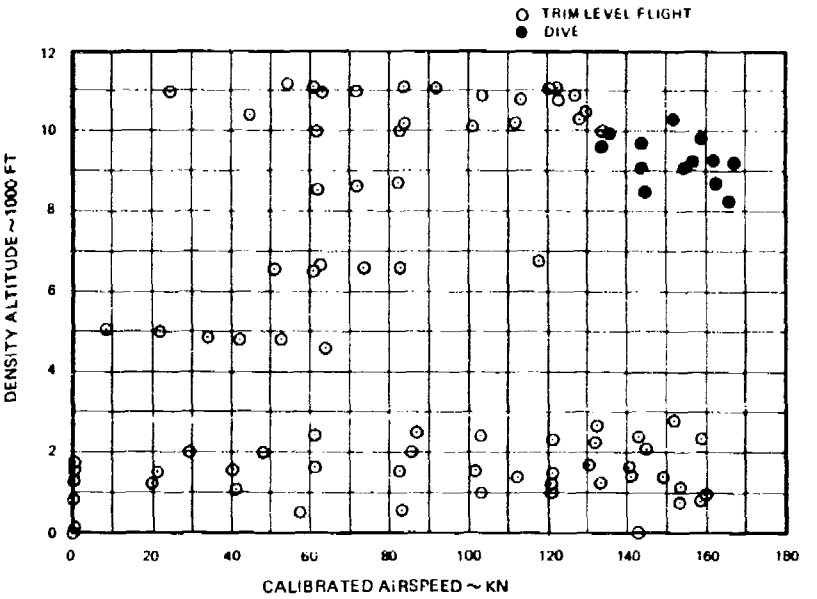

Figure 49. Altitude Envelope, Helicopter Configuration.

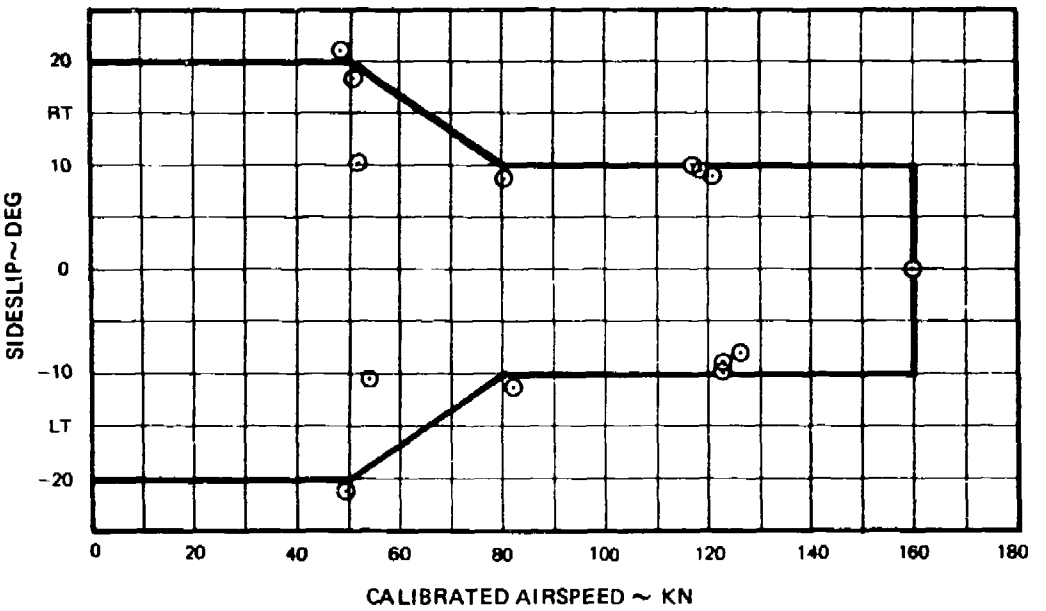

Figure 50. Sideslip Envelope, Helicopter Configuration.

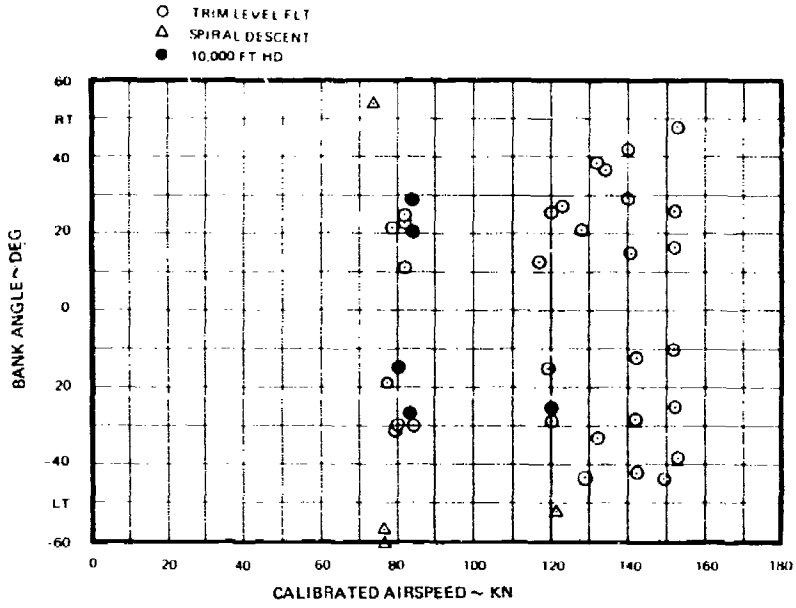

Figure 51. Bank Angle Envelope, Helicopter Configuration.

17
F

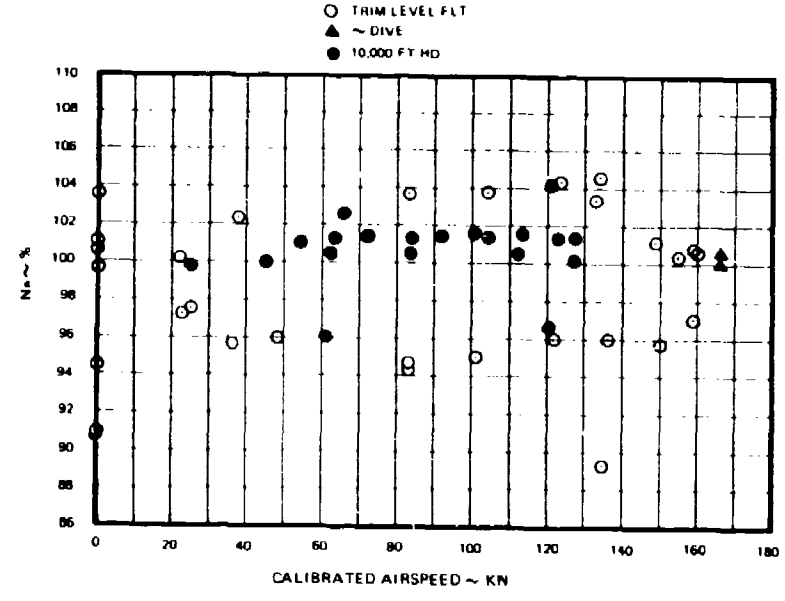

Figure 52. Power On Rotor Speed Envelope, Helicopter Configuration.

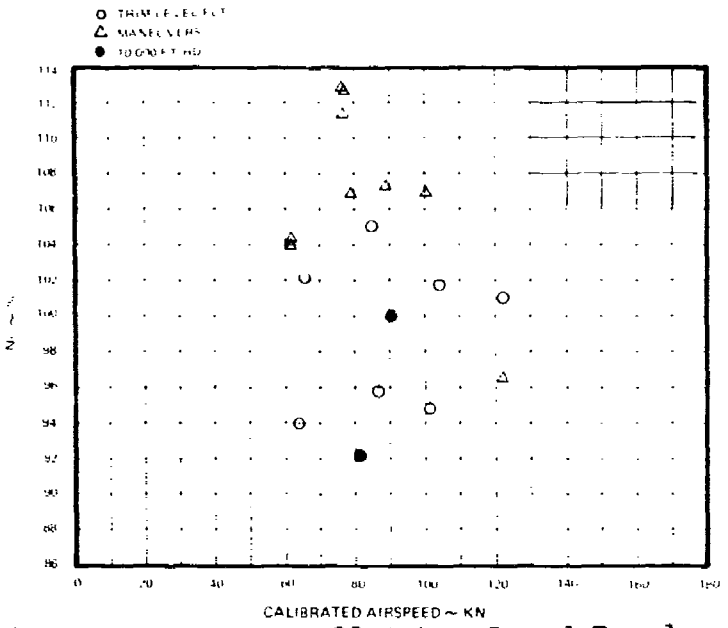

Figure 53. Power Off Rotor Speed Envelope, Helicopter Configuration.

PERFORMANCE

In the pure helicopter configuration, dedicated performance flights were flown for hover and level flight. The aircraft configuration for these flights is shown in Table 12. 17 B

TABLE 12. AIRCRAFT PERFORMANCE TEST CONFIGURATION (HELICOPTER).

	Hover	Level Flight
C.G. Location	297.0 in.	297.0 in.
SAS	ON	ON
Stabilizer Incidence	+10 deg	+10 deg
Elevator Angle	Fixed at Zero	Variable, Coupled to Collective
$\Delta\theta_{w.o.}$	100%	Auto Adjust, q Sensing
Γ	20 deg	30 deg to 80 kt, 60 deg 100 kt to V_H
A_1'	0 deg	-0.5 deg
B_1'	0 to +2 deg	0 deg
$\Delta\theta_T$	-	-0.5 deg

Hover Performance

Free flight hovering performance tests were conducted at 10,000 lb and 11,000 lb gross weights at wheel clearances of 10, 20, 35 and 75 feet. Wheel clearances were established using a weighted, calibrated rope. Power requirements at each wheel clearance were measured at $N_R/\sqrt{\theta}$'s of 92, 95 and 100 percent. Additionally, B_1' was varied between 0 and 2 degrees while hovering OGE. This changes the rotor lift distribution in such a way as to increase the interrotor moment. Test results are plotted in the nondimensional form of C_W versus Cp in Figures 54, 55, and 56. Test data points are coded to retain identification by $N_R/\sqrt{\theta}$, but curve fairings were made without regard to tip Mach number. Figure 56 indicates that on the average, power requirements increase with increased B_1'.

The derived transmission efficiency (η) of .95 and calculated vertical drag of 6 percent were used to extract main rotor thrust and power from these data. This yields a main rotor figure of merit of .79 at a nondimensional blade loading (C_T/σ) of approximately 0.1 (Figure 57). A comparison of the aircraft system figure of merit (based on gross weight and total power required) between the XH-59A and several existing aircraft is shown in Figure 58. The 11 percent improvement in hover efficiency shown over the most advanced current aircraft is derived both from improvements provided by the coaxial rotor system and absence of a tail rotor.

Level Flight Performance

Level flight performance was tested throughout the airspeed range from 20 knots to V_H at W/δ's of 11,000 lb and 13,000 lb at 100 percent $N_R/\sqrt{\theta}$, thereby depicting power requirements at C_W's of 0.01084 and 0.01281. Additionally, high-speed level flight performance (100 knots to V_H) was tested at 105 percent $N_R/\sqrt{\theta}$ for C_W equals 0.01084 to determine the effect of advancing blade Mach number (compressibility) on level flight power requirements. Γ was then varied between 30 degrees and 68 degrees, to the extent that blade tip clearance and structural considerations would permit, in the 80-knot to 120-knot speed range to optimize the Γ versus airspeed schedule from a performance standpoint. Γ schedule optimization was flown at W/δ equals 11,000 lb, $N_R/\sqrt{\theta}$ equals 100 percent, C_W equals 0.01084.

Figure 59 presents level flight power required data corrected to standard sea level conditions for 11,000 lb and 13,000 lb gross weight at 100 percent N_R. Figure 60 shows level flight power required data in the nondimensional form of Cp and M_{ADV} versus M for C_W equals 0.01084 at $N_R/\sqrt{\theta}$'s of 100 and 105 percent, and Figure 61 shows nondimensional Cp and M_{ADV} versus

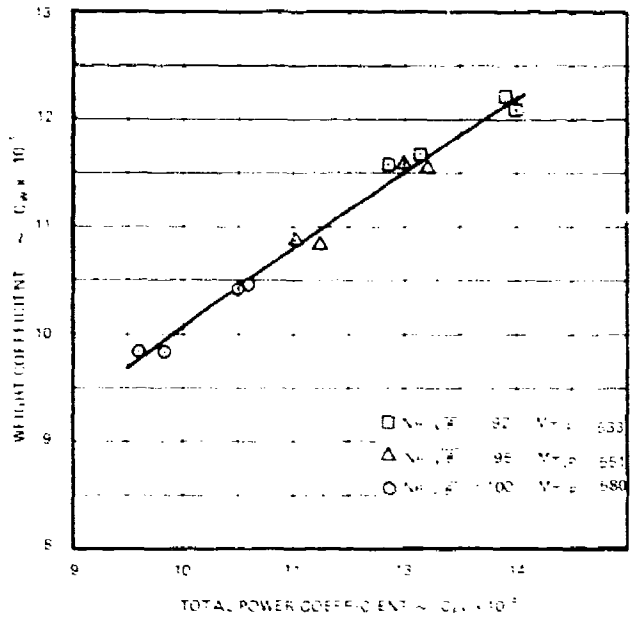

Figure 54. Nondimensional Hovering Performance 10 Ft. Wheel Clearance.

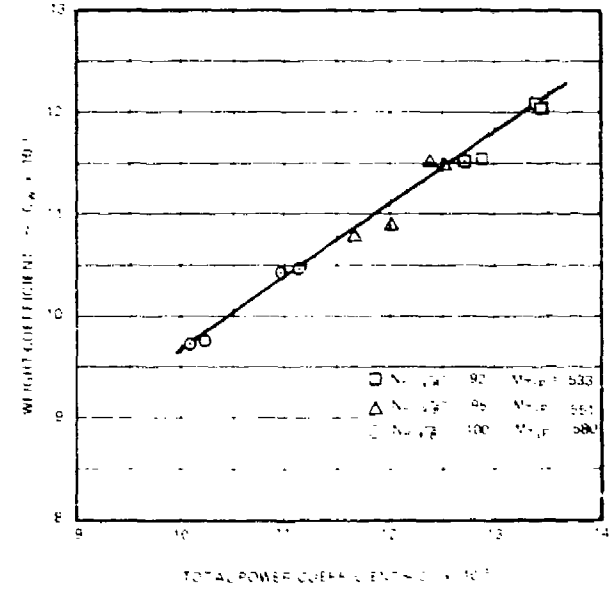

Figure 55. Nondimensional Hovering Performance 20 Ft. Wheel Clearance.

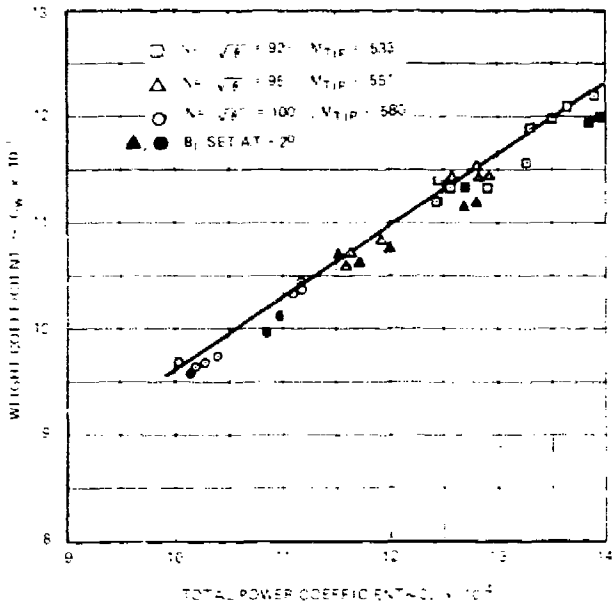

Figure 56. Nondimensional Hovering Performance Out-of-Ground Effect.

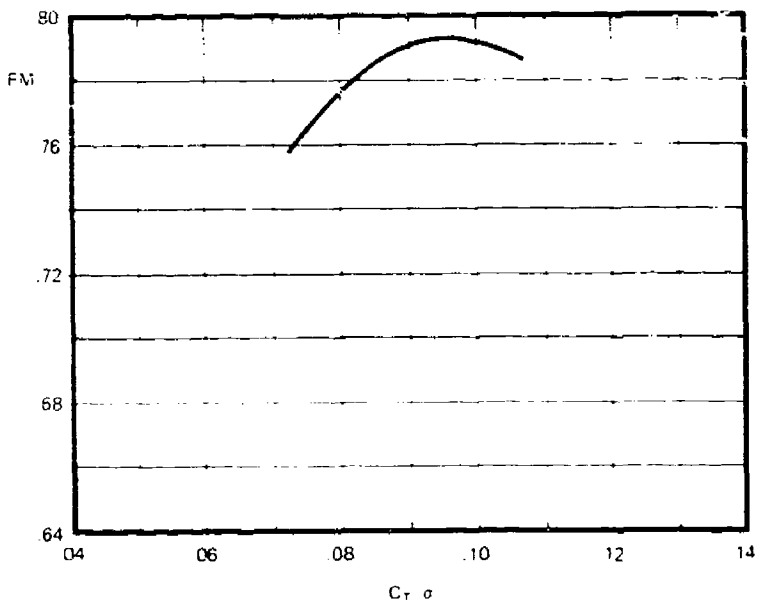

Figure 57. Main Rotor Figure of Merit.

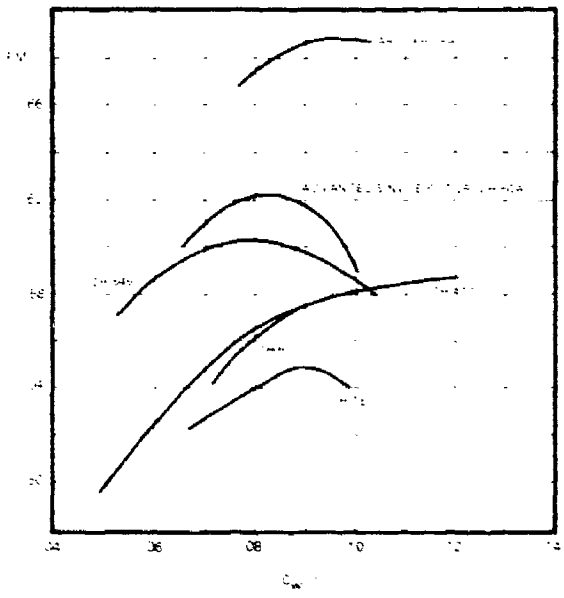

Figure 58. Aircraft System Figure of Merit.

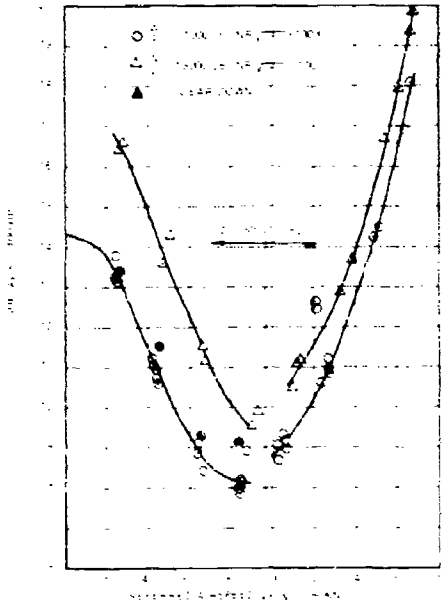

Figure 59. Level Flight Performance, Helicopter Configuration.

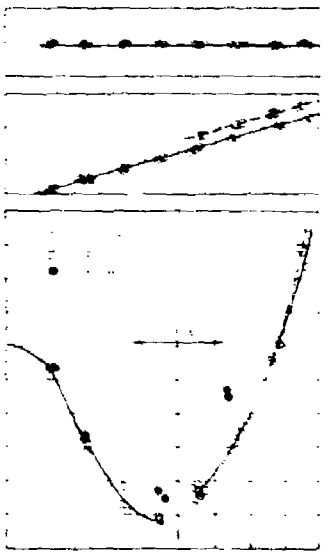

Figure 60. Nondimensional Level Flight Performance, Helicopter Configuration.

μ data for C_W equals 0.01281 at 100 percent N_R/θ. Figure 62 shows power required data record for all Γ settings. Data points are coded to retain identification by Γ angle. Figure 63 was constructed to optimize Γ at each airspeed for which Γ variations were performed. Deviations from the main airspeed within each data group were accounted for by applying the speed-power curve slopes. These data substantiate predicted trends, shown by solid lines, indicating that level flight power requirements could be minimized by flying the following schedule:

Airspeed	Γ
30 to 80 kt	30 deg
100 kt	40 deg
120 kt	50 deg
140 kt to V_H	60 deg

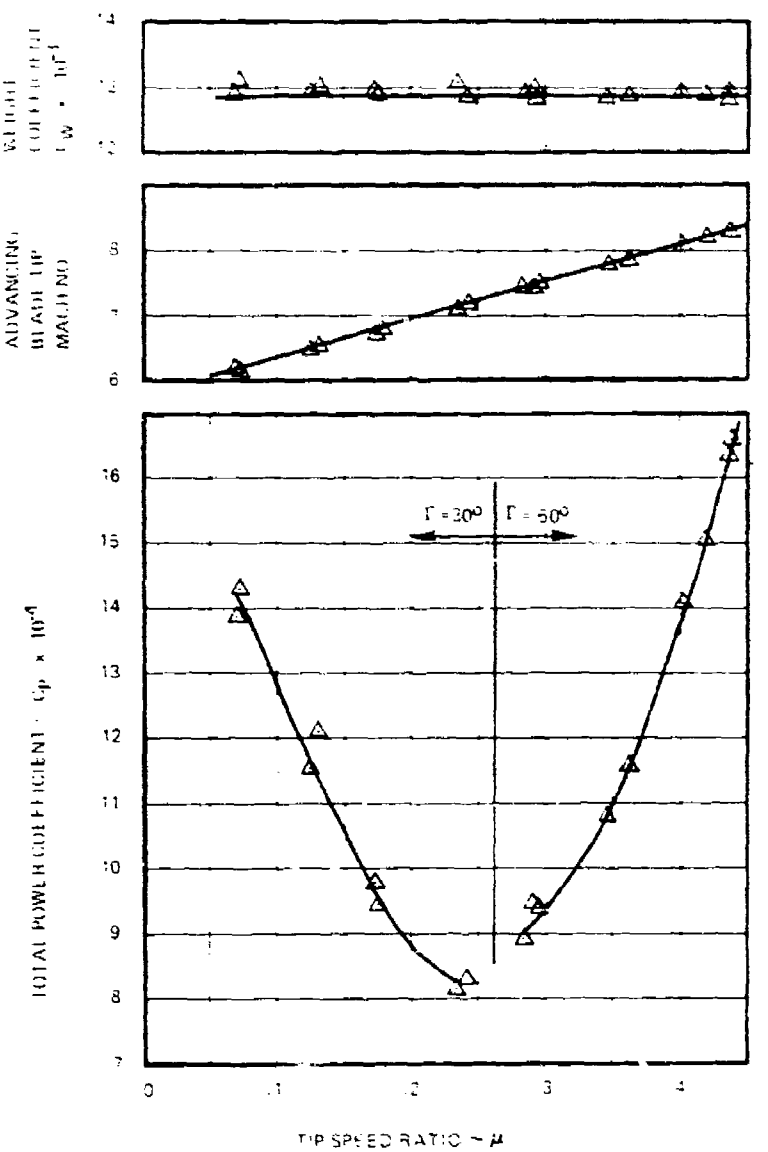

Figure 61. Nondimensional Level Flight Performance, Helicopter Configuration.

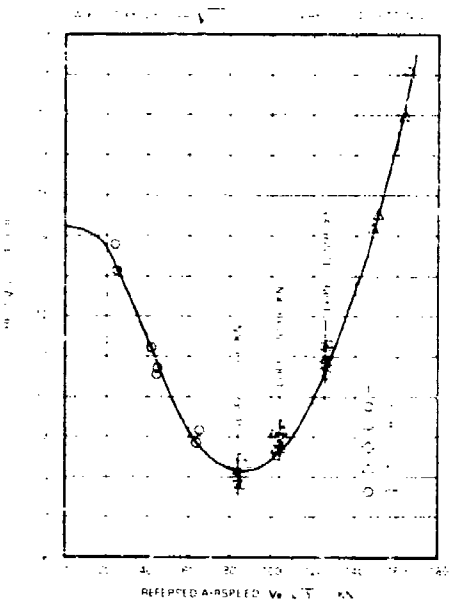

Figure 62. Level Flight Performance, Helicopter Configuration.

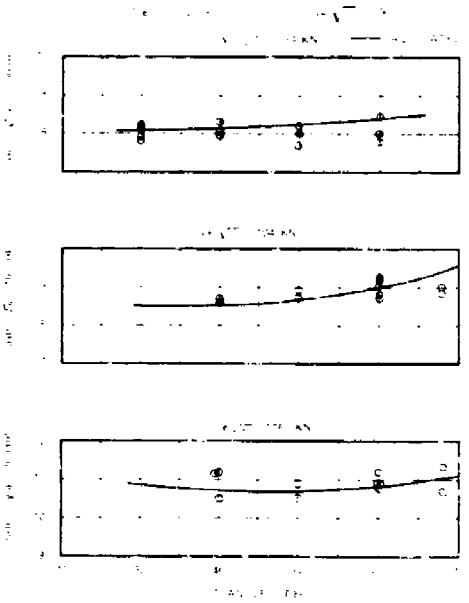

Figure 63. Level Flight Performance, Helicopter Configuration.

Figures 64 and 65 present dimensional and nondimensional level flight power required curves for the optimized schedule.

Figure 64 also shows the impact of installed instrumentation (primarily the instrumentation cam installed between the two rotors) on power required. This instrumentation increases equivalent drag 2 square feet. The dashed line in Figure 65 shows what the power required would be without the instrumentation installed.

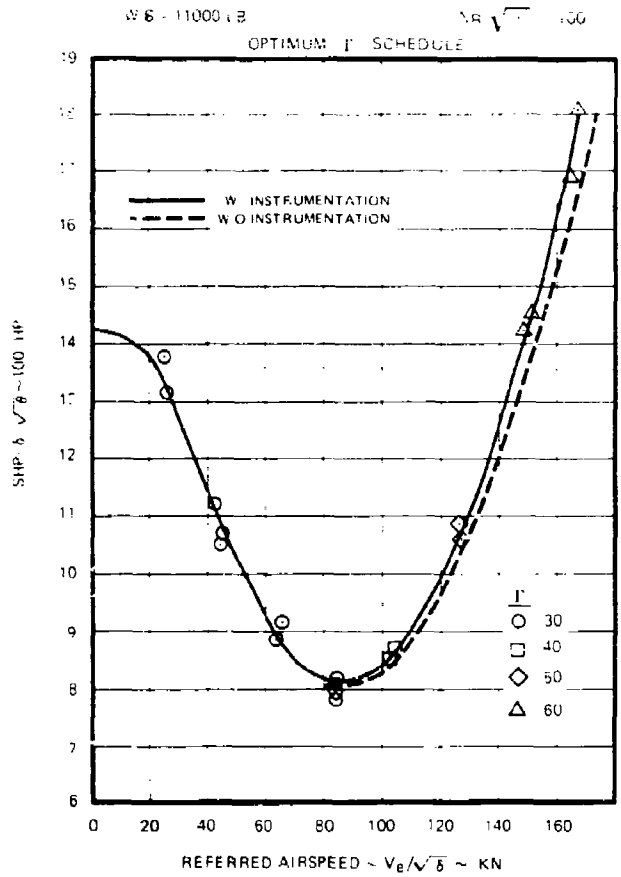

Figure 64. Level Flight Performance, Helicopter Configuration.

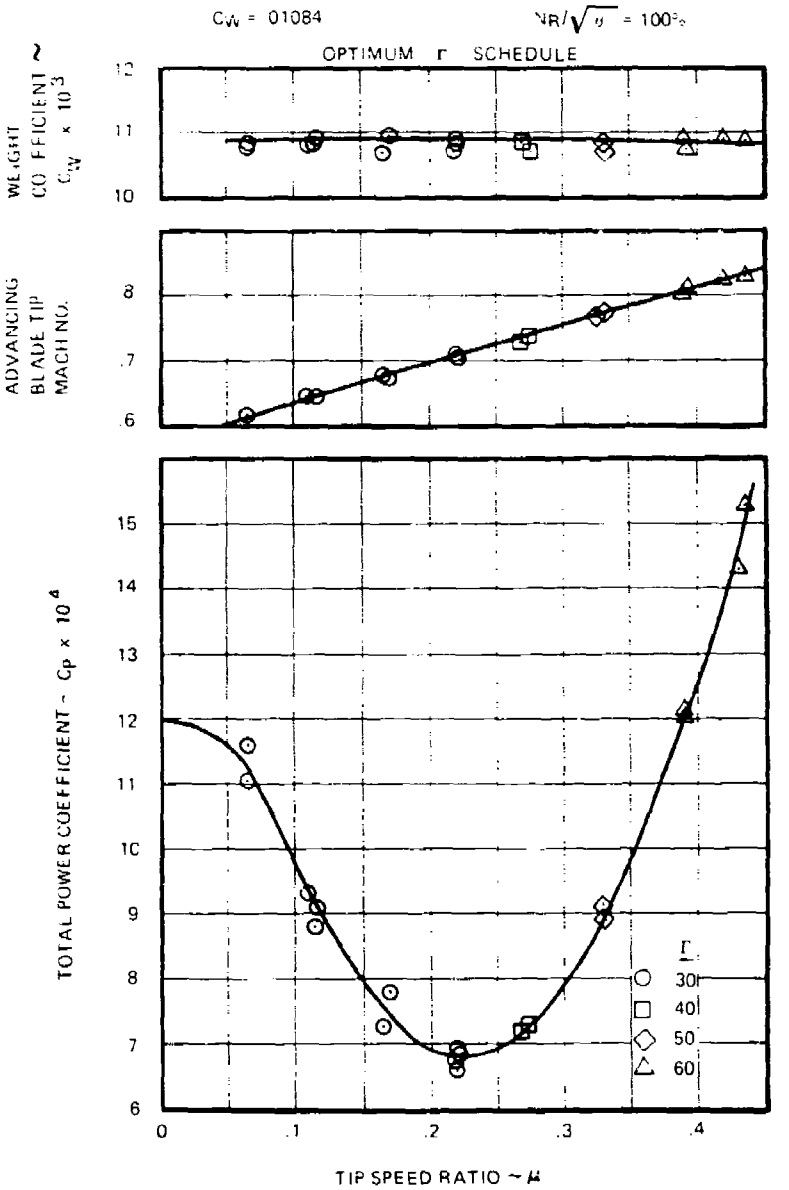

Figure 65. Nondimensional Level Flight Performance, Helicopter Configuration.

HANDLING QUALITIES

Stability, control and handling, and flying qualities were evaluated in detail during the 66.6 flight hour ABC Pure Helicopter Flight Research Program. In the initial tests, 6.1 hours of hover and low-speed flying were used to checkout all systems including the cyclic stick dampers and stability augmentation system (SAS). A subsequent 6.3 hours were used to optimize SAS gain and to evaluate control power, control margins, lateral/directional static stability, control phase angle (Γ), flare capability and simulated SAS hardovers, all at forward flight speeds up to 80 knots. In the final 54.2 hours, these handling qualities characteristics were explored at level flight speeds to 156 KTAS and dive speeds to 186 KTAS.

Hover and Low-Speed Flight

Ground Taxi:

Forward taxi to 15 knots ground speed and left and right taxi turns were performed. Adequate yaw control was available and control orientation was normal with rotor control phase angles up to 40 degrees and with the collective stick set at 25 percent. With the collective stick setting of 15 percent, no yaw control existed. Pedal movement, stop-to-stop, produced no heading change. With collective stick lowered to full down (negative rotor thrust), yaw control was reversed and fairly strong.

Hover:

Control Sensitivity Buildup and SAS Optimization:

The initial 10 flights were conducted to investigate increases in pitch and roll axes control sensitivity and damping in hover. Control sensitivity was increased by discrete changes in control linkage geometry, and damping was increased by feedback gain adjustments in the rate channel of the SAS. Low initial cyclic control sensitivities were used as a precaution to avoid pilot-induced-oscillation (PIO) with the high control power ABC rotor system. No PIO tendencies were encountered in either the pitch or roll axes. Initial and final hover values for control sensitivity and damping are shown in Figures 66 and 67 for the pitch and roll axes, respectively. Note that control sensitivity in pitch was essentially finalized at a setting of -.15 degree cyclic feathering per degree per second. This final SAS-on damping to control sensitivity provided a terminal rate of 7.2 degrees per second per inch of longitudinal cyclic input and a Cooper-Harper rating of 3.0. Control sensitivity in roll was initially doubled for flight

and a SAS rate gain setting of -.065 degree cyclic feathering per degree per second roll rate was used. This gave a terminal rate of 5.0 degrees per second per inch and a Cooper-Harper rating of 3.0. Subsequent side flight tests suggested that more lateral sensitivity was desirable; a 25-percent increase was implemented. Terminal rate was increased to 6.0 degrees per second per inch and pilot rating remained unchanged and therefore no further adjustment was made to SAS rate gain. SAS-off testing in hover was found to be acceptable (Cooper-Harper rating of 6.0) although terminal rates of 15.5 degrees per second per inch in pitch and 11.9 degrees per second per inch in roll were attained.

For the ABC rotor system, using differential torque between the upper and lower rotors resulting from differential collective application through pedals, the MIL-H-8501A criteria are not valid since they were developed for tail rotor systems. The differential collective used on the ABC system allows high yaw rates (in excess of 45 deg/sec) to result from 1 inch pedal step inputs that are easily arrested by opposite pedal input. This allows large rapid heading changes with little tendency to overshoot.

Directional characteristics available with differential collective between the rotors was rated good by the pilot although damping is below MILH-8501A minimum criteria and control sensitivity is only marginally above the minimum criteria (Figure 68).

Hover Trim Control:

The effects of wind direction on aircraft trim control positions for a 10-foot wheel height hover are presented in Figure 69. The aircraft was trimmed in successive increments of 45-degree heading changes to the left in a 2- to 3-knot wind condition. Control variations are small with the low wind, but the cyclic control was always into the wind; forward stick for nose into the wind, left stick for left side to the wind, etc. Stabilized hovers with controls fixed were maintained quite easily.

The effect of ground proximity on control positions in hover is shown in Figure 70. For wheel heights from 2 to 25 feet above the ground, collective control position increased by about 14 percent and total engine power increased almost 30 percent. Longitudinal, lateral and pedal control positions were not significantly changed.

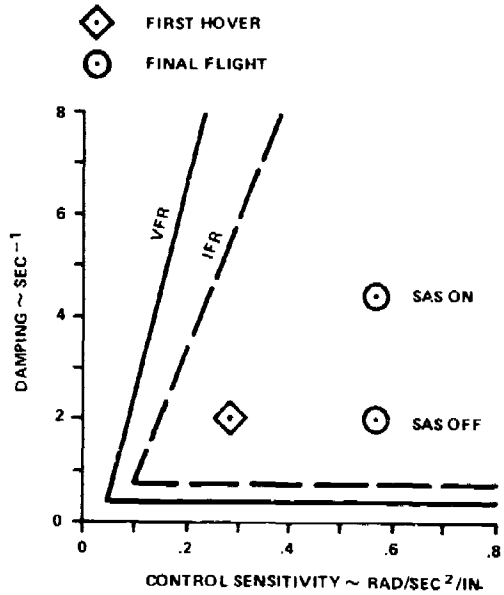

Figure 66. Hover Pitch Control Power-Damping Characteristics, Helicopter Configuration.

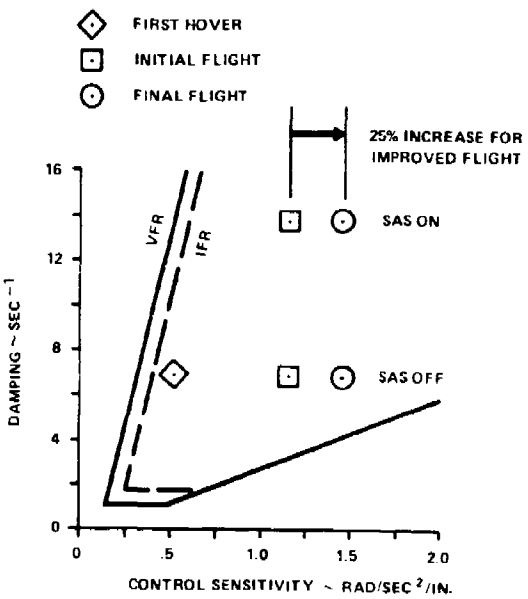

Figure 67. Hover Roll Control Power-Damping Characteristics, Helicopter Configuration.

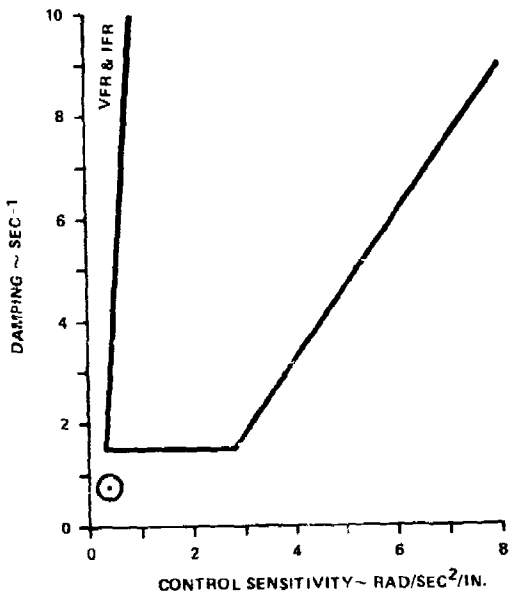

Figure 68. Hover Directional Control Power-Damping Characteristics, Helicopter Configuration.

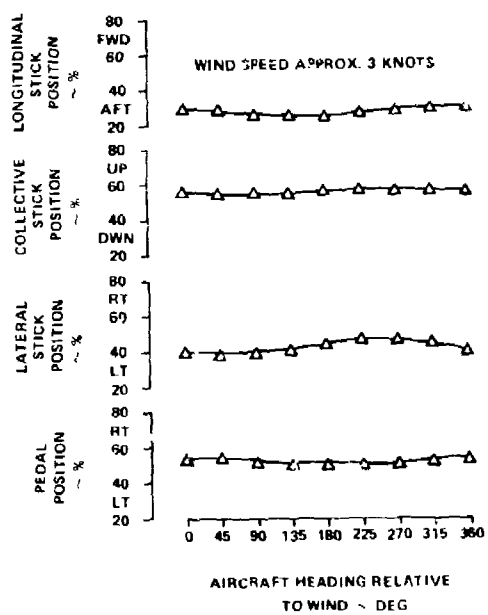

Figure 69. Effects of Wind Direction on Trim Control Hover, Helicopter Configuration.

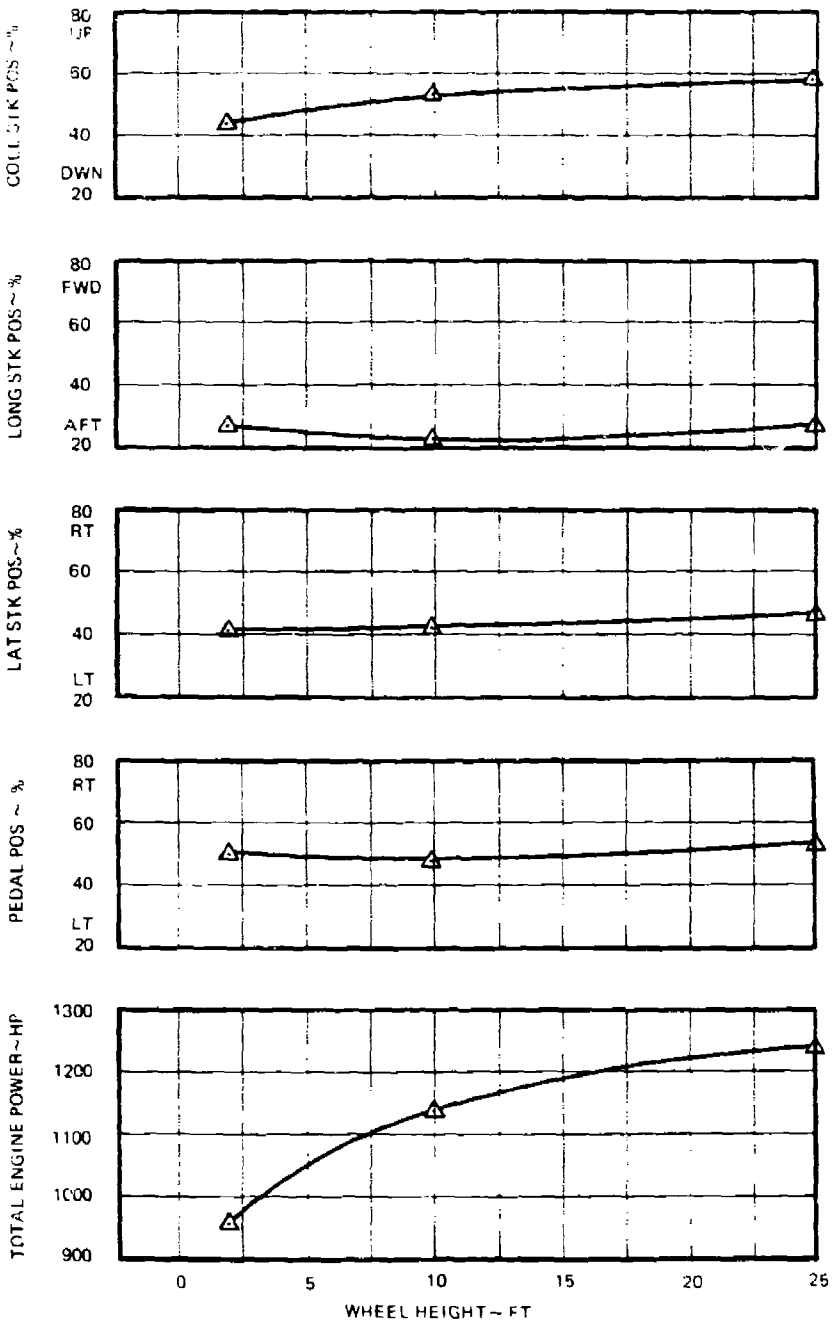

Figure 70. Controllability in Hover, Helicopter Configuration.

Hover/Low-Speed Turns:

Rapid hover turns were performed in both left and right directions. The time history of a right turn is shown in Figure 71. Note that the aircraft demonstrates a relatively smooth turning characteristic. Cross coupling into pitch or roll, as frequently encountered on single-rotor helicopters, is noticeably absent. In general, turns were easier to perform with the ABC than with conventional helicopters. Full 360-degree turns were completed in 6 to 10 seconds with very accurate final heading control. Note in Figure 71 the flat attitude of the aircraft throughout the turn. Surface winds were 5 to 10 knots and are reflected in the 10 percent longitudinal and 20 percent lateral stick motion. Pedal movement was up to 81 percent for turn initiation and up to 43 percent for recovery from the turn.

The pilot task in performing zero sideslip turns at speeds below 30 knots was considerable, due to pedal requirements for coordination. This workload dropped very quickly at speeds above 40 knots. Turn maneuvers were conducted at bank angles to 40 degrees at 60 knots. No pitch-roll coupling was evident during the normal rates used for the turns.

Hover Dynamic Stability:

The pitch and roll SAS-ON damping provided the aircraft with dynamic stability characteristics that exceeded MIL-H-8501A requirements (Figure 72). This is also substantiated by the aircraft response to a typical longitudinal control reversal in hover (Figure 73). During all low-speed maneuvers, aircraft stability was good. This was also true for SAS hardover responses and SAS-OFF flight.

Single channel SAS hardovers were evaluated for both single and dual axes for a number of hover flight conditions. Response of the aircraft to hardovers was very mild. In most cases, no corrective action was taken by the pilot for several seconds. Hardovers were five percent control authority and the operating channel tended to compensate for the hardover channel. An example of a simultaneous aft-right hardover at hover is shown in Figure 74. Pilot corrective action was taken about 3 seconds after the hardover. Attitude data were not available but pitch rate reached 15 degrees per second and roll rate about 6 degrees per second. Lift-off, hover and landing were conducted with both channels of SAS turned off. Aircraft response was mild and the aircraft remained easily controllable although the reduced aircraft damping, about halved as shown in Figures 66 and 67, was apparent to the pilots.

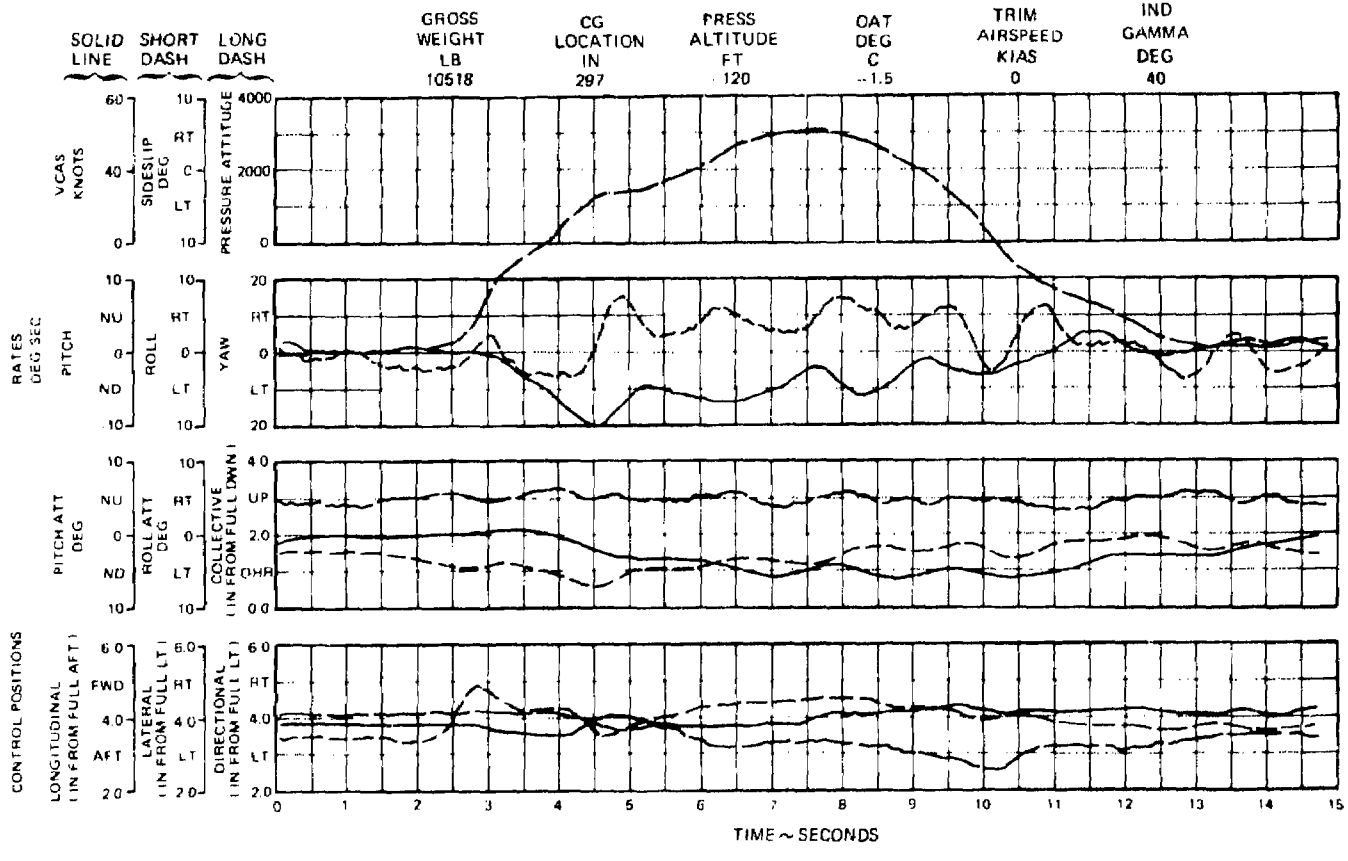

Figure 71. Rapid Hover Turns in Both Left and Right Directions, Helicopter Configuration.

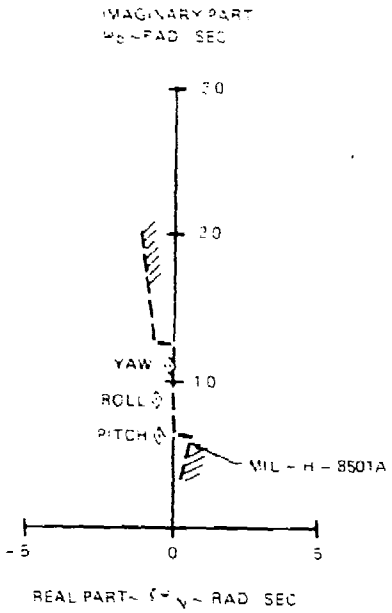

Figure 72. Hover Dynamic Stability Characteristics (SAS On), Helicopter Configuration.

Yaw Oscillation/Side Force Disturbance:

Aircraft random yaw oscillations and lateral translations were apparent when hovering in ground effect (wheel heights below 10 feet). Random yaw and lateral translation, equally strong in either direction, required pedal displacements of up to ±20 percent to contain the yawing moment, while a displacement of the lateral cyclic in the same direction was required to hold a stationary point over the ground. As the external forces acting on the aircraft reversed randomly, the control displacements required created a heavy pilot workload. Crosswind hovers at 10-foot wheel heights with doors on or off were stable, but with slightly different trimmed control positions.

It was theorized and confirmed by observation of tufts mounted on the airframe that unsteady separation of rotor downwash flow around the nose of the aircraft was creating the forces. In an attempt to stabilize the flow, flow separators or strakes were attached to the sides of the fuselage to trip the flow of rotor downwash and fix the separation point. The addition of strakes along the lower sides of the aircraft reduced the magnitude of the disturbing force to a level that required only small annoying control motions. Figures 75 and 76 provide a comparison of the disturbing forces with strakes

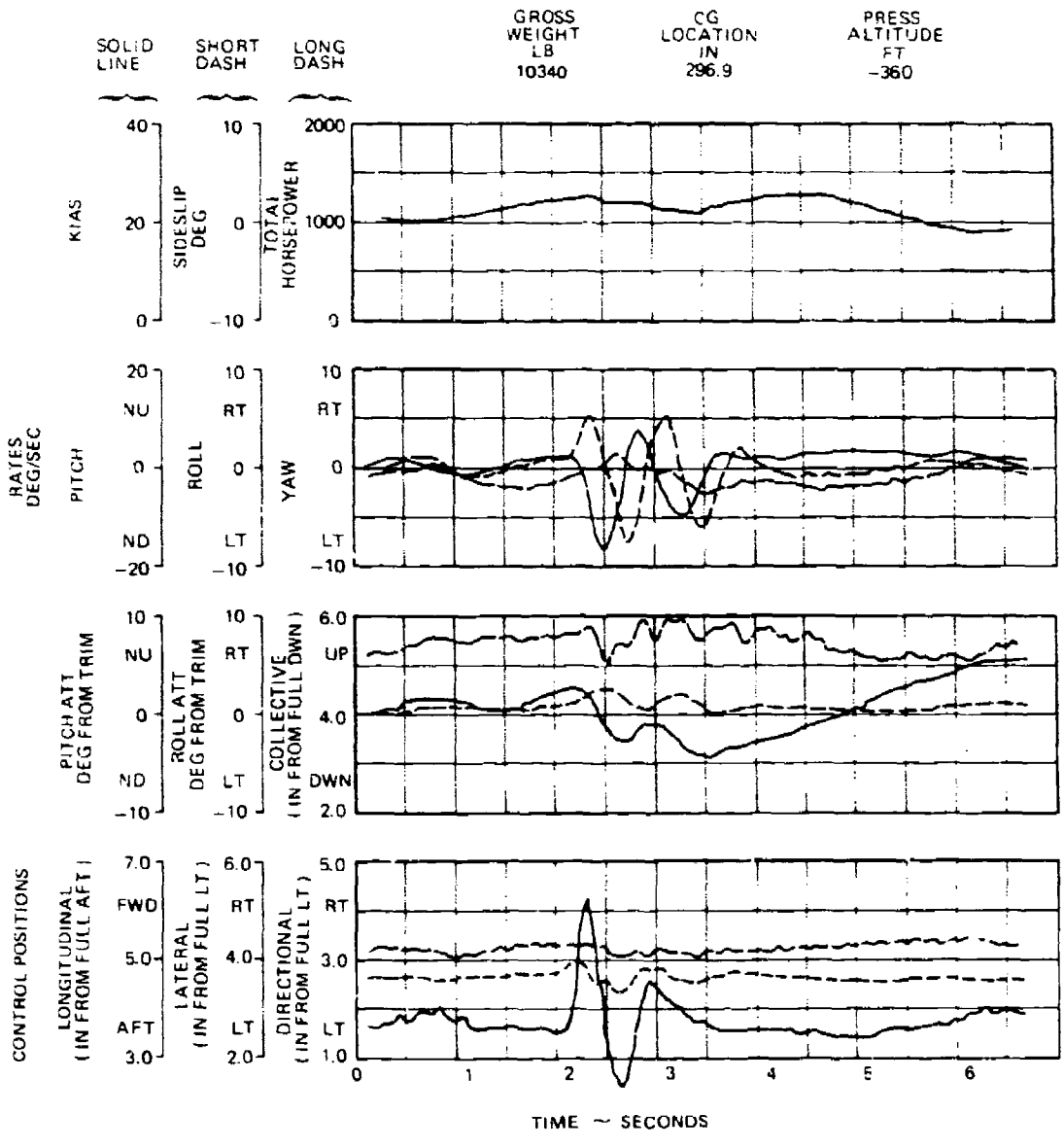

Figure 73. Longitudinal Reversal in Hover, Helicopter Configuration.

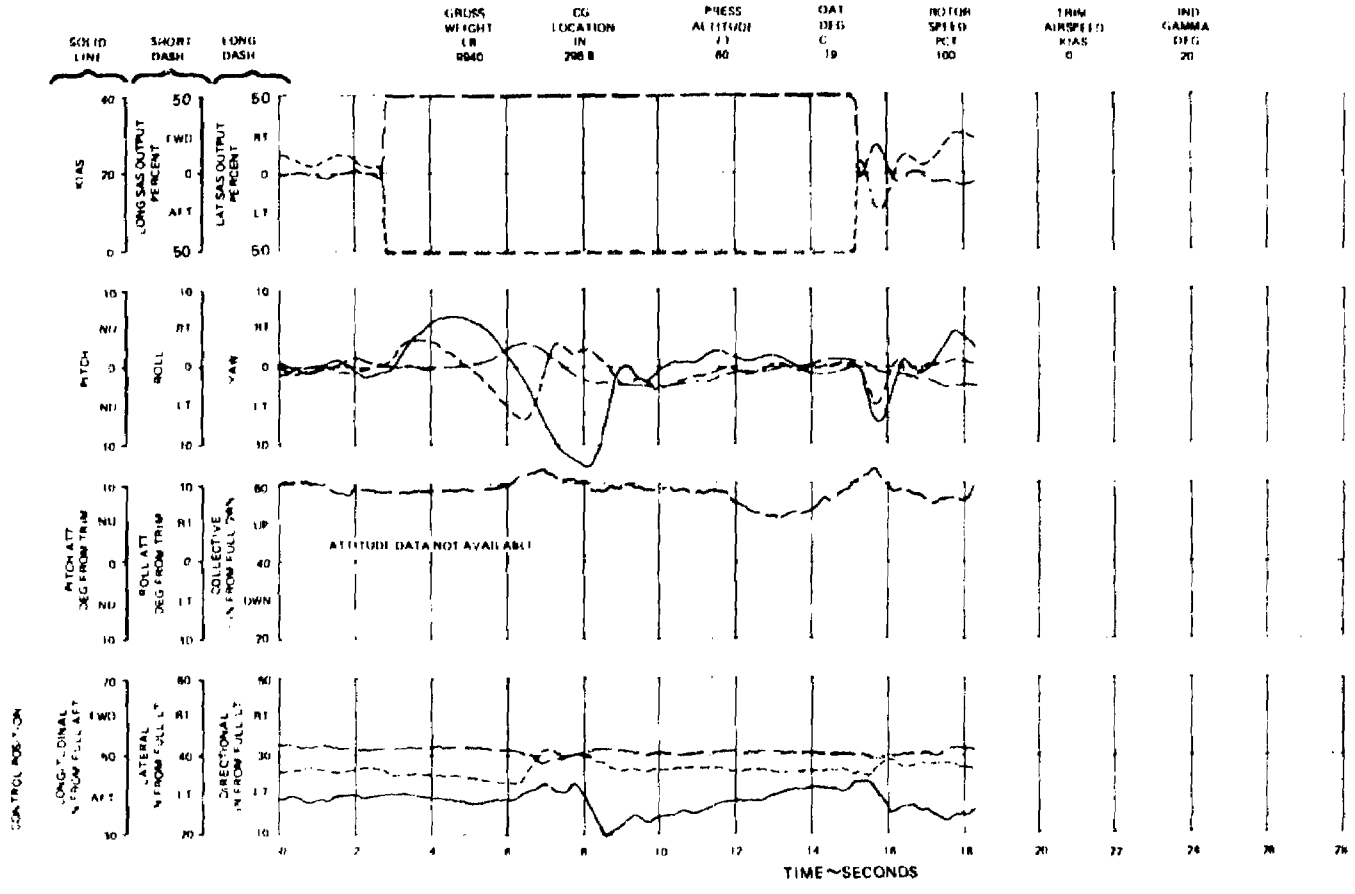

Figure 74. Hover - Aft/Right Hardover, Helicopter Configuration.

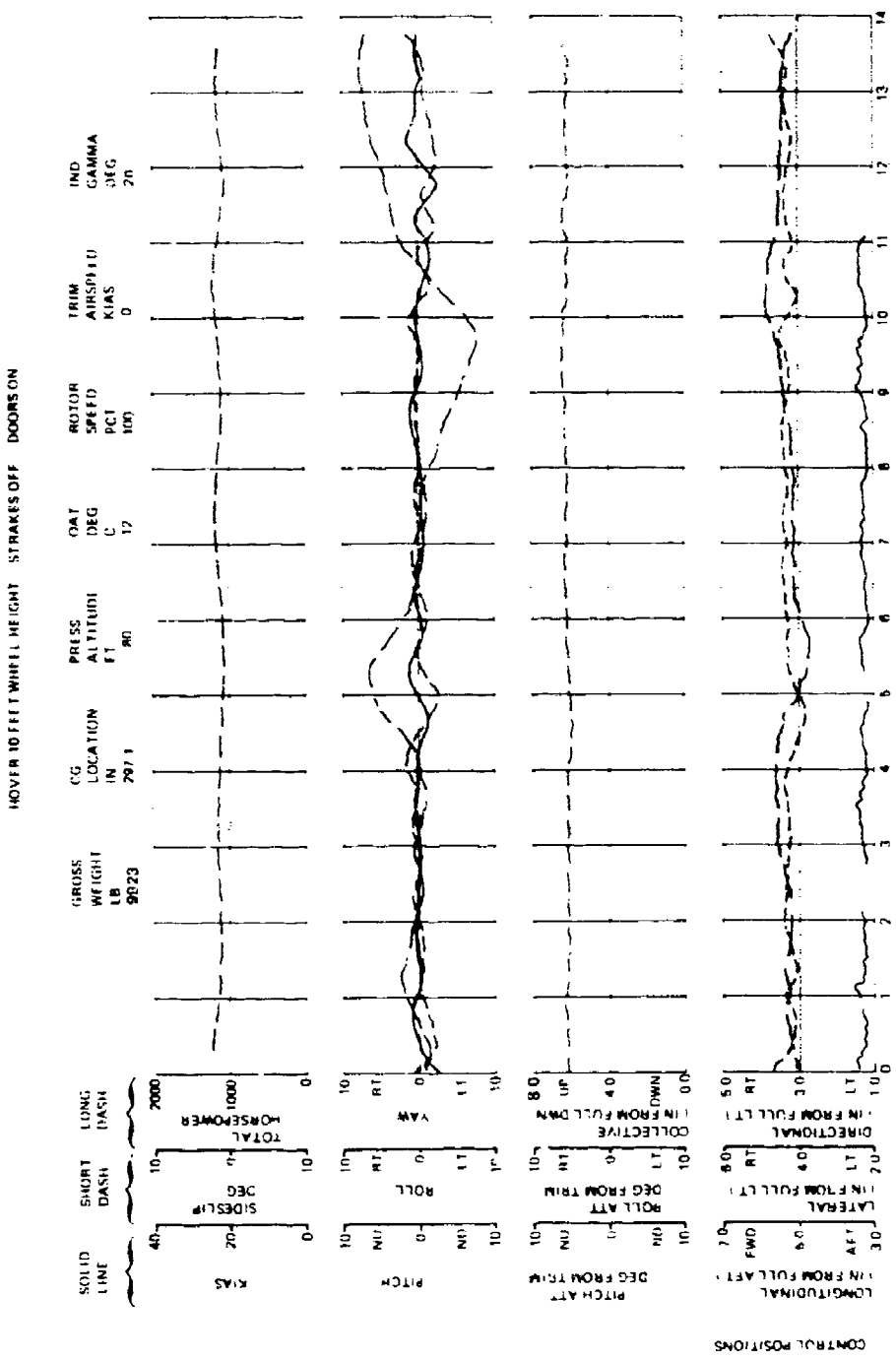

Figure 75. Hover Strakes Off, Helicopter Configuration.

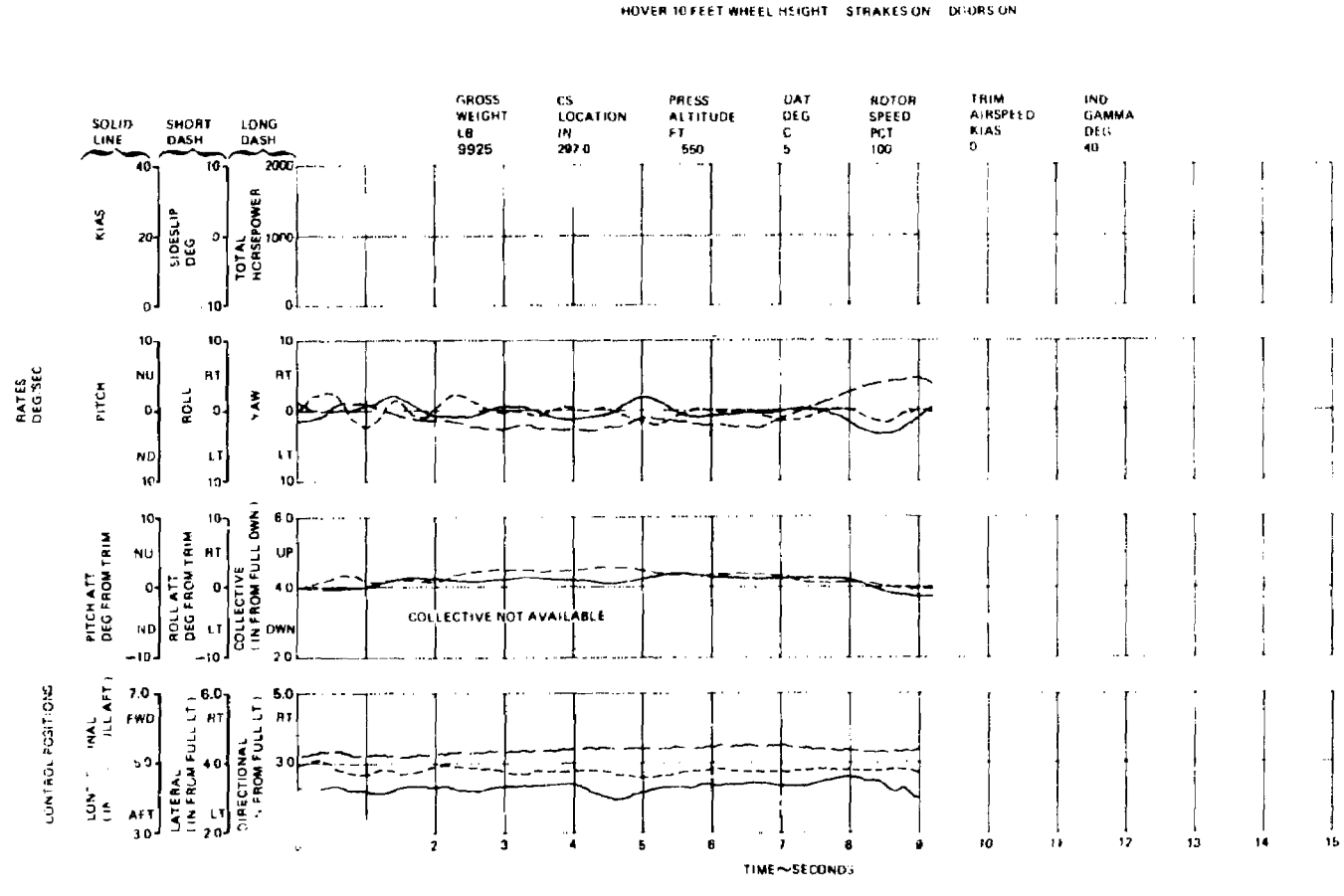

Figure 76. Hover Strakes On, Helicopter Configuration.

on and off for a 10-foot hover. Note in Figure 76 that yaw rate diverges to the right at 4.5 seconds and to the left at 8 seconds without a pedal input. Yaw accelerations of 8 to 15 degrees/ second^2 were typical without strakes. Some disturbances remain with strakes (Figure 75), but the amplitudes are generally reduced by 50 percent. The strakes installed for most of the testing were 1-1/2-inch-high fences installed at approximately waterline 130 from station 165 to 275 on both sides of the aircraft.

The unsteady flow phenomenon is apparently related to the perfectly circular cross section of the XH-59A fuselage. Since the problem is not related to the ABC rotor system, no attempt at a permanent "fix" was made and the strakes were removed prior to the start of forward flight testing.

Sideward Flight Trim:

Initial sideward flight tests resulted in a 20-knot maximum left sideward flight speed capability while retaining a 10-percent control margin. A 25-percent increase in lateral cyclic range was implemented as previously discussed. This lateral control change provided a sideward flight envelope of 40 knots right to 35 knots left with controllability as shown in Figure 77. Roll attitude, lateral cyclic control and pedal control are all stable. Note that at 40-knot right sideward flight a 20-percent lateral control margin remains. At 35 knots left sideward flight, only a 10-percent lateral control margin remains. The nonsymmetry in lateral control is a result of the differential collective pitch from the pedal position to maintain heading. In left sideward flight, right pedal is used to hold heading against the weathercock stability of the vertical tail surfaces. A right pedal input increases upper rotor collective blade angle and reduces lower rotor collective blade angle, resulting in an increasing percentage of the thrust load being carried by the upper rotor. The proportionately stronger upper rotor wake skews over and impacts on the right side of the lower rotor, inducing a strong restoring moment that must be overcome with additional lateral control displacement. Conversely, in right sideward flight the lower rotor assumes a larger share of the thrust load. The weakened upper rotor wake induces less restoring moment as it impacts the left side of the more heavily loaded lower rotor; and thus about 10 percent less lateral control is required.

Rearward Flight Trim:

The rearward flight controllability characteristics were tested by pacing airspeed with a calibrated test support vehicle. Results of rearward flight testing are shown in Figure 78. Rearward flight speed was limited to 30 knots

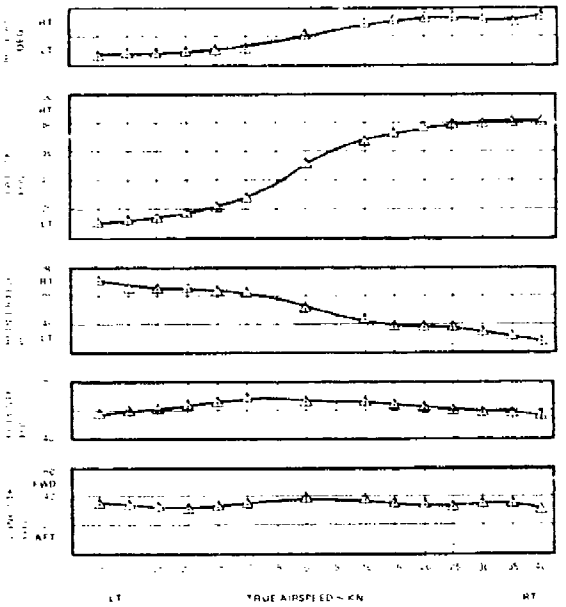

Figure 77. Sideward Flight, Helicopter Configuration.

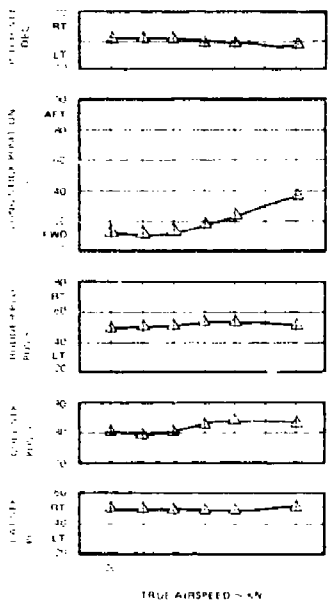

Figure 78. Rearward Flight, Helicopter Configuration.

during test by available field length even though control margin was not encountered. Note that aft longitudinal cyclic control and collective control show the start of a gradient change in the 25- to 30-knot rearward speed range. This gradient change is caused by the start of horizontal stabilizer download. The positive 10-degree incidence setting results in a download increase in rearward flight. The download causes the normal collective drop with advance ratio to cease, and the negative moment created relieves the aft cyclic requirement. No significant workload increase was reported by the pilot in association with this speed range.

Forward Flight

Level Flight Trim:

Level flight trim characteristics of the aircraft to 154 knots are shown in Figure 79. A high positive longitudinal stick gradient exists from hover to about 40 knots due to a strong low-advance-ratio speed stability of the stiff rotor system and horizontal stabilizer download at about 17 to 18 knots which persists to about 60 knots. In the 60- to 100-knot regime, longitudinal control position gradient is negative with increasing airspeed. Through this range of minimum power requirements, downwash on the horizontal stabilizer reduces, causing an aft cyclic control motion and attitude to begin going nose down. This stabilizer induced longitudinal reversal is not ABC rotor related. From 100 knots to V_H, where collective control requirements increase, the longitudinal stick gradient is positive. Migration of lateral stick is slightly left with airspeed and the maximum variation in rudder pedal position is only 5 percent from neutral and occurs at 40 knots. Aircraft pitch attitude is essentially zero through 60 knots, then varies linearly to 11 degrees nose down at V_H of 156 knots. There have been no adverse pilot comments regarding the nose-down attitude.

Level flight trim characteristics at 10,000-foot altitude are similar to those at 2000-foot altitude. Minimum and maximum airspeeds are limited, however, by an 810°C, T5 temperature to 40 knots and 150 knots true airspeed.

Effect of Control Phase Angle (Γ):

Control phase angle, Γ, introduces components of longitudinal cyclic control input, A_{1S}, in the lateral direction as a differential lateral blade feathering, B'_{1S}. At hover and low airspeeds, low values of Γ are used to have a high amount of longitudinal control power available and keep the lift distribution of each rotor toward the advancing side. In high-speed flight, high values of Γ are used to control the outboard

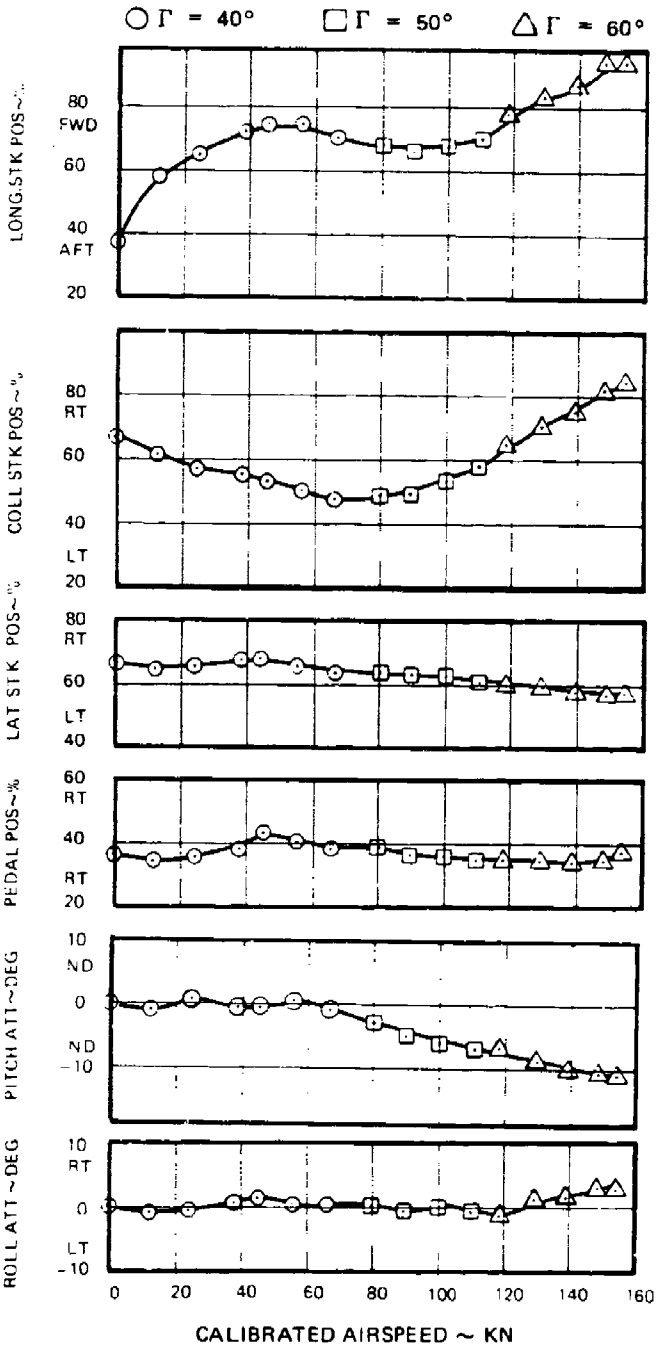

Figure 79. Level Flight Trim Characteristics, Helicopter Configuration.

movements of the lift onto the advancing side. Unrestrained lift migration on the advancing side would induce shaft bending loads exceeding allowables. This is apparent in the rolling moment data of Figure 80. The envelope of control phase angle (Γ) developed in test is shown in Figure 81. High values at low airspeed require excessive forward cyclic and leave inadequate maneuver control available, while low values at high speeds would result in shaft bending stresses at 1P exceeding allowables.

Effect of Differential Lateral Blade Control, B_1':

Elimination of the variable B_1' would allow for significant control system simplification.[1] To simulate this condition, the aircraft was flown through the full airspeed envelope using differential lateral control, B_1', with a fixed 30-degree control phase angle. Trim characteristics for level flight between 40 knots and V_H are shown in Figure 82. Comparison of fixed B_1' and variable Γ data with fixed Γ and variable B_1' data verifies that the results are essentially the same. Variable B_1', fixed Γ flight requires somewhat less forward longitudinal control than flight at high Γ values. Variable B_1' then is a viable design alternative to variable Γ.

Effect of Differential Longitudinal (A_1') and Collective Control ($\Delta\theta_t$):

Differential longitudinal cyclic pitch, A_1', was varied during flight at 130 knots airspeed and a of 60 degrees to assess controllability. Fuselage attitudes and cockpit control positions as a function of A_1' are presented on the left side of Figure 83. Lateral control position is the only parameter that varies significantly with changes in A_1'. Positive A_1' inputs require right lateral cyclic of 7.4 percent control per degree A_1'. In explanation, positive A_1' input with lateral control fixed applies a forward cyclic feathering to the lower rotor along its control axis and aft cyclic feathering to the upper rotor along its control axis. Because of the control phase angle, both rotors have left lateral feathering applied in the shaft axis and produce left rolling moment. Right control displacement is required to balance the aircraft laterally.

Effects of differential collective trim ($\Delta\theta_t$) on control positions at 130 knots are shown on the right of Figure 83. Positive application of $\Delta\theta_t$ increases upper rotor collective pitch and equally decreases lower rotor collective pitch. As a result, more advancing side lift is produced on the upper rotor while less advancing side lift is produced on the lower rotor. This creates a left rolling moment that requires right lateral stick to balance. Stick variation with $\Delta\theta_t$ is 6.0 percent per degree $\Delta\theta_t$. Attitudes and other controls are relatively unaffected by either differential control variation.

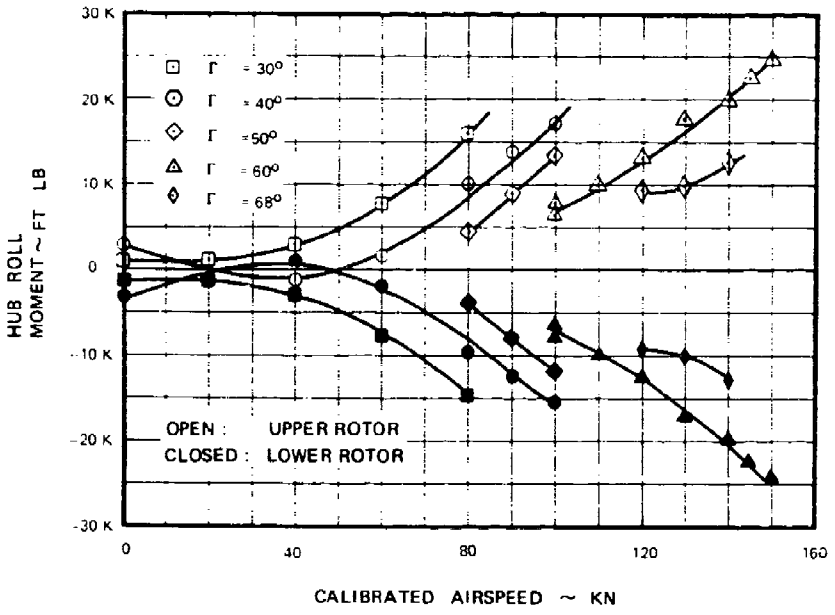

Figure 80. Hub Roll Moments Versus Airspeed, Helicopter Configuration.

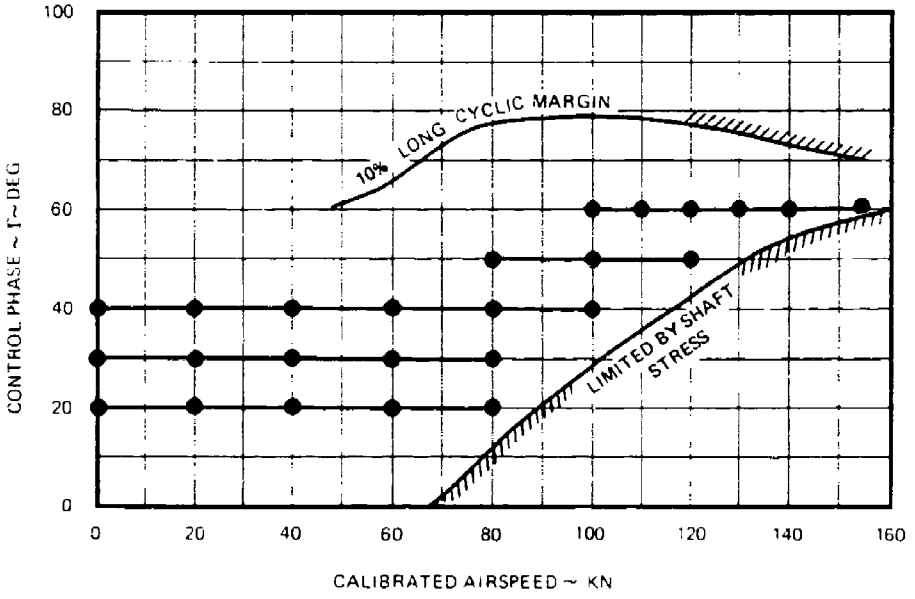

Figure 81. Control Phase Angle (Γ) Envelope for Level Flight, Helicopter Configuration.

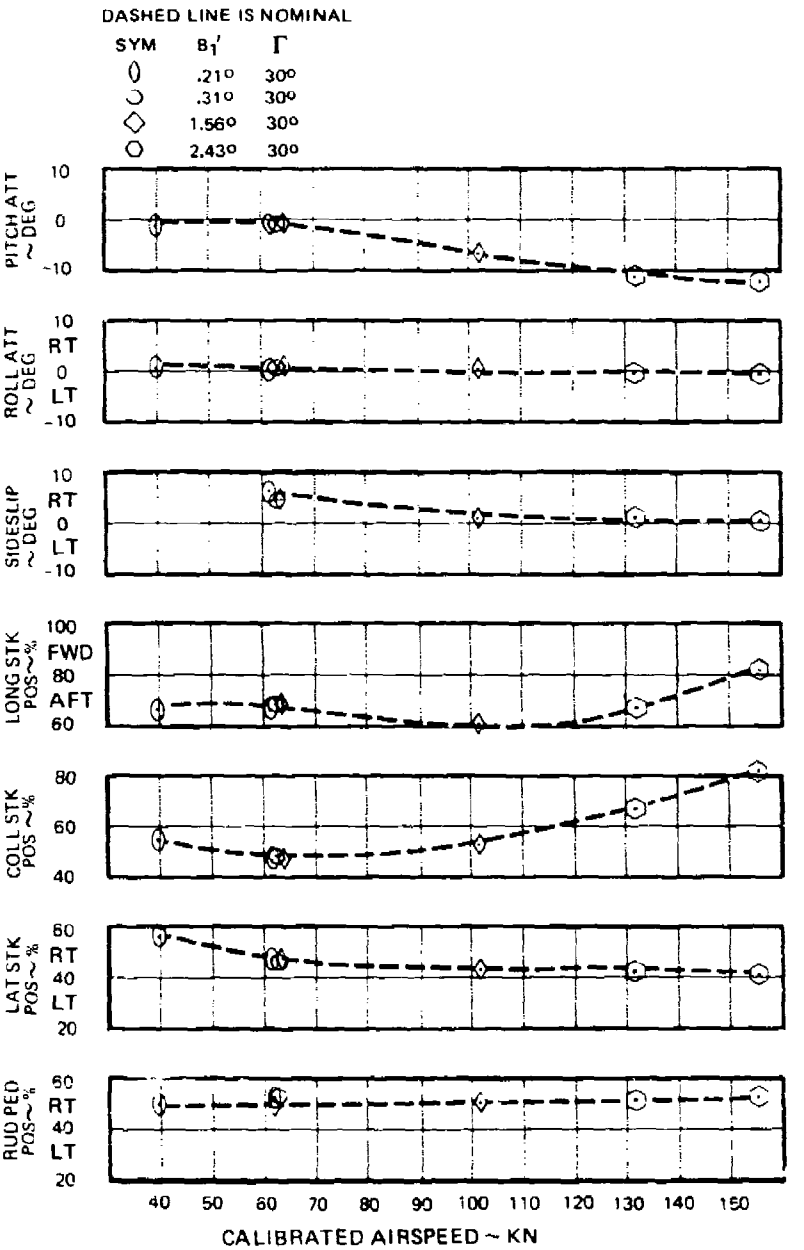

Figure 82. Cyclic Trade-Off Effects in Level Flight, Helicopter Configuration.

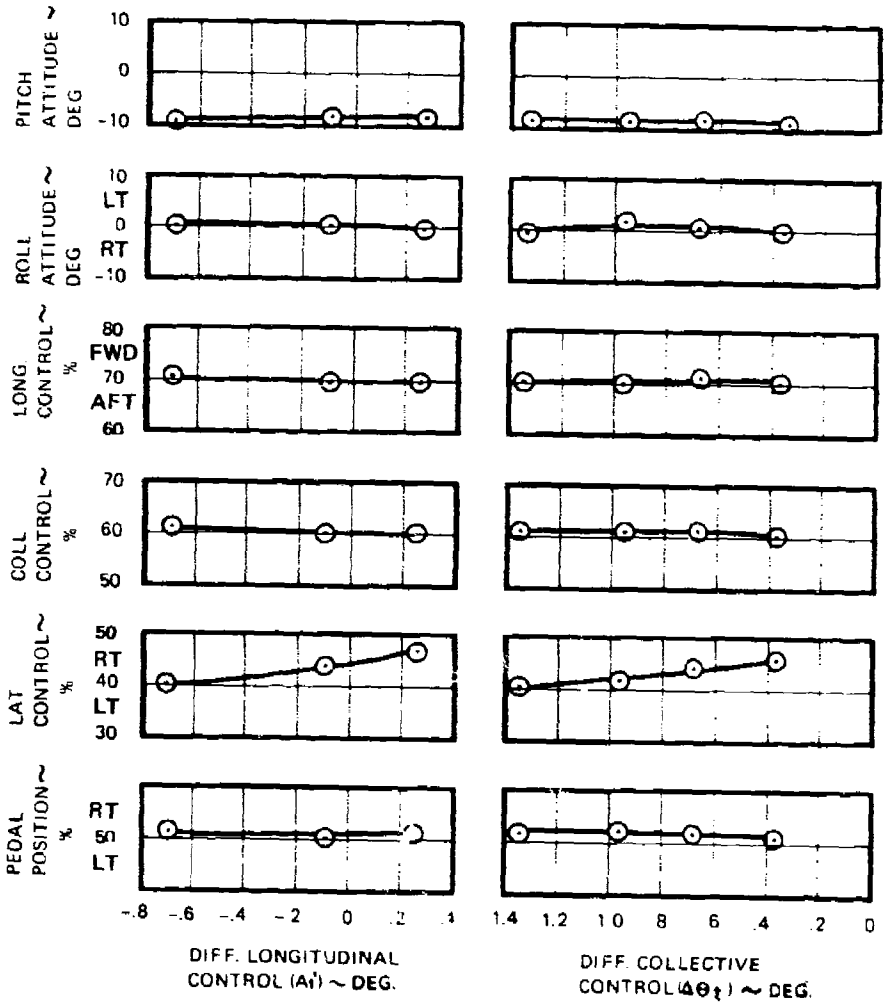

Figure 83. Effect of Differential Longitudinal (A_i') and Differential Collective (θ_t) Control on Level Flight Controllability at 130 KCAS, Helicopter Configuration.

Effect of Rotor Speed:

The effect of rotor speed on trim level flight controllability was evaluated at numerous airspeeds. Data for 50 and 130 knots are presented in Figure 84. The primary effects on aircraft trim characteristics and controllablity are collective and longitudinal stick positions. As would be expected, increasing rotor speed reduces both the collective and forward longitudinal stick requirements. The lowest gradient is exhibited at 50 knots where collective and longitudinal stick changes with rotor speed are 0.75 and 0.68 percent control per percent rotor speed. At higher speeds the gradients increase with values of 0.99 and 0.77 at 130 knots.

Comparison of the data for 50 and 130 knots shows more lateral control, roll attitude and sideslip variation at 50 knots than at 130 knots. The higher rotor speed to lateral coupling at 50 knots results from two separate rotor phenomena, one aerodynamic and the other control system design. The aerodynamic reason is that significantly more interrotor aerodynamic interference exists between the upper and lower rotors at 50 knots than at 130 knots. Increase in rotor speed therefore creates more differential torque change at 50 knots, with the upper rotor increasing torque more than the lower rotor. Secondly, dynamic pressure sensing is used to decouple differential collective pitch from the pedals linearly between 40 and 80 knots airspeed. Thus at 50 knots the pedal inputs change rotor differential collective pitch, which exaggerates the resulting differential rotor torque. Sideslip results, through dihedral, cause roll and lateral control requirements.

Effect of Elevator/Collective Coupling:

Elevator to collective coupling substantially reduced shaft structural loads in descending flight and reduced control requirements in level flight. Coupling employed is shown in Figure 85 as elevator angle against collective stick position. Full-up collective gave a 7-degree trailing-edge-down elevator position and full-down collective gave a 13.9-degree trailing-edge-up position with a linear variation. Shown in Figure 86 are collective and longitudinal stick positions for level flight trim with the elevator fixed at 0 degree, the elevator removed, and the elevator coupled to the collective control. These data show that the collective requirement is reduced about 3 percent by the coupling and forward longitudinal control required is reduced by up to 6 percent at V_H. The trailing-edge-down elevator associated with high collective produces a diving moment on the aircraft, thus requiring less forward cyclic.

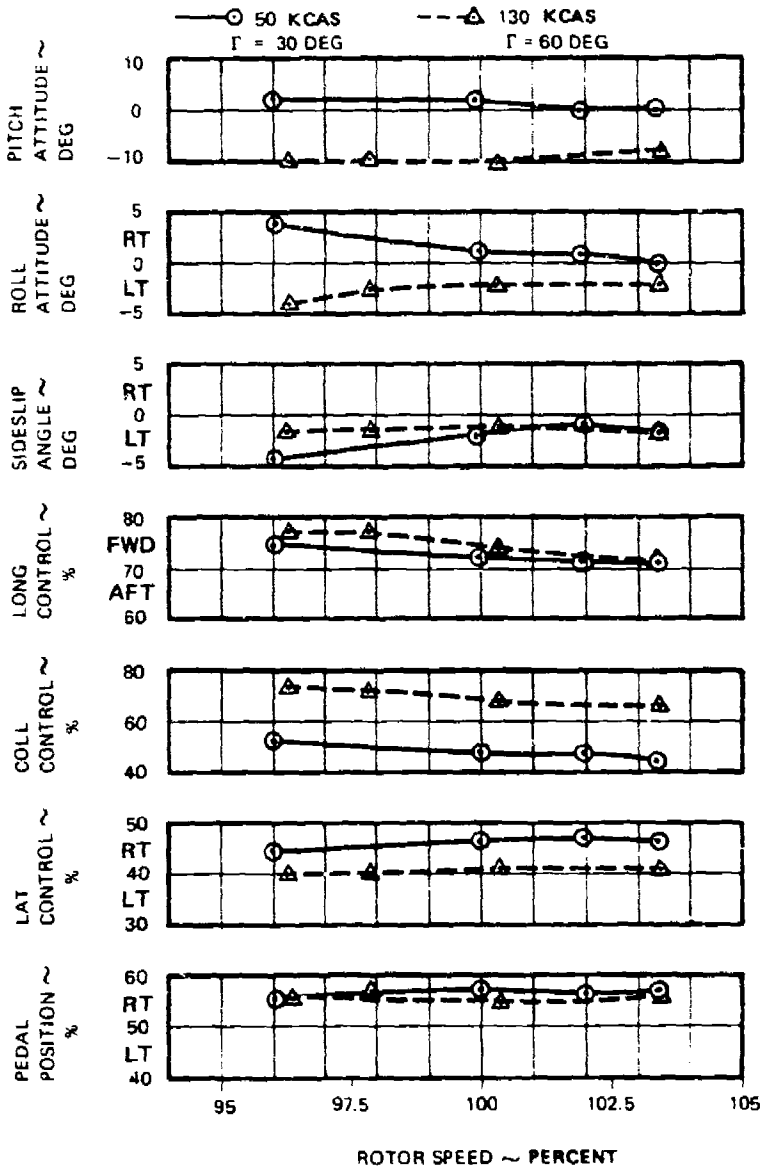

Figure 84. Effect of Rotor Speed on Level Flight Controllability, Helicopter Configuration.

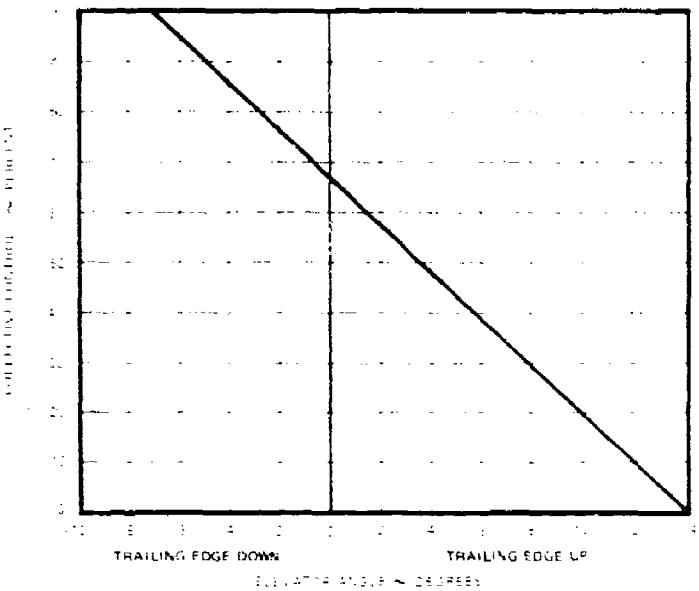

Figure 85. Elevator to Collective Coupling, Helicopter Configuration.

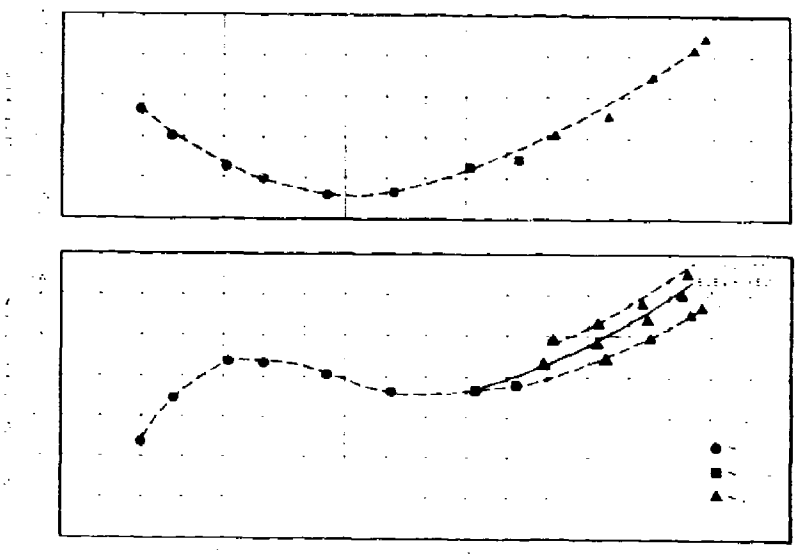

Figure 86. Longitudinal and Collective Variations with Airspeed Elevator Off, Fixed and Coupled, Helicopter Configuration.

Sideslip Flight:

Trim characteristics in sideslip flight at 120 knots are shown in Figure 87. The aircraft exhibits a positive dihedral effect. Right stick is required to balance the rolling moment induced by right sideslip and left stick for left sideslip. Positive directional stability is evident by the requirement for more left pedal to hold increasing right sideslip and right pedal to hold left sideslip. No control limitations were encountered to slip angles of 10 degrees in either direction. Adequate margins remain for maneuvering. Dihedral and directional stability become more positive as airspeed increases. Also, bank angle is in the proper direction and the gradient is strong at 120 knots due to the higher side force developed. Positive lateral/directional static stability was demonstrated for all speeds from 80 knots to V_H. No tests were conducted at speeds below 80 knots.

Maneuvering Flight:

Maneuverability of the ABC rotor system was evaluated in flight throughout the developed airspeed envelope. This maneuver envelope expansion included turn characteristics, climbing and descending flight, diving flight to airspeeds in excess of V_H, autorotations and recoveries, pullups, pushovers, and low-speed longitudinal and lateral agility.

Banked Turn Characteristics:

Banked turns were tested at selected airspeeds from 80 knots to 150 knots, .97 V_H level flight. Turns were initiated from straight and level flight with lateral stick. Collective control was held constant and altitude was sacrificed to maintain airspeed. Turns at all airspeeds were characterized by the turns at 150 knots, the control characteristics of which are shown in Figure 88. Lateral control demonstrates a stable gradient with bank angle. The aircraft is well coordinated as demonstrated by virtually no sideslip or pedal variation over the range of bank angle. A slight aft longitudinal control, stable maneuver stability, is required to increase angle of attack at the higher load factors. No structural or control system limits were encountered that would prevent banked turns at angles to 60 degrees, the design load factor limit for the airframe.

Climb and Descent:

A substantial variation in longitudinal control occurred between climbing and descending flight. The pitching moments that were being balanced emanated primarily from horizontal

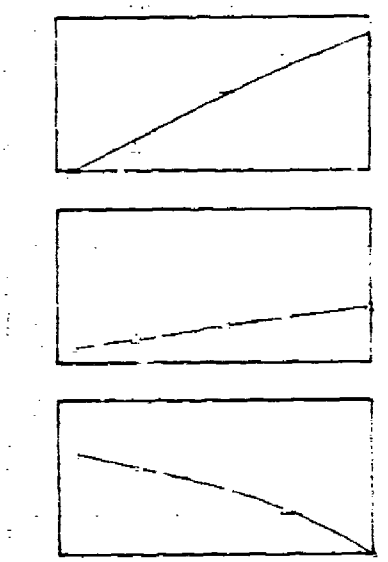

Figure 87. Sideslip Flight Characteristics, Helicopter Configuration.

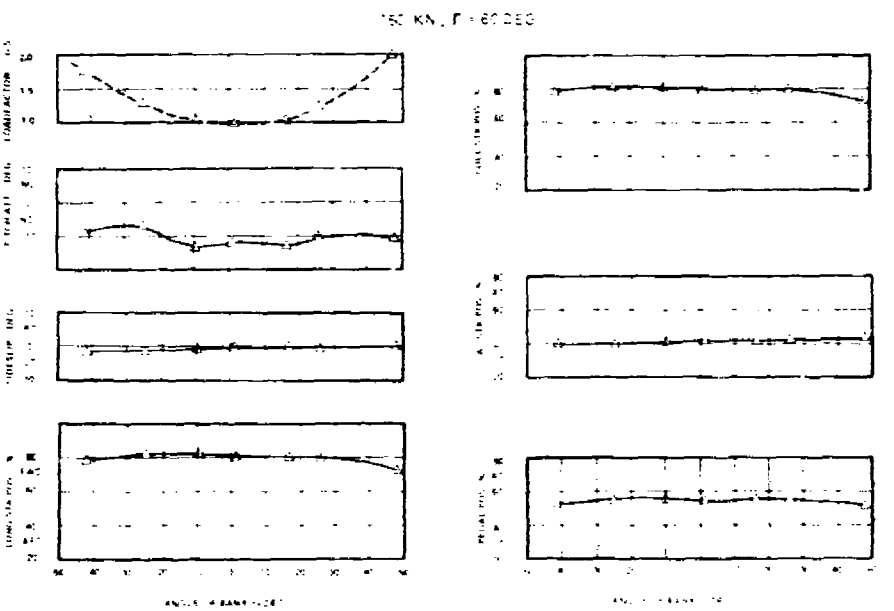

Figure 88. Controllability in Banked Turns, Helicopter Configuration.

stabilizer airloads. The amount of control migration experienced was substantial. At higher airspeed conditions, attainable rates of descent were limited by high shaft bending moments (which are discussed in the structural section of this report). Trim collective and longitudinal control requirements in climbs and descents at airspeeds from 80 to 130 knots are shown in Figure 89. The upper curves show fixed elevator characteristics while the lower show elevator coupled characteristics. Climbs and descents were also flown at 130 knots airspeed with moderate changes in fixed elevator deflection, differential collective pitch, differential longitudinal cyclic pitch; and one change occurred in the combination of control phase angle (Γ) and differential lateral cyclic pitch (B_1'). None of these control changes influenced the sensitivity of controls to rate of climb or descent.

The stabilizer-induced envelope limits on descending flight could be substantially eliminated by either reducing the stablizer area or coupling the elevator angle into the collective control. To maintain a conservatively large stabilizer for the balance of the testing and to avoid a major structural change, a decision was made to couple the elevator to the collective control as a means of reducing longitudinal cyclic excursions and resulting shaft bending moments in descending flight. The effect of the elevator/collective coupling on rate of descent capability at cruise airspeeds is shown in the lower curves of Figure 89. Full autorotation descent was attainable at 120 knots, where prior to coupling that condition was well beyond structural limits. The extent of improvement in the descending flight envelope is shown in Figure 90. No structural or control limits were encountered in climbing or descending flight within this envelope.

Dives:

To evaluate the ABC coaxial rotor system at airspeeds in excess of level flight V_H, shallow dives were conducted from 12,000-foot density altitude. Descent rates to 2000 fpm and 186 KTAS (159 KCAS) were demonstrated at 8000 to 9000 feet H_D. The technique used was to trim the aircraft in level flight and then build up speed by pushing over into a shallow dive. Dives from level flight at 100 KCAS are shown in Figure 91. Pitch attitude is stable with airspeed; nose down with increasing speed. Diving from a 100 KCAS trim, where collective was 70 percent and pitch attitude was 4 degrees nose down, results in a rearward longitudinal control position variation with speed. The unstable gradient is caused by the 10-degree leading-edge-up horizontal stabilizer incidence creating more nose-down moment with increasing airspeed. Maximum dive speed from this 100 KCAS trim condition was limited by altitude loss, increasing cockpit lateral vibrations, and rates of descent up to 2300 fpm. Tip clearance was acceptable at each attained airspeed for this diving flight.

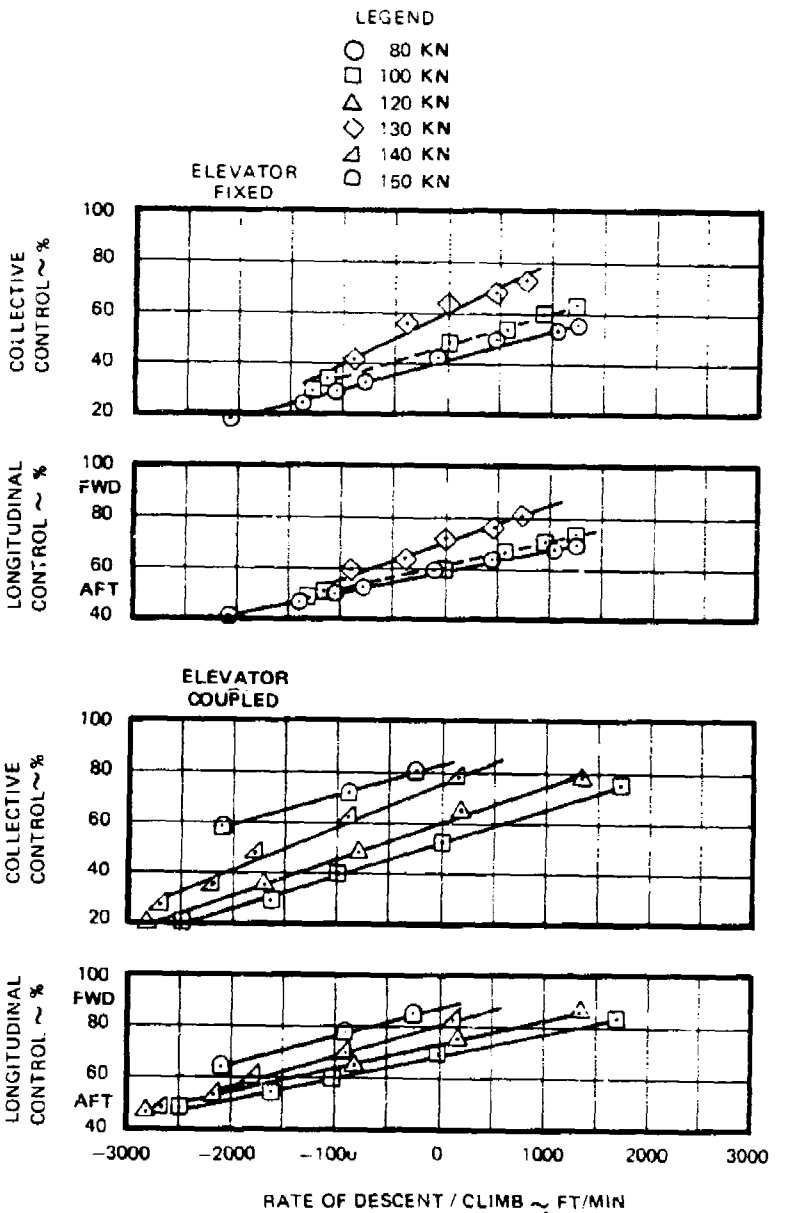

Figure 89. Collective/Longitudinal Cyclic Controllability for Climbing and Descending Flight, Helicopter Configuration.

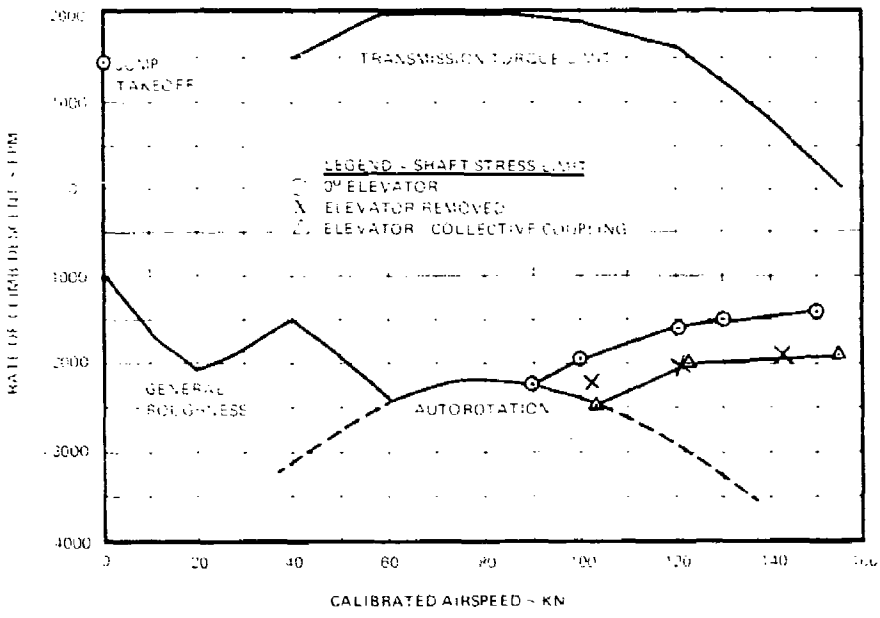

Figure 90. Climb and Descent Limitations Versus Airspeed, Helicopter Configuration.

Autorotation and Flare Recovery:

During descending flight tests, when differential collective control was retained on the pedals by deactivating the dynamic pressure sensed washout, mild directional control reversals were encountered prior to reaching autorotative descent rate at 60 and 70 knots airspeed. Recognizing that flare recovery from autorotation could result in directional control reversals as airspeed decreased and differential collective control automatically phased back onto the pedals, flight tests were conducted to establish autorotative flare and landing techniques. Different combinations of flare attitudes, autorotative rotor speeds, and differential collective-to-pedal linkages were evaluated by flaring at altitude to a target speed of 40 knots and applying a pedal step in the process. From these tests, a technique for flaring from autorotation with differential collective washout in the automatic mode was established. This technique was tested in flight and the resulting maneuver is shown in Figure 92. From trimmed autorotation at 80 knots and 95 percent N_R a 20-degree cyclic flare was conducted with a left pedal step applied as the aircraft reached 50 knots. Differential collective washout reached 40 percent at the time when the pedal step was applied. Yaw acceleration

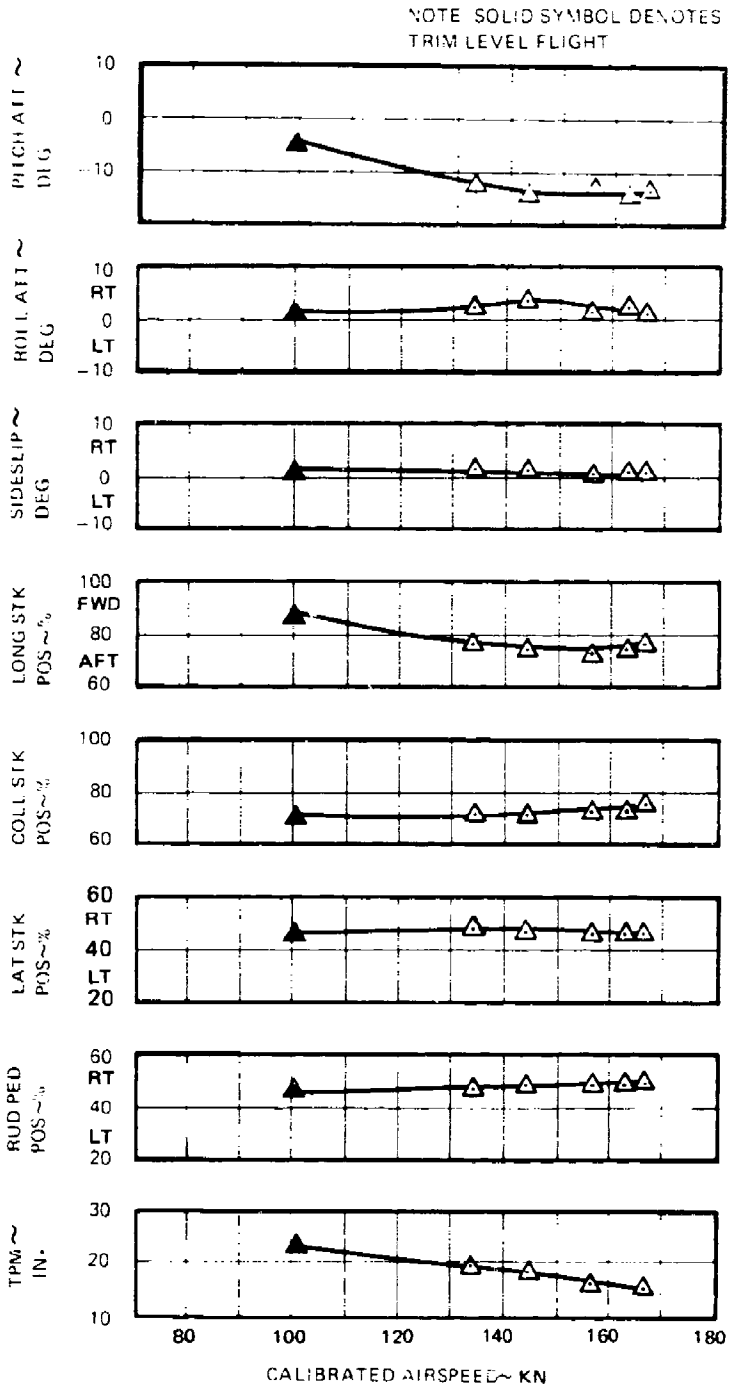

Figure 91. Dive Characteristics - 10,000 Feet, Helicopter Configuration.

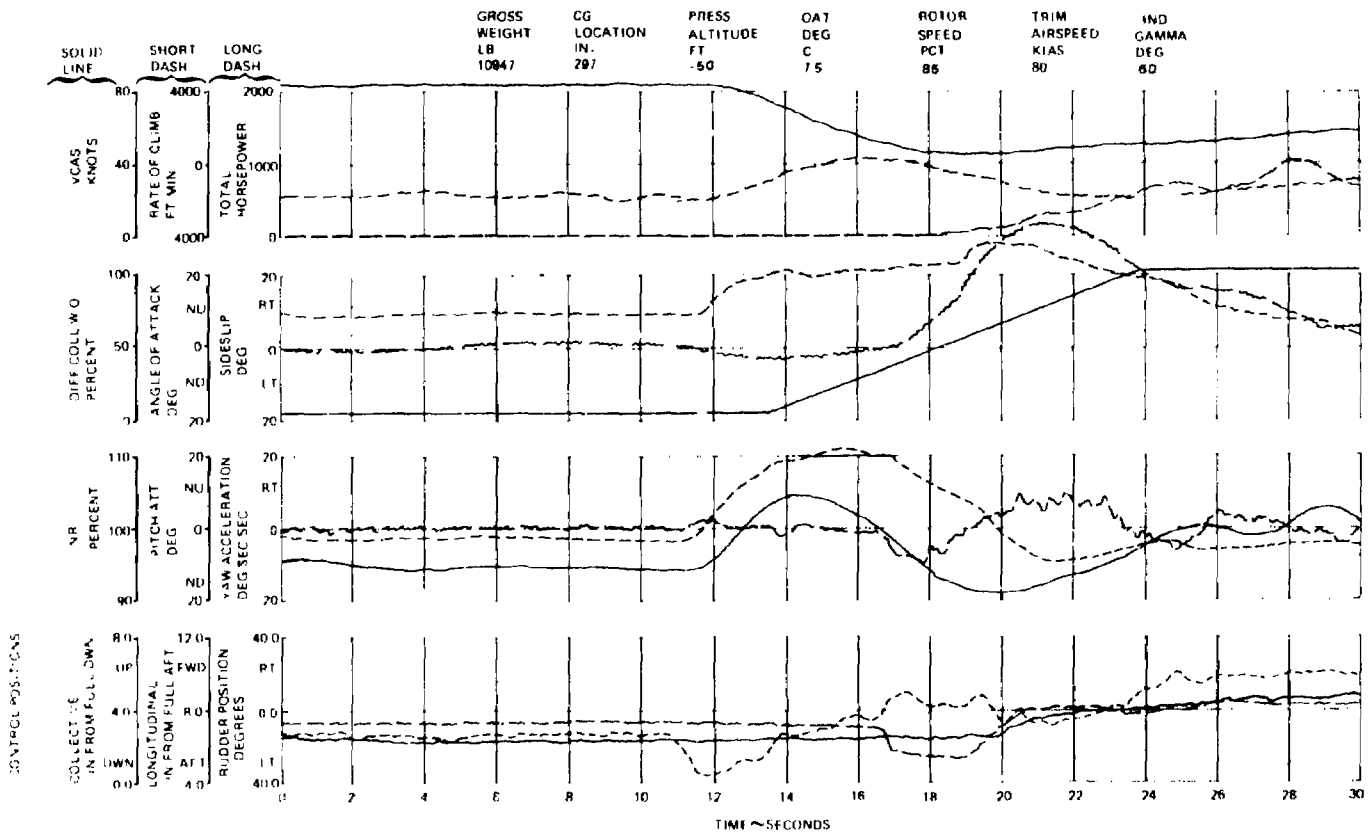

Figure 92. Autorotation Recovery with a Left Pedal Step Applied During Recovery, Helicopter Configuration.

and sideslip response to the pedal step shows that a strong positive directional control is available. Rate of descent was arrested at 50 knots and the aircraft could have landed at that point.

Agility (SAS on):

Both longitudinal and lateral acceleration and deceleration capability (agility) of the aircraft were evaluated. The results are shown in Figures 93 and 94. The maneuvers were performed at incremental pitch and roll attitudes while accelerating to a predetermined airspeed, stabilizing at that speed, and then decelerating to a hover. Both peak instantaneous acceleration and average value are presented for each target airspeed. Pitch attitudes on the order of 15 to 20 degrees were most comfortable for the longitudinal maneuvers. Peak forward accelerations of 0.5g were readily achieved (Figure 93). Agility in the left direction, however, was appreciably reduced (Figure 94). It appears that the pilot in the right seat has better ground visibility out the right window; thus he is comfortable with maneuvers to the right and therefore will command more performance from the aircraft to the right than to the left.

Stability and Control Characteristics:

Control Sensitivities and Couplings:

Longitudinal, lateral and directional control sensitivities were evaluated by application of step control inputs at level flight conditions from hover to V_H. Control steps were applied in both directions to determine tendencies toward either control or response nonlinearities. Angular acceleration about each principal axis was recorded to assure that any control couplings would be identified. In addition, pedal steps were applied in low-speed descending flight conditions to determine sensitivity reductions associated with rate of descent. These steps were applied at 40 and 60 knot descent and with pedal providing rudder inputs only and providing both rudder and differential collective inputs. SAS was kept on for all step control applications.

Longitudinal, lateral and directional control sensitivies as they vary with airspeed are presented in Figure 95. Pitch and roll control sensitivities as they vary with airspeed are presented in Figure 96. Pitch and roll control sensitivities generally increase with airspeed. Directional control sensitivity decreases up to 80 knots airspeed because collective pitch is decreasing, resulting in less differential torque per unit differential collective and phasing of differential collective from the pedals in the 40- to 80-knot range. Sensitivity above 80 knots, where rudders only are used,

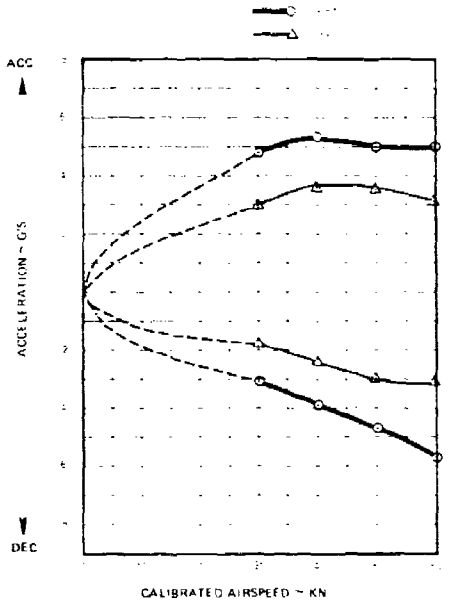

Figure 93. Flight Demonstrated Longitudinal Agility, Helicopter Configuration.

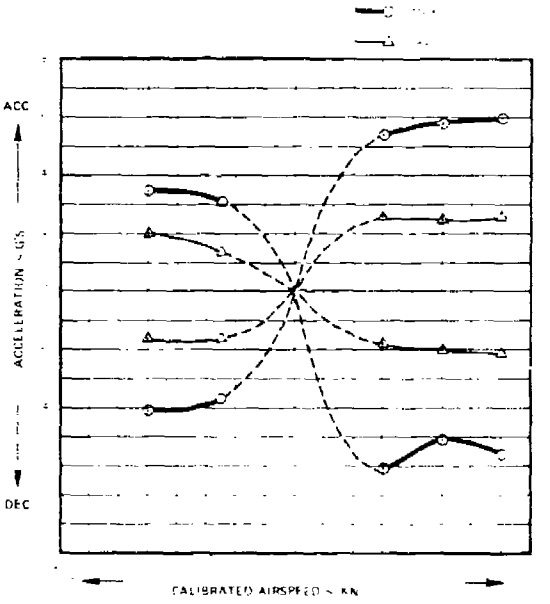

Figure 94. Flight Demonstrated Lateral Agility, Helicopter Configuration.

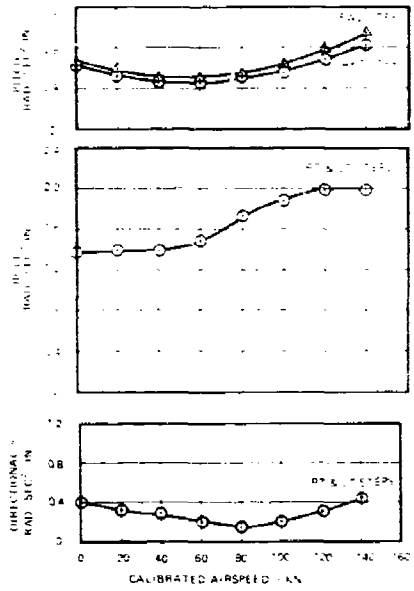

Figure 95. Variation in Control Sensitivity with Level Flight Airspeed, Helicopter Configuration.

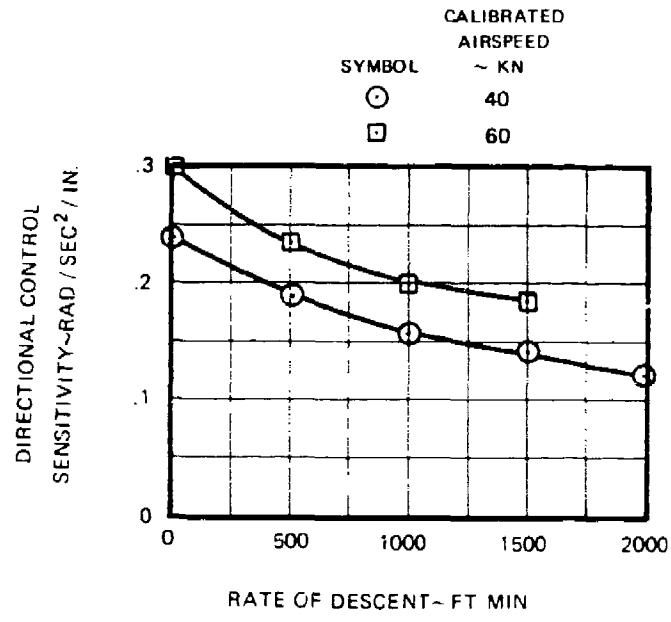

Figure 96. Variation in Low-Speed Directional Control in Descending Flight, Helicopter Configuration.

increases in proportion to dynamic pressure. Magnitude of roll and directional control sensitivity are independent of input step direction. Longitudinal sensitivity, however, is consistently higher for forward inputs than for rearward. This behavior is caused by a number of system nonlinearities that combine in various proportions at different airspeeds. The mechanical control system, particularly on the upper rotor, has nonlinearities because of small radius bellcranks and internal blade pitch horns. Additionally, the control displacement to rotor moment response is not orthogonal at forward airspeeds. This results from azimuthal variation in blade Lock No. and associated azimuthal variations in blade precession angle. These phenomena apparently combine such that forward control sensitivity is consistently higher than aft control sensitivity.

Directional characeristics were examined for effects of low-speed descending flight and coupling into roll with rudders plus differential collective and rudders only. Variations in directional control sensitivity with rates of descent are presented in Figure 96 for 40- and 60-knot airspeeds. At both airspeeds, control sensitivity decreases as descent rate increases. Lowered collective results in less torque change from differential collective, and rudder hinge axis effective sweep caused by descent reduces rudder effectiveness. Roll coupling with directional control characteristics are presented in Figure 97. Rudders at 20 degrees per inch of pedal together with differential collective at 2 degrees per inch of pedal was evaluated at 60 and 80 knot airspeeds. Coupling is strongly adverse and is the principal reason that differential collective is phased from the pedals linearly from 40 to 80 knots. Step inputs with rudder only rigged at 10 degrees per inch of pedal were evaluated at 60, 80, 100 and 120 knots. The data show proverse coupling at all speeds. The coupling is essentially unity and results in lateral stick turns being well coordinated with little or no pedal input.

Finally, collective control steps were applied over the speed envelope to evaluate the pitch with collective coupling common to hingeless rotor systems. These steps were applied with elevator fixed and collective to elevator coupling. These data are presented in Figure 98 and show the expected strong coupling at higher advance ratios. Collective to elevator coupling reduced the collective to pitch coupling by almost 50 percent. The roll with collective coupling common to single rotor hingeless systems is not present in the coaxial system since the rotors cancel through the shaft resulting in no net roll moment to the airframe.

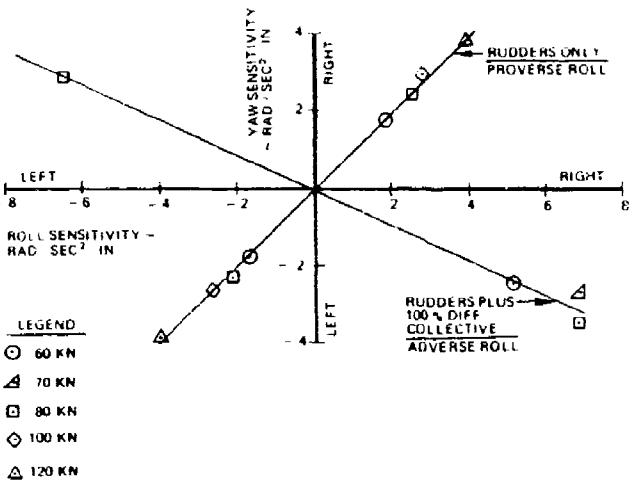

Figure 97. Directional to Roll Coupling, Helicopter Configuration.

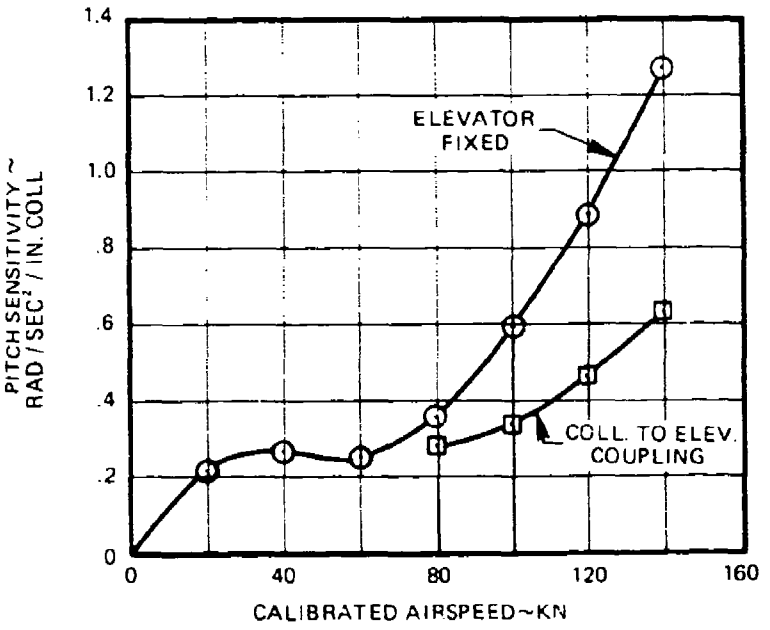

Figure 98. Variation in Collective to Pitch Coupling, Helicopter Configuration.

Dutch Roll Mode Characteristics:

Roll mode dynamics in response to lateral step inputs were stable even with SAS-OFF although some sideslip oscillation was observed. A lightly damped dutch roll mode, however, was very apparent during the response to step pedal inputs. An assessment was made of its frequency and damping and the results are presented in Figure 99 for speeds from 80 to 150 knots. The data verify that the dutch roll mode is adequately damped and is excited only by sharp pedal or lateral control step inputs.

SAS Hardover and SAS-OFF:

Single-channel single and dual axis SAS hardovers were evaluated at level flight airspeeds up to V_H. Aircraft response to all simulated SAS failure conditions was sufficiently mild to allow the hardover to be maintaned for 4 to 6 seconds without corrective pilot action. Time histories of a forward/left dual-axis hardover are shown in Figure 100. Full SAS-OFF flight was evaluated over the entire airspeed envelope, including aft longitudinal, left lateral, and up-collective step inputs up to 120 knots airspeed. Time responses of a typical SAS-OFF control step are presented in Figure 101.

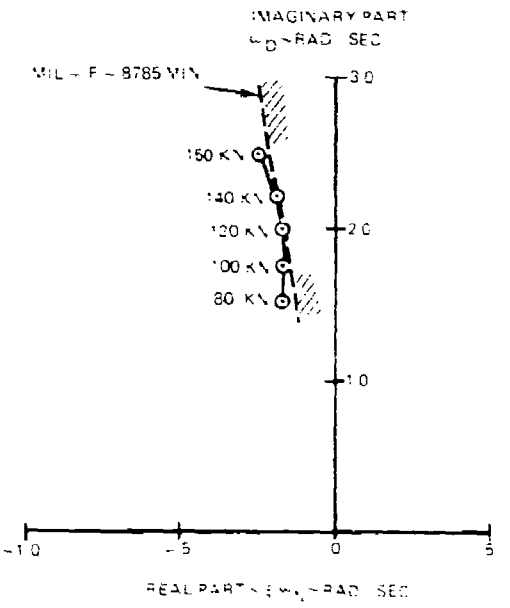

Figure 99. Cruise Flight Dutch Roll Mode Characteristics (SAS On), Helicopter Configuration.

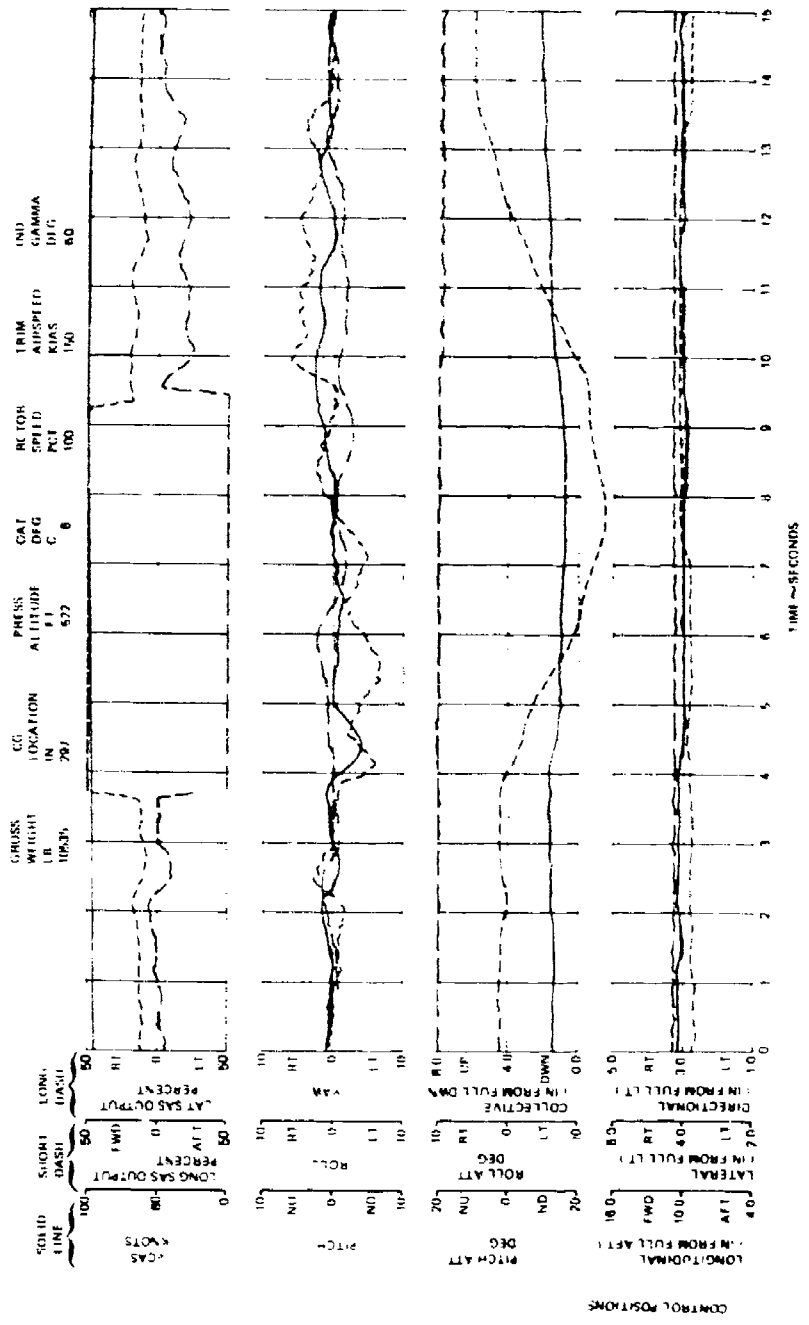

Figure 100. 150 Kn Fwd/Lt Hardover, Helicopter Configuration.

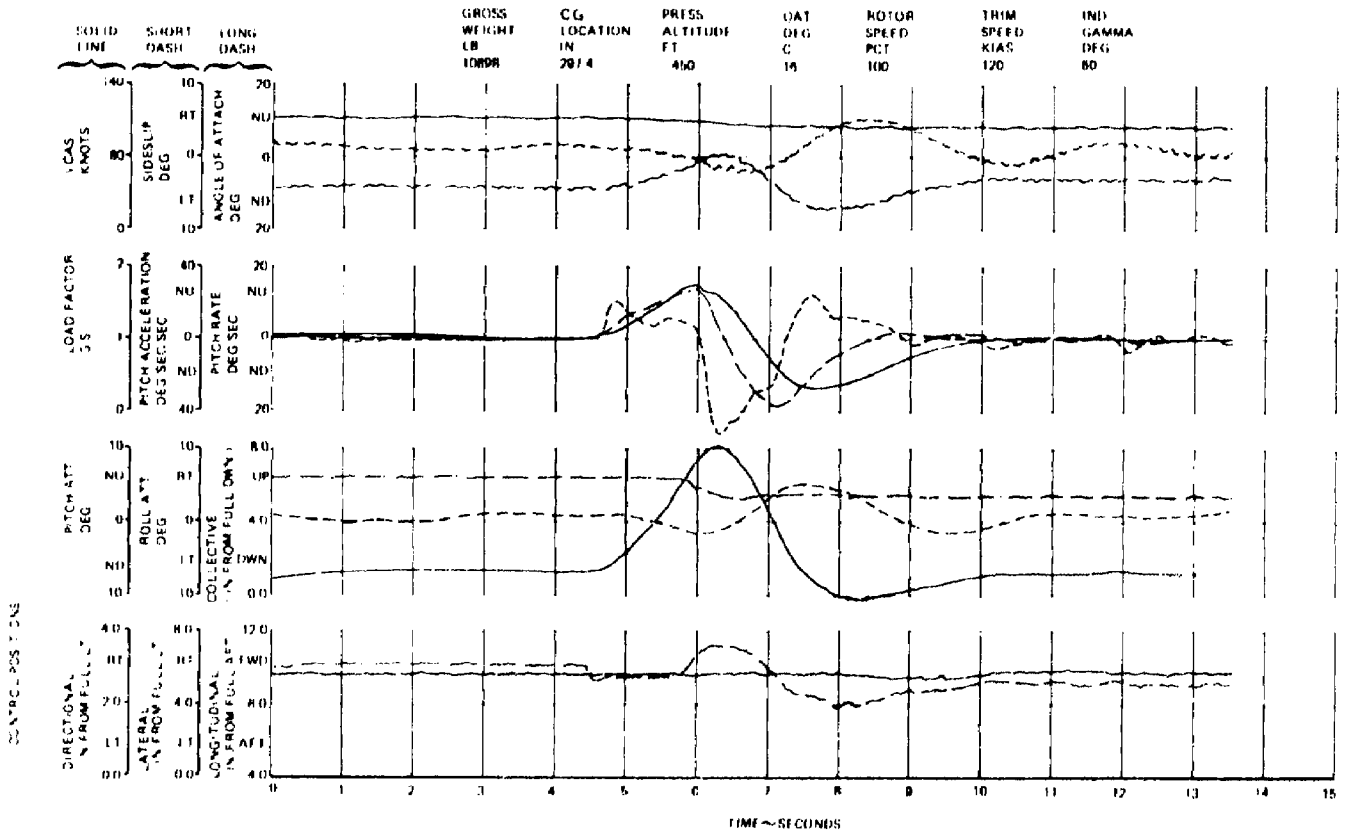

Figure 101. 120 Kn 1/2 Inch Aft Longitudinal Step - SAS Off, Helicopter Configuration.

General SAS-OFF flight characteristics are stable above about 40 knots airspeed. Unstable characteristics at hover and low speed are sufficiently mild so that they are easily controlled without excessive pilot effort. With SAS-OFF at 100 knots low altitude level flight in moderately heavy turbulence, the aircraft tends to deviate in a low frequency manner about the trim attitudes. Pilots report that this turbulence-flight motion is relatively comfortable and significantly better than the tighter, higher frequency response of the aircraft with SAS-ON.

Simulated Engine Failure:

Single-engine failures were simulated at level flight airspeeds of 100, 140 and 150 knots followed by a recovery to full power. In all cases, aircraft reaction to the single-engine cut was mild and required little or no pilot response effort. Recovery from the engine cuts disturbed the aircraft mildly, mostly as a result of engine speed governor oscillations as the engine was brought back on line. No significant pilot effort was involved in either procedure. Time responses of an engine cut at 150 knots are shown in Figure 102.

STRUCTURAL RESULTS

The helicopter mode flight test program of the XH-59A can be divided into two main sections: (1) helicopter low-speed flight and maneuverability, and (2) helicopter high-speed flight. The low-speed flight and maneuverability did not produce rotor or airframe stress levels close to the endurance limits; therefore a structural presentation is not included in this report. The only area of structural significance in yard work was the master stress gage at the base of the upper rotor shaft. This location was sensitive to total rotor pitch or roll moment and could exceed the endurance limit if too much longitudinal cyclic was used in ground taxi or if rapid longitudinal cyclic excursion occurred such as a rapid takeoff or longitudinal reversals in a hover. Data for the high-speed helicopter is presented in the following sections. Data are presented for the master parameters on the rotor and airframe. The blade bending moment at the 10 percent radius location was monitored to protect the inboard blade spar, the rotor hub and the blade spindle attachment area. These loads were primarily due to interrotor rolling moments. Upper rotor shaft bending moment was used as a backup parameter for the blades inboard bending locations as well as a secondary method for monitoring rotor tip clearance. As mentioned previously, the master stress location at the bottom of the shaft was primarily sensitive to total rotor pitch or roll moment. The upper and lower rotor pushrod loads indicate the trends and magnitude of the rotor control loads. Rotor tip clearance was a primary

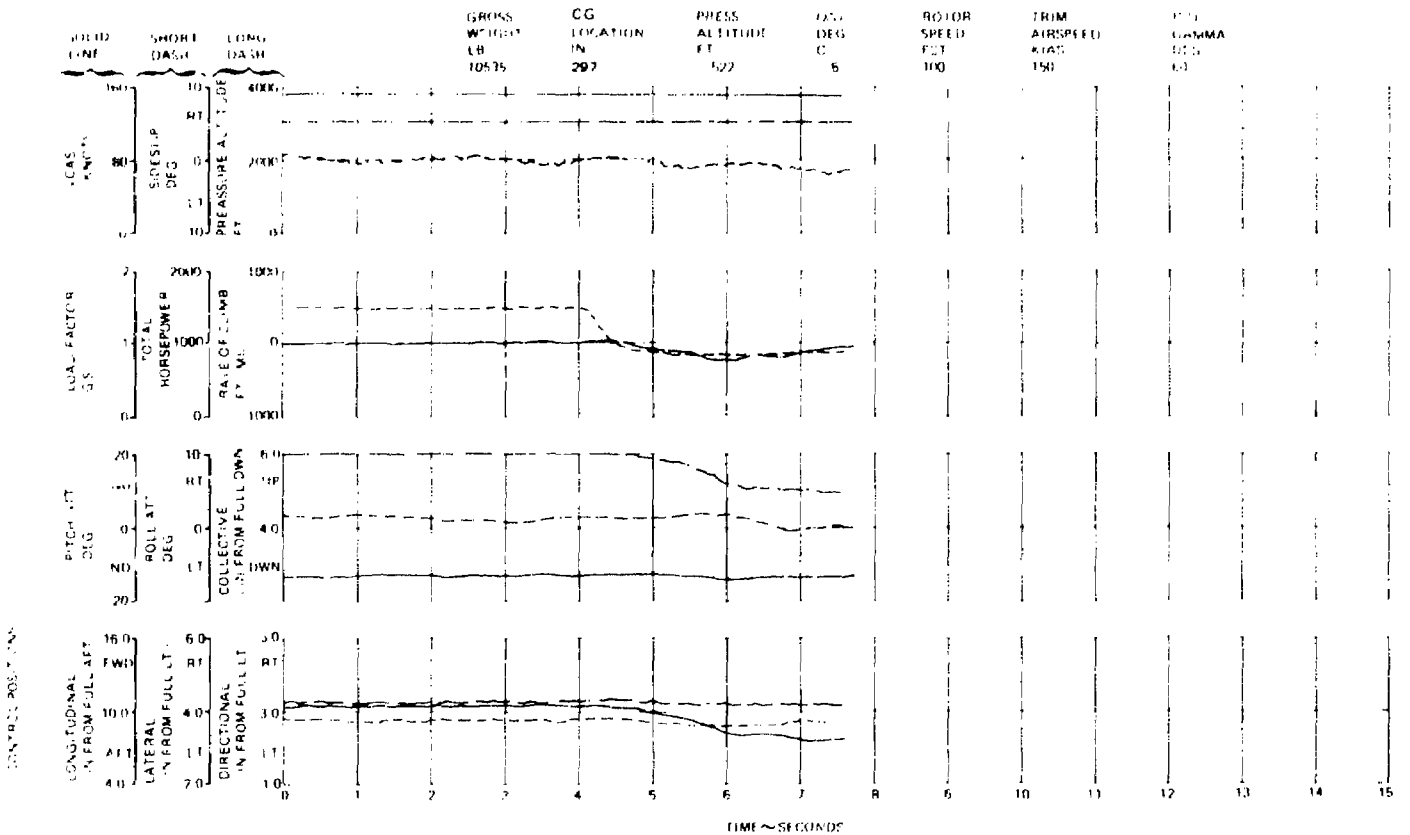

Figure 102. 150 Kn No. 1 Engine Cut, Helicopter Configuration.

safety-of-flight parameter to prevent rotor blade intersection. The master tailcone/fuselage stress and the master stabilizer attachment stress are presented to represent the XH-59A airframe. These locations were the critical stress locations known at that time. In all cases the master structural data locations resulted from structural surveys of the rotor and airframe and from rotor fatigue test and analysis

Effect of Rotor Speed

Figure 103 presents the effect of rotor speed on the rotor loads and airframe stress. Varying rotor speed within the range shown did not significantly affect the rotor loads except for the stress at the upper rotor shaft. The stress at that location increased with increasing rotor speed at 130 knots. This gage was sensitive to changes in rotor pitching moment. A review of the handling qualities data showed the longitudinal cyclic stick moved aft as rotor speed increased, indicating a change in rotor pitching moment. This characteristic is seen again in the Auxiliary Propulsion Section of this report. Figure 103 also indicates that the airframe stress was not significantly affected by changes in rotor speed.

Effect of Differential Longitudinal Control (A_1')

Changes in differential longitudinal control had no significant effect on the rotor loads or airframe stress (Figure 104). The predominant rotor loads resulted from the inter-rotor rolling moments, i.e., advancing and retreating blade azimuths. Therefore, small changes in the longitudinal axis had no significant structural effect. Differential longitudinal control primarily affected cockpit vibration and handling qualities.

Effect of Differential Lateral Control (B_1')

Figure 105 shows the effect of B_1' on the rotor and airframe with all other differential controls fixed. The data show that, if B_1' remained constant at the low value of .06 degree, endurance limits of the rotor system would be reached at a relatively low airspeed of approximately 120 knots and rotor tip clearance would be reduced below safe separation. Increasing B_1' reduced the rotor stress by decreasing blade pitch on the advancing side and increasing pitch on the retreating side of each rotor. This effectively reduced the roll moment on each rotor and opened the tip clearance.

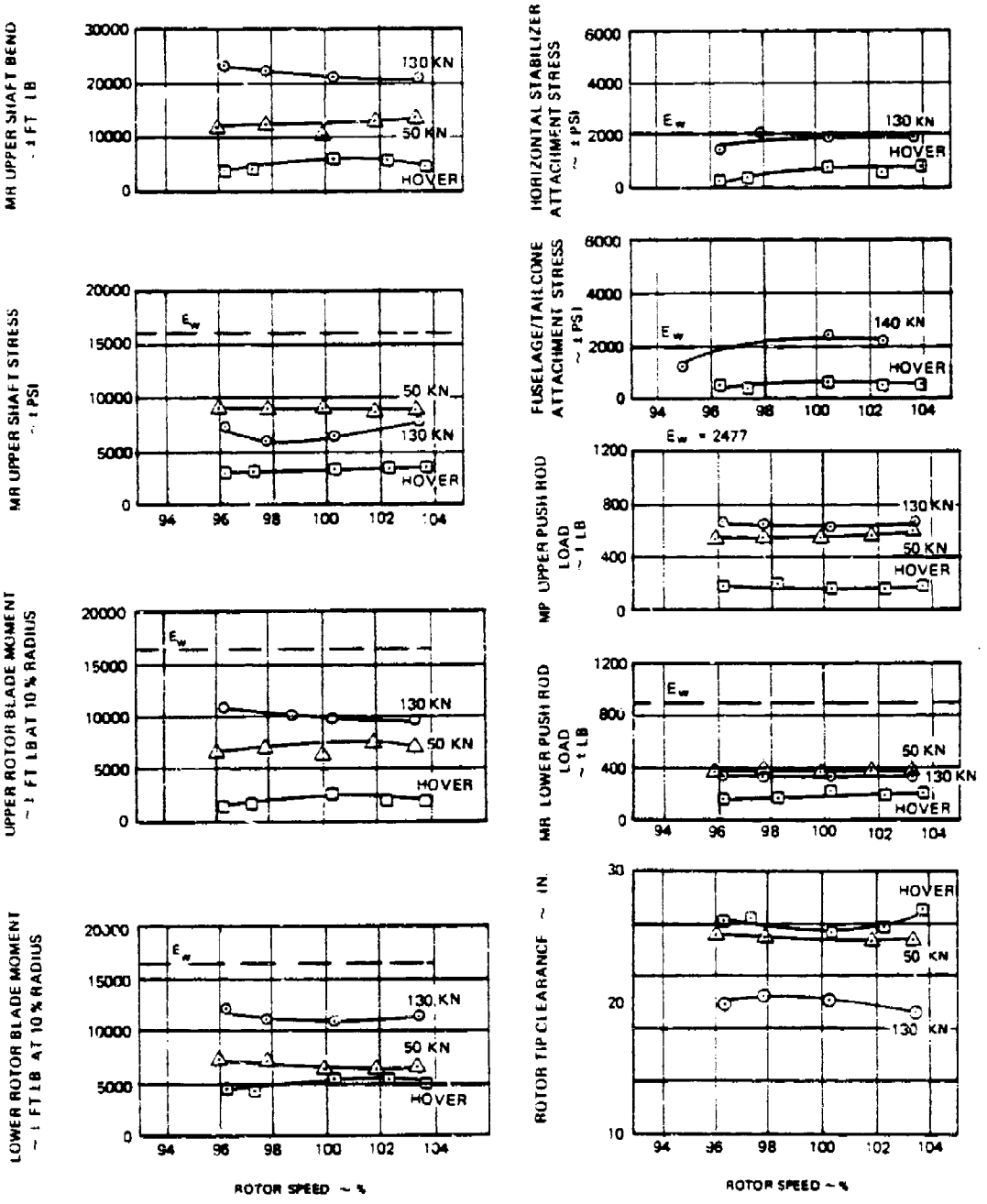

Figure 103. Effect of Rotor Speed on Rotor and Airframe Loads and Stresses, Helicopter Configuration.

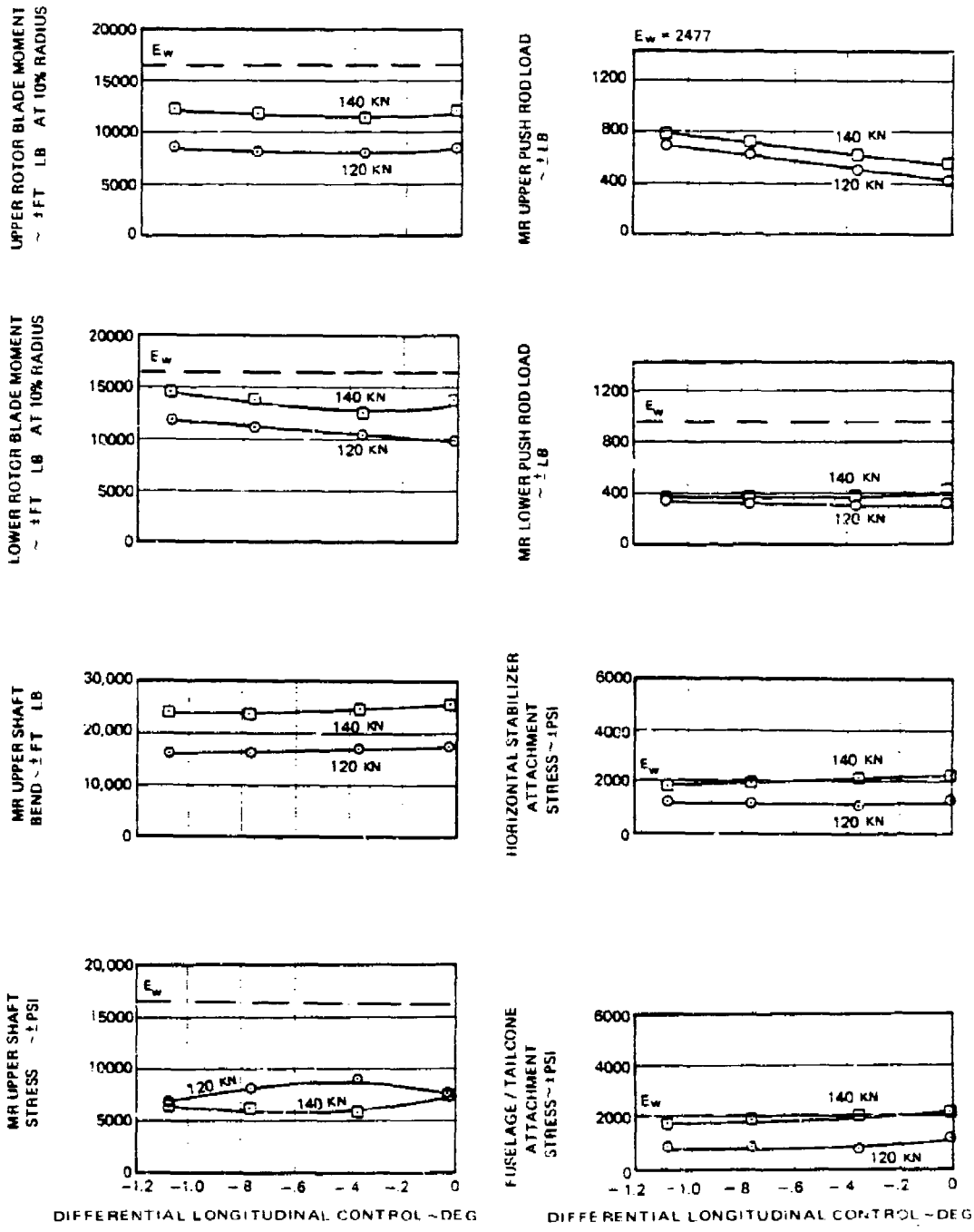

Figure 104. Effect of Differential Longitudinal Control on Rotor and Airframe Loads and Stresses, Helicopter Configuration.

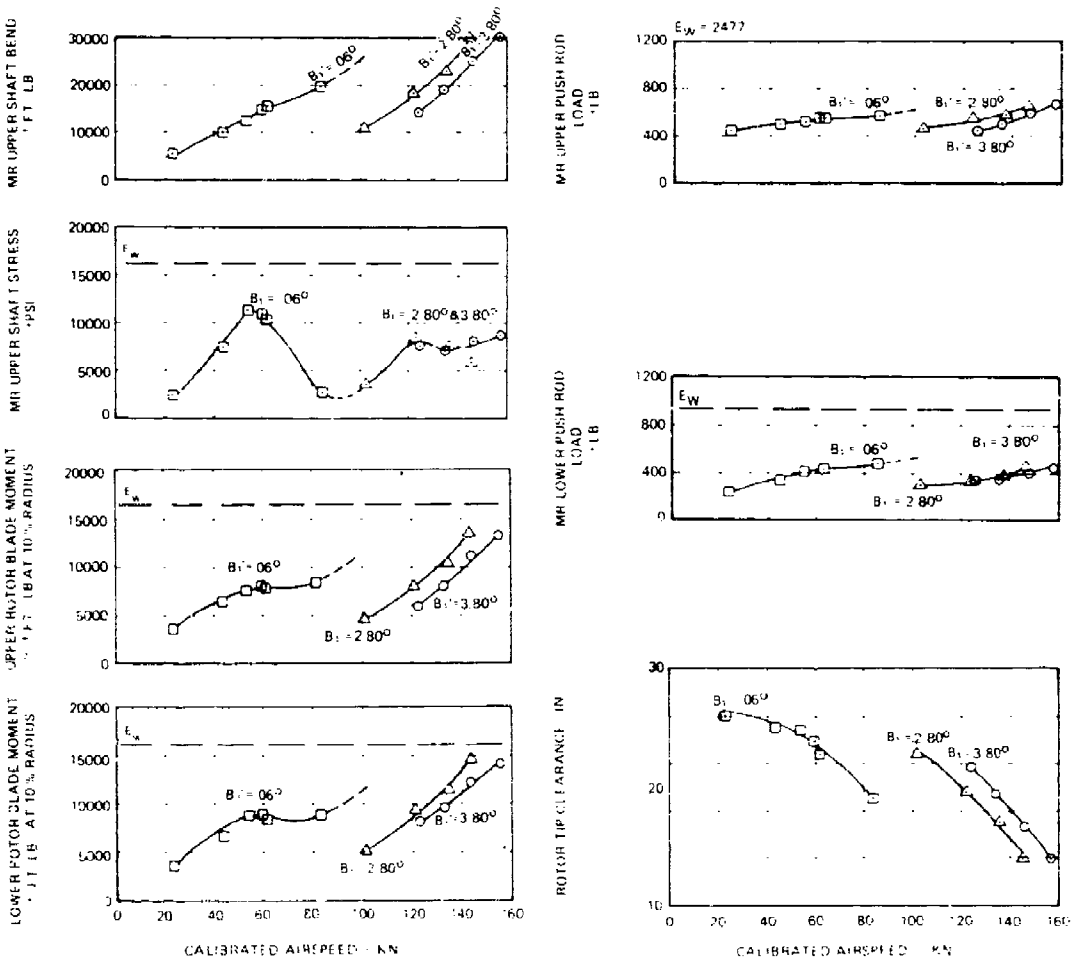

Figure 105. Effect of Differential Lateral Control on Rotor and Airframe Loads and Stresses, Helicopter Configuration.

Although differential lateral control is effective in controlling interrotor roll moments and the resulting rotor tip clearance and associated rotor loads and stresses, rotor control phase angle was found to be more effective. The effects of rotor control phase angle are discussed later in this section.

Effect of Differential Collective Control ($\Delta\theta_t$)

A positive increase in $\Delta\theta_t$ increased the collective pitch on the upper rotor and decreased the lower rotor collective pitch. Figure 106 demonstrates that changes in $\Delta\theta_t$ had very little effect in the vibratory (cyclic) loads in the rotor and airframe. However, a positive increase in $\Delta\theta_t$ did increase rotor tip clearance. This was the result of increasing the steady bending on the upper rotor and decreasing the steady bending slightly on the lower rotor. This same effect was evident in the auxiliary propulsion configuration.

Effect of Control Phase Angle (Γ)

Control phase angle (Γ) inputs to the rotor were made via secondary (analog) swashplates as described in the Flight Control Description section. The effect of varying Γ at a fixed cyclic position is the same as varying differential lateral and longitudinal controls, where increasing Γ increases the differential lateral contribution and decreases the differential longitudinal contribution. This effect provided similar control of rotor loads and stresses as can be seen by comparing data presented in Figure 105 (B_1' effect) versus Figure 107 (Γ effect).

It was obvious that either differential lateral (B_1') or control phase angle (Γ) variations, as a function of airspeed, can be used to effectively control rotor loads and stresses in trimmed flight. The choice of B_1' or Γ is of concern only in maneuvers. The use of control phase angle (Γ) variations as a function of airspeed was beneficial during maneuvering flight where the effect of rotor gyroscopics on rotor tip clearance was dramatically better using rotor control phase (Γ) than B_1'. The results of maneuver testing in the pure helicopter configuration are presented elsewhere in this section.

The data presented in Figure 108 show the final cockpit control schedule used for flight to maximum airspeed.

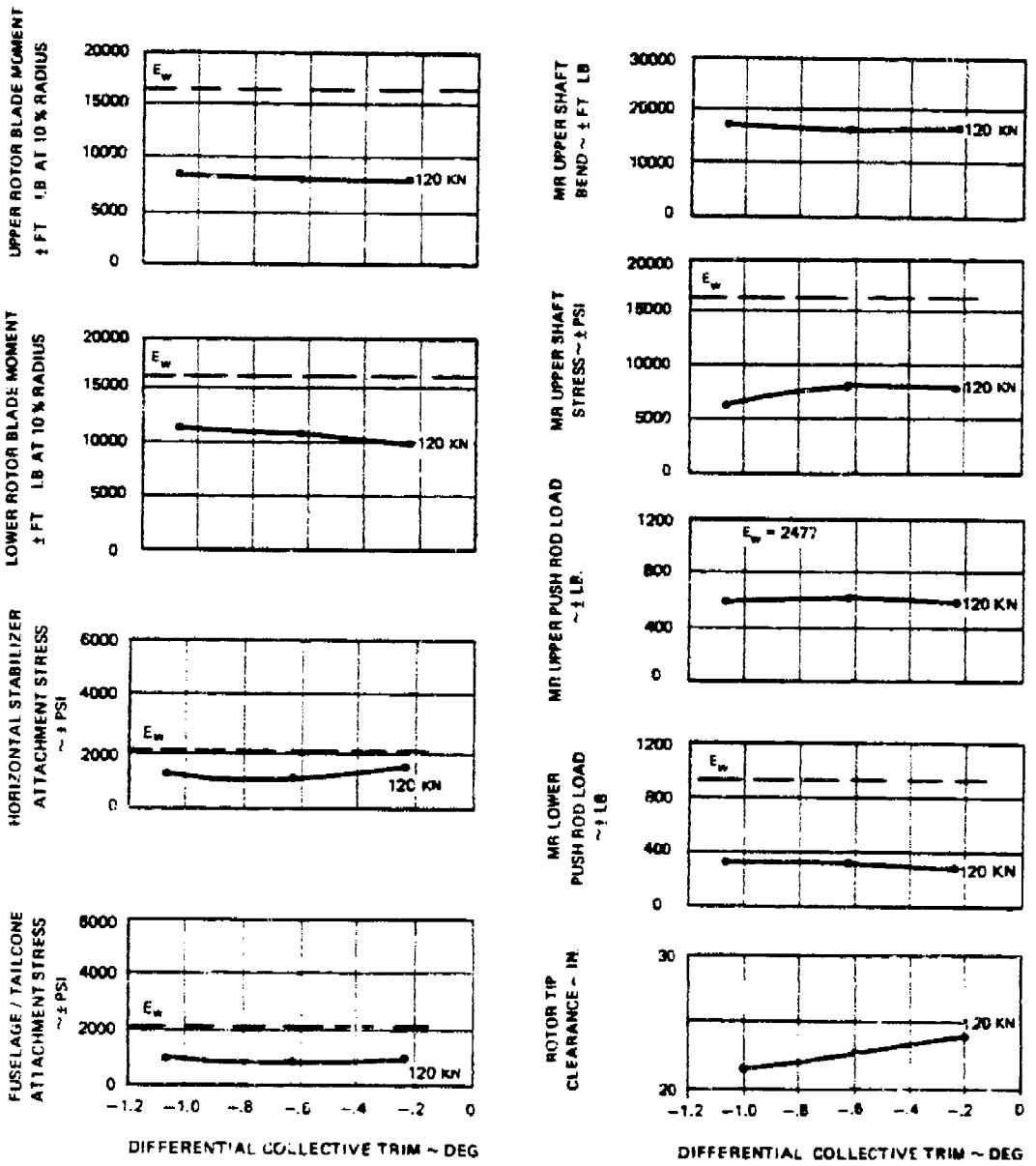

Figure 106. Effect of Differential Collective Trim on Rotor and Airframe Loads and Stresses, Helicopter Configuration.

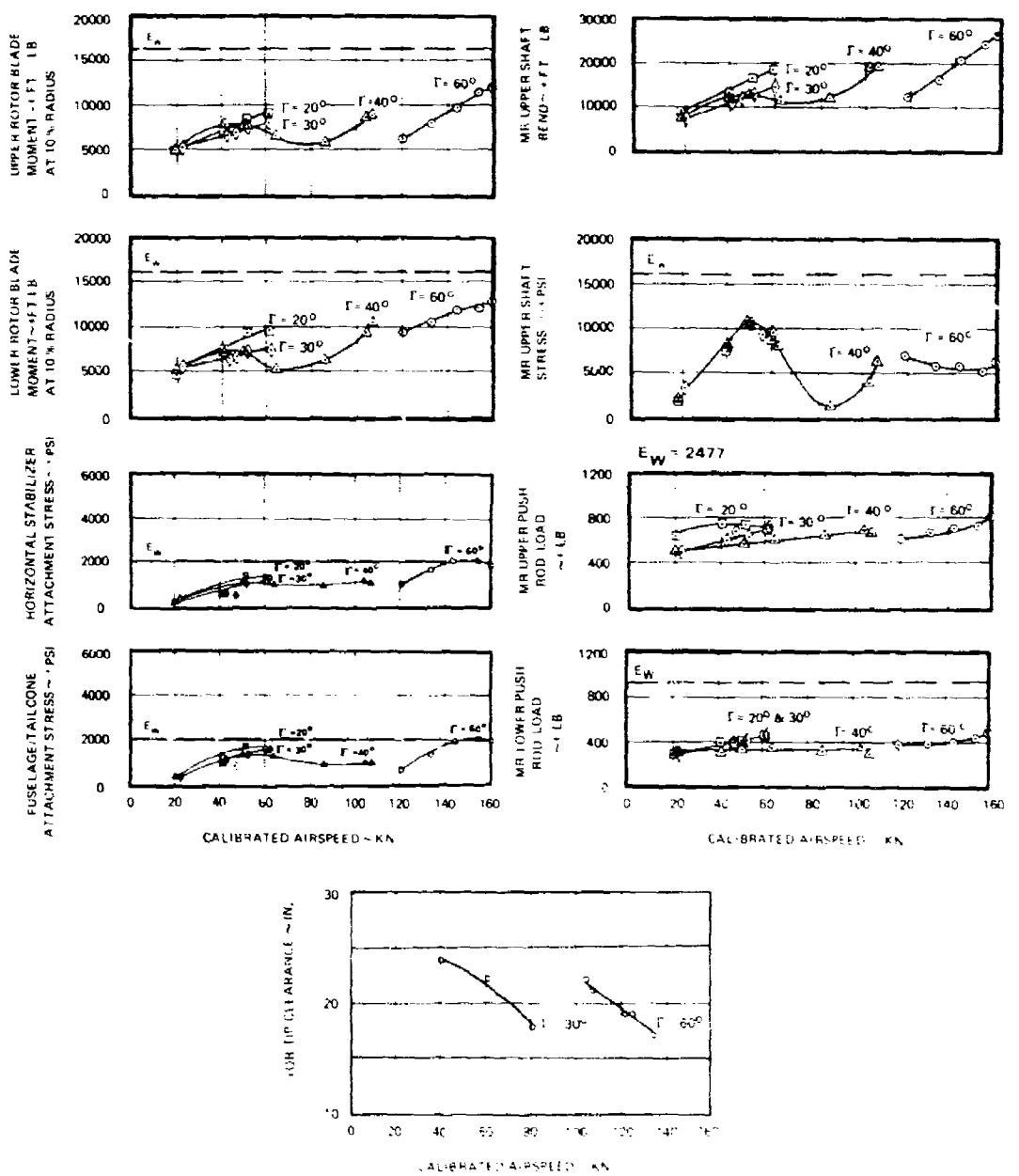

Figure 107. Effect of Control Phase Angle on Rotor and Airframe Loads and Stresses, Helicopter Configuration.

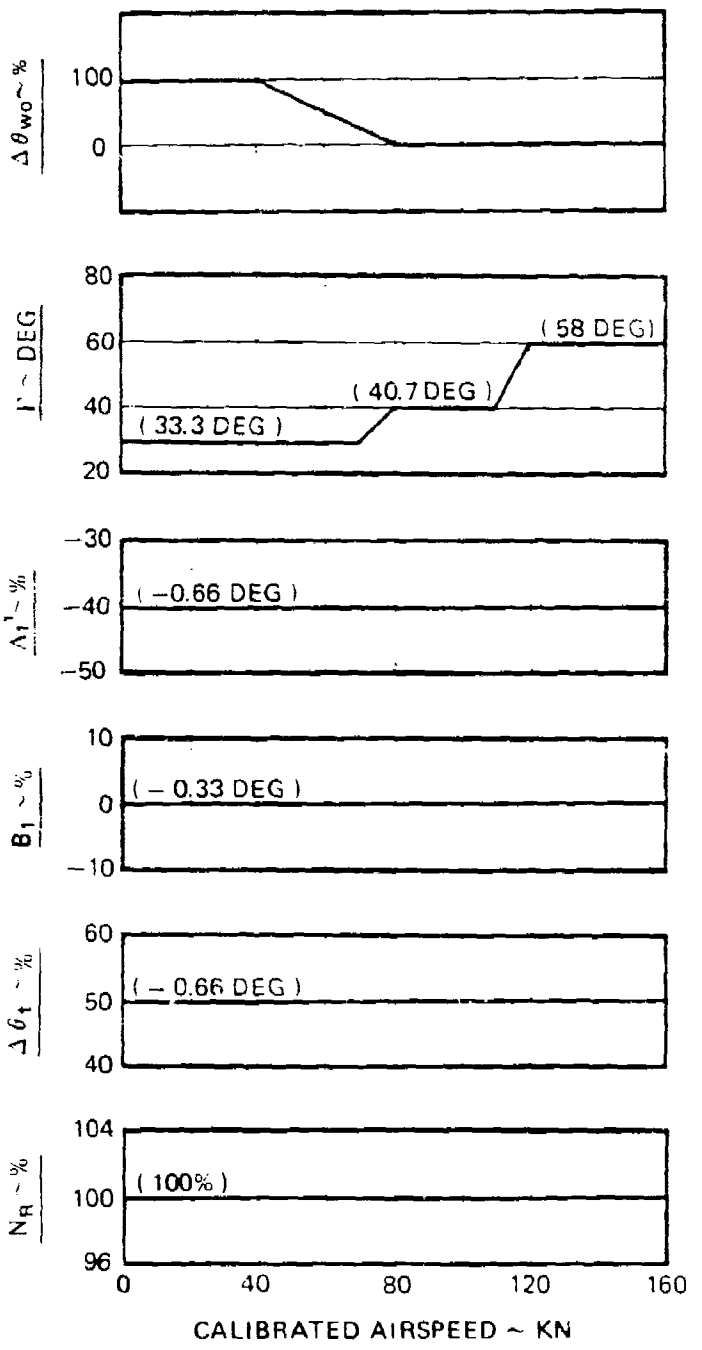

Figure 108. Cockpit Control Schedule - Helicopter Configuration.

Rotor Tip Separation - Trim Level Flight

Figure 109 presents correlation of rotor vibratory loads with tip clearance. The data shows a strong relationship of blade bending and shaft bending with tip clearance. As the rotor tips closed, the blade and shaft bending increased. However, the stress at the base of the upper shaft had no correlation with tip clearance since this location is sensitive primarily to total rotor pitch and roll moment. The minimum rotor tip clearance occurred on the left side of the aircraft where the upper rotor retreating blade is relatively unloaded and the lower rotor advancing blade is carrying high lift.

The rotor pushrods had a correlation with tip clearance. The pushrod loads were primarily a function of the blade pitching moment with blade bending providing a minor contribution to the load. Reviewing the Figure 109 data indicates that by keeping the rotor tip clearance above 13 inches, the endurance values of the rotor system were not exceeded in trimmed flight.

Structural Limitatons on Climb and Descent

Trim flight characteristics in climbing and descending flight were evaluated throughout the airspeed envelope. Figure 110 shows the boundaries established for the flight program. No structural limits were encountered during climbing flight. The climb limits were a function of rotor transmission torque only. Descending flight encountered two limits. The first limit was general aircraft roughness at airspeeds below 60 knots and is typical of all rotorcraft. The second limit was established by upper rotor shaft stress. The high stress is at the lower end of the upper rotor shaft adjacent to the bearing between the upper rotor shaft and the lower end of the lower rotor shaft. In this position the measurement responds to rotor system total pitch and roll moments. At high rates of descent the airloads on the horizontal stabilizer develop aircraft pitching moments that must be balanced by rotor pitching moments. These pitching moments caused high stress in the upper rotor shaft and limited the maximum rate of descent.

The shaft stress limits presented in Figure 110 are more restrictive than tested. For the pure helicopter testing, the upper rotor shaft master stress location endurance limit (Ew) was 23,100 psi. Prior to the start of the auxiliary propulsion configuration test program, the limit was reduced to 16,600 psi corresponding to a revised procedure regarding establishment of analytical endurance values. The information in Figure 110 has been adjusted to the new endurance limit for data continuity between aircraft configurations.

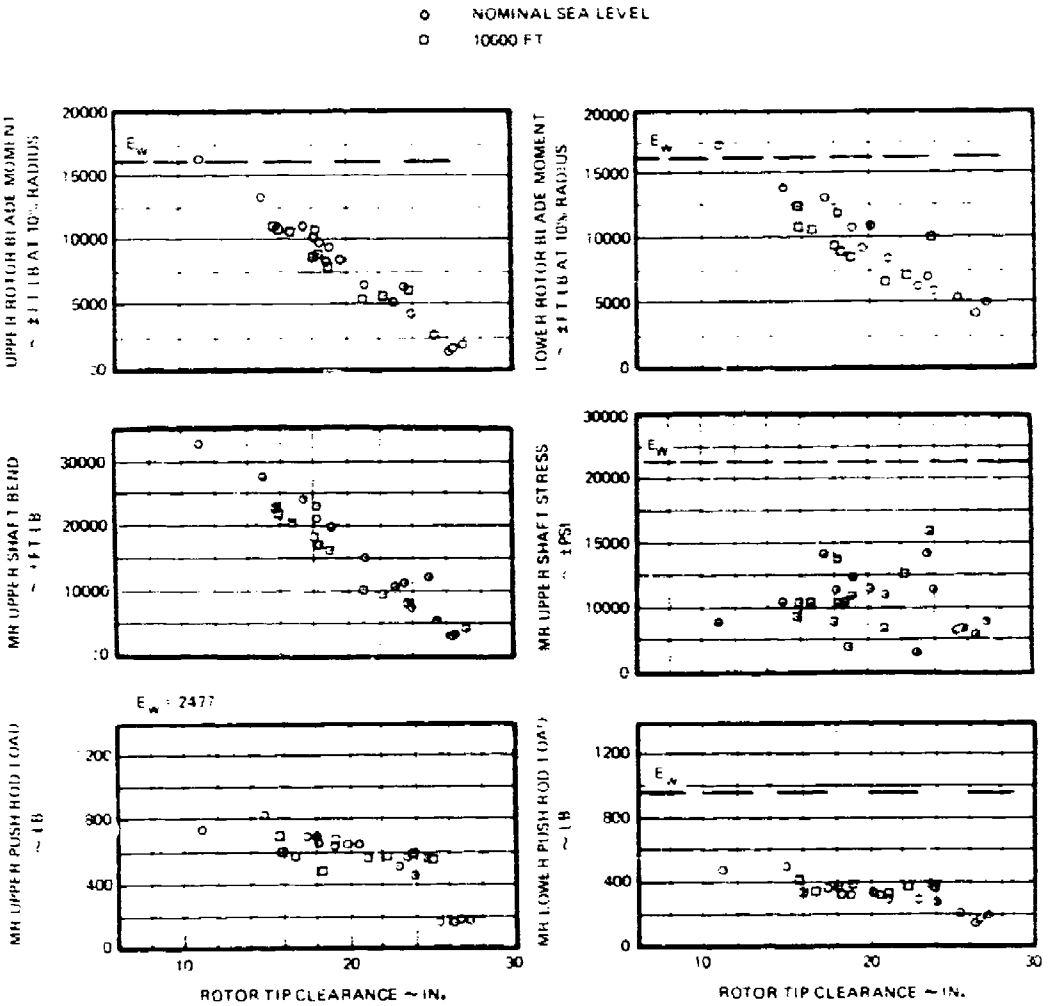

Figure 109. Rotor Tip Clearance Versus Rotor Component Loads and Stresses, Helicopter Configuration.

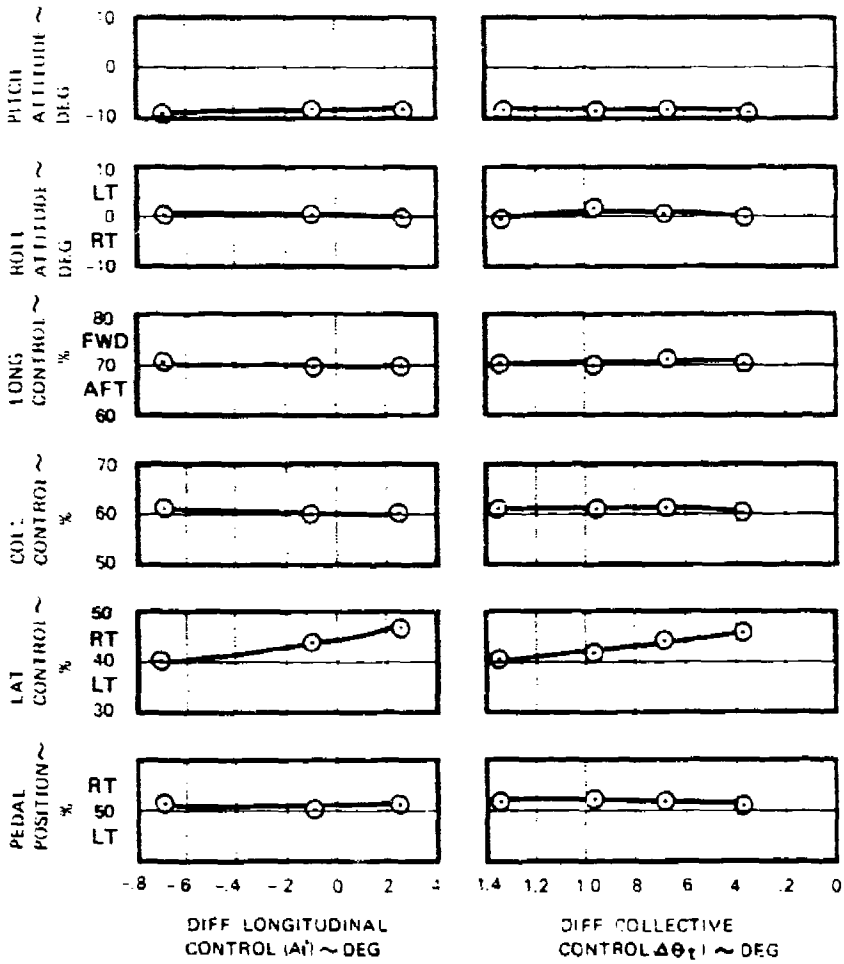

Figure 110. Climb and Descent Limitation Versus Airspeed, Helicopter Configuration.

The stabilizer-induced envelope limits on descending flight could be reduced by either reducing the stabilizer area or coupling the elevator with the collective control. Reduction of stabilizer area was simulated by flight testing with the elevator removed. Data simulating elevator/collective coupling was extracted from previous flights with variations in fixed elevator setting. The decision was made to couple the elevator to the collective control as the means of reducing the stabilizer-induced envelope limits. The chosen elevator gain with collective was established as 13.9 degrees trailing-edge-up at low collective, varying linearly with collective to 7 degrees trailing-edge-down at high collective. The descending flight limit reduction obtained both with elevator removed and with elevator coupled to the collective is also presented in Figure 110. Actual test data was obtained at substantially higher rates of descent at the higher airspeed with the pure helicopter test program endurance values.

The data presented in Figure 111 illustrates the effect of the three elevator configurations on the upper rotor shaft stress (master gage location) versus airspeed for trim level flight. As may be expected, there is little difference in the lower airspeed range. At the higher airspeeds the data reflects the variation in total rotor pitching moment for the three configurations. The upper rotor shaft stress remained well within the revised endurance limits for all elevator configurations.

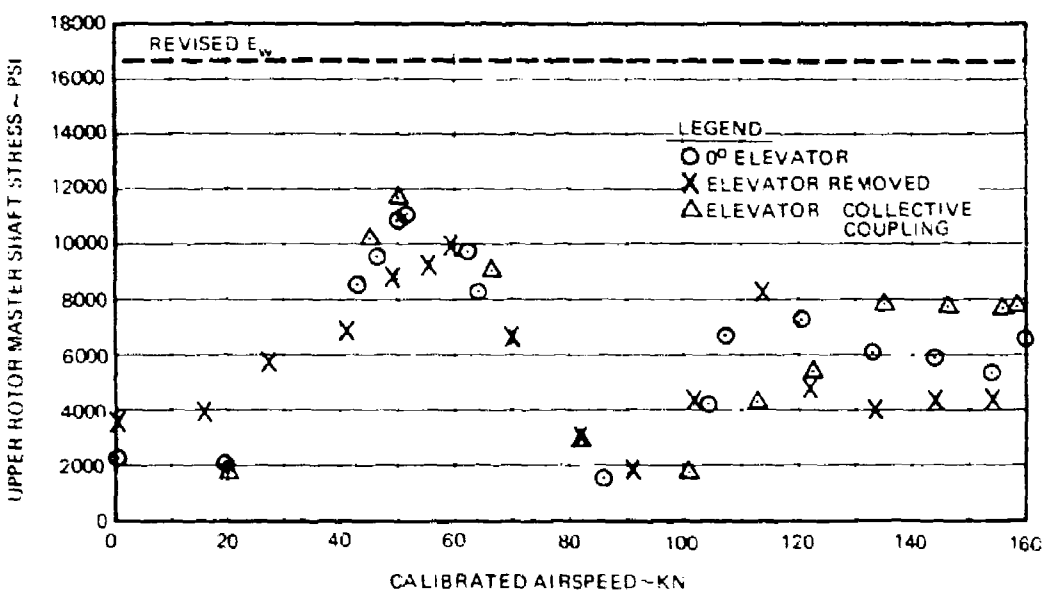

Figure 111. Upper Rotor Master Stress Versus Airspeed for Variation in Elevator Configuration, Helicopter Configuration.

Altitude

Figure 112 presents a comparison of the rotor loads and airframe stress at 3000 and 10,000 foot density altitude at the same gross weight. Figure 112 shows increased vibratory moments on the blades and rotor shaft at 10,000 foot Hd for the same calibrated airspeed. However, if the airspeeds are converted to true airspeed, the vibratory moment at altitude at the higher speed was slightly less than at sea level. The vibratory stress at the base of the shaft was not significantly affected by altitude. The control loads and rotor tip clearance had the same trend as blade bending. Airframe stress was increased slightly at the lower airspeeds at altitude, but was virtually unchanged at calibrated airspeeds above 100 knots.

Effect of Load Factor

Rotor blade tip separation as a function of load factor, airspeed and altitude is presented in Figure 113. These data show an apparent anomaly; since tip separation decreases with positive load factor at the higher airspeed as anticipated, but at low speed (80 knots) and negative load factor, the trend is reversed. This characteristic results from the high pitch rates required at lower speed to generate normal acceleration which in turn produces high gyroscopic precession forces. These forces act to separate the rotor in the critical quadrant between 225 and 315 degrees. As speed was increased, the required pitch rate decreased thereby reducing precession forces. At sea level the maximum load factor was limited by the basic static design strength of the airframe. At high altitude, however, the rotor showed evidence of stall at approximately 1.7 g's at the flight weight as shown by the reduction in tip separation and the characteristic waveform of special "hot film" gages installed on the top surface of one blade of each rotor to detect stall. In this condition the aircraft exhibited no adverse characteristic and all rotor component loads and stresses were acceptable.

High-Speed Dive Flight

Two flights were conducted to investigate general aircraft characteristics during high-speed dives from altitudes at or above 10,000 feet. Two different rotor trim techniques were evaluated. The first trim technique involved establishing trim at 12,000 feet and holding collective fixed during the pushover and subsequent incremental increased speed trim points. This testing was conducted from 100- and 125-knot level flight trim speeds. The second trim technique involved establishing a trim at 14,000 feet and lowering the collective during the pushover and subsequent incremental increased speed

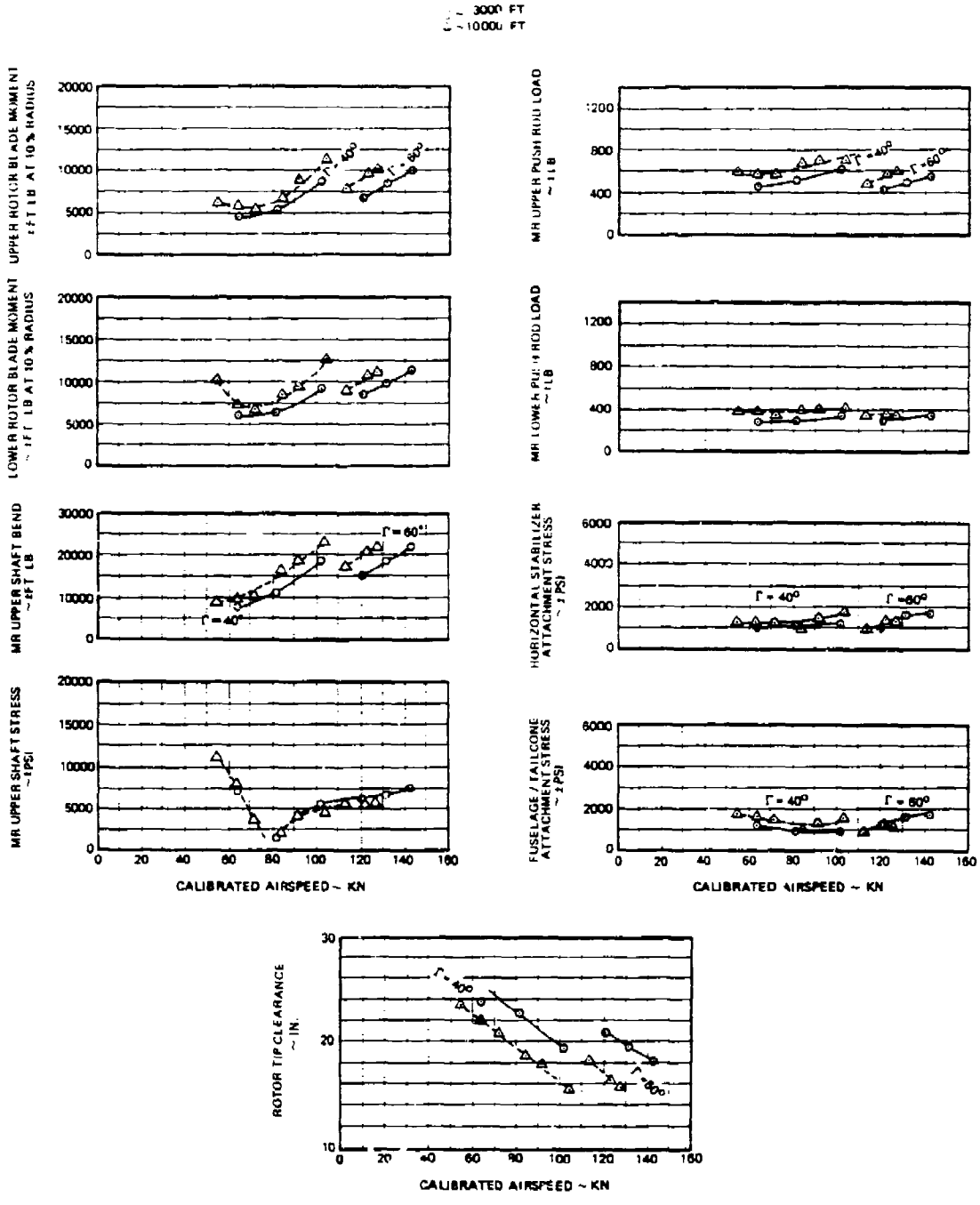

Figure 112. Effect of Altitude on Rotor and Airframe Loads and Stresses, Helicopter Configuration.

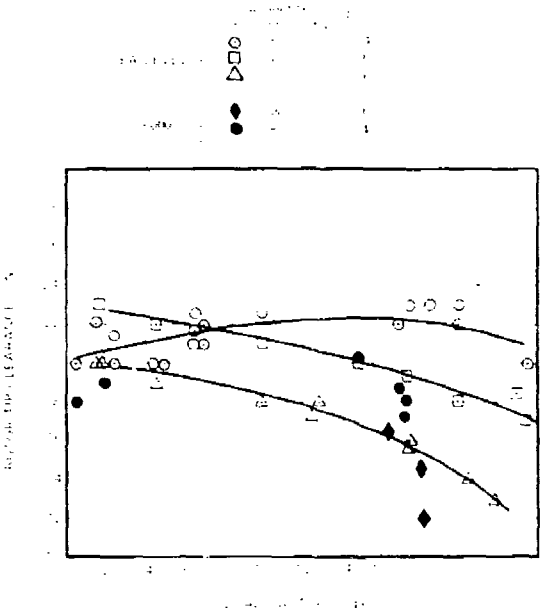

Figure 113. Rotor Tip Clearance Versus Load Factor, Helicopter Configuration.

trim points. Two lower collective settings, 50 percent and 35 percent, were evaluated. This testing was conducted to evaluate the effect of anticipated lower collective settings required for flight testing in the auxiliary propulsion configuration.

Data for the first set of dive trim points is presented in Figure 114. The maximum airspeed was 186 KTAS at 9200-feet density altitude. With the exception of exceeding the upper rotor shaft endurance limit when diving from the initial 100-knot trim point, no adverse aircraft characteristics were observed. The difference observed in the upper rotor shaft stress between the 100- and 125-knot trim dives is attributed to the difference in initial collective settings for the two trim points. With the lower collective setting (100-knot trim), additional positive rotor angle-of-attack was required to maintain lift. The additional rotor angle of attack resulted in larger rotor nose-up pitch moment for trim and a larger upper rotor shaft stress magnitude which is directly responsive to total rotor pitch and roll moments.

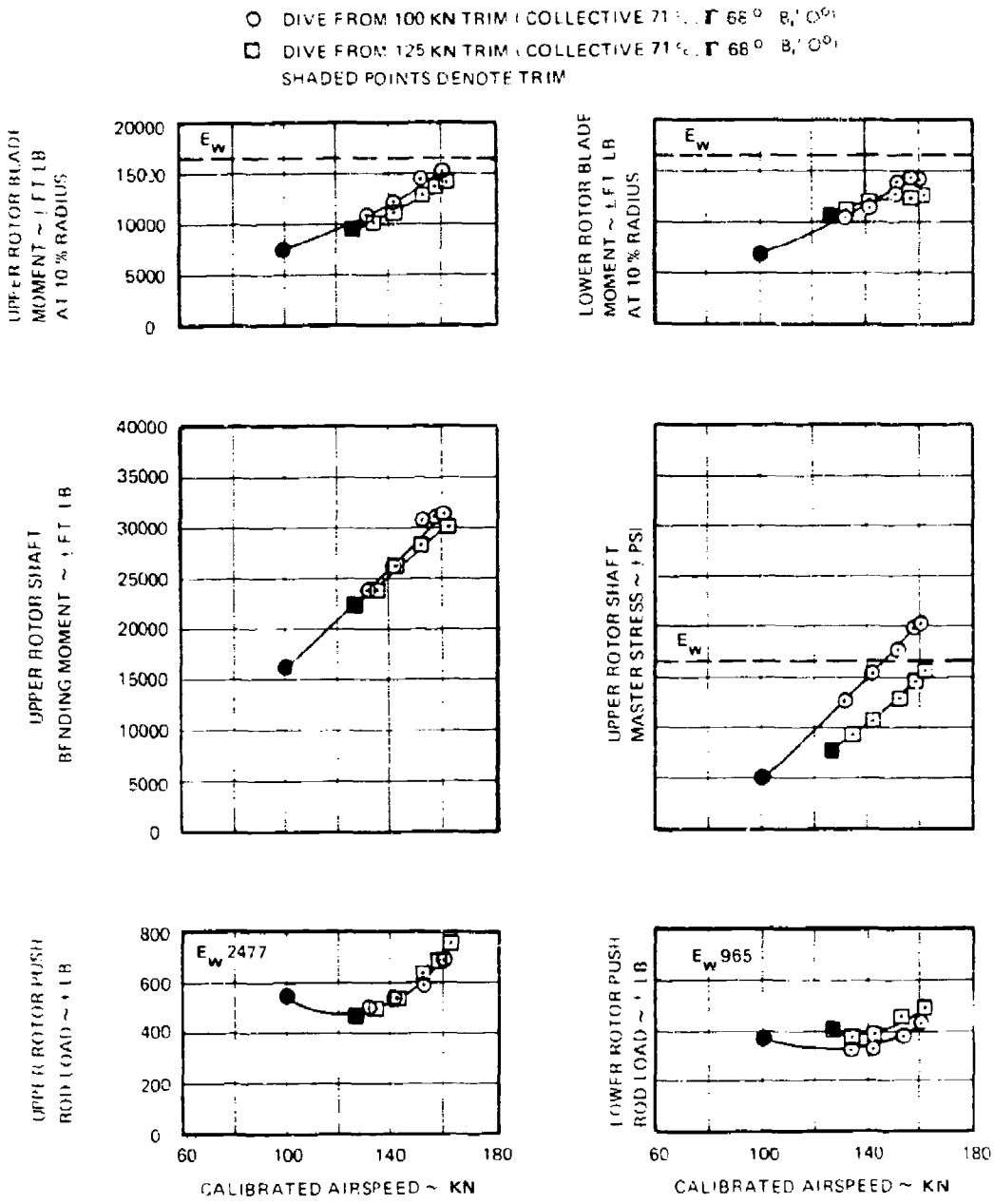

Figure 114. Dive Flight Structural Data, Helicopter Trim - 10,000 Feet, Helicopter Configuration.

Data for the second set of dive trim points is presented in Figure 115. As anticipated, the upper rotor shaft stress problem was amplified with the lower collective settings, as can be seen by comparing Figure 114 with 115. Analysis of this data confirmed that the helicopter configuration horizontal stabilizer angle of incidence of 10 degrees trailing-edge-down was improper for the anticipated rotor trim conditions required for the auxiliary propulsion test program. Further analysis ultimately established a horizontal stabilizer angle of incidence of 5 degrees trailing-edge-up for the auxiliary propulsion configuration.

An additional auxiliary propulsion simulation rotor trim condition was evaluated during the second set of dive trim points. A rotor control phase angle (Γ) of 68 degrees and differential lateral control (B_1') setting of 0 degree, consistent with high-speed pure helicopter flight, was used for the dive trim points of Figure 114. It was anticipated that a Γ of 40 degrees would be required for auxiliary propulsion testing. The second set of dive points were conducted with a Γ of 38 degrees and a B_1' of 0 degree to evaluate this condition. This trim configuration resulted in substantially larger upper and lower rotor blade moments; compare Figure 114 with Figure 115. These loads resulted from excessive outboard migration of the lift vector and the resultant large inter-rotor roll moments. It was evident from this testing that either a different Γ setting or the use of B_1' to control the lift offset migration would be necessary for auxiliary propulsion testing. After further analysis, differential lateral control (B_1') was selected for auxiliary propulsion testing.

Effects of Roll Rate

Two methods of rotor trim were employed during the roll rate test evaluations. The first method used fixed rotor control phasing (Γ) and employed differential lateral control (B_1') to control rotor lift offset. The second method used variable rotor control phasing to control rotor lift offset, and the differential lateral control was fixed at zero degree. A summary of tip clearance versus roll rate for both rotor trim configurations is presented in Figure 116.

The data summary for fixed rotor control phasing and variable differential lateral control is presented in Figure 116A. It may be noted for this rotor trim configuraton that there are two apparent discrepancies. First is the difference between tip clearance at 80 and 120 knots for zero roll rate. This difference is a function of airspeed and the differential lateral control (B_1') schedule established to control lift

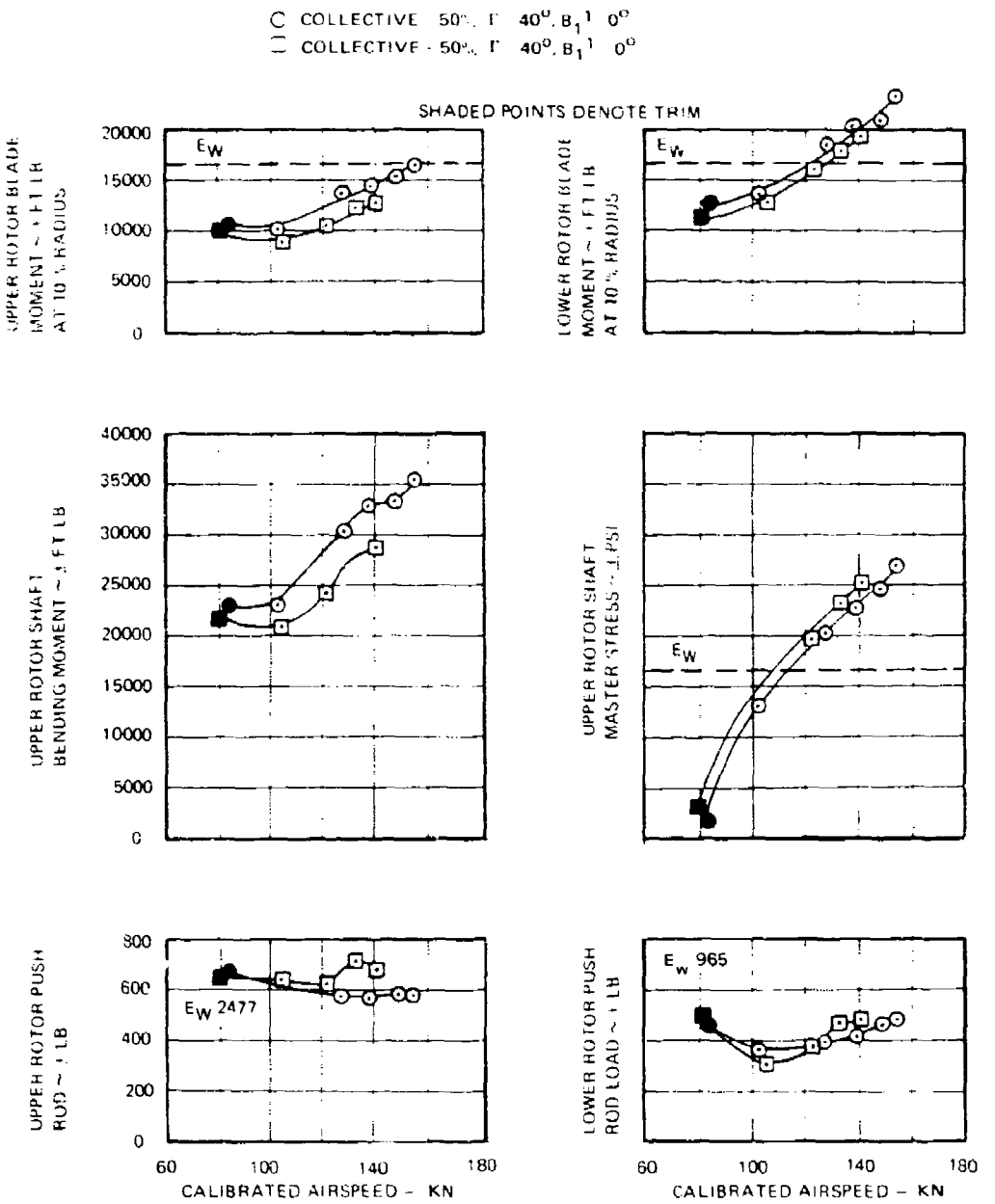

Figure 115. Dive Flight Structural Data - Auxiliary Propulsion Simulation - 14,000 Feet, Helicopter Configuration.

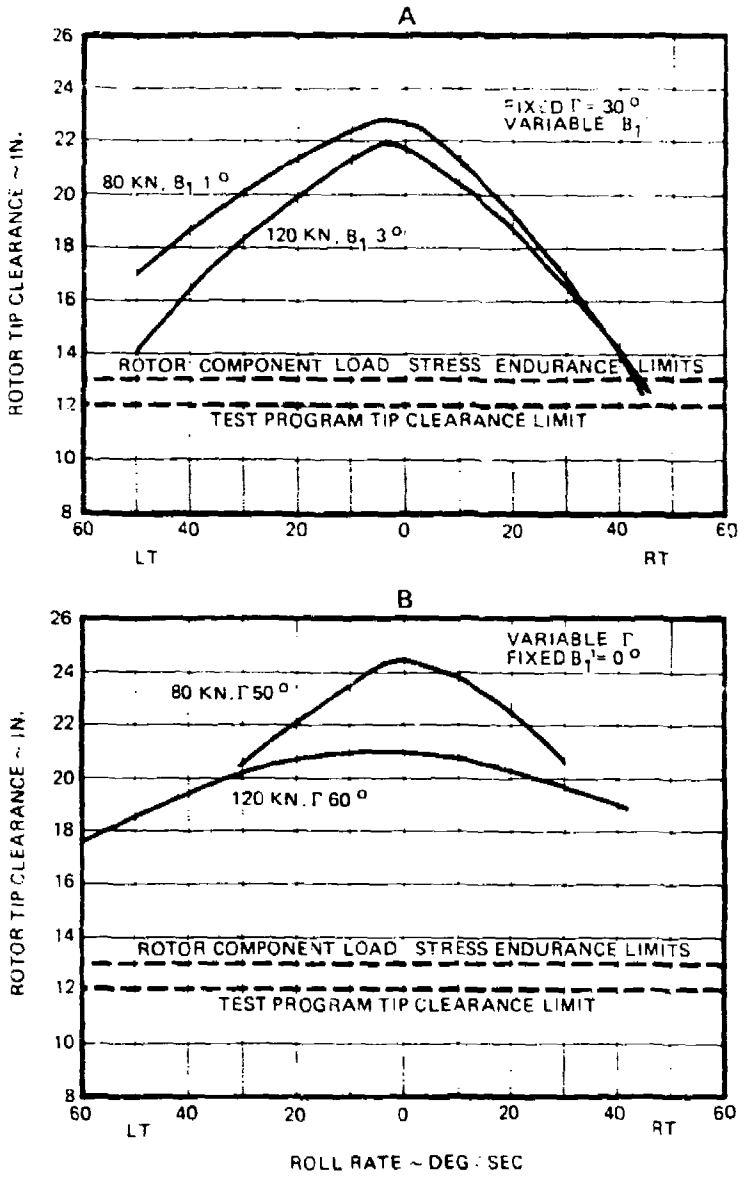

Figure 116. Effect of Roll Rate on Rotor Tip Separation and Rotor Loads and Stresses, Helicopter Configuration.

offset and the resultant rotor loads and stresses. Second is an apparent discrepancy in initial tip clearance as a function of roll direction. This is due to three major items: (1) the location of the minimum tip clearance in rotor azimuth as determined by airspeed and rotor trim settings, i.e., A_1', B_1', and $\Gamma\theta_t$; (2) rotor precession caused by the roll rate generated; and (3) the introduction of A_1' through the control phase angle with the applicaton of lateral control.

The data summary for variable rotor control phasing and fixed differential lateral control is presented in Figure 116B. This data shows the same apparent discrepancies as the data with fixed rotor control phase (Γ) and variable differential lateral control (B_1')except that there is substantially larger difference in tip clearance at 80 and 120 knots for zero roll rate. This is the result of using a rotor control phase angle schedule to control lift offset and the resultant rotor loads and stresses.

The largest difference between the two rotor trim configurations is the strong effect higher rotor control phase angles (Γ) have on reducing the rate of tip closure with roll rate. Introducing lateral cyclic through Γ also introduces a differential longitudinal control (A_1'). As the Γ angle is increased the differential longitudinal control effect becomes stronger. In the case of roll rate maneuvers, the A_1' component is compensating in terms of tip closure and reducing the delta tip closure with roll rate.

As noted from the data presented in Figure 109, 13 inches of rotor tip clearance represented a nominal separation above which the rotor system component loads and stresses remained below endurance (Ew) values. A review of the data of Figure 116 shows that rotor loads and stresses did not inhibit the roll rate maneuvers.

Both control configurations are feasible and selection of one or the other would be dictated by specific design mission requirements.

Summary of Helicopter Structural Results

1. Changes in rotor speed between 96 and 104 percent N_R did not affect the rotor loads or airframe stress except for the stress at the base of the upper shaft. This stress increased with increasing rotor speed at 130 knots due to changes in rotor pitching moment.

2. Differential longitudinal control did not affect rotor loads or airframe stress.

3. Differential lateral control scheduling with airspeed effectively controlled rotor loads and rotor tip clearance.

4. Control phase angle scheduling with airspeed effectively controlled rotor loads and tip clearance. It also maintained greater tip separation in roll reversals than differential lateral control.

5. Differential collective pitch did not significantly affect rotor loads or airframe stress. However, increasing differential collective pitch increased rotor tip separation.

6. Maintaining rotor tip clearance above 13 inches in trim flight resulted in rotor loads below the endurance limits.

7. Partial power descents and autorotation were limited by the stress at the base of the upper shaft resulting from the increased pitching moment. Elevator collective coupling increased the autorotation speed by 15 knots.

8. Increasing density altitude increased the rotor loads and decreased rotor tip clearance for a given calibrated airspeed. However, the stress at the base of the upper shaft was not affected by altitude.

9. High-speed dives at altitude indicated that at the reduced collective settings simulating the auxiliary propulsion configuration, the stablizer incidence must be changed to reduce the stress at the base of the upper shaft.

DYNAMICS

Aircraft Aeroelastic Stability

The rotor system was demonstrated to be aeroelastically stable up to 156 KTAS level flight and throughout the flight envelope, including dive speeds to 186 KTAS and full autorotative descents up to 3500 feet per minute. The rotor was excited to check edgewise damping during envelope expansion by pilot inputting longitudinal cyclic stick pulses. The only significant mode of rotor response was a regressive inplane blade mode of each rotor at a frequency of 1.4P in the rotating system. This mode was unchanged throughout the flight envelope and involves almost pure edgewise response; no significant coupling exists between the edgewise and either blade flatwise bending, blade torsion, or airframe/ control system response.

Rotor system modal damping levels in level flight were shown to be well above the 0.5 percent critical inherent structural damping measured in the blades. Damping varied from 2.5 percent critical in hover to a minimum of 1.0 percent at 80 knots and again increased to 2.5 percent at high speeds. The variation of the regressive mode stability with airspeed is shown in Figure 117.

Minimum rotor damping levels were experienced at high rates of descent, but still were above the level of edgewise structural damping inherent in the blade. In full autorotation at 80 knots, 2400 feet-per-minute descent, minimal modal damping of 1.2 percent to 0.5 percent critical were encountered. This trend of damping in descents shown in Figure 118 was expected at high inflow angles where the change in induced drag acting in phase with the edgewise velocity in descent tends to reduce the net aerodynamic damping as shown in Figure 119.

Since the rotor is relatively stiff in torsion, with a blade torsional natural frequency near 11 to 12P at 100 percent rpm, classical blade flutter is precluded from airspeeds below 400 knots. In fact, flight results showed no indication of this phenomenon throughout the flight envelope. Stall flutter, usually evidenced by a sharp buildup of control loads with airspeed or load factor, was not evident in the XH-59A helicopter mode testing. This is due to the high torsional natural frequency which results in small coupling motions into the flatwise direction.

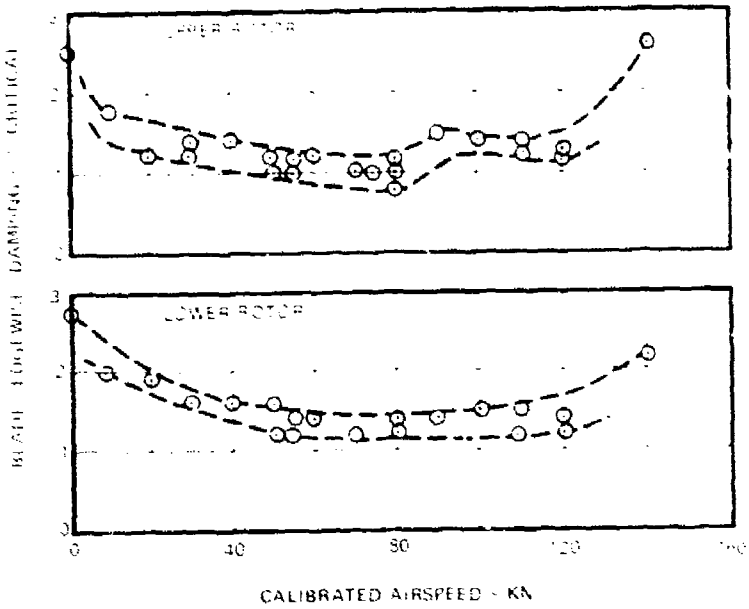

Figure 117. Blade Edgewise Damping Versus Airspeed, Helicopter Configuration.

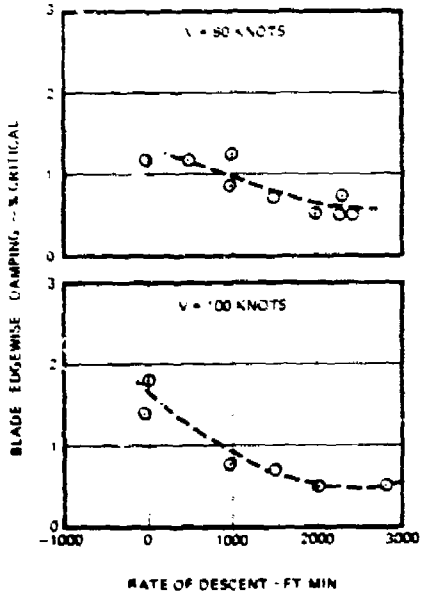

Figure 118. Blade Edgewise Damping Versus Descent Rate Upper Rotor, Helicopter Configuration.

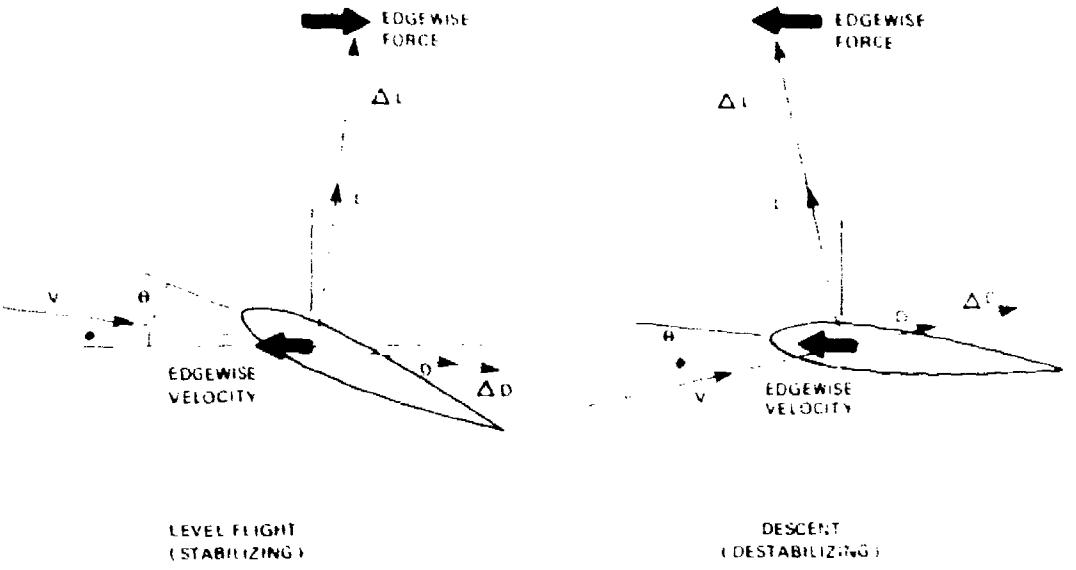

Figure 119. Blade Edgewise Damping Source.

There were no indications of surface flutter of either the horizontal stabilizer or vertical stabilizer throughout the helicopter flight testing. Predictions had shown flutter speeds for these surfaces in excess of 600 knots with the controls (rudder and elevator) locked. With the rudder active, however, a lower flutter speed was predicted unless it was mass balanced. This mass balance was done for the rudders on the XH-59A. Weight was added to the leading edge to attain a 75 in.-lb overbalance. This precluded surface flutter to well over 400 knots with the rudder active. The elevator was flown in a locked-out fixed position or driven through an irreversible hydraulic actuator located at the tail so that surface flutter for the horizontal stabilizer was not an issue.

Airframe Vibration

Cockpit vibratory response was monitored throughout the test program and agreed generally with trends predicted by analysis. The predominant cockpit response for a 90 degree cross-over, 3P pilot lateral, increased sharply above 100 knots in airspeed as shown in Figure 120. The rotors were phased to cancel 3P pitching moment, vertical and longitudinal shear forces and therefore added in the 3P yaw, roll and lateral directions. This accounts for the low 3P longitudinal and

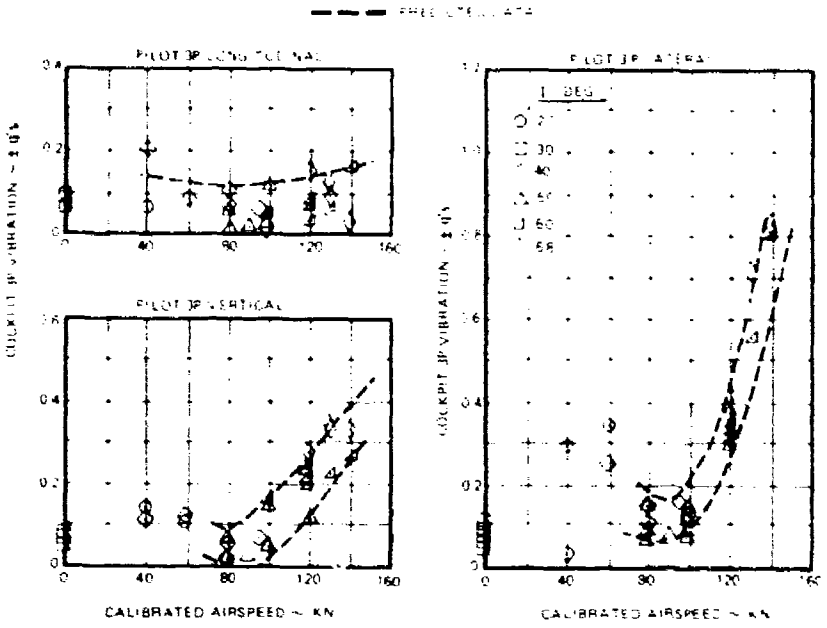

Figure 120. Cockpit 3P Vibration Versus Airspeed, Helicopter Configuration.

high 3P lateral response shown in Figure 120. The rise in cockpit 3P vertical at high speeds is not caused by higher rotor head vertical excitation but by a cockpit vertical component resulting from increased rotor head roll moment excitation.

The 3P hub roll moment generated primarily by 2P flatwise blade bending is the prime cause for the rise in cockpit 3P lateral vibration as shown by Figure 121. Blade root bending moments were harmonically analyzed (shown in Figure 122 versus airspeed) and resolved into nonrotating coordinates to calculate the hub 3P roll and pitch moment trends. The 2P blade flatwise and edgewise bending components were the dominant contributors to 3P hub roll and correlate with the rise in cockpit 3P lateral response as shown in Figure 121. In general, this correlation between 3P roll moment and 3P cockpit lateral/roll vibration held firm throughout the testing.

The aircraft design has provisions to install a vibration control system that would isolate the airframe from this roll/lateral excitation through the use of elastomeric transmission mounts. Such a system was fabricated, but initial

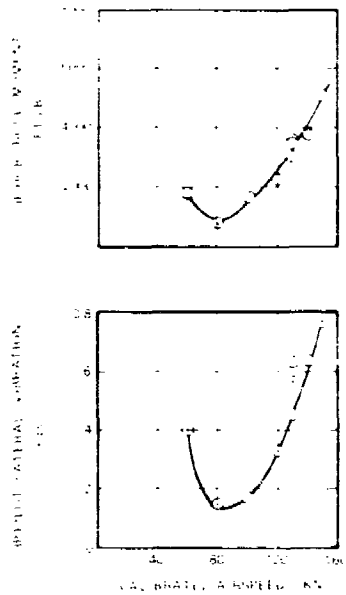

Figure 121. Correlation of Cockpit Lateral Vibration with Roll Moment, Helicopter Configuration.

flight tests to 100 knots indicated that it might not be required. Alternatively, attention was given to other means of vibration control such as control system changes allowed by the coaxial rotor system of the ABC and a fixed system absorber.

Parametric variation of the differential controls indicated that aircraft vibration could be reduced. Over the small range of Γ tested, a reduction in Γ at 120 and 130 knot speed results in a reduction in pilot lateral 3P vibration, as shown in Figure 123. As Γ is decreased, the 3P roll moment is reduced due to a sharp decline in lower rotor 2P vertical airloads as shown in Figure 124. The use of this control was limited by shaft bending and blade tip clearance considerations, since decreasing moves the advancing blade center of lift further out on the blade span.

Figure 125 shows a reduction in 3P roll moment and pilot lateral vibration as differential longitudinal cyclic pitch (A_1') is varied. Further examination of pilot 3P lateral response in Figure 125 shows that the total vibration is due both to roll and pure lateral motion at the pilot seat. As A_1' is decreased, the lateral component, out of phase with roll, actually increases due to increased 2P blade edgewise bending

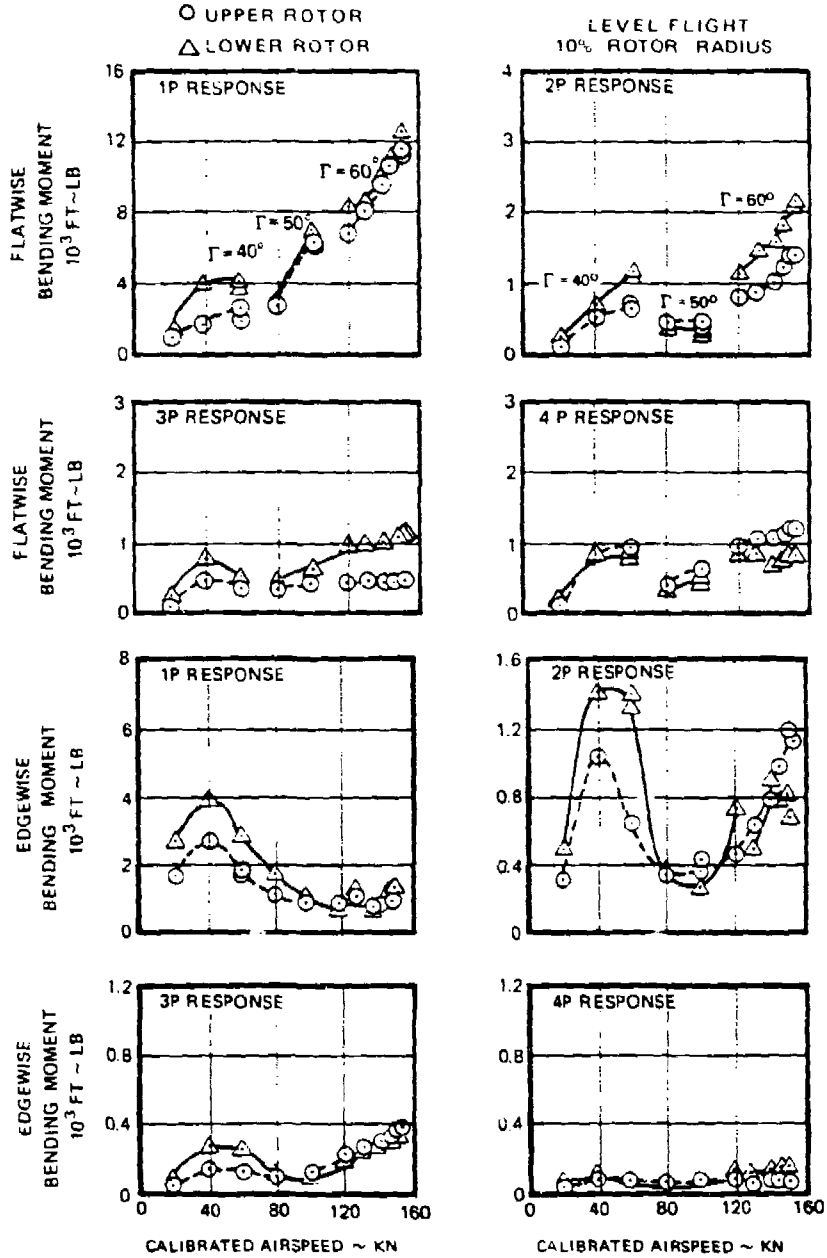

Figure 122. Harmonic Analysis of Blade Flatwise Bending - Level Flight 10% Radius, Helicopter Configuration.

loads. As shown in Figure 126 this results in cancellation and reduced net 3P lateral vibration at the pilot seat. While these control investigations were interesting, no combination was found which could reduce the vibration at high speed.

The installation of a 62-lb dynamic mass fixed system lateral absorber located on the cabin floor 40 inches aft of the cockpit contributed the most to reducing high-speed 3P pilot lateral vibration. With this arrangement an approximate 27 percent to 45 percent reduction in cockpit vertical and 33 percent reduction in pilot lateral response were obtained as shown in Figure 127. Inspection of the 3P lateral airframe response shape in Figure 128 shows that the most effective location for the absorber is as far out toward the nose as possible. The absorber tested had to be located in a much less than optimum position due to space, slightly forward of an airframe node. The improvements in vibration gained with this compromise location suggest that proper placement of the absorber could significantly improve pilot 3P vibration but this local improvement may come at the expense of increased loads and vibrations elsewhere in the vehicle.

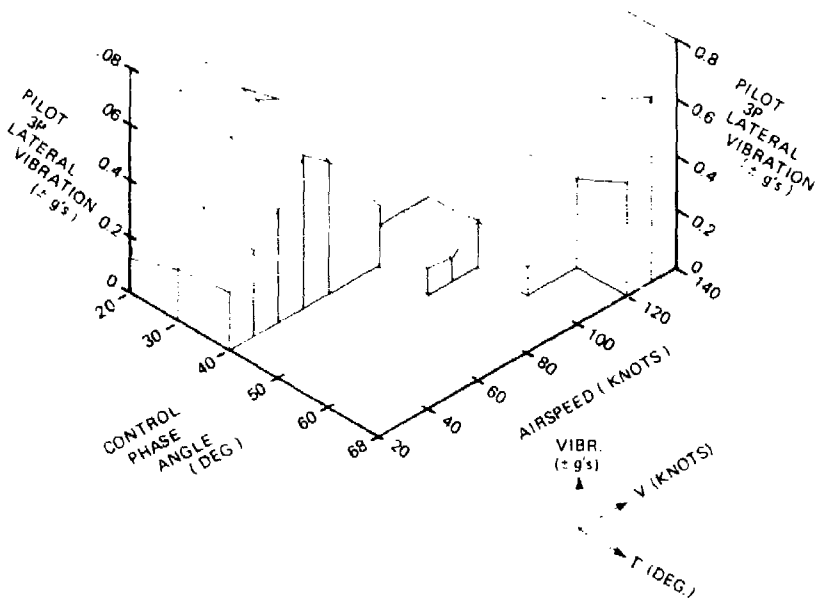

Figure 123. Increasing Rotor Lift Offset (Decreasing Γ) Reduced High-Speed Pilot Lateral Vibration, Helicopter Configuration.

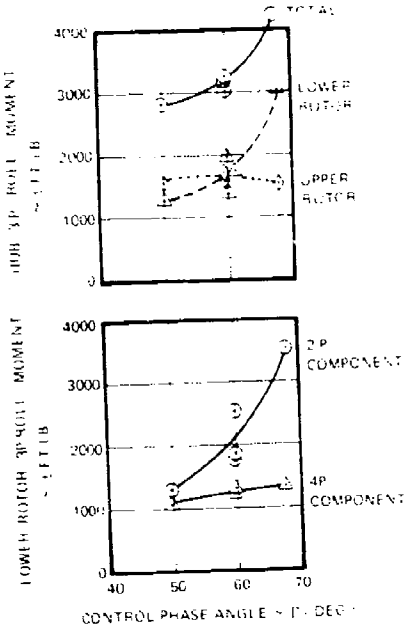

Figure 124. Decreasing Control Phase Angle Reduces 3P Roll Moment; V = 130 Kn; Helicopter Configuration.

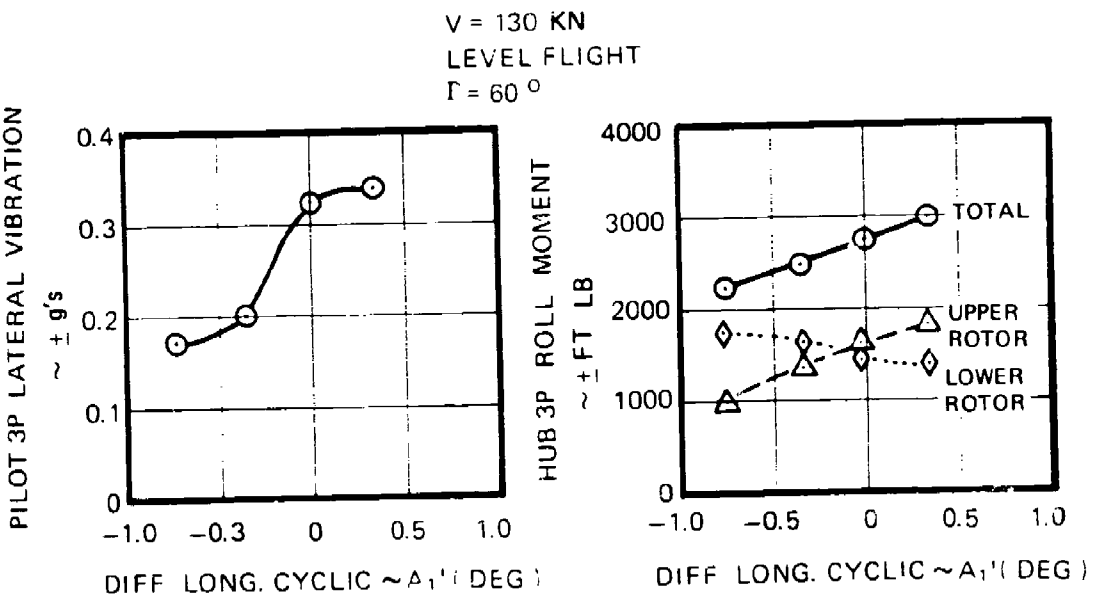

Figure 125. Decreasing Differential Longitudinal Cyclic Reduces Pilot Lateral Vibration, Helicopter Configuration.

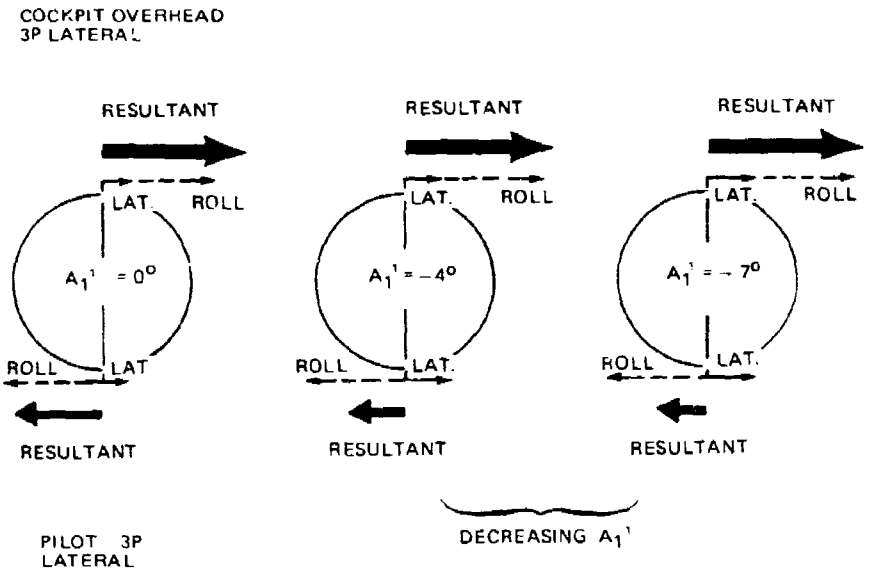

Figure 126. Roll Lateral Components of Cockpit 3P Lateral Vibration V = 130 Kn, Helicopter Configuration.

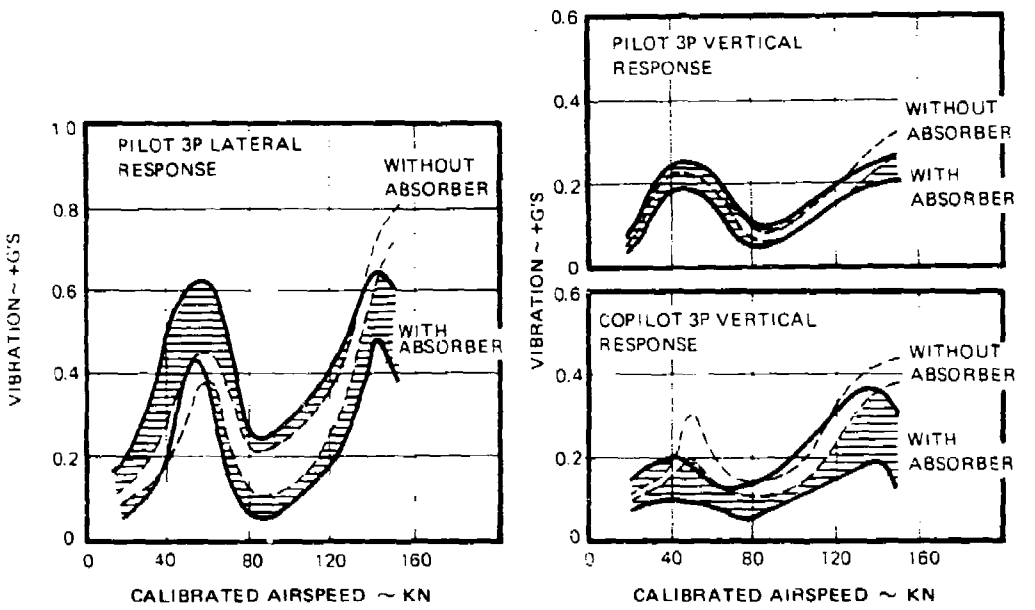

Figure 127. Cabin Lateral Absorber Improves Cockpit Vibration, Helicopter Configuration.

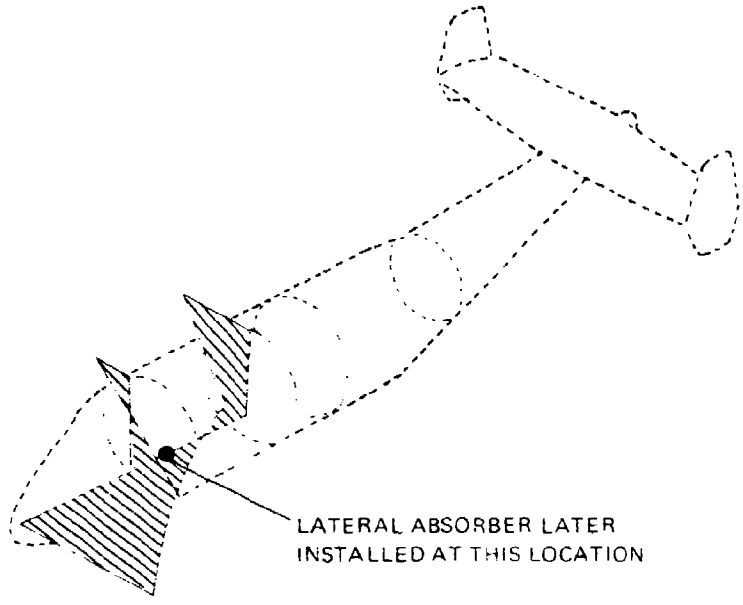

Figure 128. Cabin 3P Lateral Response Shape V = 140 Kn Level Flight Without Absorber, Helicopter Configuration.

AUXILIARY PROPULSION TEST RESULTS

FLIGHT ENVELOPE

The auxiliary propulsion envelope, like the helicopter envelope, was expanded in 20-knot increments. In addition, sideward and rearward envelopes were established to provide a safe operational envelope. Maximum speeds achieved in each axis are shown in Table 13.

TABLE 13. AUXILIARY PROPULSION SPEED ENVELOPE.

Regime	True Airspeed (knots)	Limit
Forward Flight 90-Degree Crossover -Nominal 3000 ft	204	Airframe loads and stresses
Forward Flight 0-Degree Crossover - Nominal 3,000 ft	238	(Absolute limit not achieved within the scope of this effort)
Sideward Flight - Right	20	10% Control Margin
- Left	20	10% Control Margin
Rearward Flight	20	Control Margin

The demonstrated XH-59 lift capability is shown in the load factor envelope (Figure 129) for this configuration. This figure presents the actual rotor lift developed in trim and maneuvering flight and relates it to the auxiliary propulsion design gross weight of 11,100 lb in terms of load factor.

The maximum nondimensional blade loadings (C_t/σ) developed throughout the flight envelope is presented in Figure 130.

Both Figures 129 and 130 show the maximum trim and maneuver conditions attainable due to airframe structural restraints.

The range of density altitude covered in the envelope expansion is shown in Figure 131.

Sideslip and bank angle envelopes are presented in Figures 132 and 133.

The rotor speed ranges that were investigated with power on the rotor and in trimmed autorotational flight (autogyro) are shown in Figure 134.

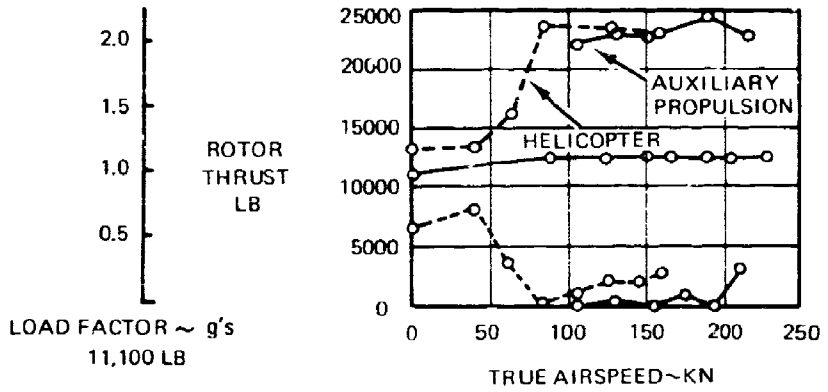

Figure 129. Rotor Thrust Capability Demonstrated.

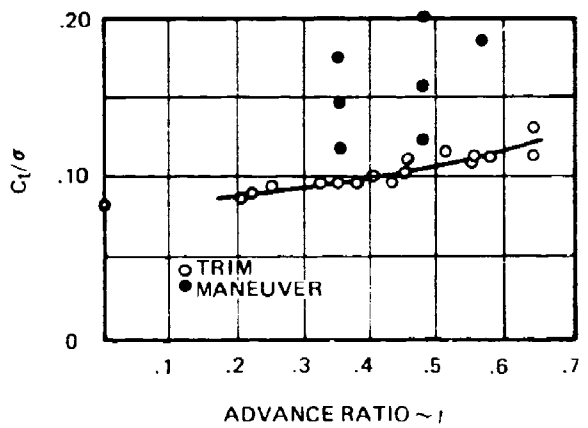

Figure 130. Maximum Nondimensional Blade Loading Demonstrated.

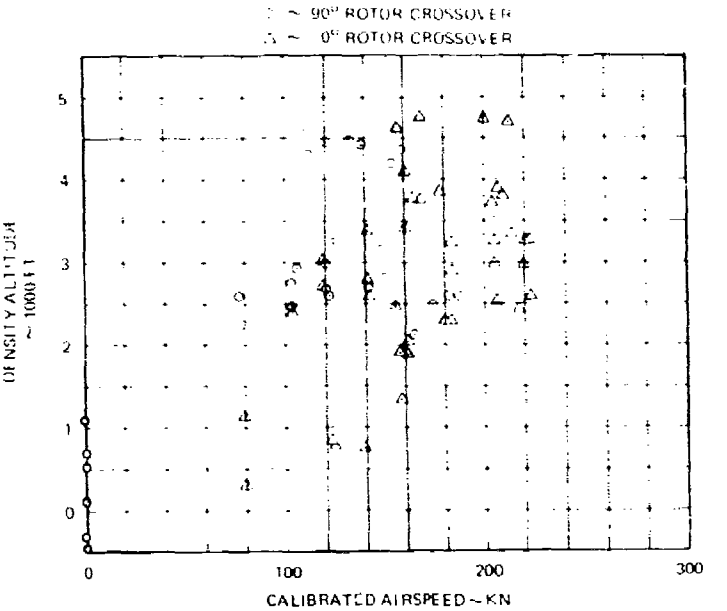

Figure 131. Altitude Envelope, Aux Propulsion Configuration.

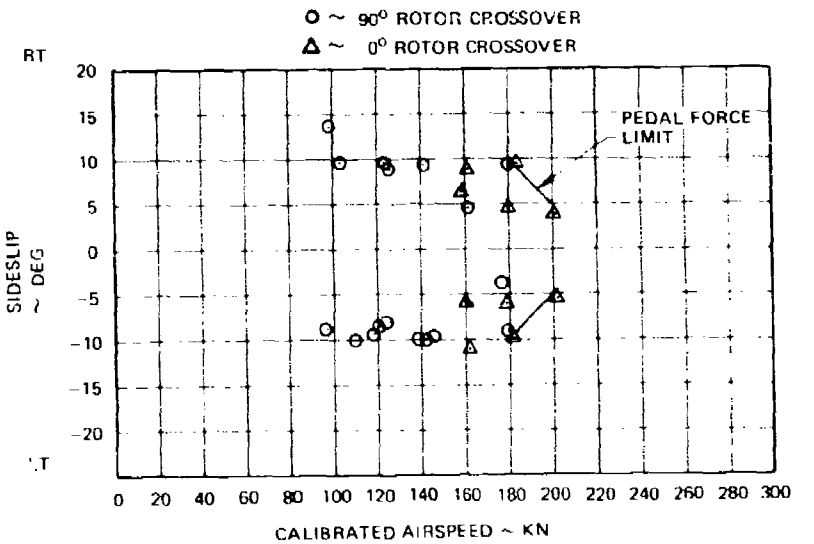

Figure 132. Sideslip Envelope, Aux Propulsion Configuration.

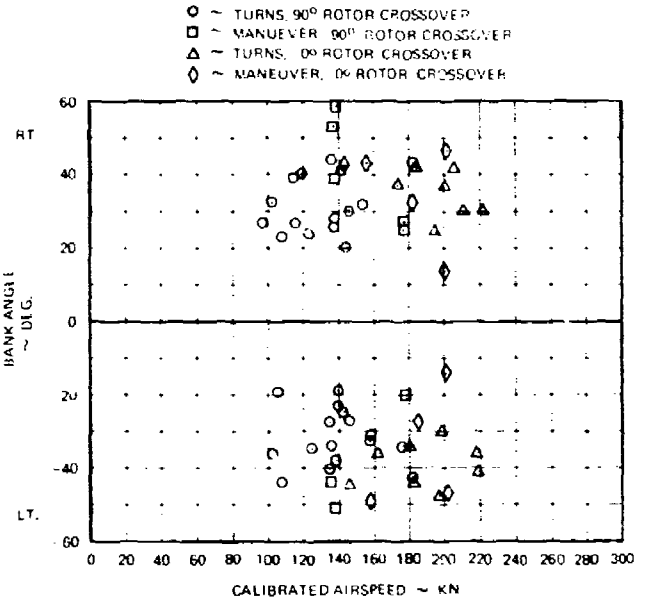

Figure 133. Bank Angle Envelope, Aux Propulsion Configuration.

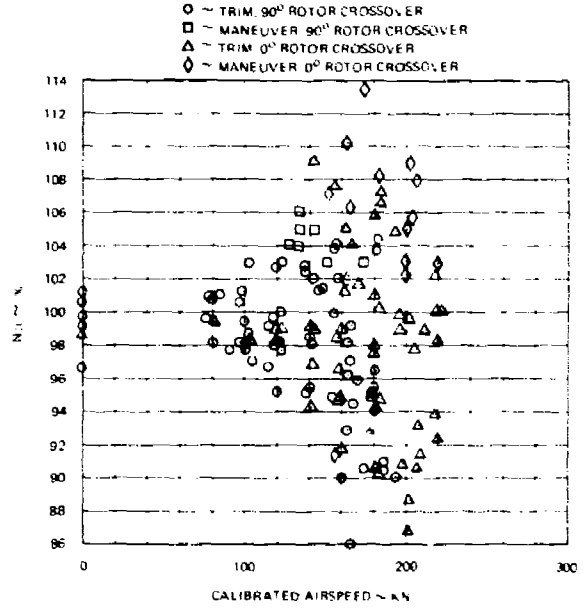

Figure 134. Level Flight Rotor Speed Envelope, Aux Propulsion Configuration.

PERFORMANCE

In the auxiliary propulsion configuration, unlike the helicopter, no dedicated performance flights were flown. Data from five flights were selected as representative of aircraft performance. However, since these flights were flown for other purposes there are differences in control trim positions (A_1', B_1' and $\Delta\theta_t$), collective position and rotor speed. Variations in these items have strong influence on power sharing between the lift and thrust engines. By converting thrust to an equivalent shaft horsepower and adding it to rotor shaft power, a good representation of aircraft performance could be developed.

Figure 135 shows the total equivalent power required for level flight corrected to standard sea level conditions. The nominal referred gross weight (W/δ) for these data is 13,300 pounds. The actual thrust and rotor horsepower (also corrected to standard sea level conditions) for each of the flights is presented in Figure 136. Here the wide variations in power sharing due to differences in collective and trim control positions and rotor speed are evident. While these power-sharing variations are significant, over the range tested there is little effect on total aircraft power required. This would indicate only small changes in aircraft system lift/drag ratio. However, it must be noted that significant power sharing was only encountered in the low-speed region (80 knots to 130 knots). While predicted aircraft performance has been verified, additional mapping of control system trim positions, collective position, and rotor speed is required to verify this trend at higher speeds and to determine the optimum trim for the best aircraft system L/D.

Shown also in Figures 135 and 136 is the impact of the installed instrumentation. The dashed lines indicate the power and thrust required without test instrumentation.

Over the range investigated there were no discernable effects on power required due to changes in rotor speed, differential lateral cyclic, or collective position. Figure 137 shows the effect of rotor speed and differential lateral cyclic at a corrected airspeed of 160 knots and Figure 138 shows the effect of collective position at a corrected airspeed of 230 knots.

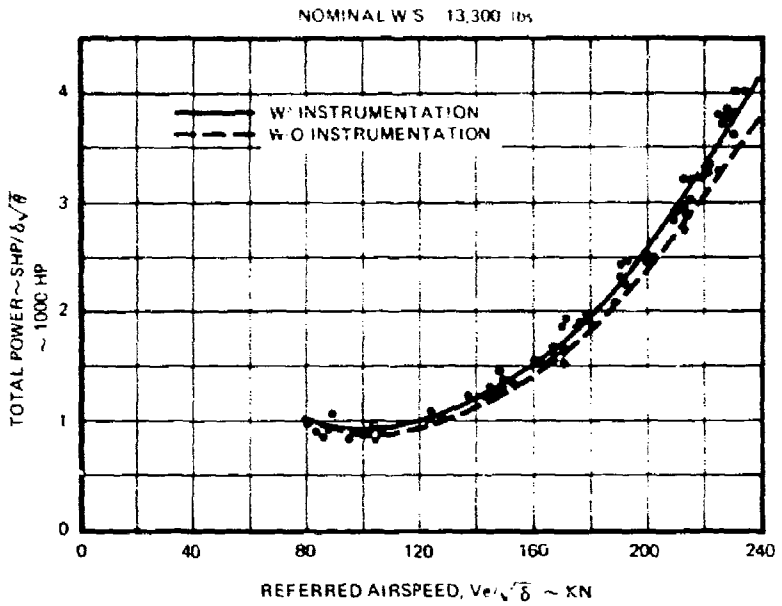

Figure 135. Level Flight Performance - Total Power Required, Aux Propulsion Configuration.

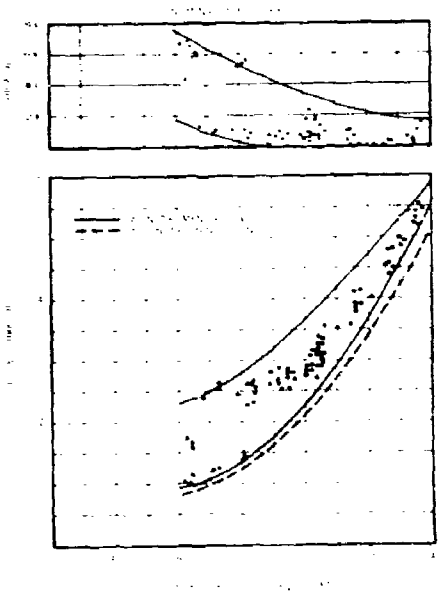

Figure 136. Level Flight Performance - Rotor Power and Thrust Required, Aux Propulsion Configuration.

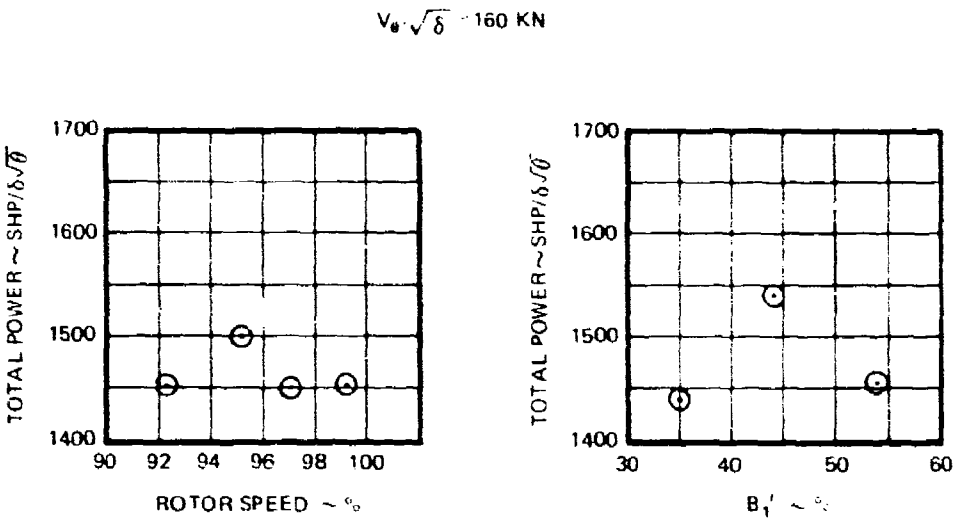

Figure 137. Level Flight Performance - Effect of Rotor Speed and B_1', Aux Propulsion Configuration.

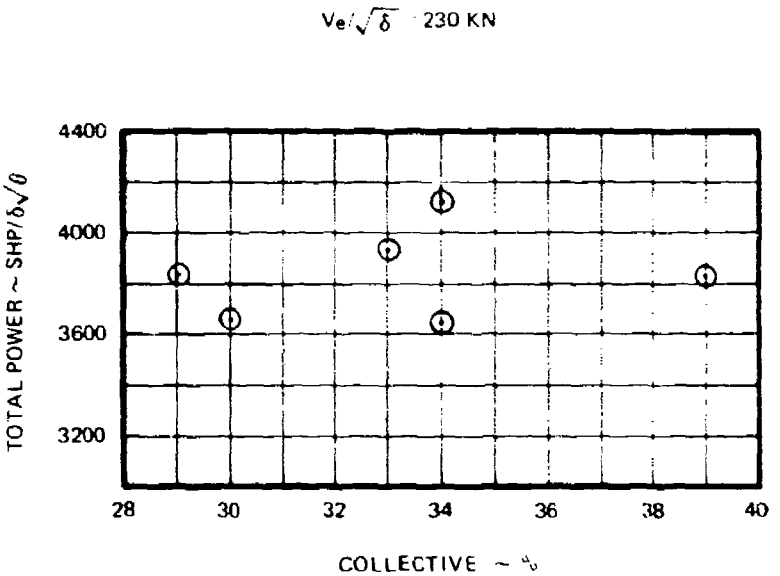

Figure 138. Level Flight Performance - Effect of Collective, Aux Propulsion Configuration.

HANDLING QUALITIES

Flight testing of the auxiliary propulsion configuration was conducted in three basic segments. Each test segment was formulated to evaluate specific characteristics and procedures necessary for progression to the next segment. Particular attention was directed toward flight safety aspects including stability, controllability and engine loss tolerance and procedures. The first segment was rotor-propelled flight with auxiliary jets installed, but cold. The purpose was to establish a jet's inoperative flight envelope. This increased the auxiliary propulsion endurance by permitting the jets to be shut down after data collection was complete. The second segment was runway takeoff and landing tests using auxiliary thrust to establish a critical decision point, rejected takeoff procedures and controllability envelope for one engine inoperable (OEI) flight capability. The third segment, auxiliary propulsion airspeed and maneuver envelope expansion, was conducted using two different upper to lower rotor rotational phasings. The first was with the rotors indexed for a 90-degree crossover in which the upper and lower blades are coincident alternately on the right and left side of the aircraft at three times per revolution (six total crossovers per revolution). This rotor index configuration was flight tested to 204 KTAS (194 KCAS). The second indexing configuration tested was 0 degree crossover in which upper and lower blades are coincident alternately over the tail and nose of the aircraft. This index configuration was flight tested to 238 KTAS (227 KCAS). Handling qualities and controllability characteristics are independent of upper to lower rotor indexing and are therefore presented and discussed together in this section.

Rotor Propelled Cold Jet Controllability

The flight testing with auxiliary jets cold was conducted at partial fuel load to assure adequate hover and simulation of test flight return at low fuel. Nominal gross weight was 11,500 pounds with a center of gravity 5 inches forward of the shaft at station 295. Longitudinal, lateral and directional control power were evaluated at hover by applying step control inputs in both directions and in each axis. Presented in Figure 139 are the control sensitivities with J-60 jets installed compared to hover sensitivities from the pure helicopter OGE condition. Lateral and directional sensitivity are slightly reduced because of the inertia increase resulting from the laterally disposed J-60 mounting. Longitudinal sensitivity is unaffected because of the J-60 mass being disposed about the center of gravity and thus not materially increasing the pitch inertia (I_{yy}). Lateral and directional control sensitivity are reduced 17 percent by the addition of the auxiliary propulsion engines.

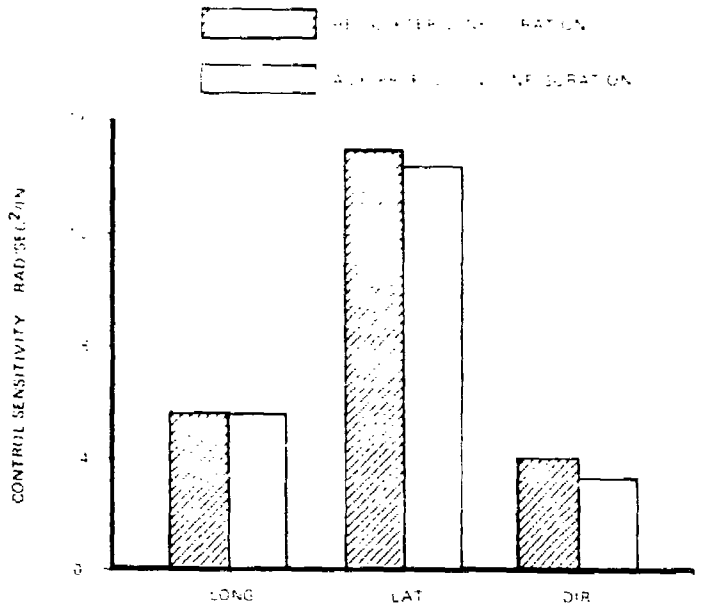

Figure 139. Hover Control Sensitivity.

Longitudinal, lateral and directional control sensitivity to damping ratios with SAS on or off are shown in relation to VFR and IFR criteria of MIL-H-8501A (Reference 9) in Figure 140. Longitudinal characteristics, (a) of the figure, show the damping-to-control sensitivity ratio to be in compliance with the criteria for both SAS on and off. The terminal rate of 8.3 deg/sec/in. with SAS on is rated excellent by all pilots who have flown the aircraft, and the relation with the minimum VFR and IFR boundaries would suggest that this would be expected. Lateral characteristics, (b) of the figure, are also rated excellent with SAS on, as would be expected by relation to minimum VFR and IFR boundaries and the 20 deg/sec/in. maximum terminal rate boundary. The terminal rate of 6.8 deg/sec/in. compared to the 8.2 deg/sec/in. in the longitudinal axis provides good control harmony. The lateral characteristics with SAS off are pilot rated as oversensitive, which proximity to the maximum rate boundary would suggest. The directional characteristics are shown to be marginally acceptable with respect to control sensitivity and not acceptable with respect to damping when compared to MIL-H-8501A criteria. The directional control characteristics are cited by pilots as an enhancing characteristic of the ABC rotor system. The directional control system also allows crosswind and tailwind

9. MIL-H-8501A, MILITARY SPECIFICATION, GENERAL REQUIREMENTS FOR HELICOPTER FLYING AND GROUND HANDLING QUALITIES.

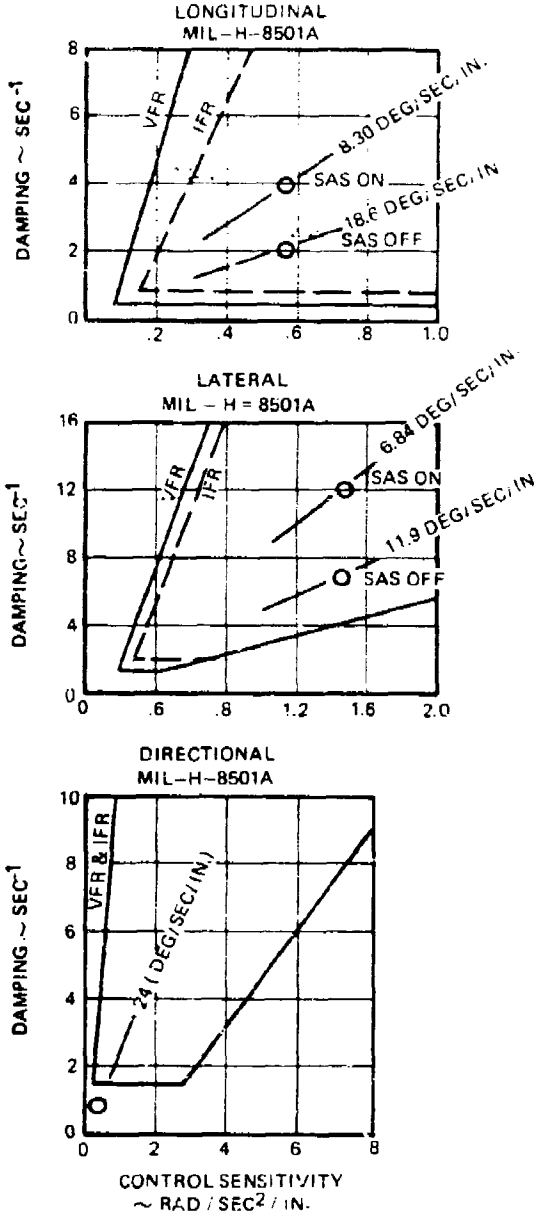

Figure 140. Hover/Low-Speed Control Sensitivity to Damping Ratio Characteristics, Aux Propulsion Configuration.

hover with only slight degradation in heading precision relative to wind on nose hover. The absence of directional instability during crosswind and tailwind hovers, typical of tail rotors, is the reason for the excellent ABC system relative wind heading characteristic.

Trim level flight was conducted with cold jets from 20 knots rearward to 80 knots forward airspeed. Controllability in level flight at a gross weight of 11,500 pounds and center of gravity at station 295 is presented in Figure 141. Shown are pitch attitude and the four control positions. Attitude data appears to be rather random. This was found to be the result of a two-degree accuracy attitude gyro instrument, and the true attitude for trim is expected to be the mean of the instrument readings shown by the curve faired through the data. Drag of windmilling J-60 engines and nacelles, plus the five-degree leading-edge-down stabilizer incidence, causes minimum collective airspeed to be about 50 knots rather than the 70 to 80 knots experienced during the pure helicopter flight testing where the stabilizer was set 10-degrees leading-edge-up. The additional drag and nose-up moment induced by the nacelles and stabilizer incidence result in a stable longitudinal control gradient with airspeed throughout the tested speed range. Lateral cyclic control positions and pedal position are relatively constant with airspeed. Small amounts of left lateral and right pedal were required over the forward speed range. Left lateral was found to be the result of a control phase delta between the rotors, with the upper having more than the lower. The right pedal that was required over the forward speed range is the result of a nonoptimum rig of collective between the rotors for the condition flown. The pedal could easily have been centered using some differential collective beep control, but was not felt to be important nor cost effective to test at that time. The impact of the configuration modifications, J-60 engine nacelles and stabilizer incidence change and the higher gross weight and associated drag, was to require higher collective and power, more forward longitudinal control, and more nose-down attitude at 80 knots than pure helicopter testing.

Takeoff and Landing Tests

At the 12,500-lb gross weight of the auxliary propulsion configuration, the XH-59A has insufficient shaft power to hover out of ground effect. Therefore, to provide maximum safety during testing, particularly in the event of an engine failure, takeoffs and landings were accomplished using STOL techniques. These techniques were developed in tests conducted at Rentschler Field in East Hartford, Ct. on the 6700-foot United Technologies Corporation main runway. Tests were conducted to identify the critical decision point during rolling takeoff, investigate controllability following single engine loss, establish rejected takeoff procedures and determine distance requirements. Controllability concerns were

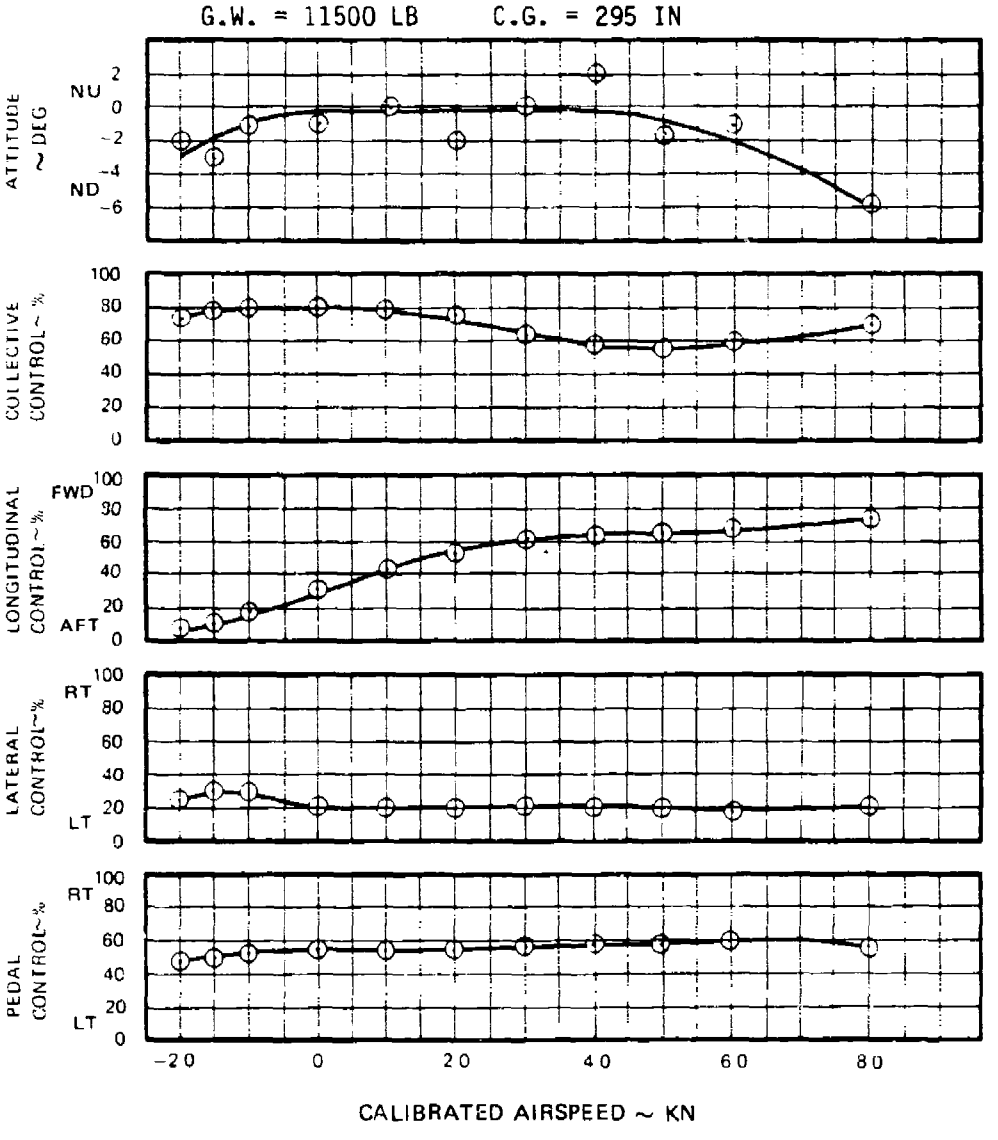

Figure 141. Level Flight Controllability (Cold Jet), Aux Propulsion Configuration.

collective control setting during takeoff to accommodate a single PT-6 loss, longitudinal cyclic control required to hold the nose gear down during acceleration, and directional control margins for accommodating a thrust engine loss and the J-60 power setting compatible with this requirement.

To evaluate the above handling qualities issues and other considerations pertinent to structures and performance, a progressive series of tests was conducted. Orderly increases in speed, collective, single and dual J-60 thrust engine power, simulated engine failures of both thrust and lift systems, wheel braking and flaring decelerations and rejected takeoffs were accomplished. The summary findings of the runway test phase are presented in Figures 142 through 145. The relationship between torque required by the rotor as a function of speed and collective control setting is shown in Figure 142. All tests were conducted with full fuel giving an aircraft weight of 12,500 pounds and a center of gravity at fuselage station 294, 6 inches forward of the rotor shaft. Airspeeds on the ground were kept at 70 knots or less to remain within landing gear design limits. Lift-off was not attained below 50 percent collective control settings but occurred at 60 knots at 50 percent collective, 40 knots at 60 percent collective, and 20 knots at 70 percent collective. A 50-percent collective, providing 60-knot lift-off speed, resulted in a 50-percent rotor torque requirement. This torque can be provided by a single PT-6 engine. Collective control setting for takeoff was thus limited to 50 percent to provide OEI lift engine capability at lift-off speed of 60 knots. The longitudinal cyclic controllability during ground roll and through lift-off as a function of collective is shown in Figure 143. Control margins are not approached for any conditions tested. The most noteworthy characteristic is the more forward longitudinal cyclic required with higher collective settings, a common characteristic of hingeless rotors resulting from collective to pitch coupling.

Directional controllability to counter a thrust engine failure during takeoff was investigated by accelerating to progressively higher speeds on a single J-60 thrust engine. Two J-60 power settings were used for these tests: 30 percent power setting giving 990 pounds of thrust creating a 4373 ft-lb yaw moment, and 40 percent power setting giving 1320 pounds of thrust, creating a 5830 ft-lb yaw moment. Data from these tests are presented as pedal position for zero slip as a function of airspeed and power setting in Figure 144. Collective was maintained at the 50 percent previously established as providing OEI lift engine capability. Two significant findings were: (1) right and left pedals required to counter a failure of either J-60 engine are symmetric and therefore one thrust engine failure is not more critical than the other,

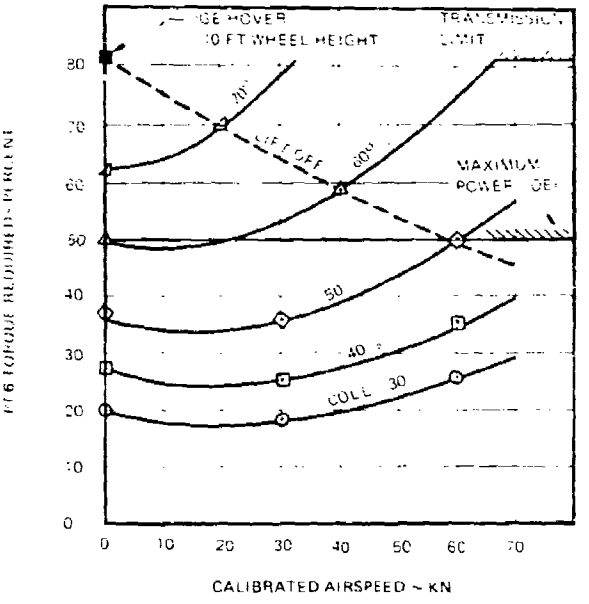

Figure 142. Torque, Collective, Airspeed, Liftoff Dependence at 12,500 Lb, Aux Propulsion Configuration.

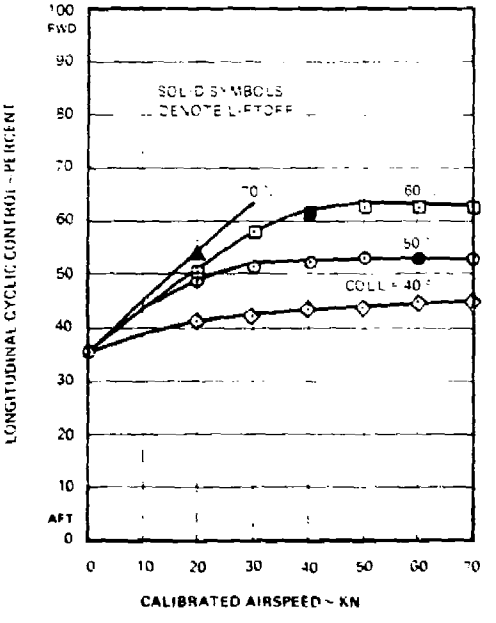

Figure 143. Longitudinal Controllability During Takeoff with Auxiliary Propulsion at 12,500 Lb, Aux Propulsion Configuration.

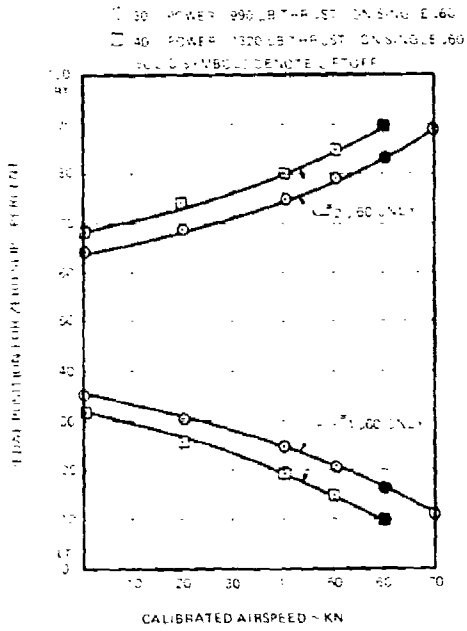

Figure 144. Directional Controllability During Runway Acceleration (One J-60 Inoperative) 50% Collective, 12,500 Lb, Aux Propulsion Configuration.

23
F

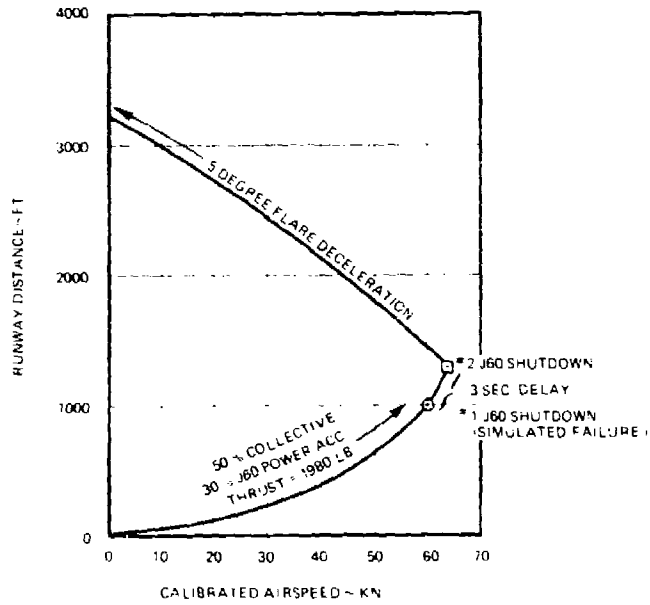

Figure 145. Rejected Takeoff Distance 12,500 Lb, Aux Propulsion Configuration.

and (2) 10 percent pedal margin or more exists at lift-off. To accommodate transient pedal motion for an actual unannounced J-60 failure a 30-percent power setting for the J-60 thrust engines was determined as takeoff condition. Subsequent tests showed this to provide for transients after a failure and still retain a 10-percent pedal margin.

Having determined collective and thrust engine power for takeoff, 60 knots became the critical decision point at which continued takeoff or reject are possible. A short deceleration test was conducted using rotor thrust to decelerate. The aircraft was accelerated from a standstill with 50 percent collective and 30 percent J-60 power, and upon reaching 60 knots, the #1 J-60 was shut down to simulate a failure. After a 3-second delay, the #2 J-60 was shut down and the aircraft was decelerated with a 5-degree flare. The runway distance for each segment from brake release to stop is shown in Figure 145. This represents the average distances measured for three takeoffs and reject runs where total distance variation was less than 200 feet or about 6-percent. Takeoff was also completed following both a J-60 thrust engine and a PT-6 lift engine simulated failure followed by 80-knot flight within the airfield confines and roll-on landings. The complete procedure was uneventful, straightforward and repeatable.

Auxiliary Propulsion Mode Flight Test

Stability and handling qualities of the XH-59A in the auxiliary propulsion configuration were excellent with no control margin limitations or unstable modes apparent. Test planning was therefore designed to evaluate aircraft structural and vibratory characteristics during envelope expansion. Handling qualities data presented and discussed are by-products of envelope expansion and not results of specific handling qualities dedicated flights. 23 B

Controllability in Level Flight

Trim level flight was conducted from 90 knots to 227 KCAS. Differential lateral cyclic input was generally increased with airspeed to control lift migration toward the advancing side of each rotor. The allowable range of differential lateral cyclic at any trim airspeed was significantly expanded by going to the 0-degree crossover rotor indexing. The range tested as a function of calibrated airspeed for 90-degree crossover and 0-degree crossover indexing is presented in Figure 146.

Controllability in level flight from about 90 knots to 227 KCAS is presented in Figure 147. Attitude, angle of attack and the four control positions are shown for both 90-degree and 0-degree crossover. The data discontinuity between the 90-degree crossover and 0-degree crossover is the result of lower collective used at 0-degree crossover and a -2.8-degree

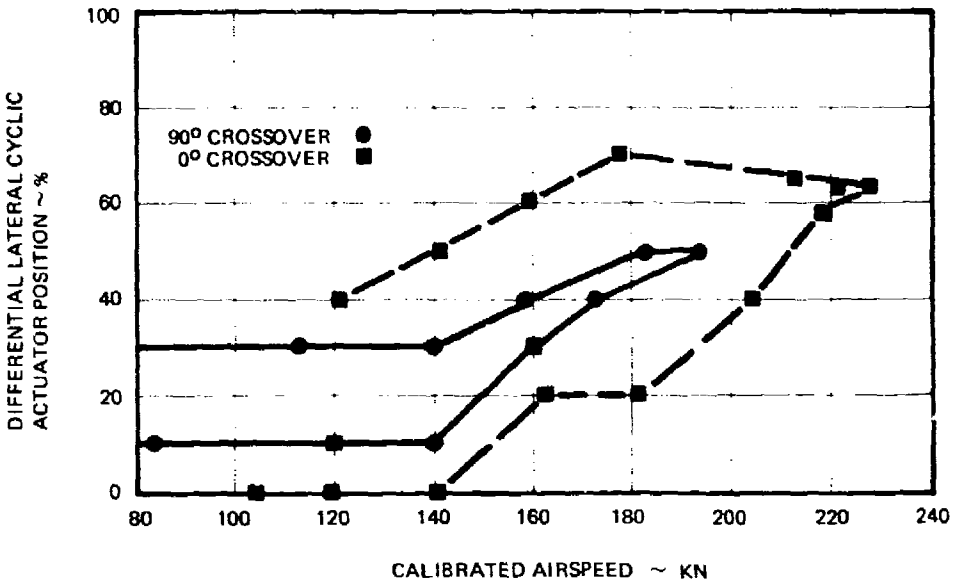

Figure 146. Differential Lateral Cyclic Range Tested as a Function of Airspeed (Level Flight), Aux Propulsion Configuration.

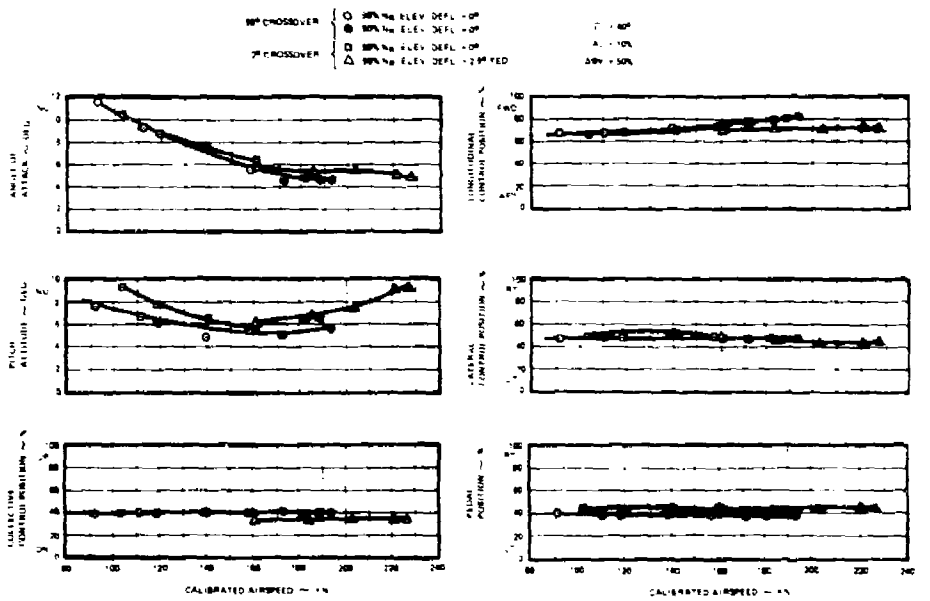

Figure 147. Controllability in Level Flight, Aux Propulsion Configuration.

elevator angle as against a 0-degree elevator position. Angle of attack and attitude differ for all aispeeds and is caused by a combination of attitude gyro bias or drift and induced flow at the angle of attack vane on the instrumentation boom. Note that lower collective in combination with a fixed -2.8-degree elevator angle, trailing edge down, reduces forward longitudinal cyclic required significantly. Longitudinal control position is stable with airspeed and lateral cyclic and pedal position are relatively insensitive to airspeed.

Figure 148 shows controllability in trim level flight with the rotor operating in autorotation. In addition to pitch attitude and the four control positions, autorotative rotor speed is shown. At low airspeed, the pitch attitude is high as is the autorotative rotor speed, while collective control is low to maintain autorotation of the rotor. As airspeed increases, rotor autorotative speed reduces, attitude reduces, and collective increases. Longitudinal control position moves steadily forward on a stable trim gradient while lateral and pedal control remain essentially constant. The 0-degree crossover index data at 160, 180 and 200 knots show higher rotor speed and less forward cyclic with a lower collective setting. This is caused by the trailing-edge-down elevator setting of -2.8 degrees. The elevator-induced diving moment results in an aft cyclic. With the control phase angle of 40 degrees, the aft cyclic creates an effective negative differential lateral cyclic application in the shaft axis. The result is more advancing blade pitch angle that is brought back down by a lower collective setting resulting in higher autorotative rotor speed. Had a zero elevator setting been retained, the autorotative points would have been the same as with the 90-degree crossover indexing. One condition was flown with 0-degree crossover index at 180 knots prior to the elevator change and compared well with 90-degree index data. The demonstrated level flight capability with the rotor autorotating assures fly-back capability with all lift engine power lost with a stable control gradient and an adequate rotor speed that will automatically increase as airspeed and collective are reduced. The low-speed attitude, although high, is acceptable for conducting a roll-on landing.

At 80 knots calibrated airspeed and the rotor system kept in autorotation at 101 percent, the aircraft was retrimmed in climb and descent. These data are shown in Figure 149. Pilot functions were collective and propulsive thrust adjustment. Angle-of-attack changes are consistent with collective changes, while attitude reflects the flight path angle. Controls are relatively constant over the 400 feet per minute climb to 250 feet per minute descent range tested. These data demonstrate the ability to approach, reject landing and climb out with lift engines inoperative, a distinct attribute of the demonstrator aircraft.

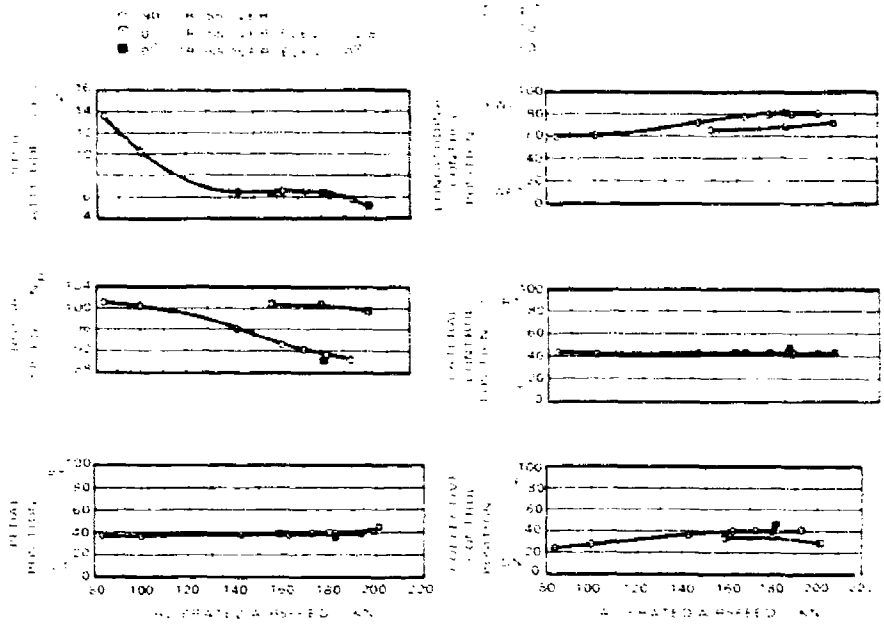

Figure 148. Controllability in Level Flight Autorotation, Aux Propulsion Configuration.

Bank turns to the right and left were conducted at various airspeeds during envelope expansion. Piloting technique was to trim at various bank angles holding constant collective position and using J-60 thrust to maintain constant airspeed and altitude use very similar to fixed-wing technique. Controllability characteristics were similar at all airspeeds tested. Data for bank turns at 180 KCAS, 90-degree crossover, and 200 KCAS, 0-degree crossover are presented in Figure 150 as representative of the controllability characteristics. Angle of attack, control positions, rotor speed and normal load factor are presented as a function of bank angle. A number of characteristics are worthy of comment. Longitudinal control position demonstrates a stable maneuver position gradient. Lateral control position is relatively insensitive to bank angle, but pedal position shows some left pedal requirement with increase in normal load factor. Data analysis of this characteristic suggest a vertical displacement of the rotor wakes at the vertical fin positions. This reasoning is generally substantiated by other configuration changes that change angle of attack and show left pedal with increase in angle of attack. The bank turns at 180 knots calibrated airspeed were initiated from a level flight trim point where the rotor was in autorotation at 94 percent rotor speed. The rotor speed increases with normal load factor as torque decreases with angle of attack reaching 104 percent at about 1.4g. The bank turns at 200 knots were initiated from a

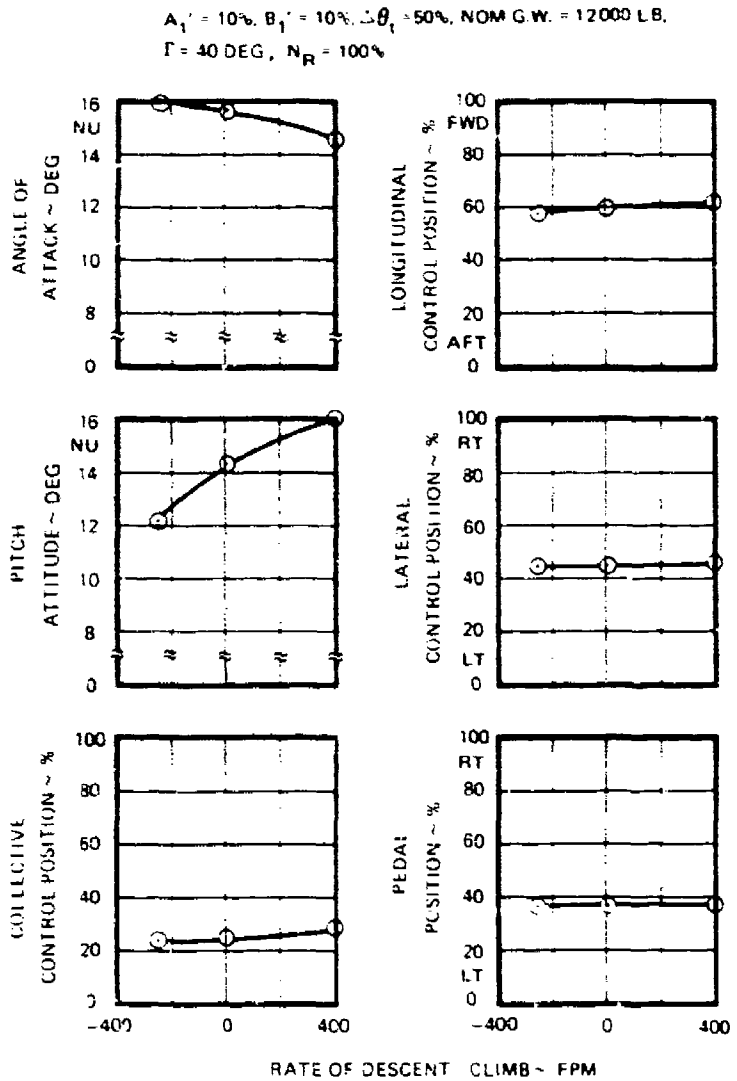

Figure 149. Controllability in Climb/Descent at 80 KCAS Autorotation, Aux Propulsion Configuration.

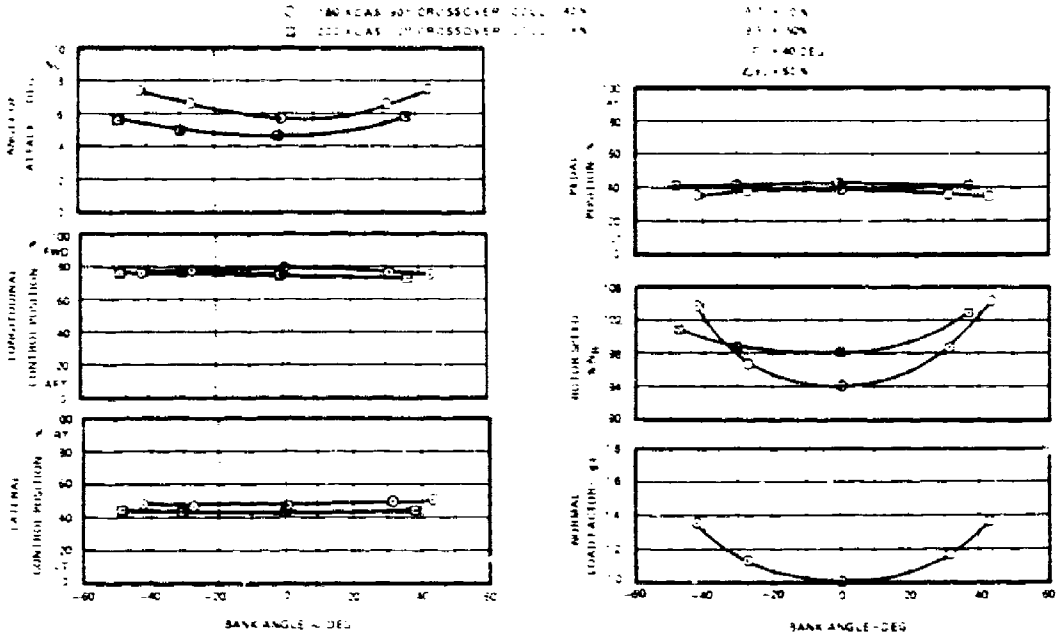

Figure 150. Controllability in Constant Altitude Bank Turns, Aux Propulsion Configuration.

low rotor torque trim at 98 percent rotor speed. Rotor speed does not increase with load factor as rapidly as at the 180 knot condition.

A design utilizing the same engines to provide both rotor torque and propulison would distribute power between the rotor and propulsion device so as to retain constant airspeed during turns at constant engine power setting.

Flight tests were conducted in which rotor speed and differential rotor trim controls were varied at constant airspeed. These data are presented in Figures 151 through 153. Influence of rotor speed on controllability at 160 KCAS is shown in Figure 151. A 9-percent change in rotor speed at 160 knots resulted in a 1.5 degree change in angle of attack and attitude. Significantly, the control positions are independent of rotor speed. Rotor speed can therefore be used to optimize vehicle performance or reduce structural resonances without changing the system controllability. The impact of varying differential collective trim ($\Delta\theta_t$) on aircraft characteristics was flight tested. Controllability with $\Delta\theta_t$ varied close to 30 percent (Figure 152), and demonstrated control to be relatively constant over the $\Delta\theta_t$ range. This control independence is important since rotor thrust sharing and numerous vibratory loads can be modified by $\Delta\theta_t$ adjustment. The most significant

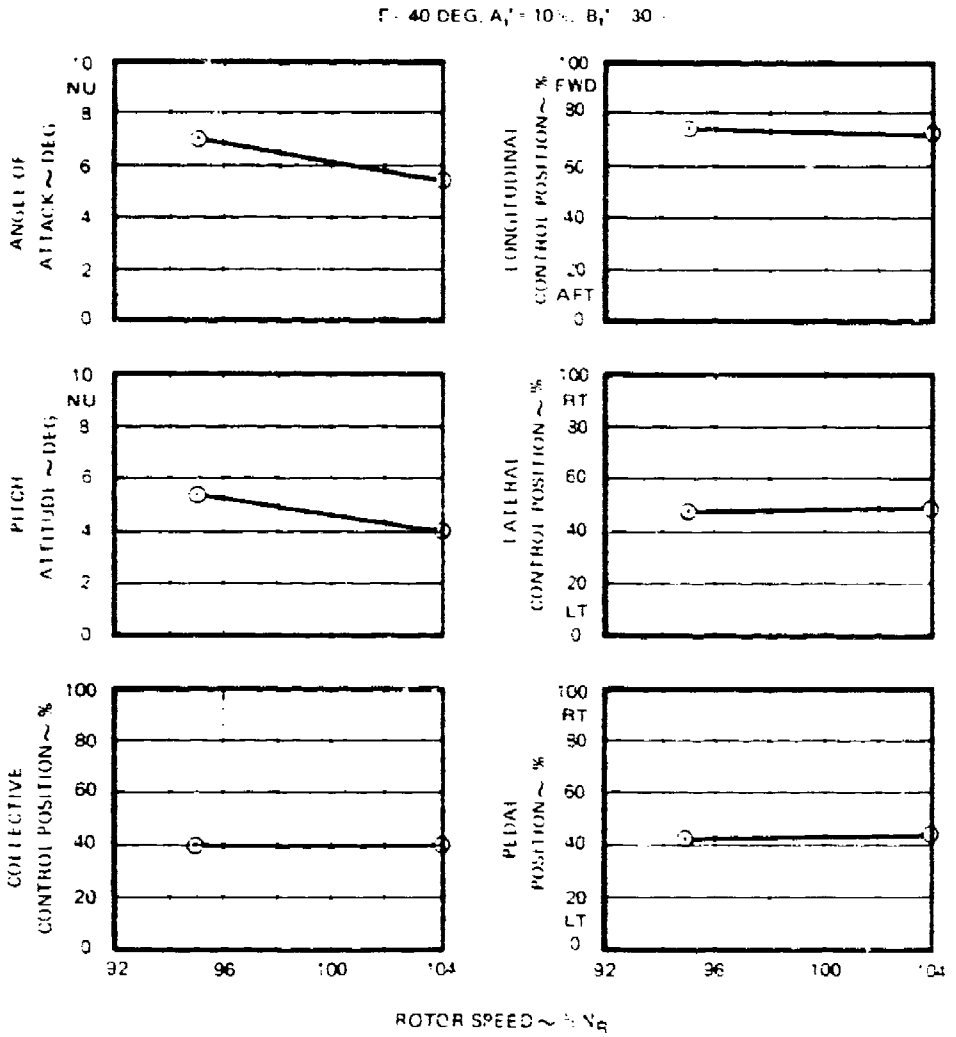

Figure 151. Controllability with Rotor Speed at 160 KCAS, G.W. = 12,000 Lb, Aux Propulsion Configuration.

differential rotor control parameter for influencing performance, rotating system structural loads, and fixed system vibration is differential lateral cyclic (B_1'). Figure 153 presents controllability data as a function of B_1' for 143, 163, and 171 KCAS.

The angles of attack and attitude changes influence performance, but control positions are independent of B_1' applied. This is important since performance, rotor structural loads and airframe vibration are controllable without adversely affecting control margins.

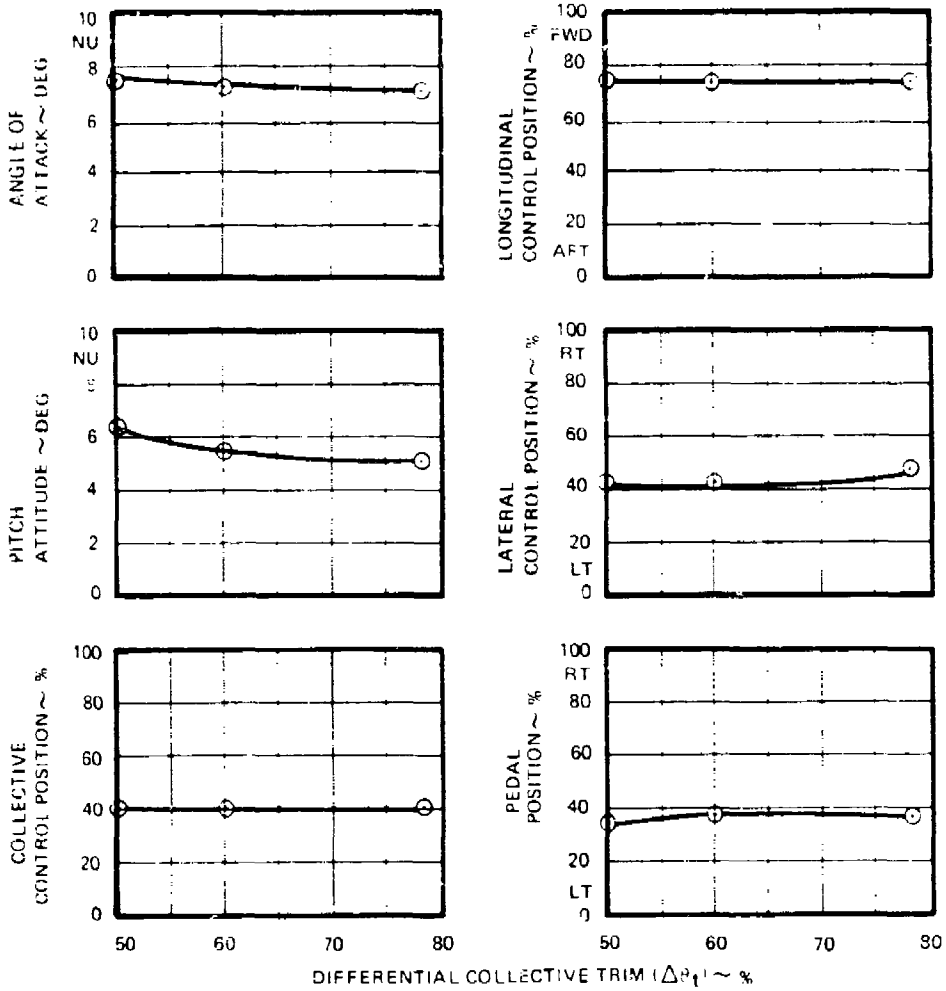

Figure 152. Controllability with Differential Collective Trim at 160 KCAS, G.W. = 12,000 Lb, Aux Propulsion Configuration.

Step control inputs were applied sequentially to longitudinal and lateral cyclic and to the pedals to assess ABC rotor system control power characteristics as a function of airspeed. Results of these tests are presented in Figure 154 as control sensitivities in radians per second squared per inch control motion as a function of calibrated airspeed. Note that longitudinal and lateral sensitivities generally increase moderately with airspeed. Directional sensitivity, however, initially drops off as differential collective is decoupled from the pedals and then increase as the square of the airspeed with rudders. The solid point at 40 knots was not tested in the auxiliary propulsion configuration but was extrapolated from pure helicopter test data by adjusting for the I_{ZZ} inertia increase.

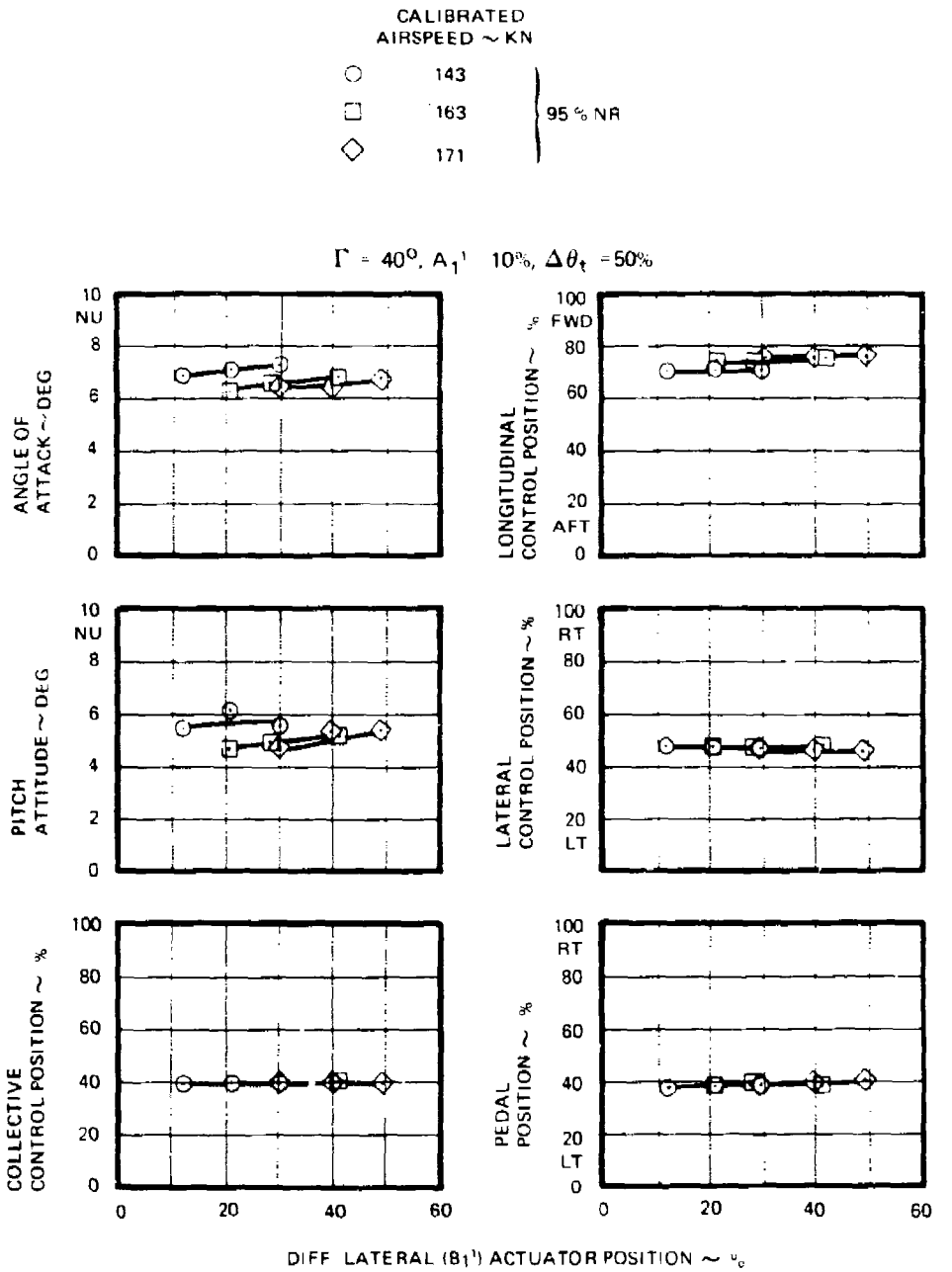

Figure 153. Controllability with Differential Lateral (B_1') Cyclic Variation, G.W. = 12,000 Lb, Aux Propulsion Configuration.

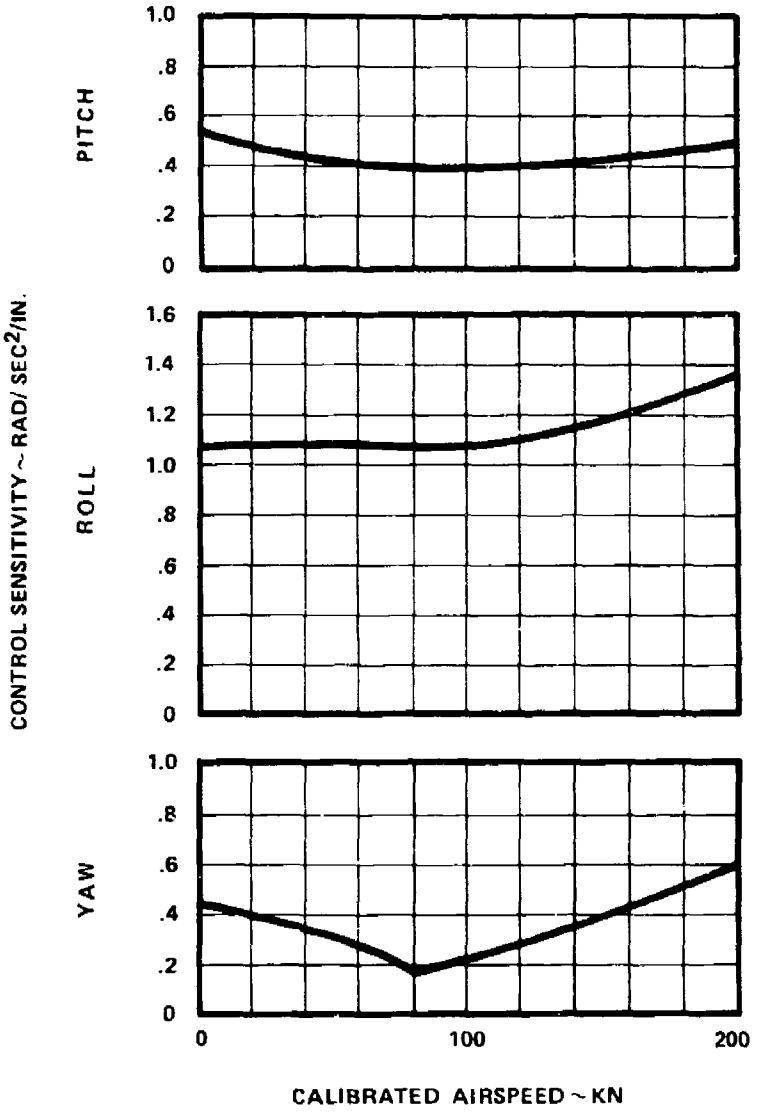

Figure 154. Control Sensitivity Variation with Airspeed, G. W. = 12,000 Lb, Aux Propulsion Configuration.

Static Stability

Longitudinal static stability was evaluated at two level flight and two climb conditions. These data are presented in Figure 155 as longitudinal control position against calibrated

airspeed. The solid symbols denote the trim conditions from which speed changes were initiated. Stability from level flight at 144 knots and 183 knots was evaluated for two different configurations. The lower speed was with 90-degree crossover rotor indexing and a 0° elevator setting while the higher speed was with 0° crossover rotor index and a trailing edge down elevator setting of -2.8°. Static stability exists at both speeds with only the initial cyclic position reflecting the elevator angle difference. In climbing flight, 200 fpm at 144 knots and 1200 fpm at 120 knots, the configuration was 90° crossover rotor index and 0° elevator angle. Both climb conditions are statically stable to about the same degree as level flight, approximately 0.3 percent or .04 inch per knot.

Lateral directional static stability was tested as part of maneuver envelope expansion testing at 100, 140 and 180 knots. The XH-59A demonstrated stable lateral directional static characteristics as shown by the data presented in Figure 156. Dihedral, lateral control for sideslip, is stable and nearly constant with airspeed. Directional stability, pedal for sideslip, is stable and also nearly constant with airspeed. Roll with sideslip slope increases with increasing airspeed and is linear to ±10 degrees of sideslip.

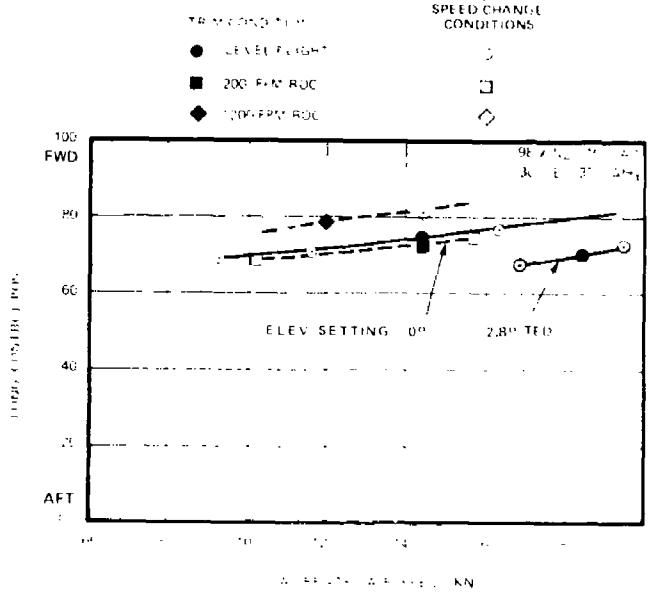

Figure 155. Longitudinal Static Stability, Aux Propulsion Configuration

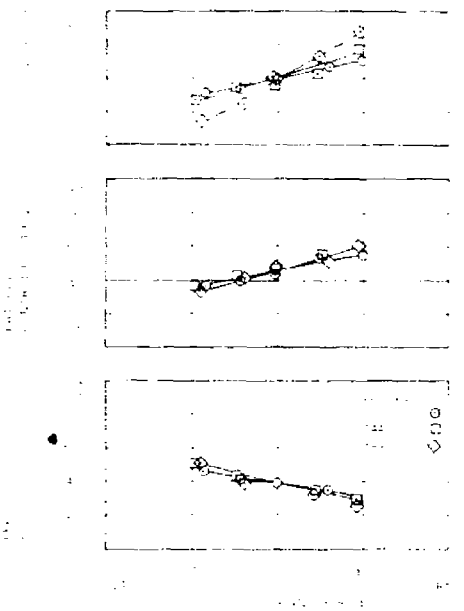

Figure 156. Lateral/Directional Static Stability, Aux Propulsion Configuration.

Dynamic Stability

Dedicated dynamic stability flights were not flown. Assessment of aircraft transients following control steps, pulses, and doublet inputs allowed extraction of most of the dynamic stability characteristics in the 120- to 180-knot speed range. Longitudinal pulse and doublet inputs were made with SAS on and off to assess phugoid characteristics where rotor speed variations get involved during low or zero shaft torque flight conditions. The degree of rotor speed participation during phugoid oscillations is a function of load factor, as previously discussed for banked turns. The stability mode roots for phugoid, longitudinal short period, dutch roll and roll modes are shown in Figure 157. The migration of roots with airspeed, as speed increases from 120 to 180 knots, is also presented. The XH-59A is dynamically stable in all modes over the demonstrated range of airspeed. Variation in characteristics with the SAS on and off was only discernable in the phugoid mode. The derived rate feedback SAS, pitch and roll axis, with a 0.1-second derivation lag, had no identifiable effect on the other stability modes at any airspeed above 80 knots. The SAS was provided to improve hover and low-speed handling qualities where the high ABC rotor system

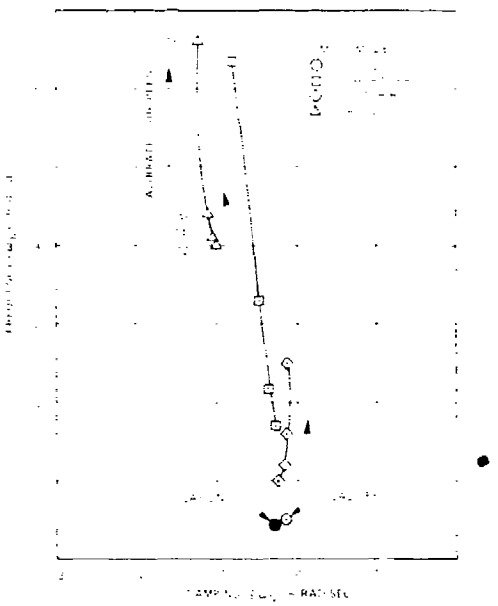

Figure 157. Dynamic Stability, Aux Propulsion Configuration.

control power could possibly have resulted in pilot induced oscillation problems. At forward airspeeds, the dynamic stability is dominated by the damping of the horizontal and vertical tail surfaces. Phugoid damping is increased by SAS because of the long period and the interplay of rotor speed. Phugoid roots are not, however, substantially changed over the airspeed range evaluated. Spiral mode could not be identified during any of the responses because of either a very stable characteristic or inadequate data response duration time.

STRUCTURAL RESULTS

Auxiliary Propulsion Testing - 90-Degree Rotor Crossover

This phase of the test program was conducted through a series of 27 flights from November 6, 1978 through May 17, 1979. The buildup in aircraft airspeed envelope was initiated at 100 KCAS and expanded in 20-knot increments to a maximum of 195 KCAS (204 KTAS). With each 20-knot airspeed expansion the maneuver envelope was expanded to the maximum permissible.

Rotor Trim Mapping:

It became evident early in this phase of testing that adjustments of the interrotor differential controls and earlier than anticipated reduction of rotor speed were necessary to contain rotor and airframe loads and stresses within endurance (Ew) limits. For this reason a limited amount of rotor trim and rotor speed mapping was included as a standard test technique with each speed increment buildup.

The mapping presented is not complete. Rotor speed and differential controls were varied only as required to determine a combination to allow an incremental increase in airspeed. Also, these maps are not pure in the strict sense of the word. These maps are primarily influence lines; i.e., the trends of master rotor hub stress versus differential lateral control (B_1') at 160 KCAS and at 180 KCAS may not have been flown at the same differential collective control ($\Delta\theta_t$). Therefore, only a given influence line on given maps is pure, and no attempt should be made to cross plot among the maps.

Three control variables that have not been explored at this time are control phase angle (Γ), collective control and elevator position.

Effects of Rotor Speed:

The graphs of Figures 158 and 159 present the effects of rotor speed on the rotor and airframe. Note that most rotor parameters (Figure 159) were insensitive to rotor speed. The total stress at the upper rotor shaft (master stress location), which was primarily affected by changes in rotor pitching moment, shows increasing stress with increasing rotor speed. This correlates with handling qualities data which showed increasing nose-down pitching moment on both rotors as rotor speed is increased.

Figure 159 presents the trends of the XH-59A airframe stress with rotor speed. This data shows the stress in the tail cone and the horizontal stabilizer attachment peaking at 100 to 101 percent rotor speed. However, stress at both thrust engine attachment areas increased steadily as rotor speed was decreased. This high stress condition was a major obstacle in exploring rotor behavior at reduced rotor speed. This structural problem is related to the XH-59A design and not the ABC rotor concept.

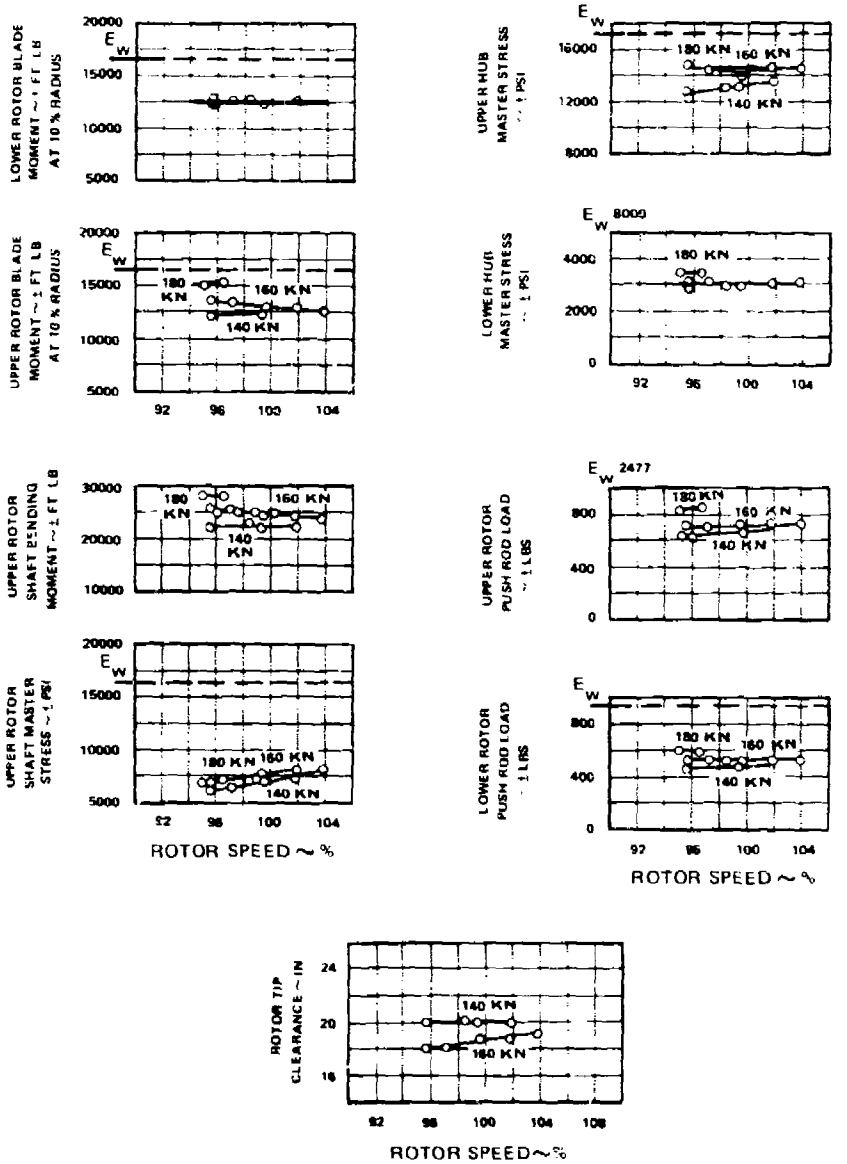

Figure 158. Effect of Rotor Speed on Rotor Component Loads and Stresses, Aux Propulsion Configuration.

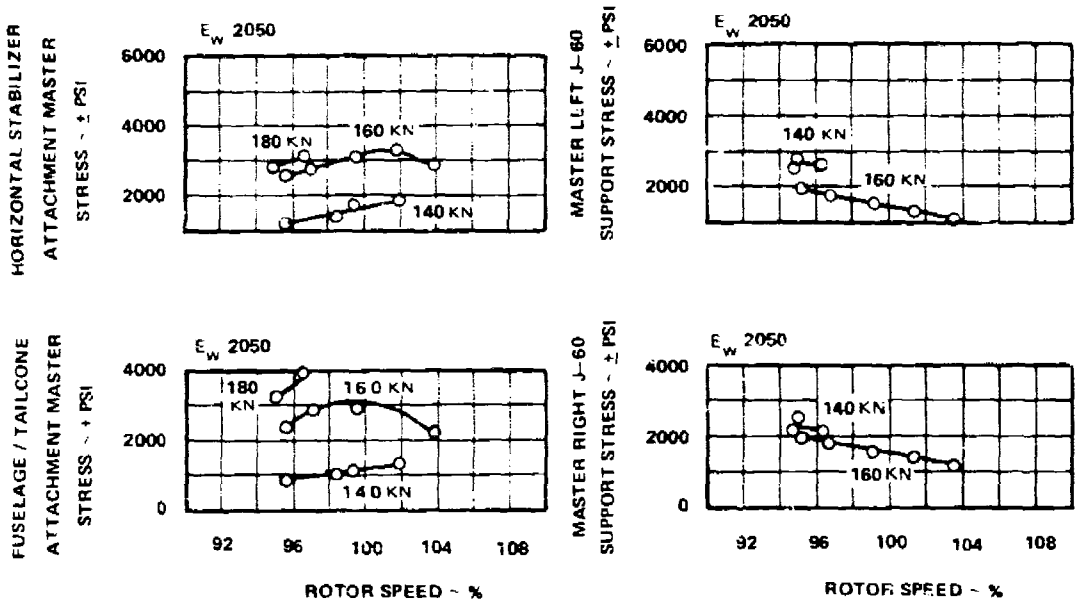

Figure 159. Effect of Rotor Speed on Aircraft Loads and Stresses, Aux Propulsion Configuration.

24
F

Effects of Differential Longitudinal Control (A_1'):

Figure 160 shows the influence of differential longitudinal cyclic control on the various rotor loads and stresses. Increasing positive differential longitudinal control increased the nose-up moment on the upper rotor and decreased the nose-up moment on the lower rotor. The net effect was opening the tip clearance over the nose. However, the greatest portion of the rotor loads were not generated with the blades at the fore and aft azimuth positions. Therefore, as expected, the differential longitudinal control had a very minor effect on the rotor parameters.

The effect of differential longitudinal control on the airframe is shown in Figure 161. The airframe was virtually unaffected by differential longitudinal control up to 160 knots. However, at 180 knots the tailcone and horizontal stabilizer attachment had minimum stress at +8 percent differential longitudinal control setting. The 8 percent setting was also acceptable for cockpit vibration and was used for the remainder of the 90-degree crossover testing.

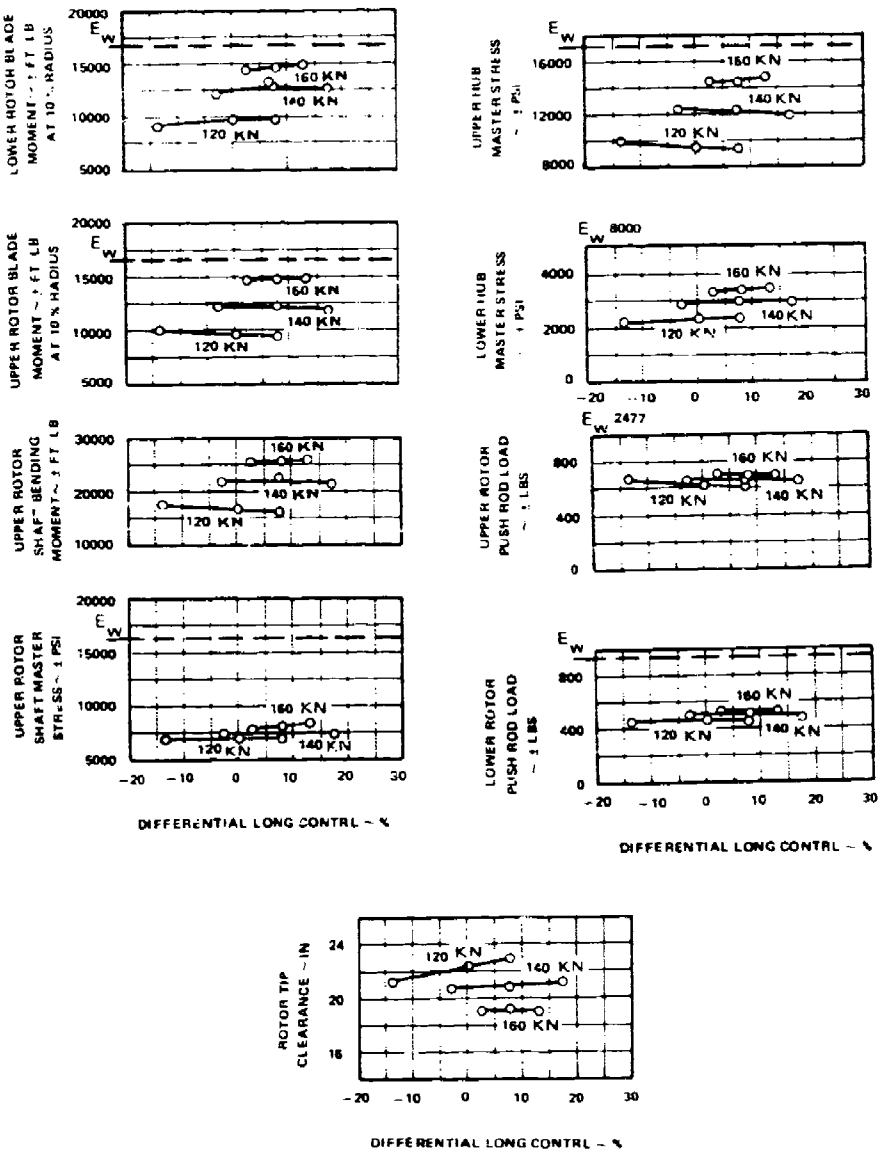

Figure 160. Effect of Differential Longitudinal Control on Rotor Component Loads and Stresses, Aux Propulsion Configuration.

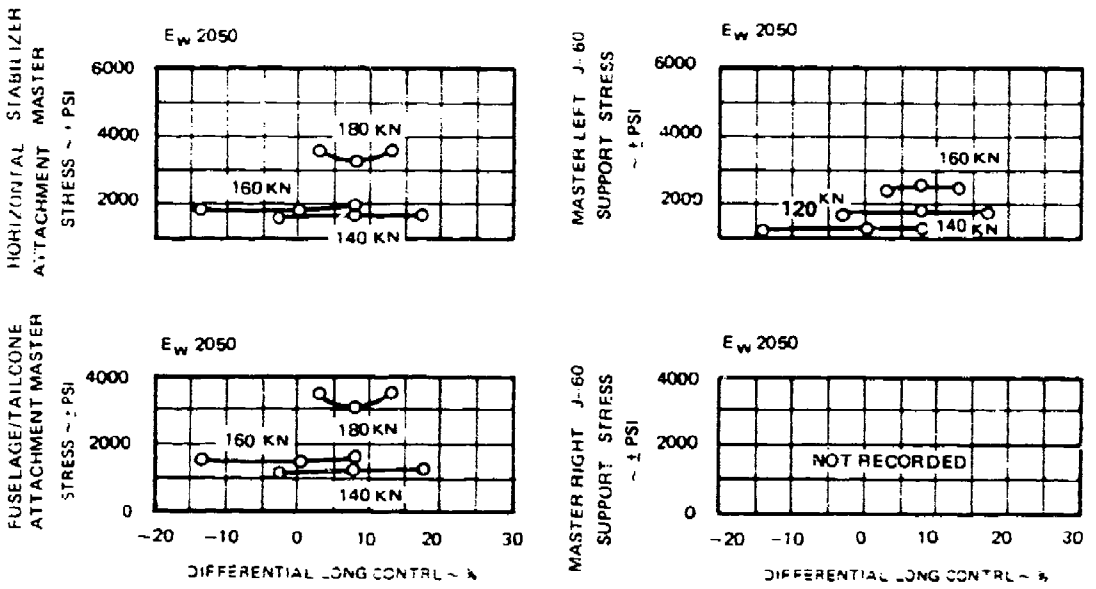

Figure 161. Effect of Differential Longitudinal Control on Airframe Loads and Stresses, Aux Propulsion Configuration.

Effects of Differential Lateral Control (B_1'):

Differential lateral control was chosen to control tip clearance as a function of increasing airspeed rather than (Γ) as was used for the pure helicopter testing. Increasing differential lateral control decreases blade pitch on the advancing side, increases blade pitch on the retreating side, increases rotor tip separation, and reduces blade and rotor head loads and stresses. Shown in Figure 162 is the effect of adjusting differential lateral control on rotor loads and stresses. The data shows a strong influence on tip separation, rotor blade bending and rotor hub stresses. Control loads were not significantly changed. However increasing differential lateral control caused an increase in perceived cockpit vibration, thus making it desirable to maintain minimum differential lateral control trim sufficient to control rotor loads, stresses and tip separation.

The data presented in Figure 163 show the effect of differential lateral control on master airframe loads and stresses. It is evident that there is only a slight increase in airframe

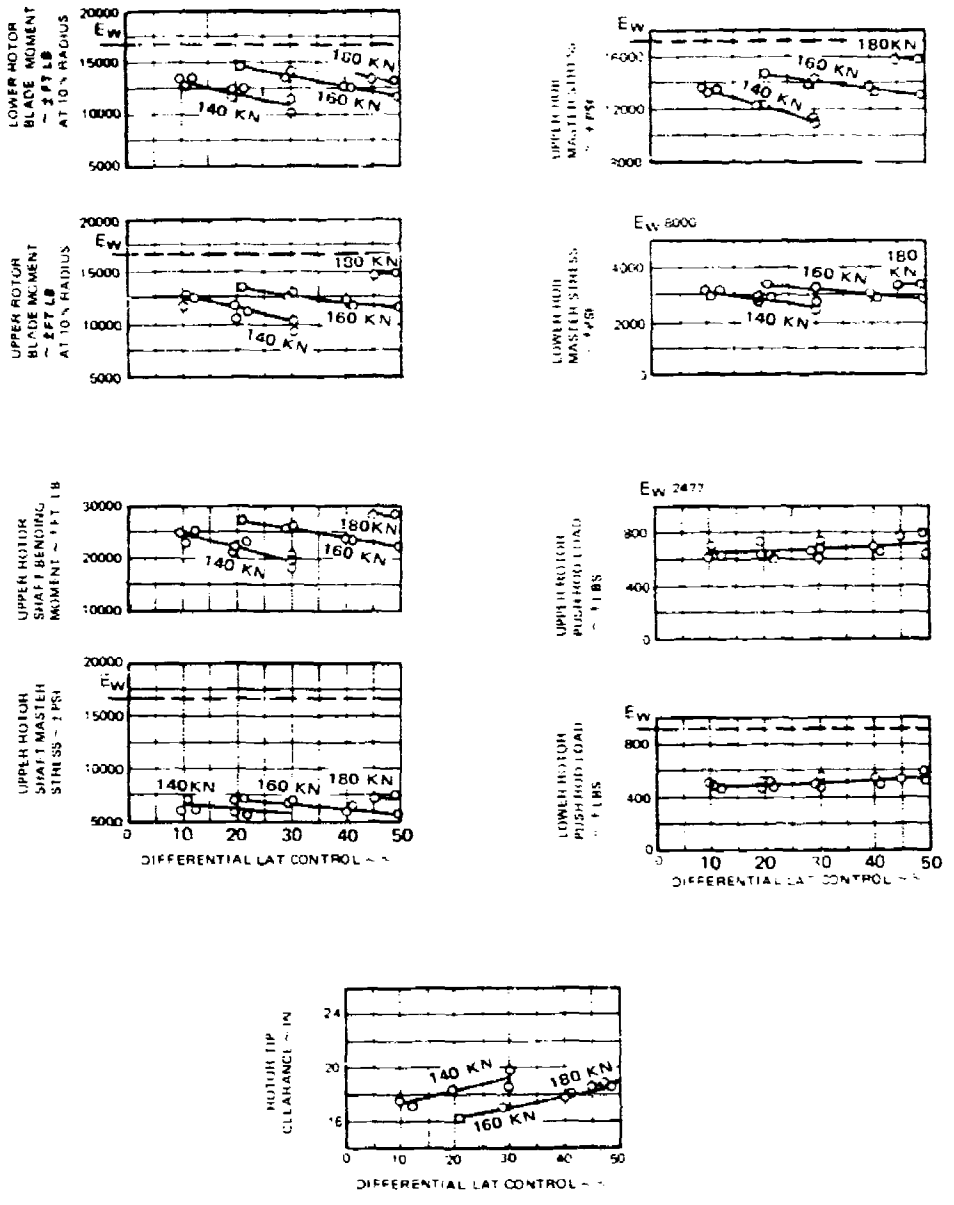

Figure 162. Effect of Differential Lateral Control on Rotor Component Loads and Stresses, Aux Propulsion Configuration.

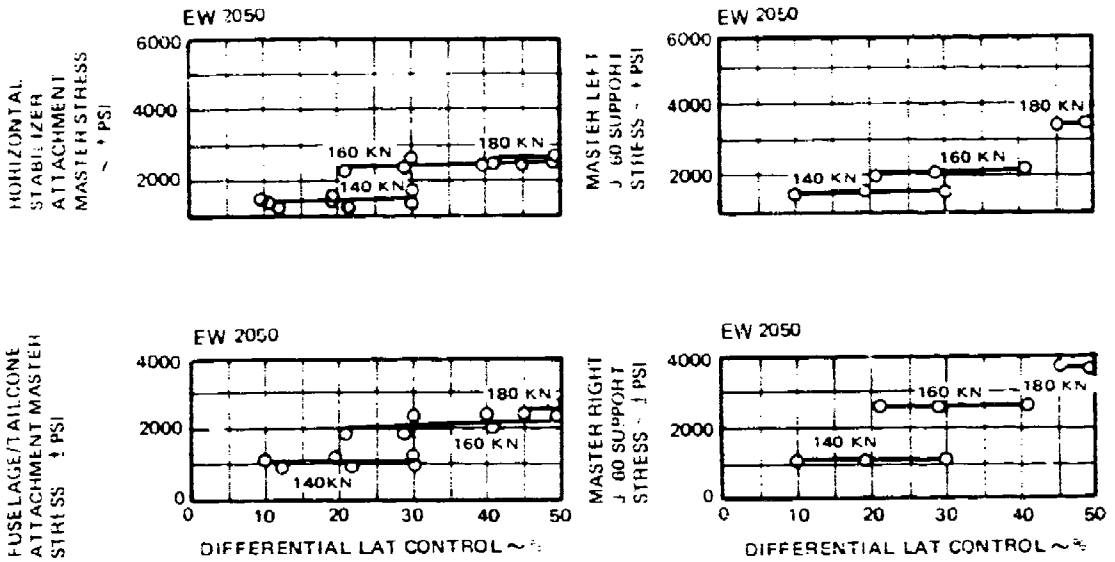

Figure 163. Effect of Differential Lateral Control on Airframe Loads and Stresses, Aux Propulsion Configuration.

stress with increased control trim. This data shows that while differential lateral control is very effective in controlling rotor parameters, it is ineffective in controlling airframe stresses.

Effects of Differential Collective Control ($\Delta\theta_t$):

Figures 164 and 165 illustrate the influence of differential collective trim ($\Delta\theta_t$) between the rotors. Increasing differential collective trim increased the collective pitch on the upper rotor and correspondingly decreased the collective pitch on the lower rotor. Changes in differential collective trim produced only minor changes in rotor loads/ stresses. However, increasing differential collective trim did increase the rotor tip clearance by virtue of the fact that the lower rotor blade steady bending decreased slightly. No effect was seen on the airframe.

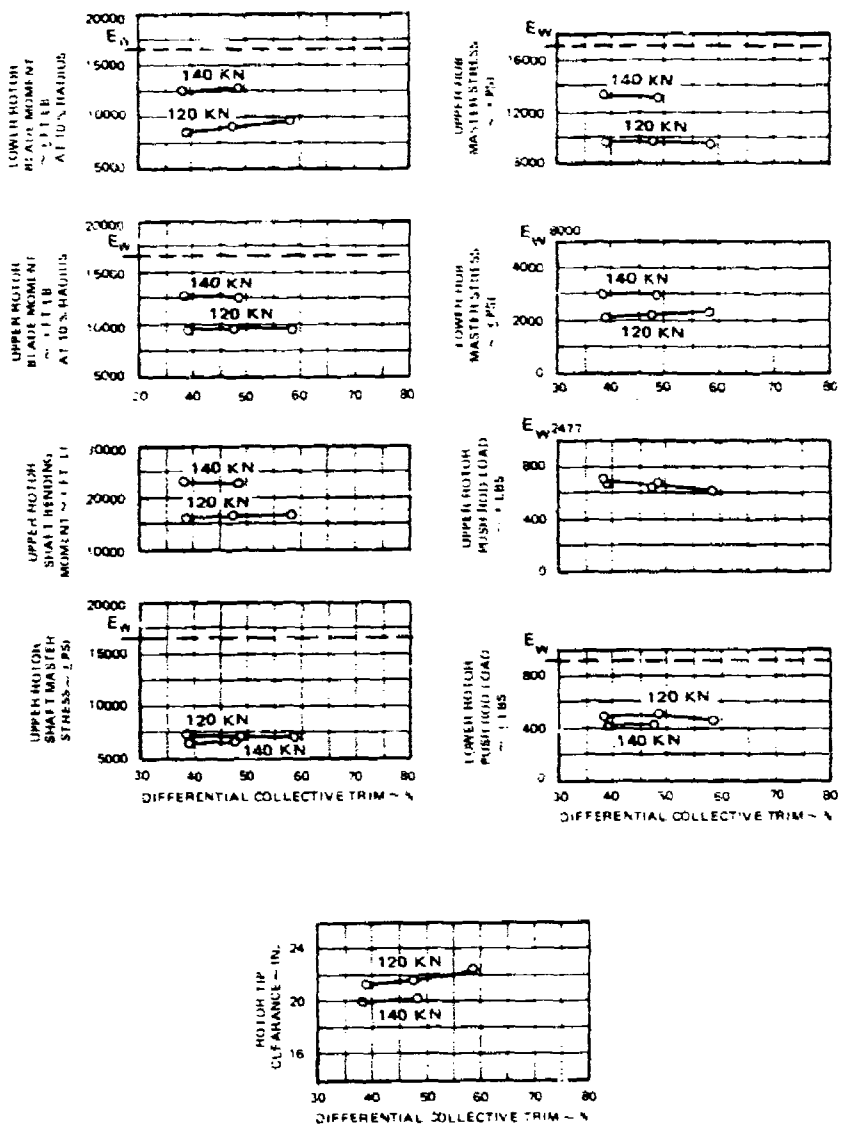

Figure 164. Effect of Differential Collective Trim on Rotor Component Loads and Stresses, Aux Propulsion Configuration.

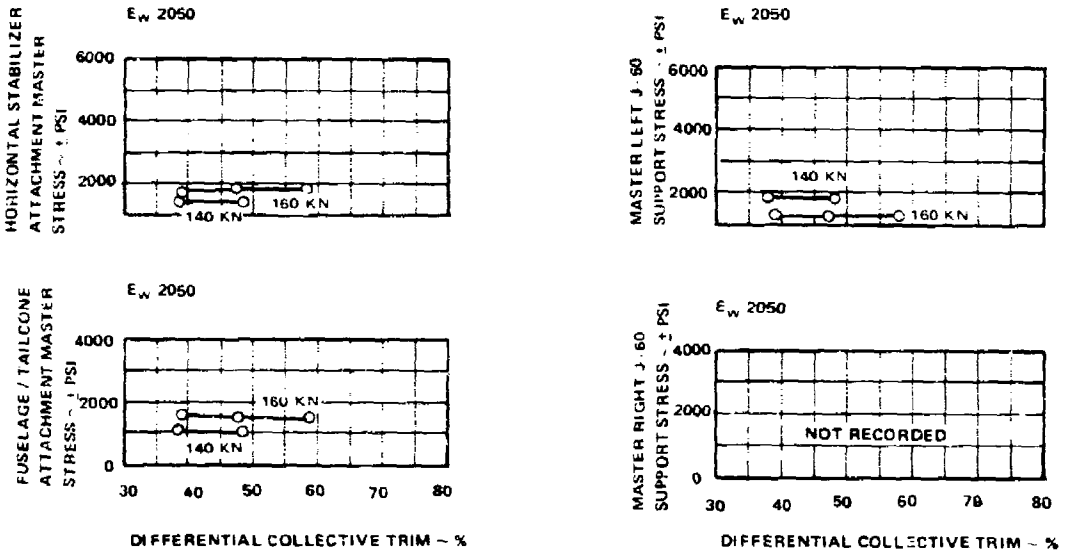

Figure 165. Effect of Differential Collective Trim on Airframe Loads and Stresses, Aux Propulsion Configuration.

Rotor Tip Separation - Trim Level Flight:

Figure 166 presents the relationship of the various rotor loads/stresses to rotor tip clearance. The data presented are for an array of airspeeds, rotor speeds, and rotor differential control positions to trim level flight. Figure 166 demonstrates a direct relationship between decreasing tip clearance and increasing vibratory rotor loads. The lone exception was the total stress at the base of the upper shaft. This parameter is primarily affected by rotor pitch moment.

Flight to Maximum Speed - 90-Degree Rotor Crossover:

The maximum airspeed achieved in trim level flight was 204 KTAS. This speed was achieved after completing each increment of airspeed envlope expansion in conjunction with expansion of the aircraft maneuver envelope at a lower speed. Adjustments of the interrotor differential controls and earlier than anticipated reduction of rotor speed were necessary to contain rotor and airframe loads and stresses.

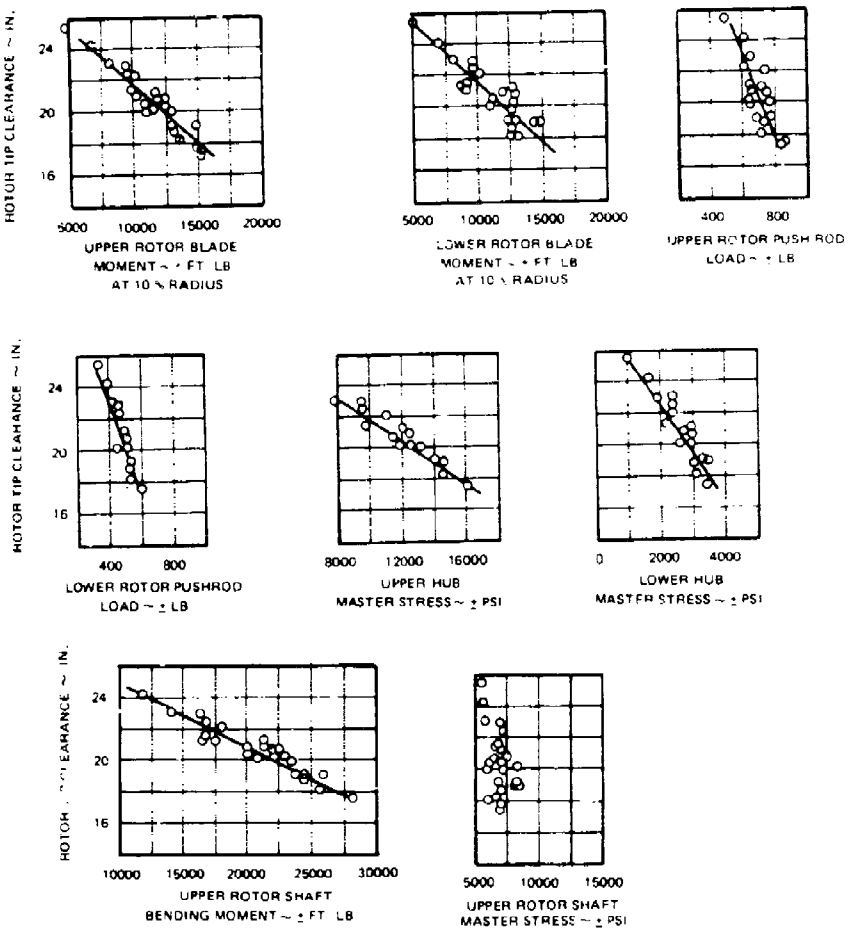

Figure 166. Rotor Tip Clearance Versus Rotor Component Loads and Stresses, Aux Propulsion Configuration.

The data presented in Figure 167 depicts the final individual control settings selected to provide the most acceptable rotor and airframe loads, stresses and vibration to maximum airspeed with 90 degree rotor crossover. This control schedule was also tailored to reduce pilot workload in that three of the five variables remained fixed for the entire speed range. Differential lateral control (B_1') was used to control rotor loads, stresses, and tip separation. Rotor speed was reduced in an attempt to reduce airframe loads and stresses. The data presented in Figure 168 shows that all rotor-related

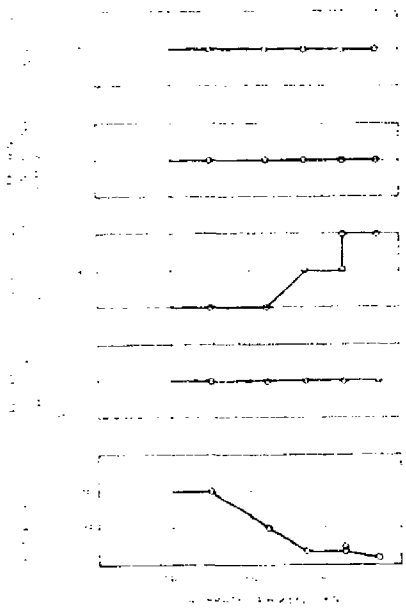

Figure 167. Cockpit Trim Control Schedule Versus Airspeed, Aux Propulsion Configuration.

component master loads and stresses were contained within the allowable limits. The data presented in Figure 169 shows, however, that the master airframe stresses were running higher than predicted even though a rotor speed reduction schedule was followed. The primary cause of the airframe stress problems was the airframe response to the 3-per-revolution vibratory roll and lateral rotor forces generated with 90 degree rotor crossover.

It was evident at this point that either some method of reducing airframe response or increasing the load-carrying capability of the critical airframe hardware was necessary to continue airspeed envelope expansion without accumulating excessive fatigue damage. It was then decided to reindex the rotors to cross over at 0 degree azimuth position to change the nature of the rotor-induced vibratory forces and moments.

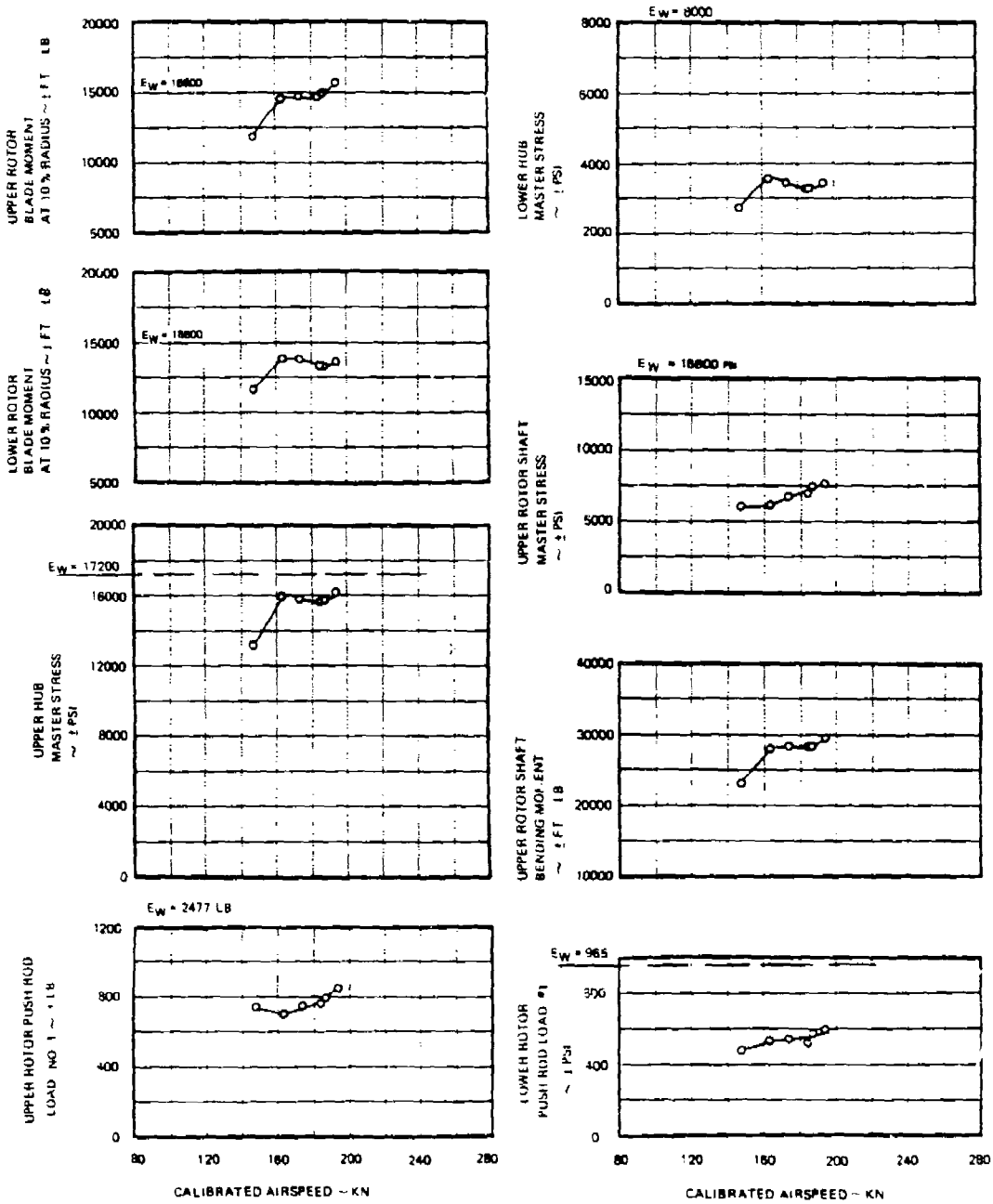

Figure 168. Rotor Structural Parameter Variation with Airspeed, Aux Propulsion C nfiguration.

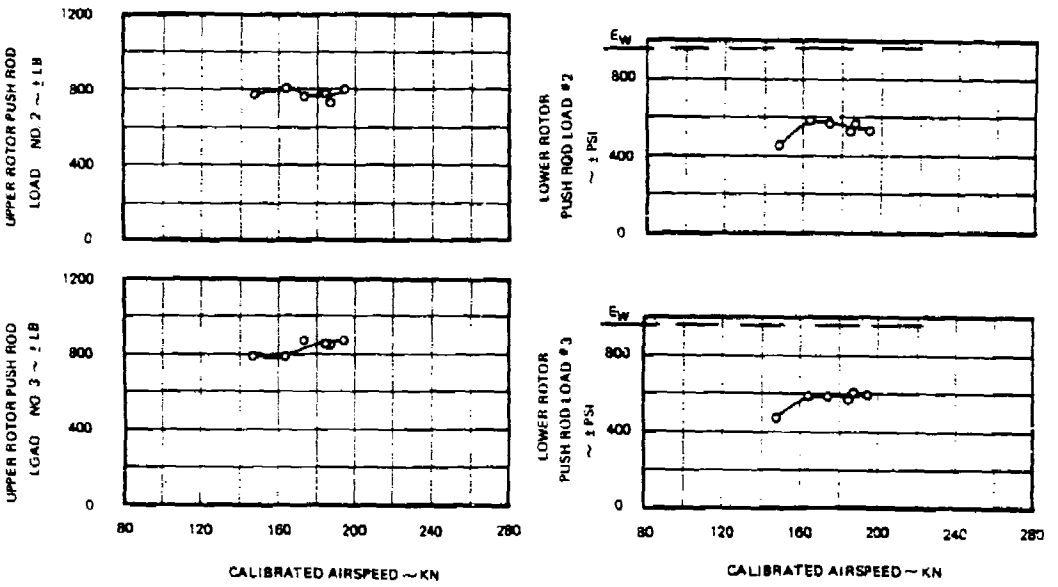

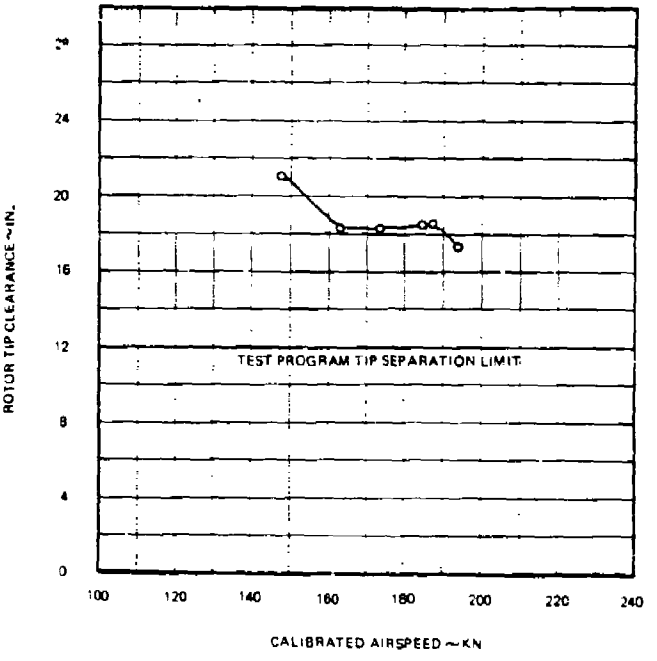

Figure 168. Continued

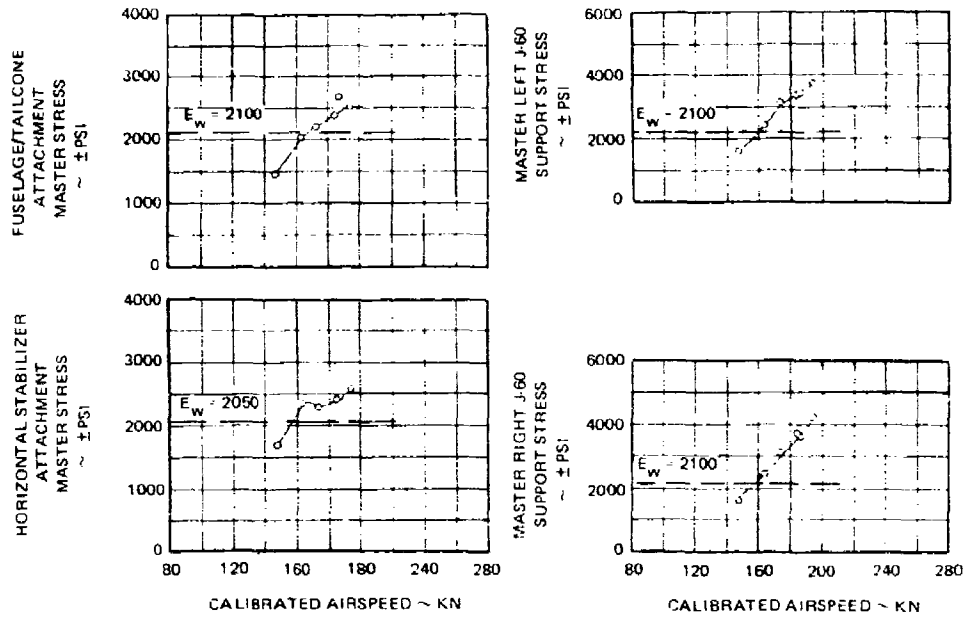

Figure 169. Airframe Structural Parameter Variation with Airspeed, Aux Propulsion Configuration.

Maneuvering Flight:

After each 20-knot increase in aircraft envelope expansion, the maneuvering envelope was expanded at the previous airspeed. The maneuvering envelope expansion consisted of evaluating the effects of load factor, roll rate, sideslip, simulated single lift engine power loss, simulated single and dual thrust engine power loss, turn to 45 degree angle of bank, and simulated stability augmentation system hardover malfunctions. Of these test conditions the most significant maneuvers were load factor, roll rate and sideslip. The remaining maneuvering tests contained one or more of these three conditions. However, in no case did they approach the limits evaluated during these three specific test maneuver evaluations.

Effects of Load Factor:

Presented in Figure 170 is the effect of load factor on rotor tip clearance and rotor pushrod loads for 100, 140 and 180 knots. Rotor pushrod loads are essentially linear with load factor and show no tendency to develop a knee in the curve due to rotor stall as experienced with normal articulated helicopters. In addition, a review of the pushrod instrumentation

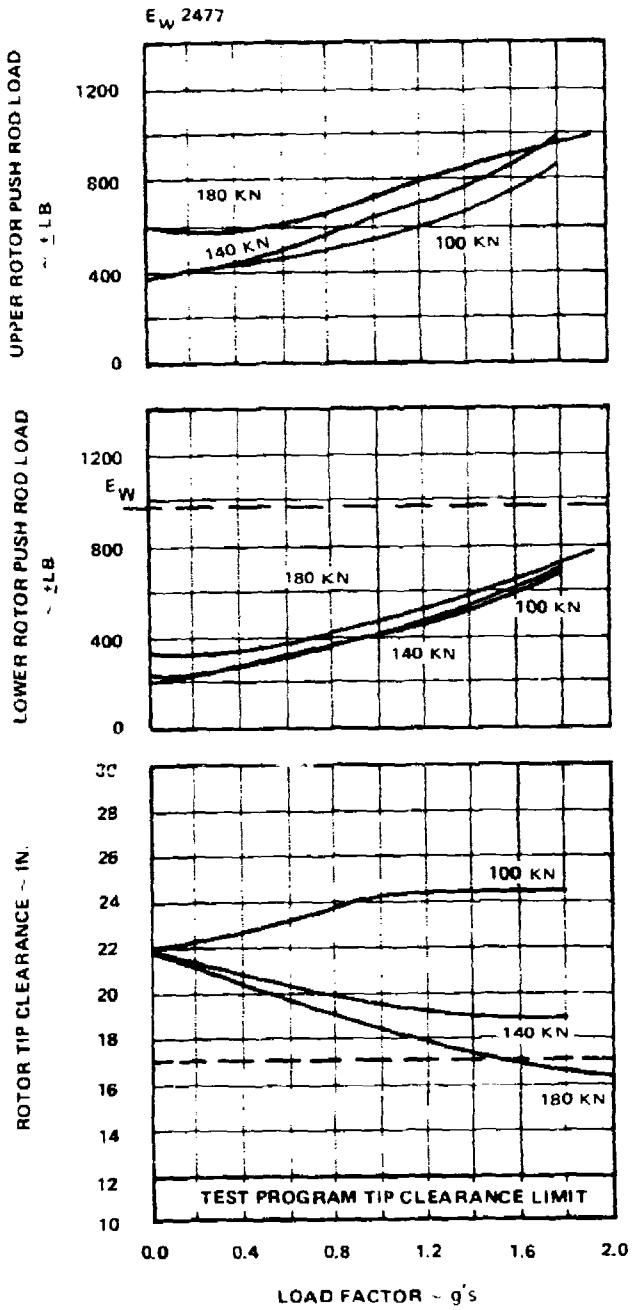

Figure 170. Effect of Load Factor on Tip Separation and Rotor Control Loads, Aux Propulsion Configuration.

data revealed no evidence of blade stall. The pushrod load magnitude remained well within endurance limits through 1.8g's.

The rotor tip clearance versus load factor data shows the same apparent discrepancy as with the pure helicopter. Tip clearance at 140 and 180 knots reduces with positive load factor as anticipated but remains constant at 100 knots. Here again, as with the pure helicopter, the tip clearance at low speed is more dependent on rotor gyroscopics due to the larger required pitch rates to generate load factor. As airspeed increases, a smaller pitch rate is required to develop the same load factor. The minimum rotor tip clearance achieved during these maneuvers was approximately 16 inches at 1.95g's and 180 knots. At no time did the tip clearance approach the 12-inch limit. All rotor component loads and stresses remained below endurance except for load factors above 1.45g's at 180 knots.

Effects of Roll Rate:

Presented in Figure 171 is a summary of rotor tip separation versus roll rate for two airspeeds. The difference between tip separation at 140 and 180 knots at zero roll rate is a function of airspeed and the differential lateral control (B_1') schedule established to control lift offset and the resultant rotor loads and stresses. These trim points can be directly compared to the rotor tip separation data presented in Figure 169 for a typical set of level flight trim points. The difference in attainable roll rate, left and right, before tip separation reaches the established test program limit of 12 inches is due to rotor precession caused by the roll rate generated, and the introducton of A_1' through the 40-degree control phase angle (Γ) with the application of lateral control.

Effect of Sideslip:

Sideslips, although not a classic dynamic maneuver, represent a substantial steady-state deviation from level flight trim. A steady-state sideslip envelope of ±10 degrees was established up through 180 knots calibrated airspeed for the auxiliary propulsion configuration.

The data presented in Figure 172 depicts typical rotor loads and stresses for sideslip conditions at 180 knots. The angle of attack data presented shows that the aircraft exhibits a slightly nonsymmetric angle of attack versus sideslip characteristic which is also reflected in some of the rotor system loads and stresses. The upper shaft master stress

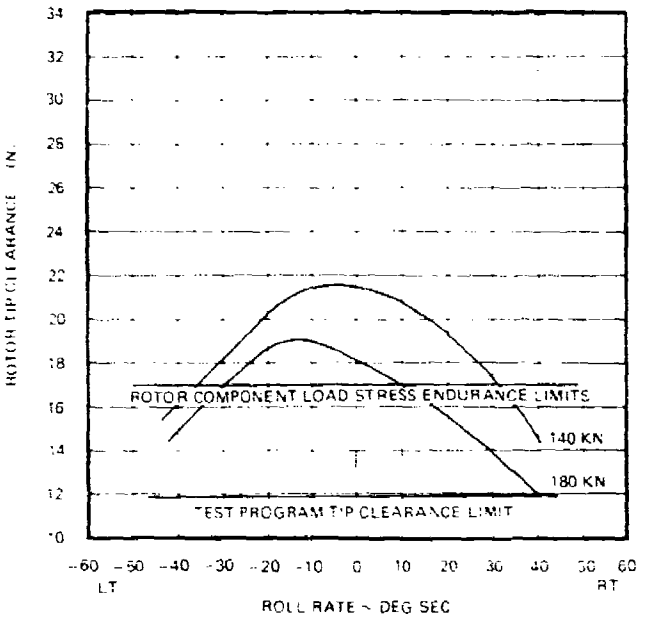

Figure 171. Effect of Roll Rate on Rotor Tip Separation and Rotor Loads and Stresses, Aux Propulsion Configuration.

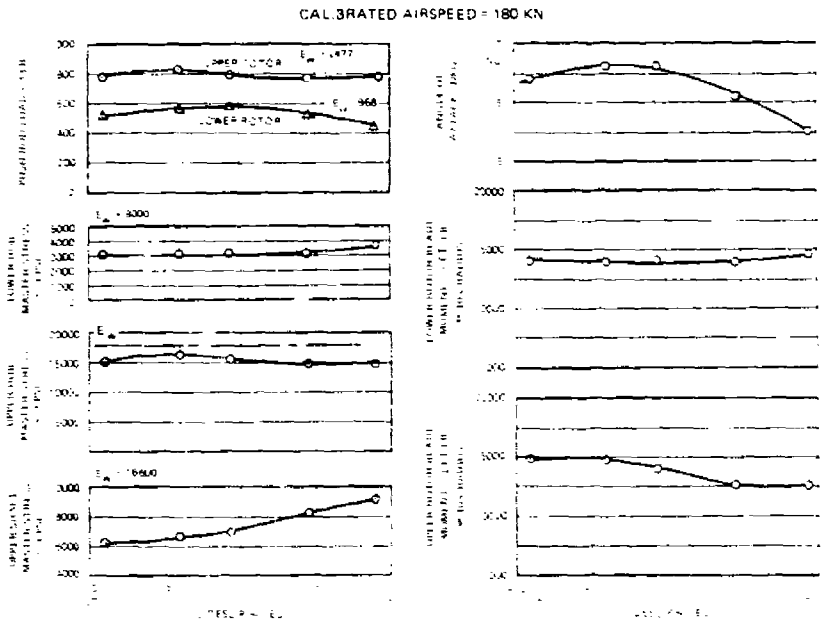

Figure 172. Rotor Structural Parameter Variation with Sideslip, Aux Propulsion Configuration.

measurement, which is predominantly responsive to rotor pitching moment, exhibits the largest change in magnitude, responding to the variation in angle of attack. The remaining master parameters exhibit less response. All rotor loads and stresses remained well within acceptable limits.

The data presented in Figure 173 depicts typical loads and stresses for the tailcone/empennage area of the airframe versus sideslip for the same 180-knot sideslip conditions. Unlike the rotor loads and stresses where the effect of sideslip was small, the effect of sideslip on the tailcone/empennage is more pronounced.

A shake test was conducted on the tail of the aircraft, inputting vertical vibratory forces separately at the tailcone centerline and at the right vertical fin. Of the several modes defined, two were predominant at rotor blade passage frequencies. The first predominant mode was an antisymmetric (roll) mode of the empennage/tailcone. This mode adversely affects both the tailcone/fuselage attachment area and the horizontal stabilizer/tailcone attachment area. The second predominant mode was an empennage (horizontal stabilizer) symmetric mode which exhibited less effect on the horizontal stabilizer/tailcone/fuselage atttachment areas but showed a strong influence on both elevator and rudder rod loads. The symmetric mode (vertical shake at the tailcone centerline) affected the elevator rod loads due to the inertia effects of the elevator and the resulting elevator hinge moments. The rudder surfaces are designed with antiflutter overbalance weights located at the top of the control surface. It was theorized that the overbalance weights were responding in opposite directions, with the tail responding in the symmetric mode. Due to the kinematics of the rudder control system, the rudder rod loads (rudder hinge moments) increased with the magnitude of the empennage symmetric mode response. The theory was proven during the shake test when the rudder rod loads reduced to near zero with the overbalance weight removed.

The variation of loads and stresses in the tail section versus sideslip shows the effect of both the symmetric and antisymmetric tail response to rotor forcing functions plus an apparent downwash impingement from the lower rotor. The rotor forcing functions are affected by changes in the individual rotor effective control phase angle (Γ) due to the sideslip angle. In addition, the impact of the downwash impingement is modified by the location of the tail in relation to the rotor wake with sideslip.

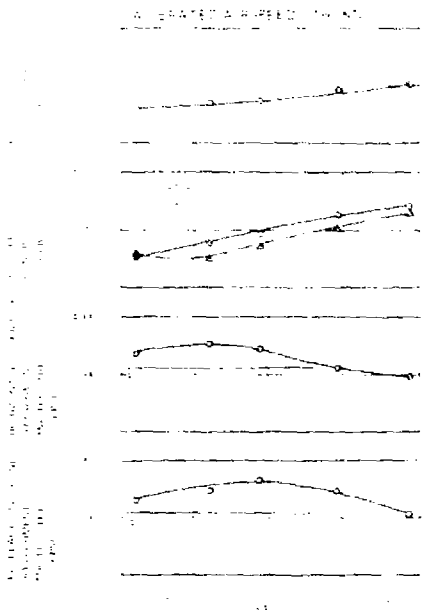

Figure 173. Airframe Structural Parameter Variation with Sideslip, Aux Propulsion Configuration.

Summary of 90-Degree Crossover Auxiliary Propulsion Structural Results:

1. Changes in rotor speed between 90 and 104 percent N_R did not significantly affect rotor loads and stresses. However, the stress at the tail of the aircraft was maximum at 100 to 101 percent N_R and the stress on the thrust engine support structure increased as rotor speed decreased, hampering the effort to effectively demonstrate the ABC concept on the XH-59A airframe.

2. Differential longitudinal cyclic control did not significantly affect rotor loads/stresses. However, the tail stress was minimized at +10 percent control.

3. Differential lateral cyclic control had a very strong influence on rotor loads and stresses, but did not affect the airframe.

4. Differential collective primiarily produced minor changes in rotor tip clearance.

5. Evidence indicated rotor wake impingement on the tail area at all forward speeds.

6. Most rotor loads correlated with rotor tip clearance.

7. Tip clearance and rotor loads were successfully controlled to 204 KTAS.

8. XH-59AA airframe response was a limiting factor in demonstration of the ABC limitations.

9. The XH-59A demonstrated the absence of rotor blade stall at 180 KCAS through a $C_T/\sigma = 0.21$.

10. Gyroscopic effects were evident in the ABC rotors during rolling reversals.

Auxiliary Propulsion Testing - 0-Degree Rotor Crossover

This phase of the test program was conducted through a series of 34 flights from November 11, 1979 through May 29, 1980. The buildup in envelope expansion was initiated at 140 knots with a maximum airspeed of 227 KCAS (238 KTAS) being achieved. The aircraft envelope expansion technique used for the 90-degree crossover test phase was retained for this phase of testing.

25
B

Rotor Trim Mapping

As with the 90-degree rotor crossover testing, a limited amount of rotor trim and rotor speed mapping was necessary with each increment of airspeed. In addition, collective control and elevator angle mapping were also investigated.

Effects of Rotor Speed

The effects of rotor speed on the primary structural parameters for the 0-degree rotor crossover configuration are presented in Figure 174. The data show that the rotor parameters were not significantly affected by rotor speed in the range evaluated. Comparison with the data in the 90-degree rotor crossover data lead to the same conclusion. There are slight variations in the shallow slopes of the data due in part to normal data scatter and to an impedance change of the rotor system resulting from the rotor index change.

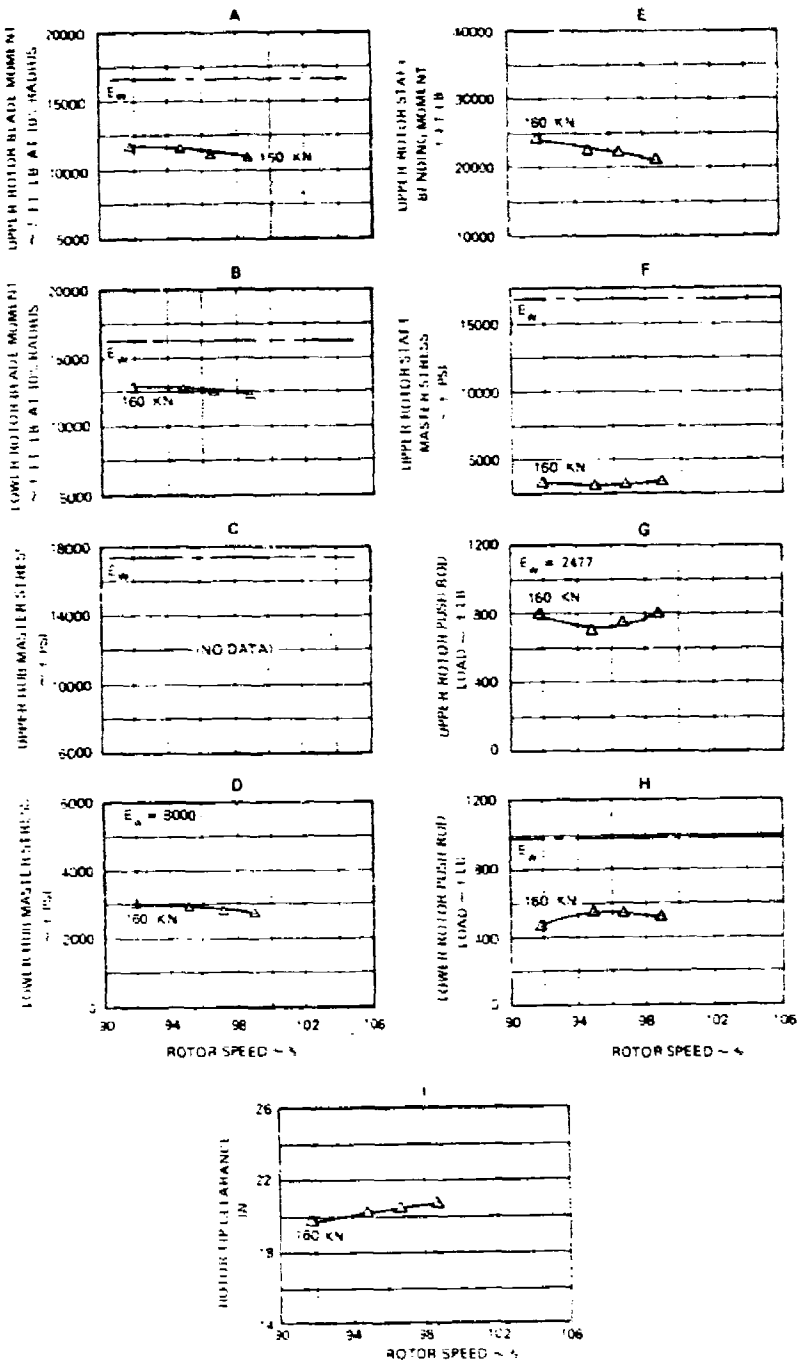

Figure 174. Effect of Rotor Speed on Rotor Component Loads and Stresses, Aux Propulsion Configuration.

Figure 175 presents the effect of rotor speed on the airframe parameters. The J-60 engine attachment structure (Figure 175B) had the same sensitivity to reduced rotor speed as in the 90-degree crossover configuration; however, the vibratory stress was reduced to well below the endurance limit in the 0-degree crossover configuration.

The vibratory stress master stress locations on the tailcone and stabilizer attachment areas (Figure 175C and D) were not as sensitive to variation in rotor speed at 160 knots when compared to the 90-degree crossover data. The vibratory stress was also substantially reduced as a result of the rotor index change. It should also be noted that the horizontal stabilizer attachment fittings were changed from aluminum to steel at the same time, providing greater attachment hardware strength.

Figure 175E and F show the response of the rudder vibratory control loads to rotor speed. The response was the same as with the 90-degree crossover configuration; however, the amplitude was increased. This increase resulted from exciting the symmetric mode of the horizontal stabilizer which in turn caused the rudder overbalance weights to generate high vibratory control rod loads.

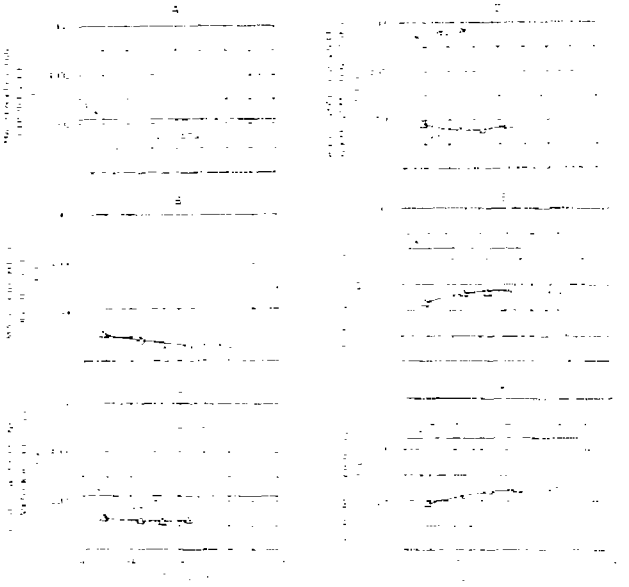

Figure 175. Effect of Rotor Speed on Airframe Loads and Stresses, Aux Propulsion Configuration.

Effects of Differential Longitudinal Control (A_1'):

Figure 176 shows the influence of differential longitudinal cyclic control on the rotor loads and stresses. At 160 knots the rotor remained insensitive to A_1', similar to the results obtained with 90-degree rotor crossover at 160 knots and below. The influence at 180 knots changed for rotor inboard blade bending (Figures 176A and B) as well as upper rotor shaft stress (Figure 176F). This effect was influenced by higher airspeed, changes in elevator setting and the use of different values of positive A_1' required to retrim the rotor with the change in elevator setting.

The airframe vibratory stress at the J-60 attachments (Figure 177A and B) and the rudder rod vibratory loads (Figure 177E and F) remained insensitive to A_1'. The tailcone and stabilizer stresses (Figure 177C and D) show some increase in stress levels with increasing differential longitudinal control.

Effects of Differential Lateral Control (B_1'):

The effects of B_1' on the rotor loads, stresses and tip clearance for the 0-degree crossover configuration are presented in Figure 178. Rotor blade bending, hub stresses, upper rotor shaft bending, and tip clearance had the same strong gradient with B_1' as the 90-degree crossover configuration. Figure 179 again shows that B_1' did not have a significant effect on airframe stress.

Effects of Differential Collective Control ($\Delta\theta_t$):

Figure 180 shows that variation of $\Delta\theta_t$ did not significantly affect the rotor loads. Minor changes to the curve slopes for the 0-degree crossover were evident for the rotor blade and hub load/stress. These slope changes relative to the 90-degree crossover data were probably due to the rotor system impedance change associated with the rotor index change. The gradient of rotor tip clearance to $\Delta\theta_t$ remained unchanged.

The airframe parameters again were only mildly sensitive to variations in $\Delta\theta_t$ as was shown for 90-degree rotor crossover indexing (Figure 181).

Effect of Collective:

As the airspeed envelope was expanded beyond 180 knots, it became evident that variations in rotor differential controls were not sufficient to keep the rotor loads and the main transmission foot loads within their working endurance limits. Data from isolated test conditions where small collective changes had been made indicated that the rotor loads and some airframe components were significantly affected by collective position. Systematic changes in collective position were evaluated for stress/load reductions and handling qualities consideration.

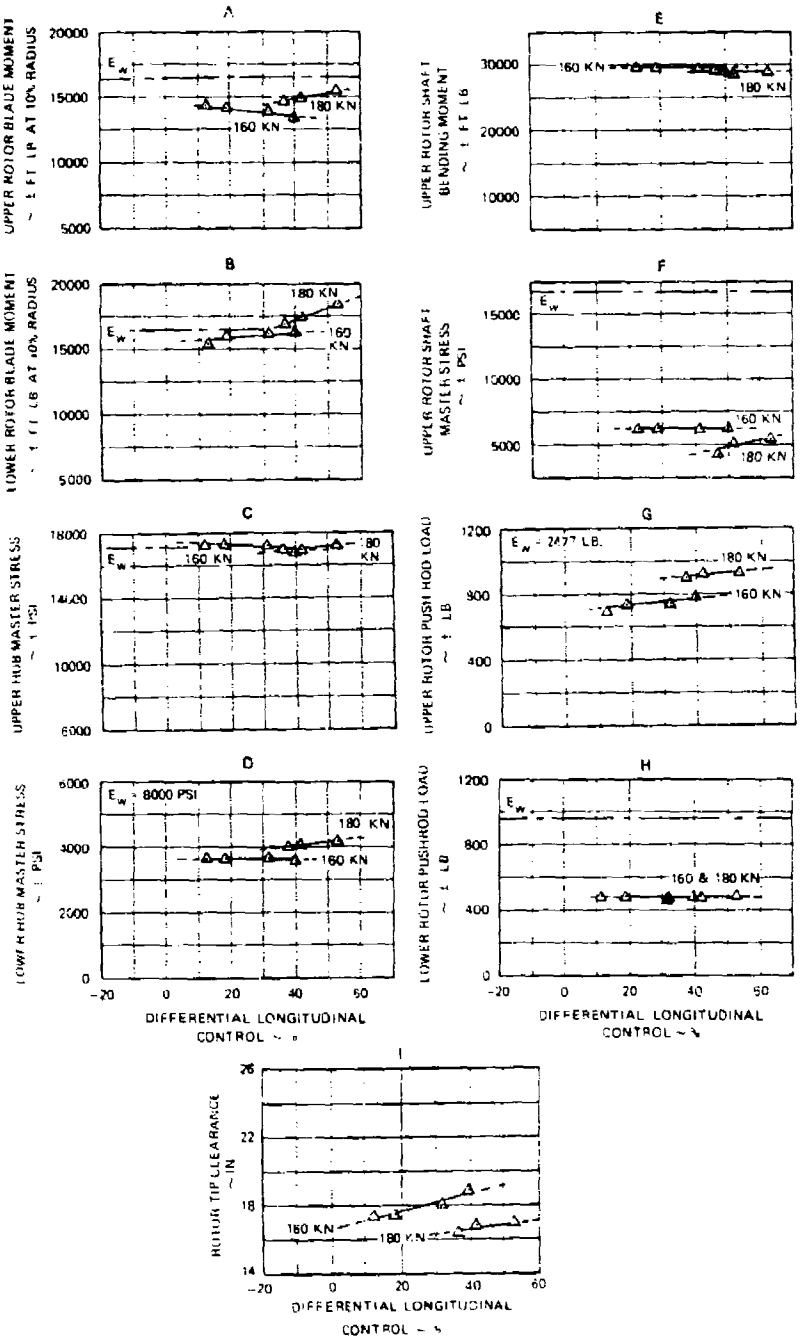

Figure 176. Effect of Differential Longitudinal Control on Rotor Components Loads and Stresses, Aux Propulsion Configuration.

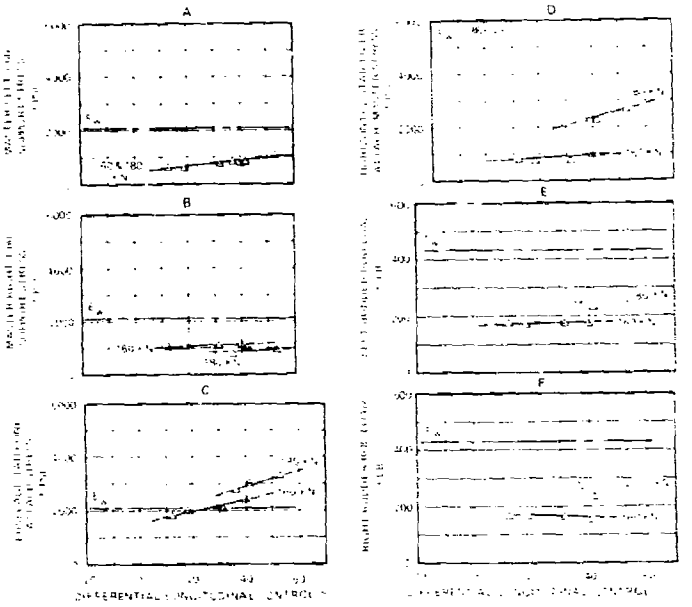

Figure 177. Effect of Differential Longitudinal Control on Airframe Loads and Stresses, Aux Propulsion Configuration.

Figure 182 presents the effect of collective position on rotor loads. The data show that except for the control loads (Figure 182G and H), the rotor loads were very sensitive to increasing collective. As airspeed increased, the sensitivity to collective position became more critical. Upper rotor hub stress, lower rotor blade bending at 10 percent radius, and upper rotor shaft stress were the most critical locations on the rotor system. Note that lowering the collective decreased the hub and blade vibratory loads but increased the stress at the base of the upper rotor shaft (Upper Rotor Shaft Stress, Figure 182F). For airspeed of 220 knots and above, the collective position will be critical.

Note also the characteristic of the upper rotor shaft stress (Figure 182F). At the lower airspeeds, the stress increased with increased collective; at the higher speeds, the stress decreased with increased collective. This gage location was sensitive to rotor pitching moment. It is believed that this slope change was due to the change in direction of the rotor pitching moment, i.e., the pitching moment went through zero. These slopes can also be affected by how the pitching moment is shared between the two rotors and by elevator angle. More work is needed to accurately determine this influence.

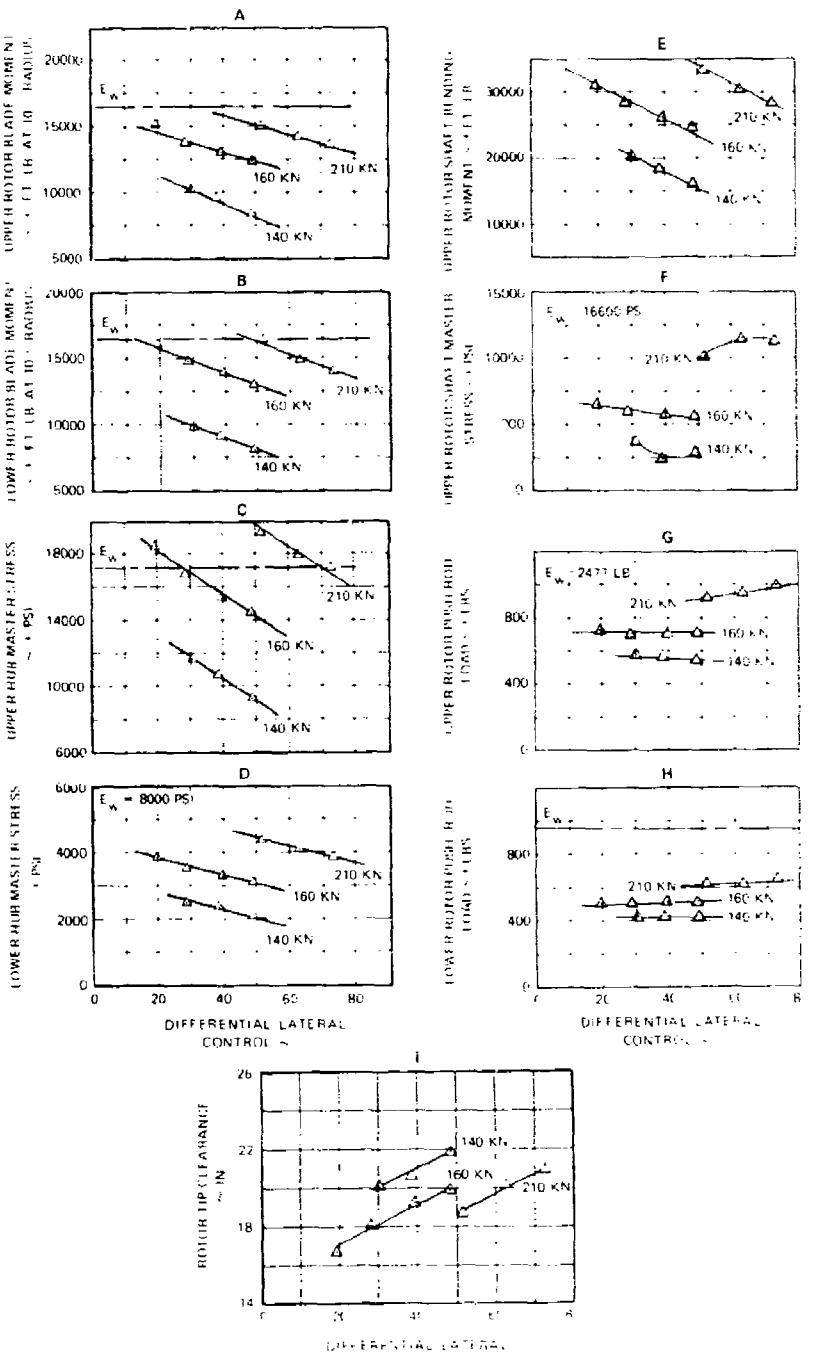

Figure 178. Effect of Differential Lateral Control on Rotor Component Loads and Stresses, Aux Propulsion Configuration.

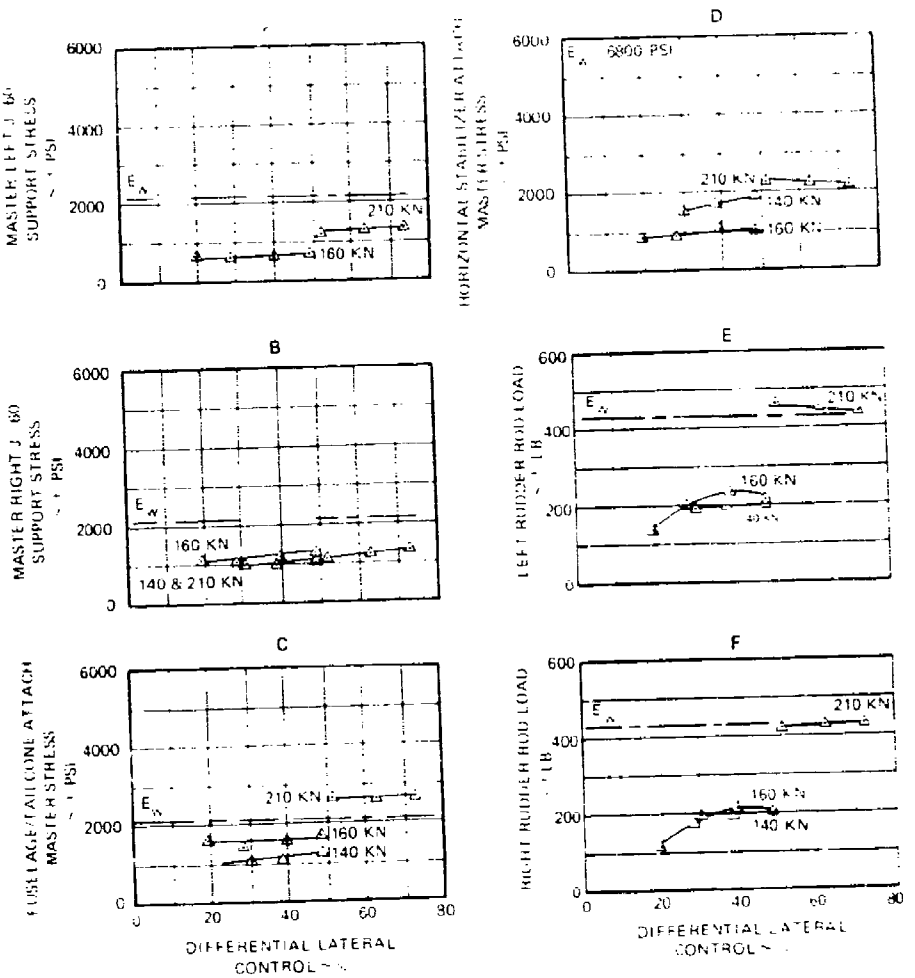

Figure 179. Effect of Differential Lateral Control on Airframe Loads and Stresses, Aux Propulsion Configuration.

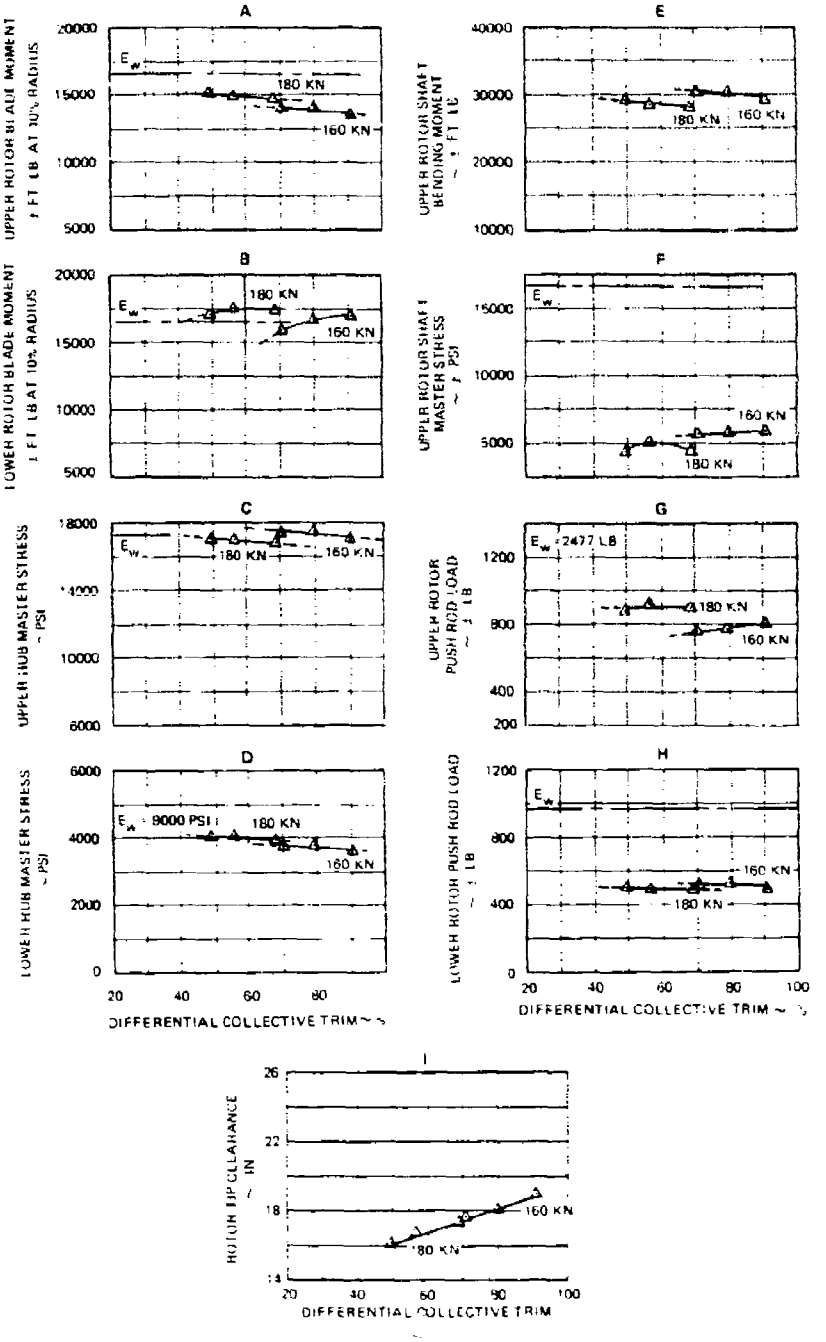

Figure 180. Effect of Differential Collective Trim on Rotor Component Loads and Stresses, Aux Propulsion Configuration.

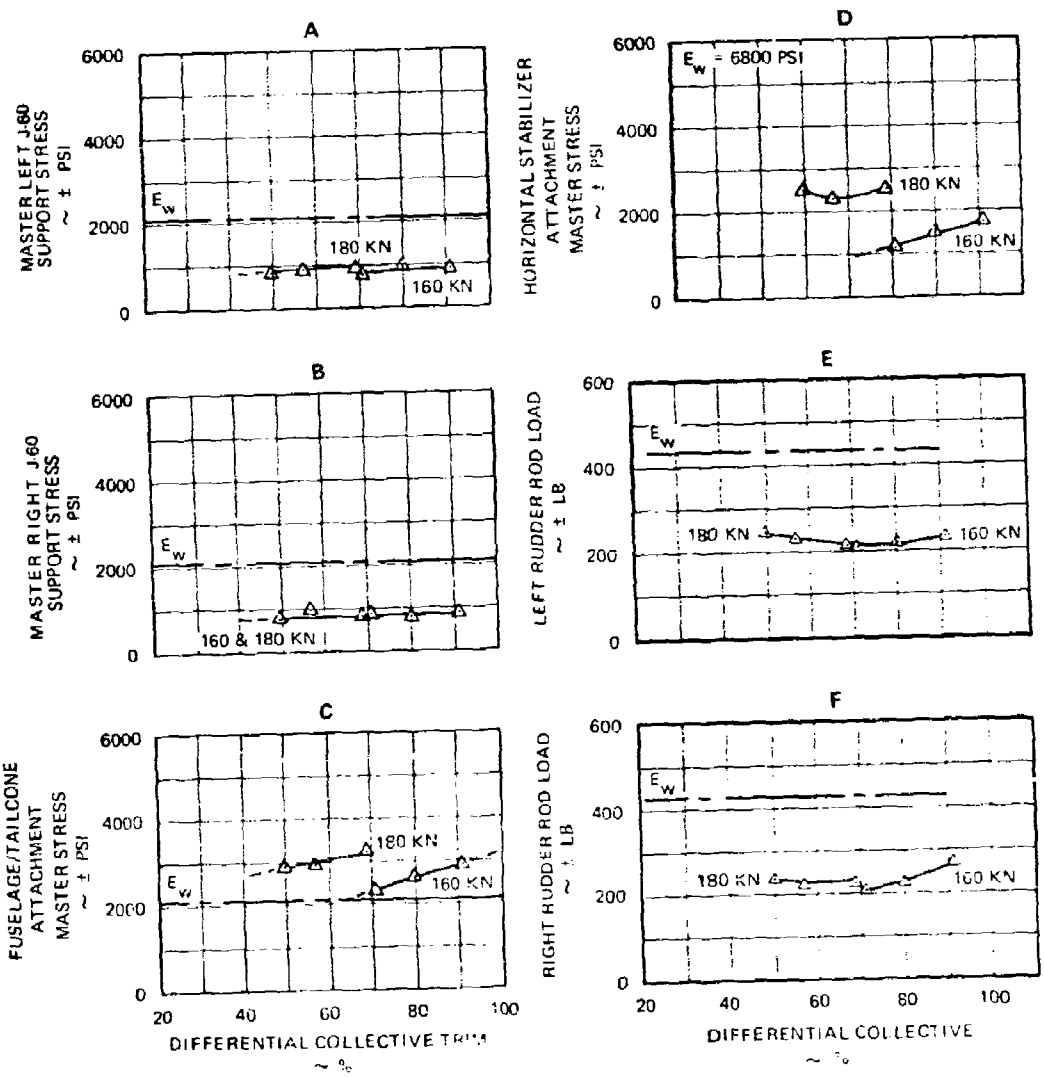

Figure 181. Effect of Differential Collective Trim on Airframe Loads and Stresses, Aux Propulsion Configuration.

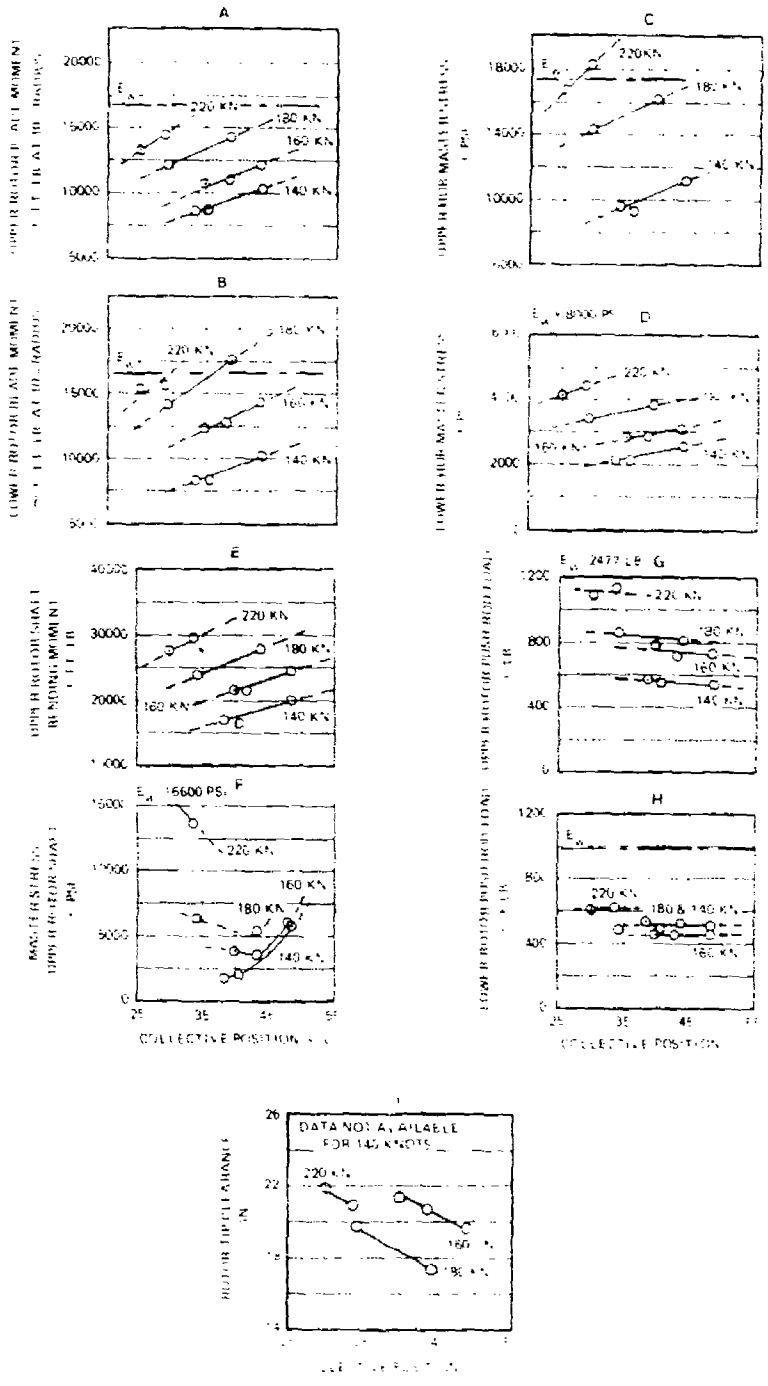

Figure 182. Effect of Collective on Rotor Component Loads and Stresses, Aux Propulsion Configuration.

Figure 182I also demonstrates that lowering the collective increased the rotor tip clearance. This same result was seen by increasing B_1'. The mechanism is effectively the same. Both control methods reduce rotor blade pitch on the advancing side and move the spanwise lift inboard.

The influence of collective position on the airframe and rudder rods is shown in Figure 183. The J-60 support structure and the rudder rod vibratory loads were not significantly affected by collective. The tailcone and stabilizer attachments showed a steep gradient with increased collective at 200 knots.

The vibratory loads at the main transmission attachments are presented in Figure 184. The data indicate the vibratory loads at 200 knots were significantly reduced by reducing collective. The vibratory loads at 180 knots were not significantly affected by collective position.

The collective schedule established to fly to 227 KCAS was predicated upon keeping the rotor loads and main transmission feet loads within their respective working endurance limits. Figure 185 shows the steady loads at the main transmission attachments.

Effect of Elevator Angle:

Changing the rotor crossover configuration from 90 degrees to 0 degree resulted in excessive elevator control rod loads by 160 knots. These loads were caused by elevator inertia when the elevator responded to the vibratory pitching moments that are transferred to the stationary system in the 0 degree crossover index. To eliminate the problem, the elevator was strapped to the stabilizer across the hinge line. The initial flights in this configuration resulted in dramatic changes in some of the rotor loads and stresses. Analysis of this data and previous data indicated that the unstrapped elevator had been making small angle changes in flight due to some control rod hysteresis and minor attachment backup structure deformation. The analysis also indicated that small elevator changes had a larger than anticipated effect on rotor component loads and stresses. To assess this effect, changes in elevator angle were evaluated.

The effects of elevator angle on rotor component loads and stresses is presented in Figure 186. The trends, based on 160 knots, show that an elevator angle of -1 degree to -1.5 degree provided minimum loads and stresses. Data at higher airspeed reflect this trend, however, the data set is not complete. Changes in elevator angle showed insignificant effect on tip clearance (Figure 186I).

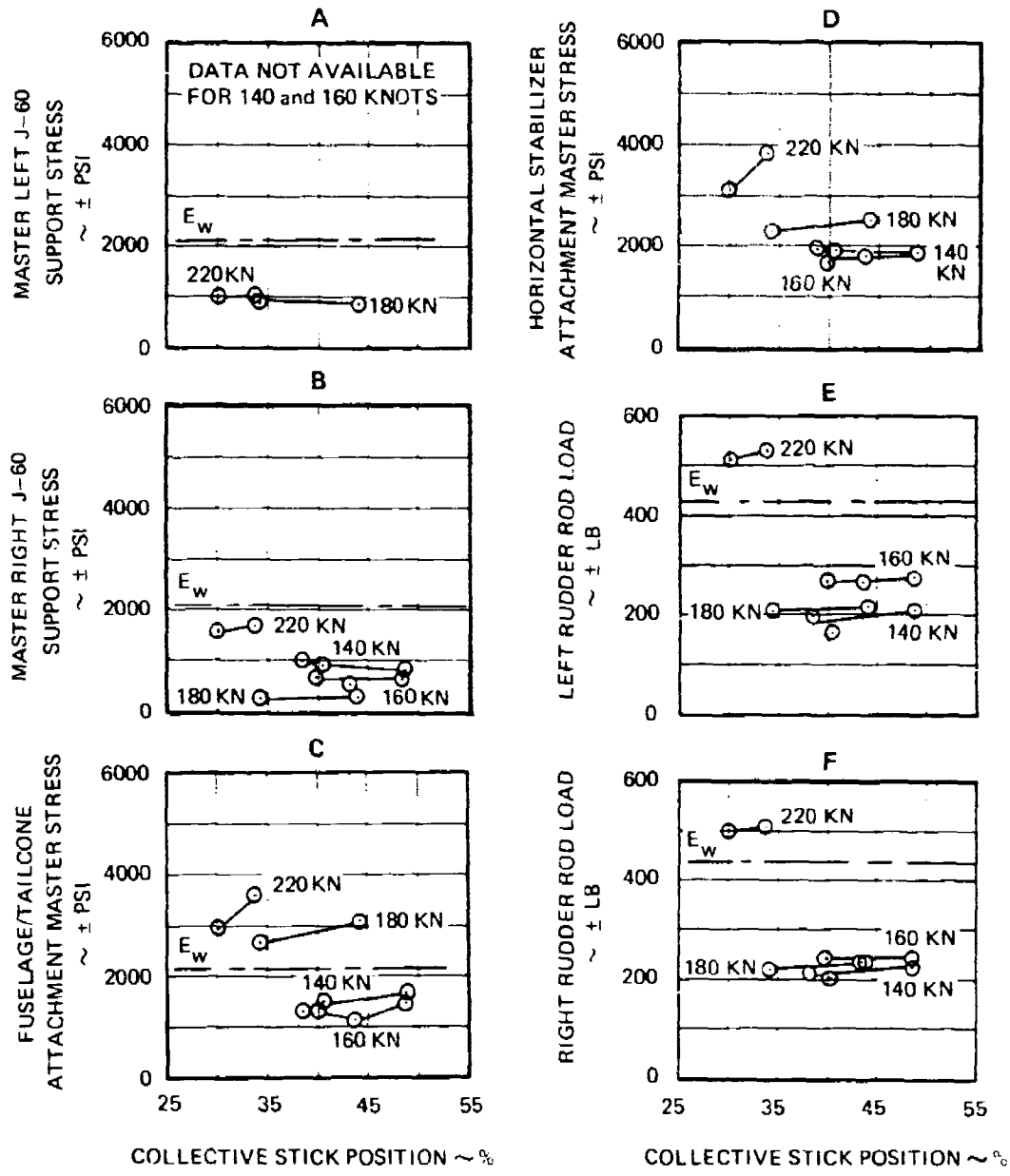

Figure 183. Effect of Collective on Airframe Loads and Stresses, Aux Propulsion Configuration.

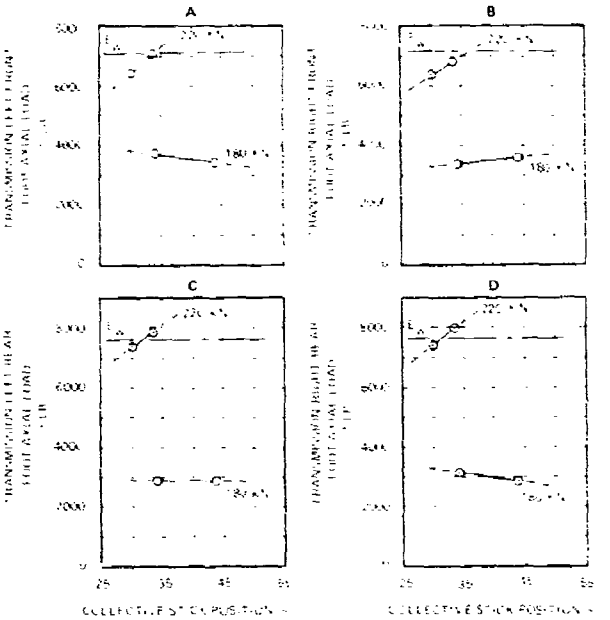

Figure 184. Effect of Collective on Transmission Foot Loads (Vibratory), Aux Propulsion Configuration.

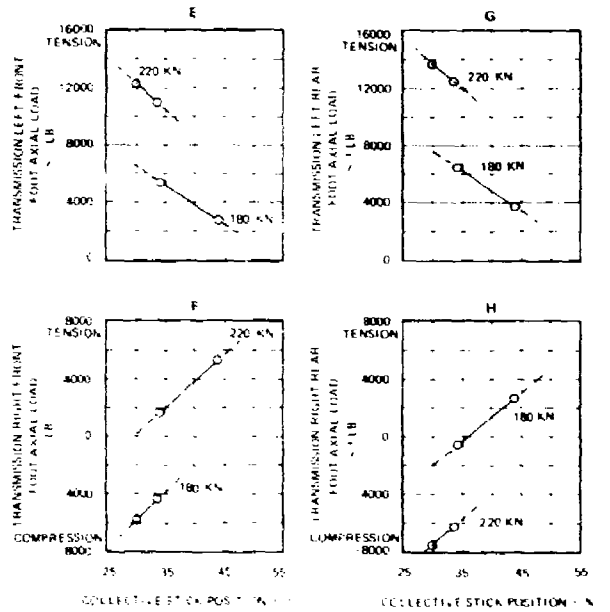

Figure 185. Effect of Collective on Transmission Foot Loads (Steady), Aux Propulsion Configuration.

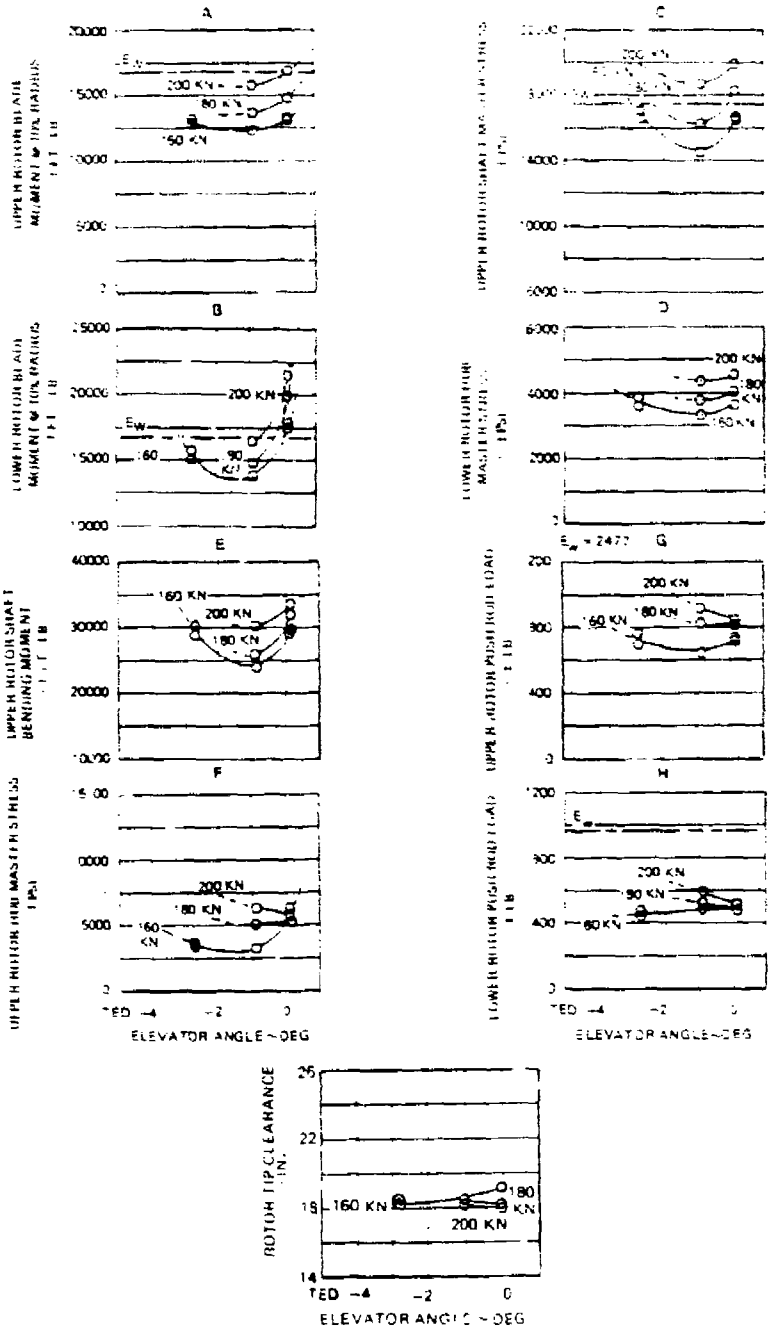

Figure 186. Effect of Elevator Angle on Rotor Component Loads and Stresses, Aux Propulsion Configuration.

The trends of elevator angle on airframe loads and stresses (Figure 187) were mixed with the most dramatic effect taking place in the fuselage tailcone attachment area (Figure 187C) and the horizontal stabilizer attachment (Figure 187D).

Flight to Maximum Speed:

The data in Figures 188 through 190 present a comparison of the results obtained during flight to maximum speed for both the 90-degree crossover and 0-degree crossover aircraft test configurations. The maximum airspeeds attained were 194 KCAS (234 KTAS) for the 90-degree crossover configuration and 227 KCAS (238 KTAS) for the 0-degree crossover configuration.

The information in Figure 188 depicts the difference in significant cockpit control trim parameters plus the difference in elevator angle used for the two rotor crossover configurations. With the exception of elevator angle which had not been optimized, the most significant trim changes were collective and rotor speed. The trim changes for differential longitudinal control (A_1') and differential collective trim ($\Delta\theta_1$) were consistent with balancing upper and lower rotor lift and pitching moments as a function of elevator angle.

The first significant difference between 90-degree and 0-degree rotor crossover is the fact that a premature reduction in rotor speed to reduce tail stresses was unnecessary with the 0-degree rotor crossover. On the negative side, however, the rudder rod loads (Figure 189F) exceeded the established endurance limits (Ew) which, as previously discussed, is directly attributable to the horizontal stabilizer symmetric response to 0-degree rotor crossover. The fuselage/tailcone attachment area stresses were unchanged (Figure 189C). The horizontal stabilizer attachment stress improvement (Figure 189D) is attributed both to the change in stabilizer response from an antisymmetric response with 90-degree rotor crossover to a symmetric response with 0-degree rotor crossover plus the hardware material change from aluminum to steel.

All master rotor component loads and stresses remained within their respective endurance limits (Figure 190). The upper rotor hub master stress was controlled at speeds up to 200 knots with differential lateral control (B_1') and was controlled for speeds above 200 knots with a combination of differential lateral control (B_1') and a step reduction in collective from 34 percent to 30 percent. This effect can also be observed in other rotor component master load and stress parameters as well as rotor tip clearance. The difference in rotor tip clearance shown in Figure 190 is not due to the change in rotor crossover. It is due to the difference in control settings used, as shown in Figure 188.

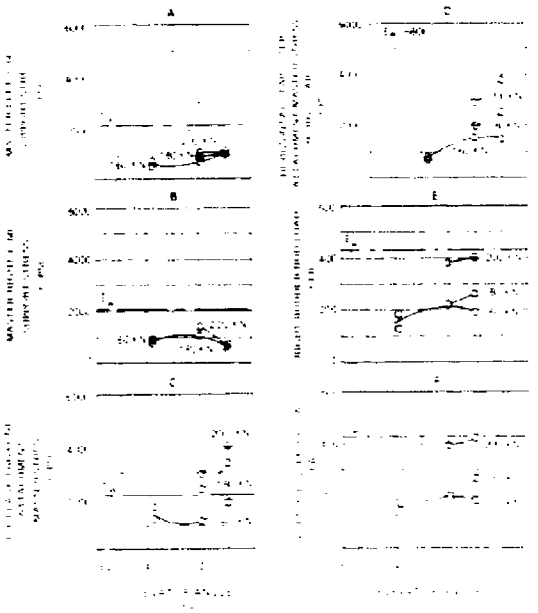

Figure 187. Effect of Elevator Angle on Airframe Loads and Stresses, Aux Propulsion Configuration.

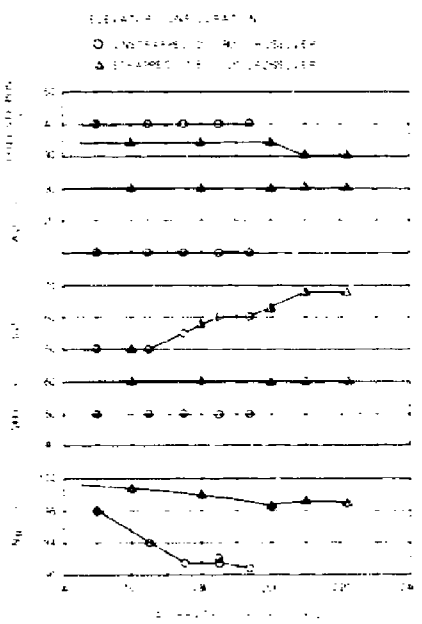

Figure 188. Cockpit Control Schedule, Aux Propulsion Configuration.

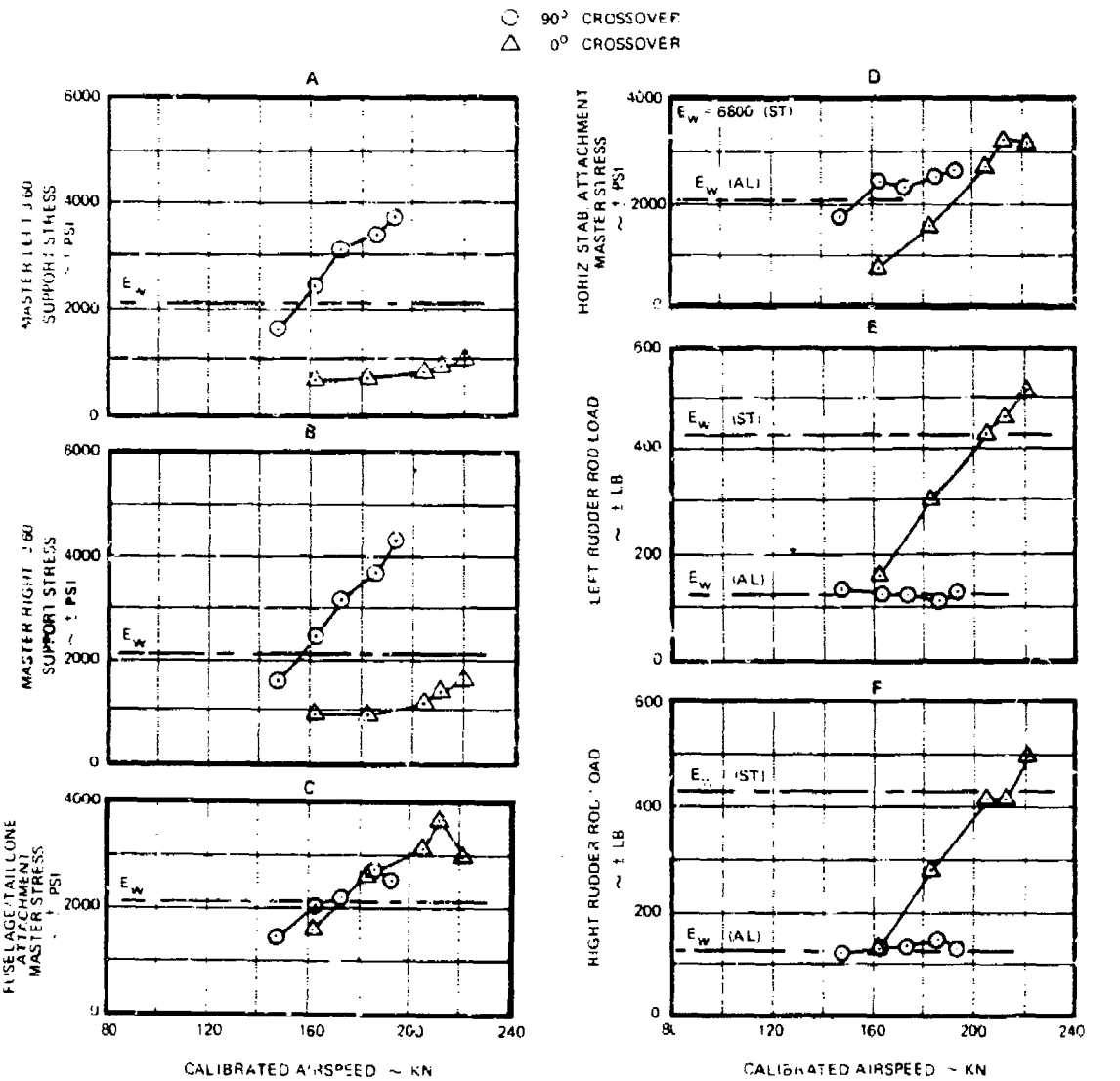

Figure 189. Effect of Airspeed on Airframe Loads and Stresses, Aux Propulsion Configuration.

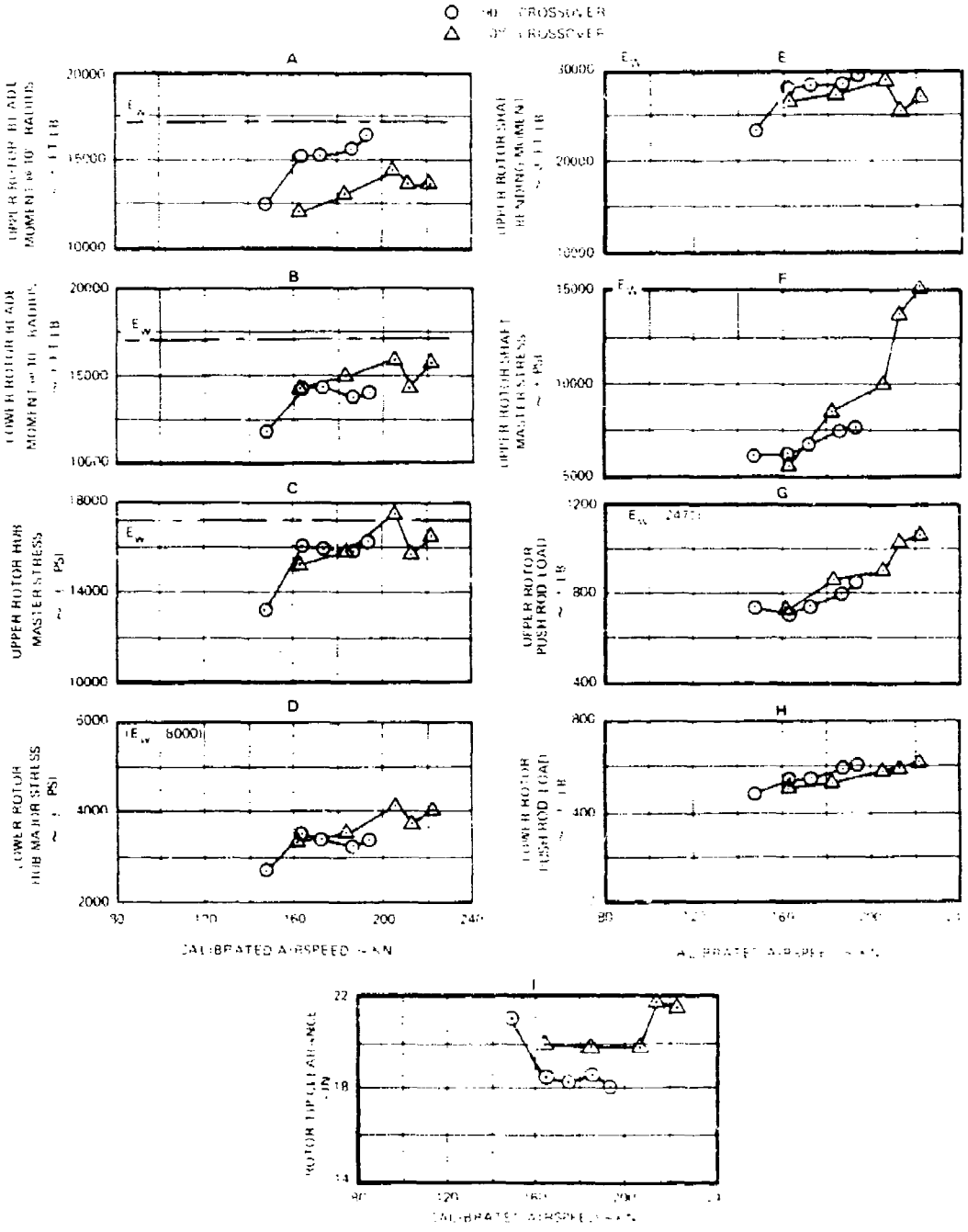

Figure 190. Effect of Airspeed on Rotor Component Loads and Stresses, Aux Propulsion Configuration.

The upper rotor shaft master stress, which as noted earlier responds to total rotor pitching moment, was approaching endurance at maximum airspeed (Figure 190F). This dramatic increase in stress was the result of two parameters. The first parameter was excessive negative elevator angle. The change in slope above 200 knots was the result of the collective reduction necessary to contain the upper rotor head master stress. The resultant rotor thrust reduction was compensated for with increased rotor angle of attack to maintain level flight. This in turn resulted in an increase in total rotor nose-up pitching moment due to the increase in horizontal tail angle of attack, thus causing the slope change.

Effects of Load Factor:

The effect of load factor on rotor tip clearance for the 0-degree rotor crossover configuration is presented in Figure 191. The trend of decreasing tip clearance with increased load factor was the same as obtained with the 90-degree crossover configuration previously shown in Figure 170. Comparing the results obtained at 180 knots for both rotor crossover configuratons shows agreement within one inch, which is well within the ± two-inch accuracy quoted for the tip path monitor. It may be noted that there is less tip separation closure at 200 knots than 180 knots with increasing load factor. Flight data shows that less angle of attack change per unit load factor is required at 200 knots, which results in lower gyroscopic loading of the rotor discs. Data obtained in both the 90-degree and 0-degree crossover configurations indicate that maximum tip closure with increasing load factor occurs at 180 knots and that the effect decreases as speed increases. Additional testing at higher airspeeds is required to confirm this trend.

The effect of load factor on rotor control loads for the 0-degree rotor crossover configuration is presented in Figure 192. The trend of decreasing control load with decreasing load factor agrees with the data obtained in the 90-degree rotor crossover configuration (Figure 170). The slope of increasing control load with increasing load factor is steeper with a 0-degree rotor crossover. The mechanism for this slope change was trim flight collective setting with 40 percent collective used with 90-degree crossover and 34 percent collective used with 0-degree crossover. With the lower collective setting for the 0-degree crossover configuration, larger rotor speed increases with increasing load factor were observed than with the 40-percent collective for the 90-degree crossover configuration and resulted in an incremental increase in control load when compared to the same condition with 40-percent collective.

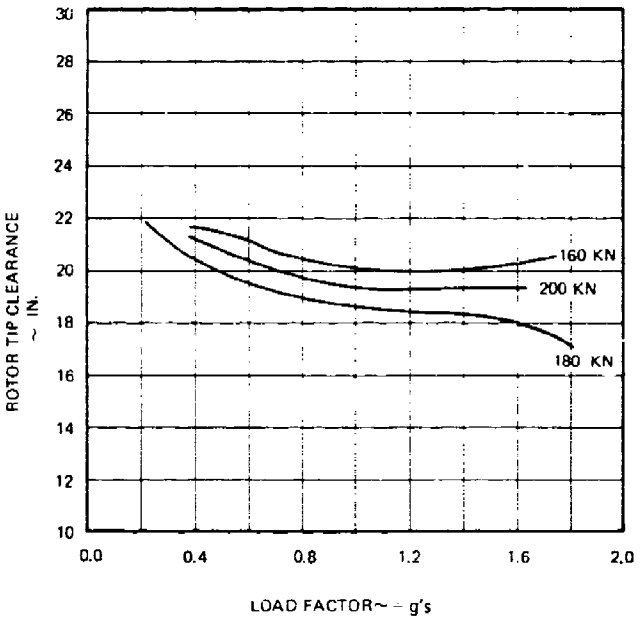

Figure 191. Effect of Load Factor on Rotor Tip Clearance, Aux Propulsion Configuration.

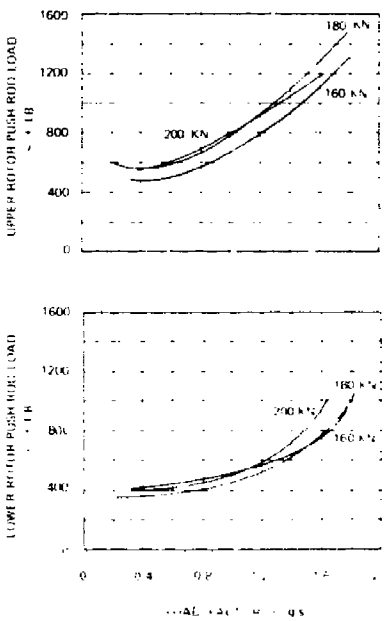

Figure 192. Effect of Load Factor on Control Loads, Aux Propulsion Configuration.

Effect of Roll Rate:

Only limited roll rate testing was conducted with 0-degree rotor crossover. The effect of roll rate on rotor tip clearance for the 0-degree rotor crossover configuration is shown in Figure 193. Comparing the 180 knot data with 90-degree rotor crossover 180-knot data (Figure 171) shows that the characteristics are essentially the same. However, the initial trim rotor tip clearance value for 0-degree crossover is lower. This is the result of trimming the rotor with a different combination of differential collective and differential longitudinal control. Both conditions were tested with 40-percent collective. The 200-knot data are similar to the 180-knot data; however, the initial trim rotor tip clearance is higher based on using 34 percent collective and more differential lateral control to control rotor stresses.

Effect of Sideslip:

Figures 194 and 195 show the effect of sideslip at 180 knots for 0-degree rotor crossover. This data may be compared to Figures 172 and 173 in the 90-degree crossover configuration. With the exception of the upper shaft master stress, only minor differences are noted. The difference in upper shaft master stress values are attributed to rotor total pitching moment differences due to using more trailing-edge-down elevator and 5 percent more collective for the 0-degree crossover configuration as the elevator was strapped. The increase in rudder control rod loads for the 0-degree crossover configuration is directly attributable to the previously-discussed horizontal stabilizer and rudder overbalance weight response.

The variation of loads and stresses in the tail section versus sideslip shows the effect of both the symmetric and antisymmetric tail response to rotor forcing function plus an apparent downwash impingement from the lower rotor. The rotor forcing functions are affected by changes in the individual rotor effective control phase angle (Γ) due to the sideslip angle, and the impact of the downwash impingement is modified by the location of the tail in relation to the rotor wake with sideslip.

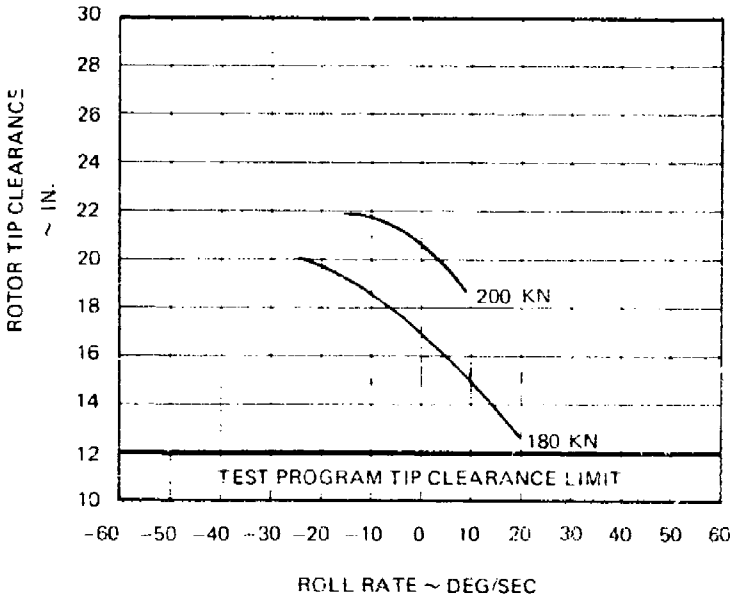

Figure 193. Effect of Roll Rate on Rotor Tip Clearance, Aux Propulsion Configuration.

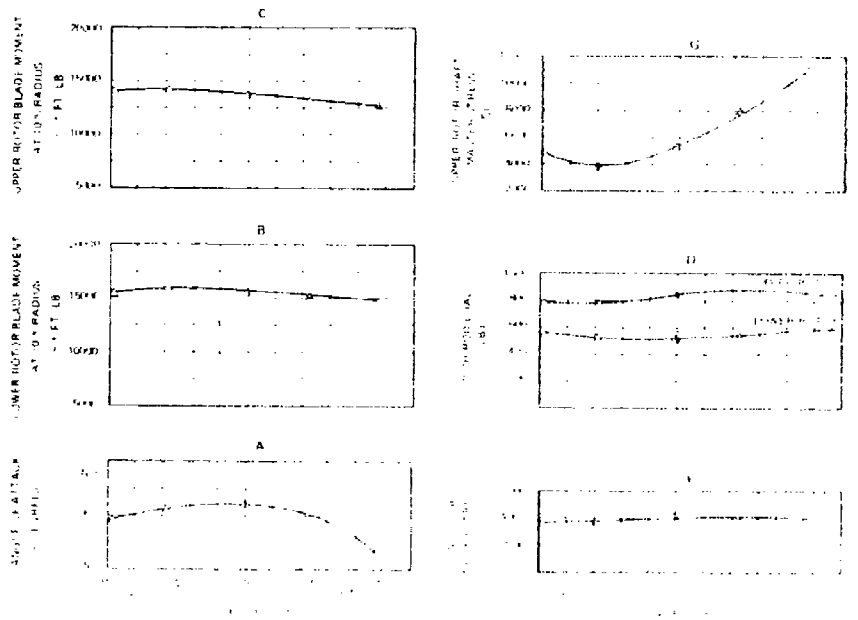

Figure 194 Rotor Structural Parameter Variation with Sideslip, Aux Propulsion Configuration

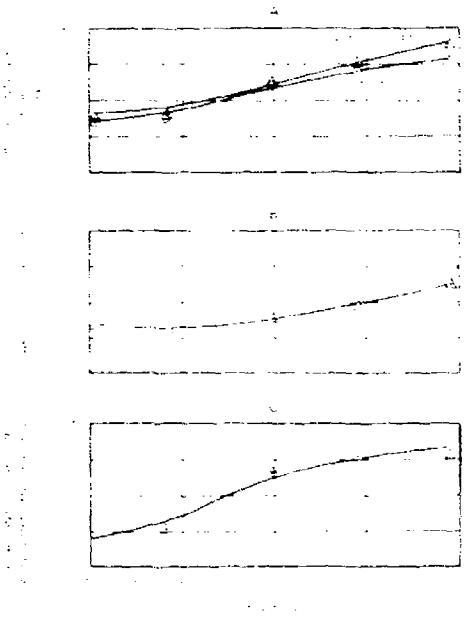

Figure 195. Airframe Structural Parameter Variation with Sideslip, Aux Propulsion Configuration.

Summary of 0-Degree Crossover Auxiliary Propulsion Structural Results

Changing the rotor crossover from 90 degrees to 0 degree:

1. Allowed a significant increase in the aircraft speed and maneuver envelopes over those flown in the 90-degree crossover.

2. Changed the impedance of the rotor system. This impedance change resulted in the upper rotor hub master stress location becoming the critical structural rotor parameter for airspeed expansion with the 0-degree crossover.

3. Changed the rotor induced 3P excitation of the airframe from roll/yaw to pitch/longitudinal. This change in direction of the 3P excitation:

   a) Reduced the stress at the J-60 engine support structure well below the working endurance limit.

b) Produced symmetrical bending of the horizontal stabilizer, causing the left and right rudder overbalance weights to work against each other via the rudder control rods. Increased rudder rod loads resulted, necessitating a change to steel rudder rods. With the aluminum rod, loads exceeded the endurance limit above 200 KCAS.

Replacing the stabilizer forward attachment fitting with a steel fitting during the rotor index change eliminated the stress problem at that location.

The stress at the tailcone/fuselage junction remained above the endurance value for both rotor crossover configurations. However, due to the redundancy of the structure in this area, the stress level was not considered critical for flight limitation.

The rotor differential control system remained an effective means of controlling rotor loads and tip clearance for the 0-degree crossover configuration. Differential lateral control (B_1') had the most significant effect on rotor loads and tip clearance below 200 knots. Collective and B_1' provided the most significant effect above 200 knots.

The rotor control loads for the 0-degree crossover data had steeper gradients than the 90-degree crossover data for load factor maneuvers.

The sideslip maneuvers indicated an apparent rotor wake impingement on the tail area for both crossover configurations.

DYNAMICS 90-DEGREE ROTOR CROSSOVER

Aircraft Aeroelastic Stability

The rotor and fixed control surfaces were demonstrated to be stable throughout the flight envelope, including trim flight to 194 KCAS. Considerable emphasis was placed upon the stability characteristics of the blade edgewise response, particularly in light of the high forward speed target and the autogyro mode of operation for the aircraft. Operation in this mode is somewhat equivalent to the minimum damping flight condition found in helicopter flight, and was therefore closely monitored. Much prior analysis and a 1/5 Froude scale model test had shown that the edgewise mode would be stable to 300 knots.

The edgewise damping trends shown in Figure 196 reflect the same basic character as seen in helicopter operation - minimum blade damping was coincident with minimum rotor power requirement. It is also seen that minimum rotor damping is nominally achieved in the range of the aircraft power bucket region, with damping then tending to increase with increasing airspeed.

Rotor and fixed system control surface flutter were also monitored as the flight envelope was expanded. Waveform analysis of critical parameters was performed to ensure that the aircraft was not approaching a flutter boundary. The blade torsional response character was tracked by examining pushrod response, which was found to demonstrate none of the characteristics descriptive of either classic or stall flutter. Positive fixed surface flutter stability margins were verified by evaluation of the nonharmonic response characteristics of the control rod loads for each surface. Nonharmonic response analysis indicated no unusual buildup of loads against airspeed which could be attributed to reduced modal stability descriptive of approaching a flutter boundary.

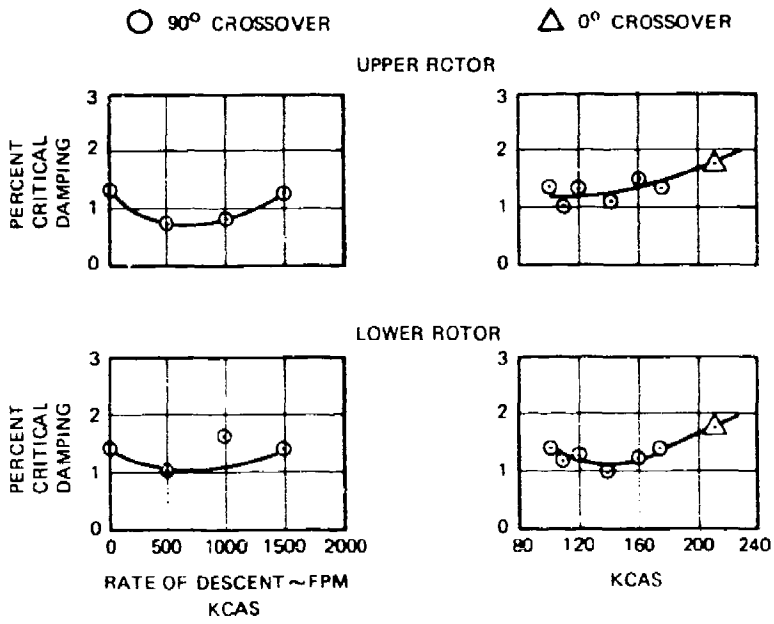

Figure 196. Blade Edgewise Damping, Aux Propulsion Configuration.

Airframe Vibration

Figure 197 shows a composite plot of the 3P cockpit vibration, thrust engine vibration, and horizontal tail fitting vibratory stress. As predicted, the lateral vibration was lower than in the helicopter mode at the same airspeeds. The change of vibration with rotor speed is also noted in Figure 197 for the airspeeds tested and is also plotted in Figure 198. The general trend of the vibration and stress is to increase with airspeed following the increasing 3P roll moment (Figure 199). As the rotor speed is changed, the 3P roll moment trend is not significantly altered so that the changes of vibration and stresses with rotor speed (Figures 197 and 198, are strictly a reflection of the dynamic characteristics of the fuselage. A subsequent shake test of the auxiliary propulsion configuration confirmed this fact.

The basic dilemma with the aircraft with the 90-degree rotor crossover was the fact that the rotor speed could only be reduced to 90 percent N_R near 200 knots. As shown in Figures 197 and 198, this had a very favorable effect on tail stresses (HSF 12) and cockpit lateral vibration, but increased the J-60 vibration and cockpit vertical. While the N_R trends shown in Figure 198 indicate this tendency of vibration to reverse due to the airframe mode at 90 percent N_R, steady-state investigation of lower rotor speeds was not possible.

Figure 199 shows the measured 3P rotor vibratory forces and moments derived from blade bending at +10 percent radius and summed into the fixed system. The total loads shown account for the rotor phasing so that for this arrangement (90-degree crossover) the major force into the fuselage is the 3P roll moments. The total pitching moment, vertical force and longitudinal force are theoretically cancelled with the 90-degree crossover. Test data in Figure 199 show a high degree of cancellation of these 3P loads indicating equal load sharing between the rotors.

It should be noted that the ABC flight results shown are with no vibration treatment in the aircraft. Most modern three- or four-bladed helicopters devote anywhere from 1-1/2 to 2-1/2 percent of their weight empty for this purpose. Addition of vibration treatment would substantially reduce the aircraft vibration levels.

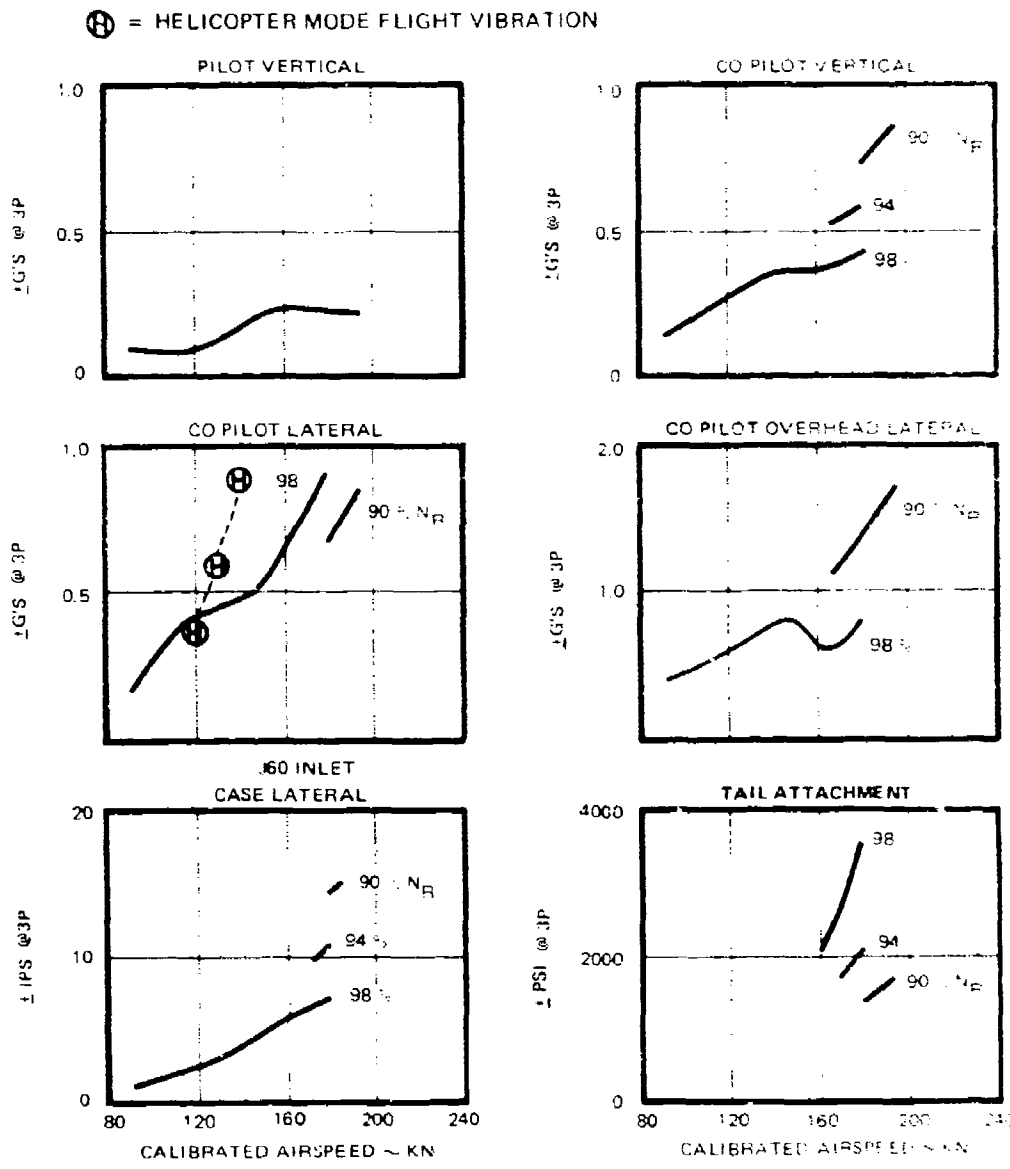

Figure 197. Airframe 3P Vibration Versus Airspeed, Aux Propulsion Configuration (90-Degree Crossover).

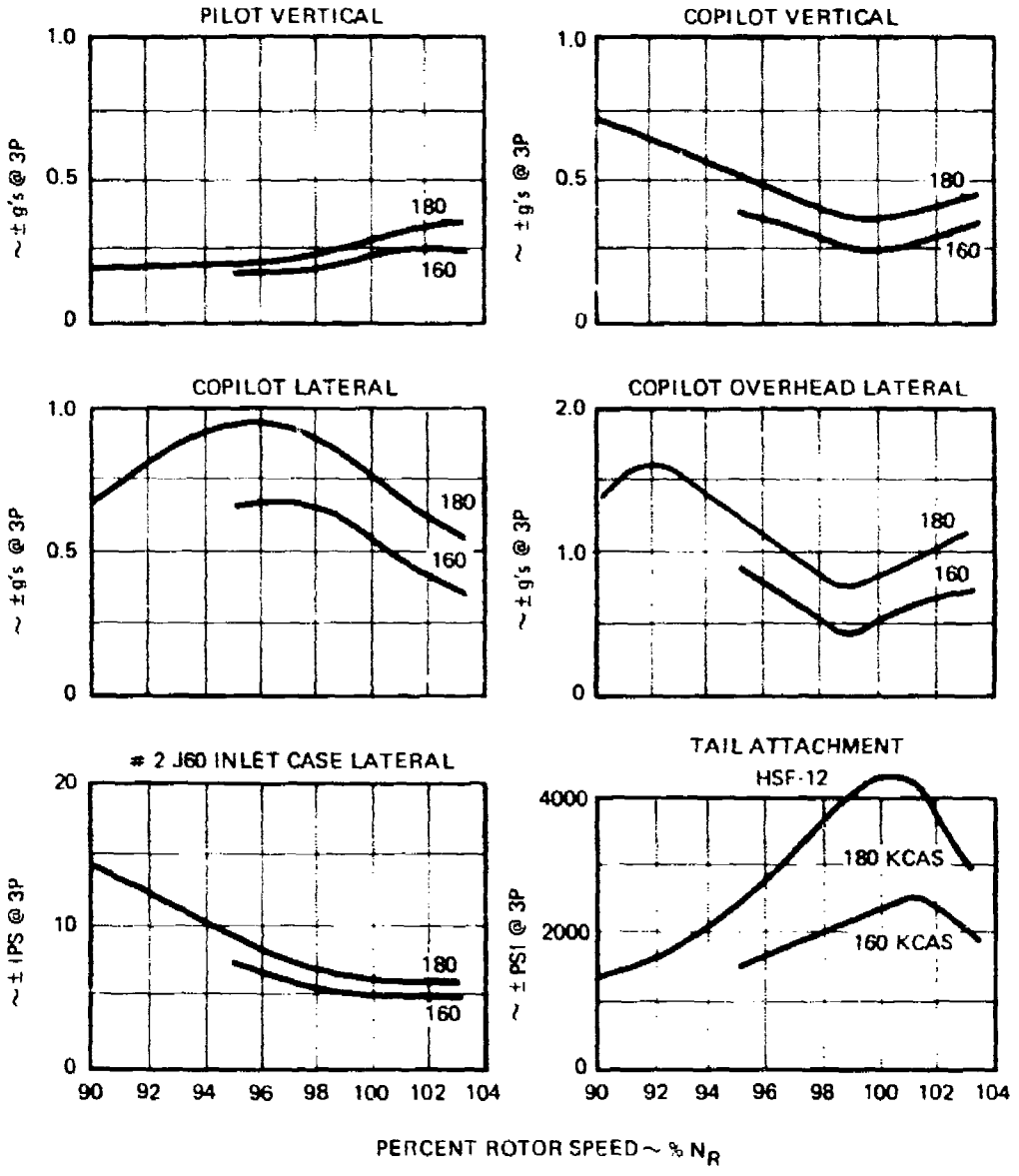

Figure 198. Airframe 3P Vibration and Stress Versus N_R, Aux Propulsion Configuration (90-Degree Crossover).

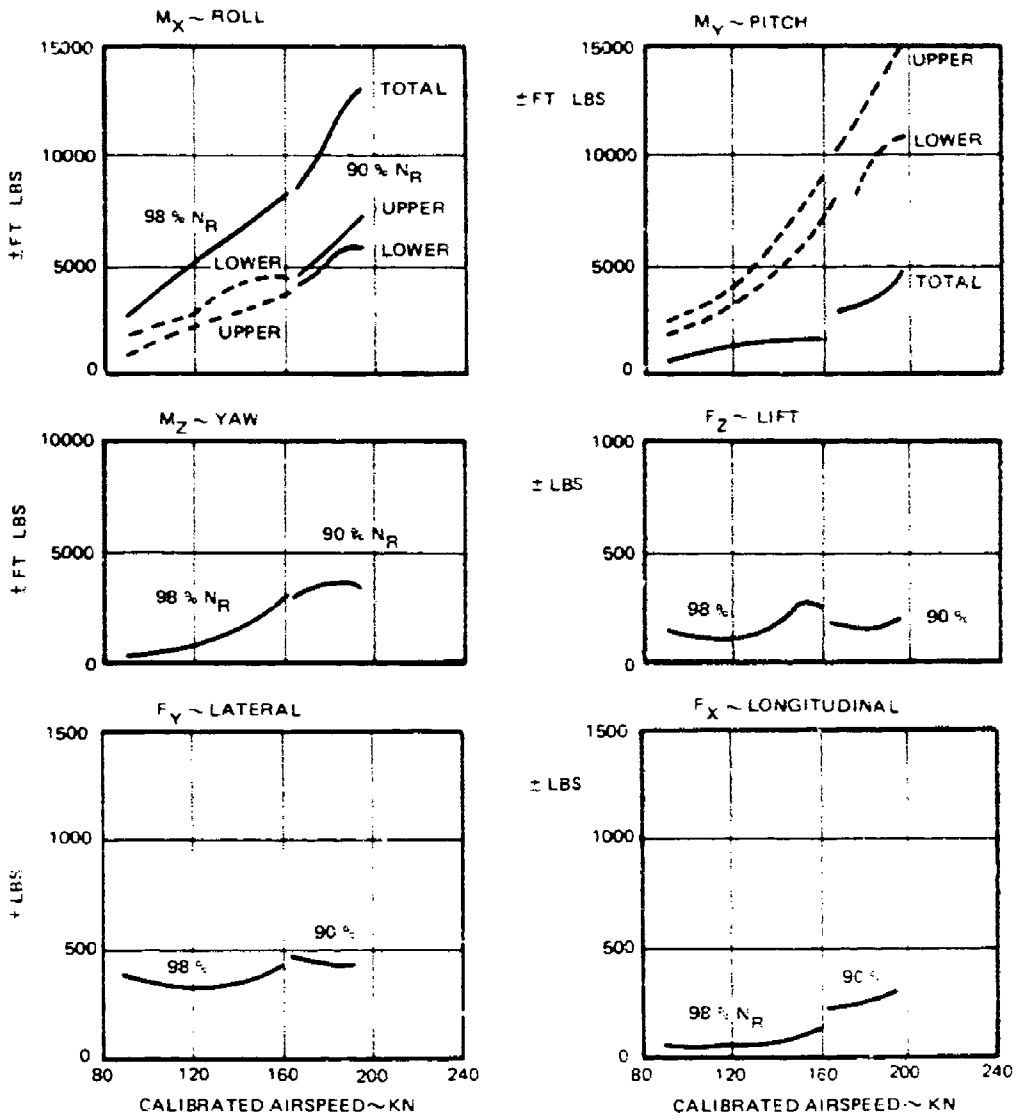

Figure 199. Measured 3P Rotor Vibratory Loads, Aux Propulsion Configuration (90-Degree Crossover).

DYNAMICS - 0-DEGREE ROTOR CROSSOVER

Aeroelastic Stability

With the rotor spatial [illegible] 0-degree crossover there is essentially no change in the aeroelastic behavior of the rotor or aircraft [illegible]. Therefore, the same monitoring and tracking procedures discussed previously for the 90-degree crossover and helicopter flight testing were employed. It was not necessary to refly the data points collected with the other rotor phasing but merely extend the airspeed envelope with the established procedures. Figure 196 shows the edgewise damping quantified for the 210-knot airspeed point with 0-degree crossover. The rotor and control surfaces were demonstrated to be stable to trim airspeed points to 238 KTAS and the demonstrated maneuver envelope.

No indications were found of any incipient aeroelastic instability of the rotor system, rotor blades or aerodynamic [illegible] surface during the entire flight program.

Airframe Vibration

After the aircraft had reached a true airspeed of 204 knots, at 90-degree crossover where lateral roll vibration and engine/tail stresses were excessive, there was an attempt to install a lateral/roll absorber in the cabin to control the vibration. This absorber configuration was never flown, however, since a decision was made to change the rotor index to 0 degree. This change would allow 3P pitch moments rather than 3P roll moments to be transmitted to the stationary system. This would excite the aircraft in a symmetrical manner at 3P and preclude the loadings that caused tail stress and engine mount problems in the previous flight testing. Without the fuselage strength problems the maximum airspeed envelope could be expanded quickly since other factors like edgewise damping and flying qualities would not be affected. Additionally, since little was known of the XH-59 fuselage response to 3P pitching moments, a hanging shake test of the airframe was accomplished.

The 3P vibration characteristics, tail stress and engine mount stress and vibration were greatly improved for this untreated aircraft with a change of rotor index. Figure 200 shows a comparison of the cockpit vibration for both rotor indexings at 200 knots. It is evident that the large lateral roll vibration is greatly reduced with 0-degree crossover while the longitudinal component is increased. This shows that the interrotor cancellation of the 3P moments works. The overall ride quality was vastly improved, probably due to the large reduction of vertical (from roll) vibration coupled with greater tolerance of man to the longitudinal rather than lateral

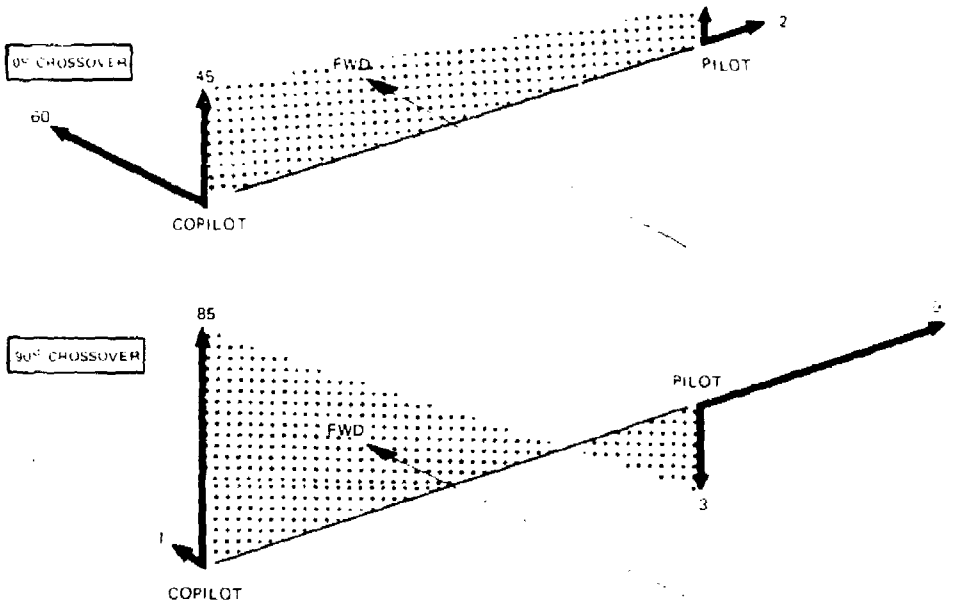

Figure 200. Cockpit 3P Vibration Comparison at 200 KIAS, Aux Propulsion Configuration.

vibration. Figures 201 and 202 show the comparison of vertical and inplane vibration with airspeed for both rotor phases for this non-vibration treated XH-59 aircraft. The change of index allowed a maximum airspeed of 238 KTAS to be flown with cockpit vertical vibration equivalent to 160 knots at 90-degree crossover. The longitudinal vibration was less than the lateral by 30 percent at 200 knots. The residual lateral with 0-degree crossover or longitudinal with 90-degree crossover were both low (0.2g) indicating that the 3P inter-rotor moment cancellation was effective. Both of these figures show that the vibration is lower at 150 knots for the XH-59A than equivalent, untreated helicopters and that the vibration could be reduced to modern-day levels with vibration treatment devices installed.

Figure 203 shows that the J-60 engine mount stresses were cut in half with 0-degree crossover to levels within the allowable. Figure 204 shows the same results for the horizontal stabilizer attachment fitting. In both cases, this large reduction was due to the elimination of the assymmetric load which occurred when the 3P roll moment was the major rotor exciting force. Vibratory airframe stress in the tailcone area and main rotor transmission attachments did become a

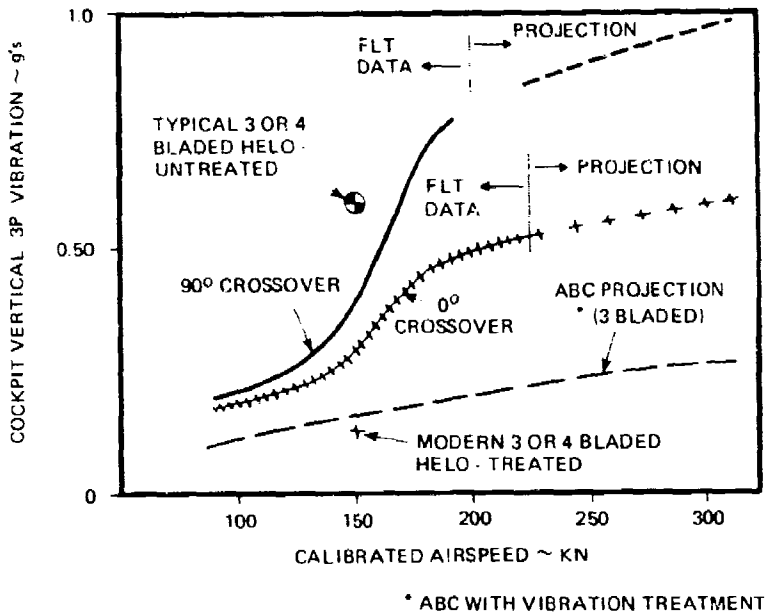

Figure 201. Vertical 3P Vibration Reduction Following Modern Helicopter Trends.

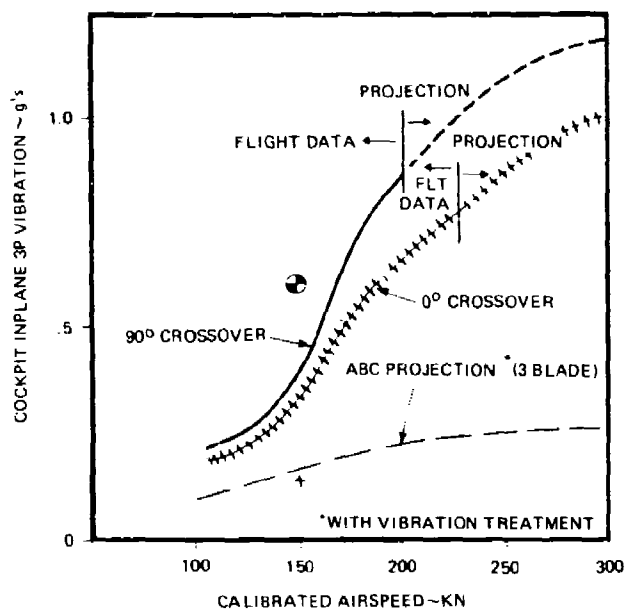

Figure 202. Inplane Vibration Reduction Following Modern Helicopter Trends.

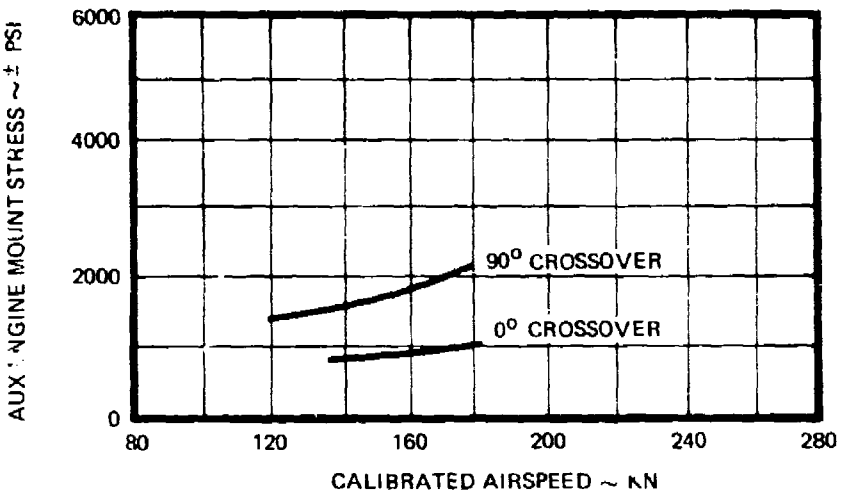

Figure 203. J-60 Engine Mount Stress Effect of Airspeed, Aux Propulsion Configuration.

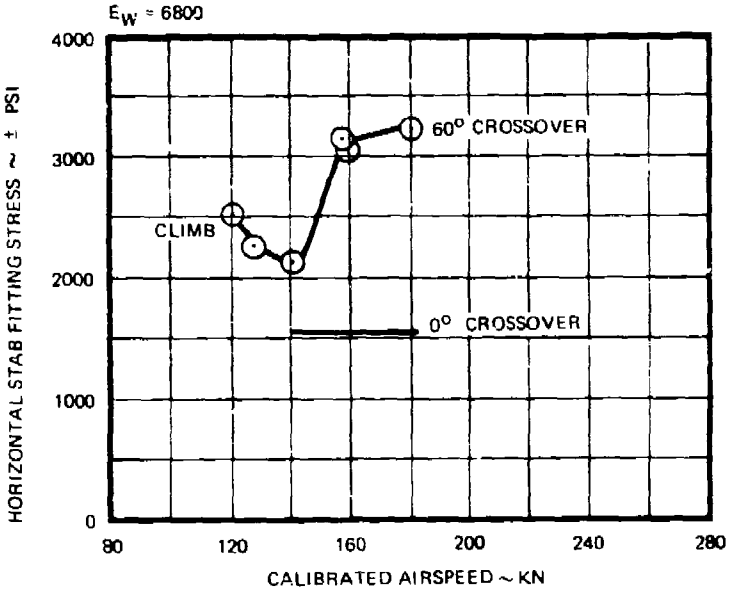

Figure 204. Horizontal Tail Lug Stress Effect of Airspeed, Aux Propulsion Configuration.

factor with the rotors indexed at 0-degree crossover. These stresses were due to an airframe symmetric mode near 16.0 Hz, which is equivalent to 3P forcing at 94 percent rotor speed.

As mentioned previously, a hanging shake test of the ABC aircraft in the auxiliary propulsion configuration was accomplished in the summer of 1979. The aircraft was extensively instrumented for both vibration and stresses in the critical areas (engine mounts, stabilizer attachments, etc) so that the response and stresses in the aircraft for the important 3P rotor loads could be measured and quantified. It was found that the 3P pitch moment or rolling moment were mainly responsible for the inflight 3P vibration or stresses in the airframe. Figures 205 and 206 show that very good correlation was attained between measured flight 3P vibration in the cockpit and calculated 3P data using the shake test mobilities (g/load) and measured inflight 3P moments at 180 knots. The match over an rpm range using only 3P roll moments as the forcing load indicates that this method could be used to predict the vibration and stress for a change of rotor index, where the 3P pitch moment is the important vibratory load. The fuselage dynamic characteristics are taken from the hanging shake test for pitch excitation. Figure 206 illustrates that the trends of the J-60 mount stress and stabilizer fitting stress were calculated well by this method for the 90-degree crossover. The absolute value of the stabilizer stress is off somewhat due to aerodynamic impingement on the vertical tail. Figure 207 shows the projected 3P cockpit vibration for the XH-59A with the rotor staging downward as the airspeed is advanced and one with a constant rotor rpm. In the case of 0-degree crossover, unlike 90-degree, the decrease of rpm required to maintain lower tip Mach number is a disadvantage from a cockpit 3P vibration standpoint although it was an advantage for the tailcone stresses.

As the flight envelope was expanded rather quickly it became apparent that the engine mount stress, tail lug stress, and cockpit vibration were much more subdued with the 0-degree crossover setting. At low speed (120 knots), the effect of collective and B_1^1 were evaluated to determine the sensitivity of the 3P pitch moment and the resulting aircraft vibration. While the collective had some effect (higher collective was higher 3P pitch moment), the B_1^1 control did not have a large effect on 3P loads or vibration. High-speed data were attained with the collective held constant and the rotor speed at 98 percent. Figure 208 shows a composite cockpit vibration plot for these flights, flown to over 235 knots. The vibration environment is much more acceptable than with 90-degree crossover which was presented in Figure 197, and compared at 200 knots in Figure 200.

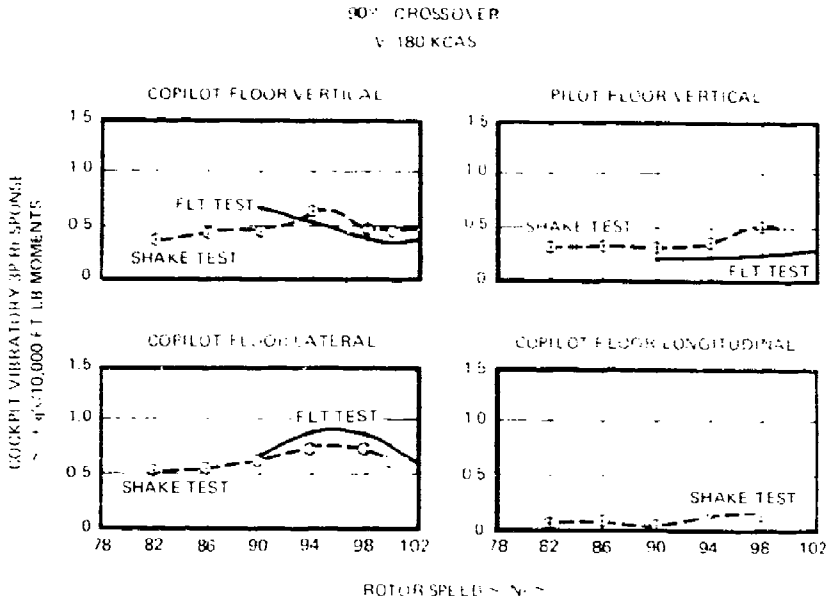

Figure 205. Shake Test Cockpit Vibration Predictions Versus Flight Test Data, Aux Propulsion Configuration.

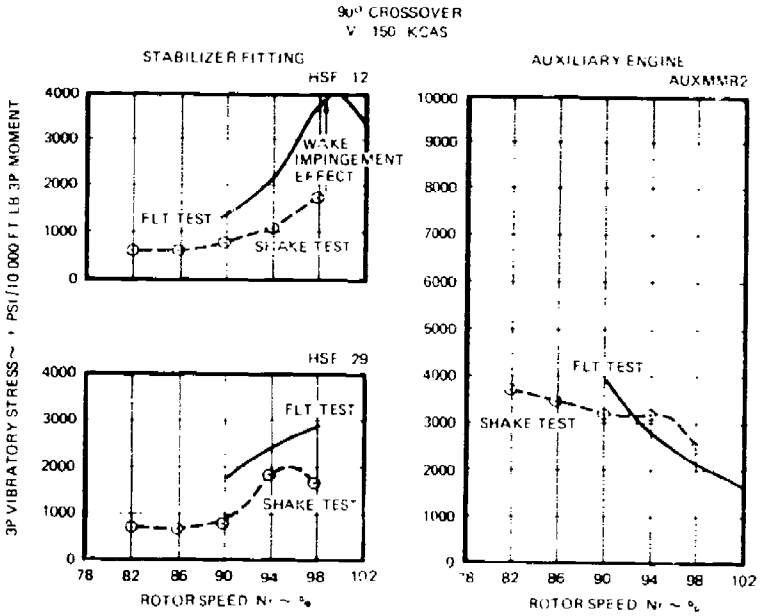

Figure 206. 3P Vibratory Stress, Aux Propulsion Configuration.

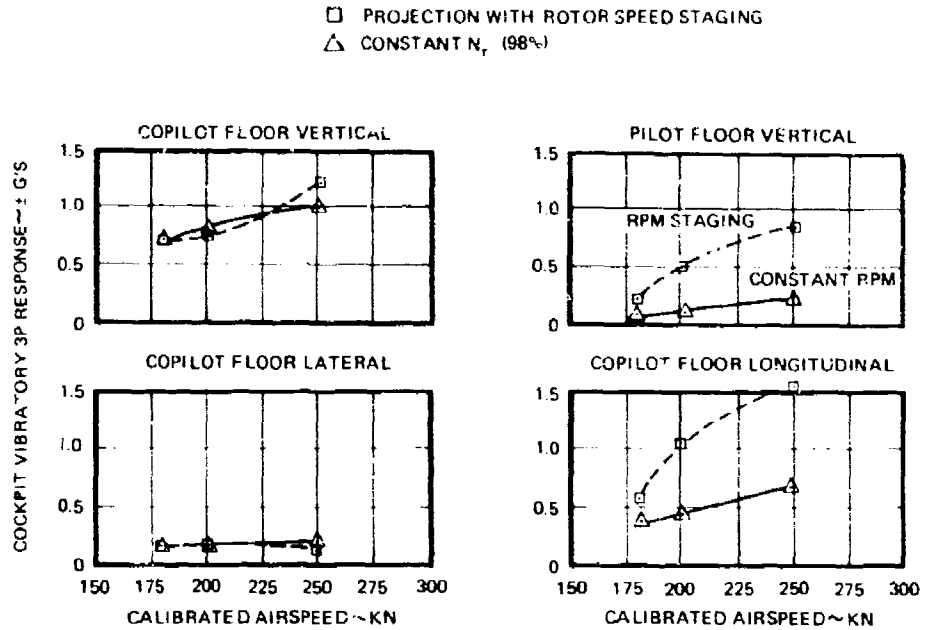

Figure 207. Projected Cockpit Vibration for 0-Degree Rotor Crossover Configuration, Aux Propulsion Configuration.

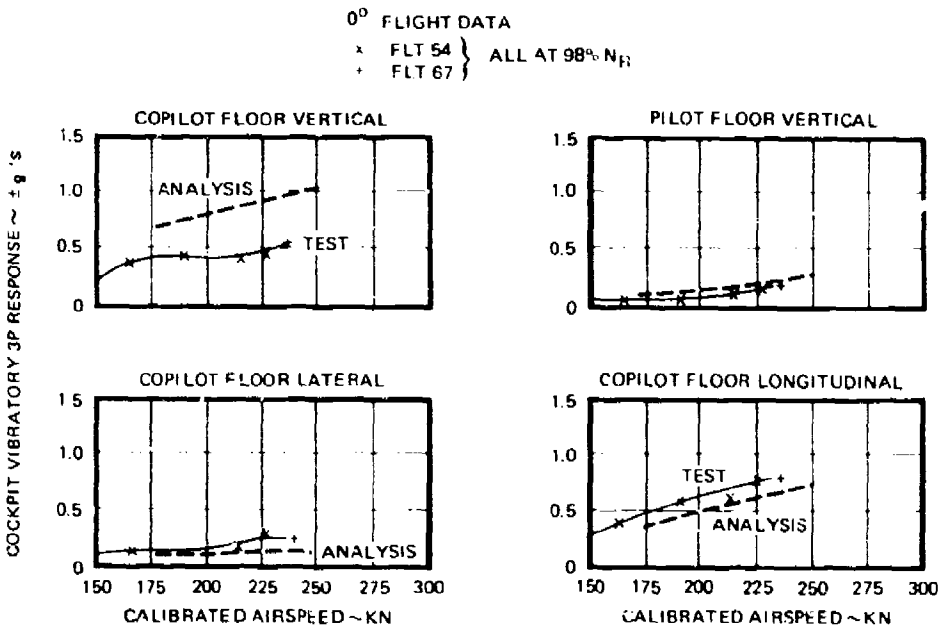

Figure 208. 0-Degree Crossover 3P Vibration - Cockpit, Aux Propulsion Configuration.

Figure 209 shows the 3P roll moment with 90-degree crossover and the 3P pitch moment with 0-degree crossover are essentially equal. The vibration and dynamic stress differences in the flight program for different rotor indexes were a function of the XH-59A fuselage structure. These differences were highlighted by the hanging shake test and indicated substantial changes dependent on the frequency (therefore rpm) at which the structure was excited. In general, the XH-59A structure and aircrew were more tolerant to the symmetrical loading of 0-degree crossover. In either case however, the basic culprit was the magnitude of the rotor vibratory 3P moments shaking the airframe. Airframe response to those moments would be substantially reduced if suitable vibration treatment were installed. Alternately, higher harmonic control has been shown analytically to substantially reduce (by 90 percent) the 3P rotor moments.

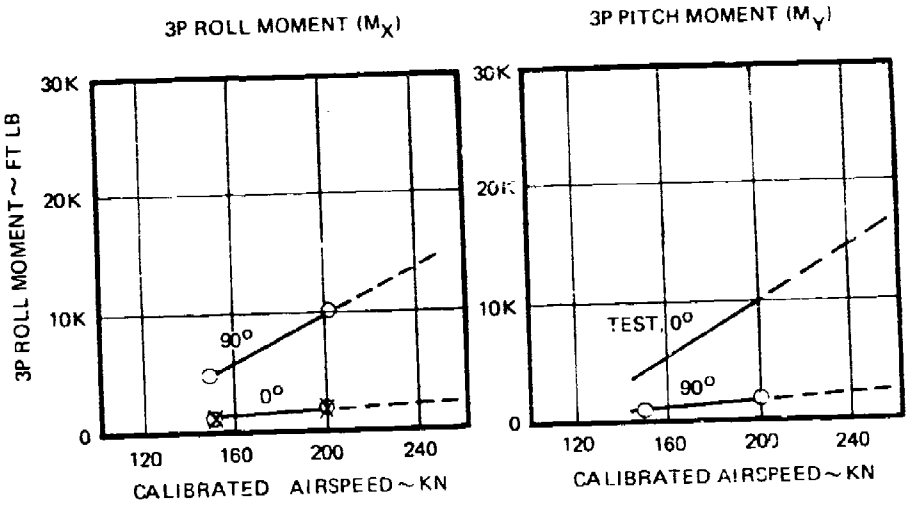

VIBRATORY MOMENTS DERIVED FROM INFLIGHT BLADE LOADS DURING 90° CROSSOVER FLIGHTS

Figure 209. 3P Hub Moments Depend on Crossover, Aux Propulsion Configuration.

RESULTS AND CONCLUSIONS

Completion of the 106-hour flight test program in both the helicopter and auxiliary propulsion flight modes supports the following major results and conclusions:

1. The ABC high-lift capability independent of airspeed has been verified up to 238 KTAS.

2. The ability of the ABC rotor to maintain airspeed at altitude has been demonstrated in the helicopter configuration.

3. Forward flight lift/drag ratios predicted for this rotor system have been verified.

4. Handling qualities have been excellent with the aircraft stable in both the low-speed and high-speed flight regimes. The entire speed envelope has been demonstrated with SAS off. The high control power available has resulted in a very maneuverable aircraft without any tendency to overcontrol.

5. Rotor stress and control loads have been controllable as predicted and remained at acceptable values throughout the level flight airspeed envelope.

6. Adequate tip clearance has been demonstrated throughout a significant maneuver envelope at all airspeeds. Stiff blades and the absence of blade stall result in very low control system loads.

7. Blade edgewise damping has remained stable; and above minimum power required airspeed, the critical damping ratio is increasing.

8. Perceived noise levels in the helicopter configuration at hover and level forward flight were 5 to 15 dB lower than those of a single rotor/tail rotor helicopter of comparable size and power.

9. The excellent agility characteristics of the ABC rotor have been demonstrated throughout the flight envelope. Particularly notable are 0 to 2g rotor load capacity through 220 KCAS, seven second 360-degree turns at hover, and excellent aircraft responses with precise control.

10. Blade twist of -10 degrees is adequate for speeds up to approximately 200 knots but less twist is desireable for higher speeds.

11. The coaxial ABC rotors have a noticeably better hovering figure-of-merit than conventional single-rotor helicopters. (A further improvement in aircraft hover performance results from not having to power a tail rotor or other type of anti-torque device.)

12. Rate of descent in autorotation is similar to other helicopters of equal disc loading. At low collective settings, the XH-59A exhibited weak (or mildly reversed) directional control, indicating a requirement for relocation or redesign of the vertical fins and/or decoupling differential collective pitch yaw control at low values of collective pitch.

RECOMMENDATIONS

Based on the completion of the flight testing to date, the following recommendations are made:

1. Flight testing should be conducted in the auxiliary propulsion configuration at higher altitude to determine the rotor capabilities at high rotor C_t/σ value and to determine how maximum airspeed varies with altitude.

2. Flight testing should be conducted at alternate center-of-gravity locations to determine the effects on stability and control and aircraft loads. Tail size reductions should be considered.

3. Numerous minor structural concerns on the aircraft should be addressed and resolved so as not to delay further productive flight testing.

4. Areas where the ABC analytical methods do not correlate with the flight test results should be resolved so that future flight testing can proceed at a more efficient pace.

5. The XH-59A speed envelope should be further expanded to determine what parameters will limit forward speed. It should be determined if this limitation is the result of the unique XH-59A aircraft or if it is an inherent ABC limitation.

6. Methods for reducing rotor system vibratory loads should be investigated. These could include higher harmonic control, which promises substantial vibration reduction with only a small penalty in aircraft weight.

7. Flight testing should be conducted to investigate in detail all the various parameters which affect the rotor performance. These would include differential lateral cyclic pitch, differential longitudinal cyclic pitch, differential collective pitch, control phase angle, and variable elevator position.

8. Additional investigation of low-speed autorotative yaw control is recommended.

9. Additional flights with government pilots should be conducted for further objective evaluation of the Advancing Blade Concept and for limited operational evaluation of the aircraft.

10. A current technology rotor and drive system should be installed to eliminate the present test restrictions of the XH-59A aircraft. A composite rotor system would allow an alternate value of blade twist and airfoil chord distribution to be investigated, while providing a substantially lighter rotor system. An integrated propulsion system with two engines powering both the rotors and an auxiliary propulsion device would provide more power to the rotor, would be lighter and more fuel efficient, and would more closely represent the type of aircraft configurations proposed to meet future production requirements.

11. Subsequent to conversion to a twin engine integrated propulsion system configuration, further investigations of rotor speed stability in maneuvering flight should be conducted.

12. Development of larger scale hardware should be initiated to determine scaling effects of the rotor system if ABC is to be considered for substantially larger gross weight aircraft.

13. Additional full-scale flight tests should be augmented by both full and reduced scale wind tunnel tests, as appropriate. Model rotor testing and model tests of interactions of rotors/tail surfaces/pusher props or fans should be conducted.

REFERENCES

1. FULL-SCALE WIND TUNNEL INVESTIGATION OF THE ADVANCING BLADE CONCEPT ROTOR SYSTEM, USAAVLABS Technical Report 71-25, Eustis Directorate, U.S. Army Air Mobility R&D Lab, Fort Eustis, Va, August 1971. AD 734338.

2. Specification No. 712B, T400-CP-400 ENGINE SPECIFICATION, Pratt & Whitney of Canada Ltd.

3. JT12 INSTALLATION HANDBOOK, Pratt and Whitney Aircraft, 14 April 1966.

4. Castles, W., Jr. and Deleeuw, J.H., THE NORMAL COMPONENTS OF THE INDUCED VELOCITY IN THE VICINITY OF A LIFTING ROTOR AND SOME EXAMPLES OF ITS APPLICATION, NACA TN-2912, 1954.

5. Glauert, H., A GENERAL THEORY OF THE AUTOGYRO, RAE R&M 1111, 1926.

6. Payne, P.R., HELICOPTER DYNAMICS AND AERODYNAMICS, Putman and Sons, London, 1959.

7. Curtiss, H.C., et al, AN EXPERIMENTAL INVESTIGATION OF THE LOW SPEED TRIM AND STABILITY CHARACTERISTICS OF A COAXIAL HELICOPTER WITH HINGELESS ROTOR ON THE PRINCETON DYNAMIC MODEL TRACK, Princeton University, TRN 1196, September 1974.

8. Phelps, A.E., and Mineck, R.E., AERODYNAMIC CHARACTERISTICS OF A COUNTER-ROTATING, COAXIAL, HINGELESS ROTOR HELICOPTER MODEL, NASA TN-78705, May 1978.

9. MIL-H-8501A, MILITARY SPECIFICATION, GENERAL REQUIREMENTS FOR HELICOPTER FLYING AND GROUND HANDLING QUALITIES.

LIST OF SYMBOLS

A_1	Longitudinal Cyclic Pitch
A_1'	Differential Longitudinal Cyclic Pitch
B_1	Lateral Cyclic Pitch
B_1'	Differential Lateral Cyclic Pitch
b	Number of Rotor Blades
C	Blade Chord
C_T	Thrust Coefficient
$C_{T/\sigma}$	Thrust Coefficient/Solidity Ratio
C_P	Power Coefficient
C_W	Weight Coefficient
$C_{W/\sigma}$	Weight Coefficient/Solidity Ratio
E_W	Fatigue Endurance Limit
FM	Figure of Merit
H_D	Density Altitude
i_t	Tail Incidence
KN	Calibrated Airspeed
K_V	Longitudinal Wake Distribution Coefficient
L	Rotor Roll Moment
M	Rotor Pitch Moment
M_{TIP}	Rotor Tip Mach Number
M_μ	Speed Stability
M_α	Angle-of-Attack Stability
N_R	Rotor Speed, rpm
$N_r/\sqrt{\theta}$	Referred Rotor Speed, rpm

N_z	Load Factor
q	Dynamic Pressure
r	Blade Radius Station
R	Blade Radius
t	Blade Thickness
u	Induced Velocity
V	Velocity, knots
V_e	Equivalent Airspeed
$V_{e/\sqrt{\delta}}$	Referred Velocity
W/δ	Referred Gross Weight
α	Angle of Attack
Γ	Control Phase Angle
Δ	Delta, a Differential
δ	Pressure Ratio, P/P_o
ζ	Damping Ratio
η	Transmission Efficiency
θ	Collective Pitch
$\sqrt{\theta}$	Square Root of Temperature Ratio, T/To
λ	Rotor Inflow Velocity
μ	Advanced Ratio, $V_T/\Omega R$
σ	Rotor solidity $bc/\pi r$
ψ	Azimuth Position
ω_D	Damped Frequency
ω_N	Natural Frequency
ΩR	Rotor Tip Speed

Subscripts

e	Equivalent
f	Fuselage
L	Lower Rotor
o	Root Blade Angle
t	Trim
U	Upper Rotor
w.o.	Washout
.75	75 Percent Blade Station